Investigation of the roles of acid sensing proteins in rheumatoid arthritis

Fawaz Saleh Albloui

A thesis submitted in partial fulfilment of the requirements for the degree of Doctor of Philosophy

The University of Sheffield
Faculty of Medicine

The University Of Sheffield.

March 2016

Acknowledgements

First, I thank The Almighty Allah for blessing, protecting and guiding me throughout my life.
Special thanks to my parents and my wife for helping and guiding me.

Also, I would like to thank my principal PhD supervisor Dr. Peter Grabowski for his endless support, advice and patience. I am deeply grateful for his help and motivations. It has been an honour and privilege working with Dr. Grabowski.

It is my pleasure to thank my co-supervisor Dr.Munitta Muthana. She has always available to guide me through all difficulties.

Also I would like to extend my thanks to Fiona Wright for her help in orders placement and purchases. Fiona has been available to help me with any shortage in materials or reagents.

It is my pleasure to thank Dr. David Buttle for his support and contributions in lab meetings which helped me to develop my knowledge.

Big thanks to the Shannon Bailey, Mai Shafi and Madhuri Doss for helping me with experiments.

Special thanks to all my Friends and colloquies in the medical school and the academic unit of rheumatology.

Finally I am very grateful to my friends Dr.Fahad Hakami, Adbulrahmaan alkhalaf and Naif Alfarraj.

The work described in this project has been supported by the Royal Embassy of Saudi Arabia.

List of Abbreviations and Acronyms

ADAMTS	a disintegrin and metalloprotease with thrombospondin motifs
AKAP150	A-kinase anchoring protein 150
AP-1	activating protein-1
ASIC1	acid-sensing ion channel 1
ASIC2	acid-sensing ion channel 2
ASIC3	acid-sensing ion channel 3
ASlC4	acid-sensing ion channel 4
ASlCs	acid-sensing ion channels
Ca^{2+}	calcium ion
CaM	calcium-modulated protein
CaMKII	Ca^{2+}/calmodulin-dependent protein kinase II
cAMP	cyclic adenosine monophosphate
CFA	complete Freund's adjuvant
CGRP	calcitonin gene-related peptide
COMP	cartilage oligomeric matrix protein
DC	dendritic cell
DMARD	disease-modifying antirheumatic drug
DRG	dorsal root ganglion
ENaC	epithelial sodium channel
Epac	exchange protein directly activated by cAMP

ERK	extracellular-regulated kinase
FBS	foetal bovine serum
FGF	fibroblast growth factor
FLS	fibroblast-like synoviocytes
GPCR (GPR)	G-protein-coupled receptor
GPLR	G-protein-linked receptors
HIF	hypoxia-inducible factor
HLA-DR	human leukocyte antigen – D related
HUVEC	human umbilical vein endothelial cell
IHC-P	immunohistochemistry paraffin protocol
IL	interleukin
JNK	c-Jun N-terminal kinase
LPC	lysophosphatidylcholine
LTP	long-term potentiation
MAPK	mitogen-activated protein kinase
MMP	matrix metalloproteinase
mRNA	messenger ribonucleic acid
Na^+	sodium ion
NF-κB	nuclear factor-kappa B
NGF	nerve growth factor
NMDAR	N-methyl-D-aspartate receptor
NSAID	non-steroidal anti-inflammatory drug
OA	osteoarthritis

OGR-1	ovarian cancer GPCR1
OPG	osteoprotegerin
PBS	phosphate-buffered saline
PDZ	post-synaptic density, Drosophila discs large, and zonula occludens-1
PICK1	protein interacting with C-kinase 1
PIP_2	phosphatidylinositol 4,5-bisphosphonate
PIST	PDZ domain protein interacting specifically with TC10
PKA	protein kinase A
PKC	protein kinase C
PLC	phospholipase C
PSD-95	post-synaptic density protein 95
RA	rheumatoid arthritis
RANK	receptor activator of nuclear factor kappa-B
RANKL	receptor activator of nuclear factor kappa-B ligand
RIPA	radio-immunoprecipitation assay
SPC	sphingosylphosphorylcholine
TBS	Tris-buffered saline
TBST	Tris-buffered saline-Tween
TDAG8	T-cell death-associated gene 8
TNF	tumour necrosis factor
TRP	transient receptor potential

TRPV1	transient receptor potential cation channel subfamily V member 1
VAS	visual analogue scale
VEGF	vascular endothelial growth factor
VGCC	voltage-gated calcium channel
VGSC	voltage-gated sodium channel
VSMCs	vascular smooth muscle cells

Summary

Rheumatoid arthritis (RA) is characterised by chronic joint inflammation, which is generally associated with destruction of articular cartilage and bone. Inflammatory cytokines, such as tumour necrosis factor (TNF), promote the up-regulation of proteases that degrade components of the extracellular matrix in cartilage and bone. Chronic joint inflammation results in reduced concentrations of oxygen (hypoxia). Hypoxic conditions cause anaerobic respiration and lactic acid build-up in synoviocytes, which are the cells that line articular joints. Acid-sensing proteins respond to these acidic conditions in the extracellular space of joints. We hypothesized that acid-sensing proteins play a critical role in the development and pathology of RA through diverse signalling and cellular functional responses. Identification of the exact signalling mechanisms and expression of acid-sensing proteins may facilitate development of effective management options for patients with RA.

In this study, by using immunohistochemistry paraffin protocol (IHC-P) and real-time polymerase chain reaction, we demonstrated that four acid-sensing proteins were expressed at variable levels in synovial biopsies from RA patients and at the messenger ribonucleic acid (mRNA) level in RA fibroblast-like synoviocytes (FLS). Expression levels of these proteins were slightly induced at the mRNA level by the inflammatory cytokine TNF. Importantly, acidic conditions that mimicked the inflamed synovial joint in RA also resulted in a significant increase in matrix metalloproteinase (MMP)-1 and MMP-9, whereas migration activity of RA FLS was reduced. Furthermore, ASIC3 and TRPV1 inhibition resulted in a significant down-regulation of MMP-1 and -9 at mRNA level in RA-FLS under low pH.

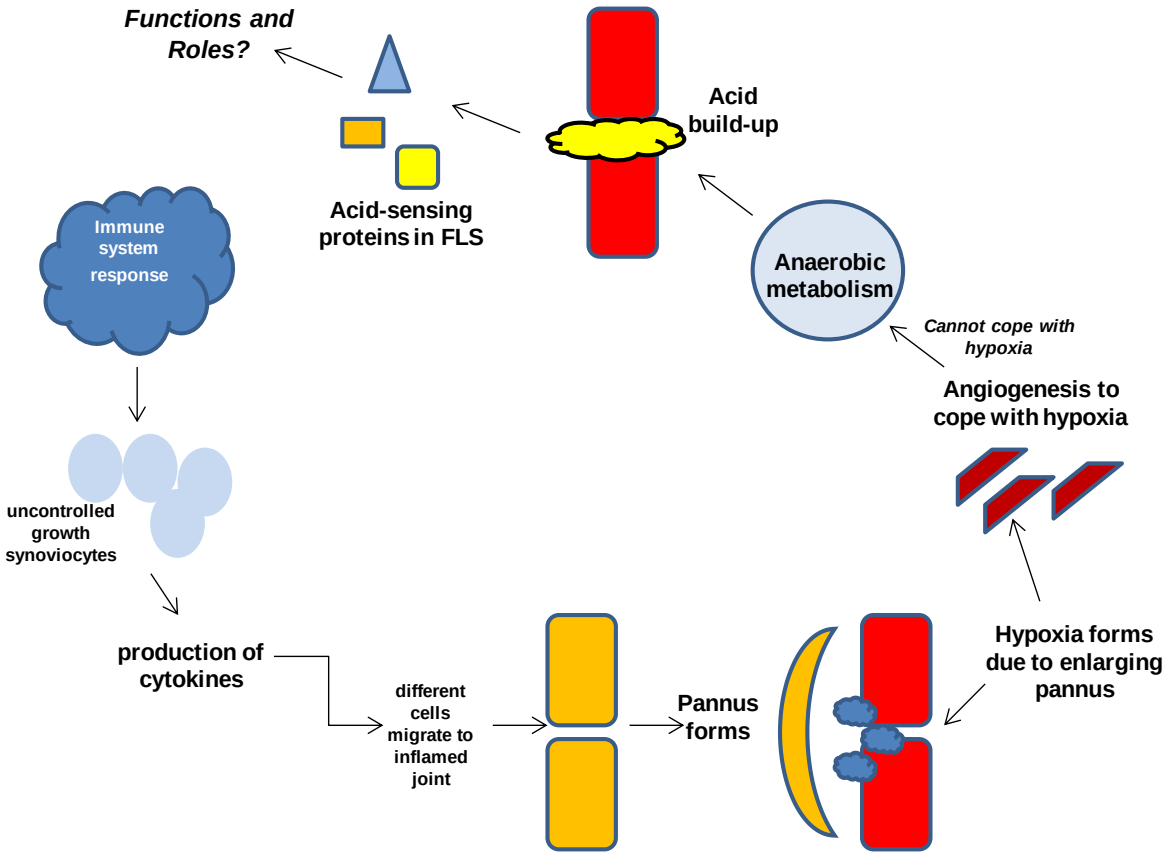

RA progression. This diagram illustrates the progression of RA starting from immune response to acid build-up in the inflamed joint. The aim of this project is to understand the function and role of acid-sensing proteins expressed by FLS obtained from the RA tissue. FLS, fibroblast-like synoviocytes; RA, rheumatoid arthritis.

Table of Contents

List of figures

1 Chapter 1: Rheumatoid arthritis

1.1 Introduction

RA is a symmetrically distributed and chronic autoimmune disorder that primarily affects the joints of the feet and hands (Gomez et al., 2011). The global incidence of RA is approximately 0.5%–1.5% according to Kobelt and Johnson (2008). Nonetheless, it most commonly occurs in people older than 50 years, although it can affect people at any age (Oliver and Silman, 2009).

1.2 Aetiology of rheumatoid arthritis

The aetiology of RA remains unknown; however, various risk factors for RA have been investigated. In the 1970s, a link between human leukocyte antigen – D related (HLA-DR) and RA was found. Researchers found that about 70% of RA patients had the HDLA-DR4 serotype, whereas only 30% of controls did, suggesting that individuals with HDLA-DR4 have a higher risk of RA (McMichael et al., 1977). Moreover, three times more females develop RA than males, which suggests that hormonal and sex-related genetic factors may be involved in RA initiation (Weyand et al., 1998). Age may also be a risk factor for RA, as reported in a study by Karlson et al. (Karlson et al., 2004), which showed that the risk of RA is elevated in women between 50 and 64 years of age as compared to women younger than 50 years of age. Furthermore, researchers have considered infectious agents, such as the Epstein-Barr virus, parvoviruses, retroviruses, bacteria, and their products as agents that may initiate RA. Bacterial products activate innate immunity through Toll-like receptors, which can lead to rapid inflammatory responses. Moreover, antigen presentation by dendritic cells (DCs) in the lymphoid

system will activate T and B cells to produce pathogenic antibodies or migrate to the joint and enhance the production of cytokines, such as interleukins (ILs), which in turn recruit other cells to the joint and activate other cells such as macrophages and FLS (Figure 1.1) (Firestein and Zvaifler, 1990). However, this hypothesis remains unproven (Firestein and Zvaifler, 1990, Wilder and Crofford, 1991). RA patients are classified into seropositive and seronegative (according to the serological status). Seropositive RA refers to RA patients with positive rheumatoid factor (RF) and/or anticitrullinated protein antibody (ACPA), seronegative RA refers to patients with negative serological test result for both RF and ACPA. It has been concluded that the majority of RA patients are seropositive, with approximately 79% RF and 70% ACPA positivity (Balsa et al., 2001, Sapir-Koren and Livshits, 2016). Seropositive RA patients tend to develop a sever course of disease progression, subcutaneous nodules (37.5%) and vasculitis (6.3%) (Alarcon et al., 1982).

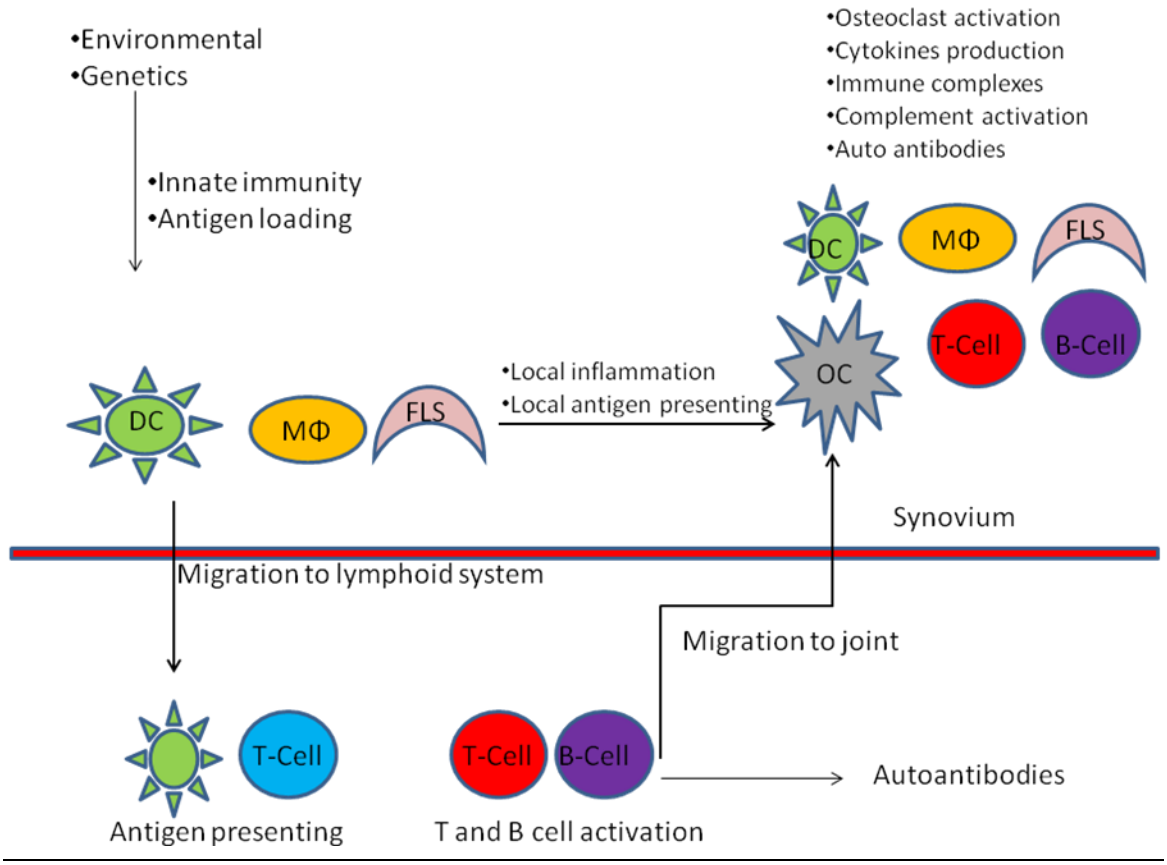

Figure 1.1 Schematic diagram of disease mechanisms that likely occur in RA

DC, dendritic cell; MΦ, macrophage; OC, osteoclast; FLS, fibroblast-like synoviocytes; RA, rheumatoid arthritis.

1.3 Extra-articular manifestations of RA

1.3.1 Rheumatoid vasculitides

Rheumatoid vasculitis is considered to be the major cause of extra-articular complications in RA. These complications are rare (affecting 1%–5% of RA patients) and mainly affect patients who are rheumatoid factor (RF)-positive. Rheumatoid vasculitides can affect any organ (e.g., skin, heart, eyes, nerves, and kidneys) and have no specific signs or symptoms. However, histopathological analysis of affected organs may help to identify vasculitides (Prete et al., 2011). Identification of acute necrotizing arteritis in small vessels of the affected organs will help in the treatment of RA Treatment of rheumatoid vasculitides is based mainly on cytotoxic drugs or steroids.

1.3.2 Skin manifestations

The skin is considered the most common target of RA (Cojocaru et al., 2010). Subcutaneous nodules occur in about 30% of RA patients and exist mainly in RF-positive patients (Prete et al., 2011). These nodules form during the progression of RA, but some may develop in early RA (before the involvement of joints). Other skin manifestations include Raynaud's phenomenon (triphasic colour change of the extremities), periungual infarcts (tiny black dots close to the corner where the distal nail touches the skin), leg ulcers, splinter haemorrhages (fingernail haemorrhage), digital gangrene (finger and toe gangrene), and sharply demarcated painful ulcerations as a result of small vessel vasculitides (Cojocaru et al., 2010, Prete et al., 2011). Most skin manifestations in RA localize in areas that are exposed to external pressure or repetitive irritation, such as the

surfaces of the forearms, fingers, and heels. Rheumatoid nodules are sometimes alleviated with standard treatment, but they may also worsen with therapy (Patatanian and Thompson, 2002).

1.3.3 Accelerated rheumatoid nodulosis

Accelerated nodulosis (AN) occurs in 8%–11% of long-term methotrexate-treated RA patients (Combe et al., 1993). There is a clear association between AN and the use of methotrexate. Reducing or replacing methotrexate with another treatment such as hydroxychloroquine or sulphasalazine suppresses the development of AN (Combe et al., 1993). However, the pathogenic mechanism behind methotrexate activity and AN remains elusive. Cases of AN have also been reported in RA patients treated with anti-tumour necrosis factor (TNF) and/or leflunomide (Cunnane et al., 2002), suggesting that pathogenetic mechanisms of RA are essential inducers of AN.

1.3.4 Pulmonary complications

Although pulmonary manifestations are detected in about 5%–10% RA patients, autopsy studies showed that pleural involvement affects about 50% of patients and is thus a significant contributor to morbidity and mortality (Bharadwaj and Haroon, 2005, Sahatciu-Meka et al., 2010). Pulmonary manifestations associated with RA include small airway disease, rheumatoid nodules, pleural effusion, and pulmonary vasculitides. The most common pulmonary manifestation is interstitial lung disease (ILD), which occurs in 25% of RA patients (McDonagh et al., 1994, Dawson et al., 2001). ILD is rarely symptomatic in the early stages of RA; only 10% of RA patients showed clinical symptoms of ILD when they were evaluated by high-resolution computed tomography. Chronic obstructive pulmonary disease is also reported more frequently in RA patients

(Nannini et al., 2013). Treatment pulmonary disease in RA patients is based mainly on systemic steroids and cyclophosphamide. Moreover, it has been reported that anti-CD20 therapy has a beneficial effect on patients with pulmonary involvement related to primary vasculitis or other connective tissue disease (Prete et al., 2011).

1.3.5 Cardiac disease

RA patients are susceptible to cardiac conditions such as pericarditis, myocarditis, valvular disease, arrhythmias, and ischemic heart disease (Sarzi-Puttini et al., 2010). In addition, myocardial infarction (MI) is twice as prevalent in female RA patients than in women without RA (Maradit-Kremers et al., 2005). Pericarditis is described as the most common cardiac disease in RA patients. Symptomatic pericarditis is rare in RA patients (affecting 1%–4%), but echocardiography and/or autopsy has revealed histopathological abnormalities in about 50% of RA patients, and early detection of pericarditis in an asymptomatic stage is essential (Turiel et al., 2010). RA patients are also prone to valvular dysfunction due to endocarditis with formation of rheumatoid nodules in the aortic or mitral valves (Ristic et al., 2010). Non-steroidal anti-inflammatory drugs or steroids are a rapid solution for symptomatic pericardial disease (Kitas et al., 2001). Immunosuppressive treatment with cyclophosphamide may be necessary when pericardial effusion recurs. Emergency intervention is required for effusive pericarditis (Turesson and Matteson, 2004).

1.3.6 Renal manifestations

Renal diseases are uncommon in RA patients. Mesangial glomerulonephritis is described as the most common renal disease, occurring in about 60% of cases of renal involvement in RA patients (Korpela et al., 1997). Secondary amyloidosis has been detected in about 25% of patients with severe proteinuria and nephrotic syndrome, but interstitial nephritis is very rare in RA patients (Korpela et al., 1997). Renal abnormalities are frequently described as iatrogenic.

1.3.7 Ophthalmic manifestations

Ocular manifestations include secondary Sjögren's syndrome, episcleritis, scleritis, keratitis, and retinopathy. Keratoconjunctivitis sicca, which is described as the most common ophthalmic manifestation of rheumatologic disease, is frequently observed with secondary Sjögren's syndrome (xerostomia) and affects about 10% of RA patients (Cronstein, 2007). Episcleritis (i.e., inflammation of the layer superficial to the sclera) may lead to a severe form of scleritis known as necrotizing scleritis (scleromalacia perforans). Scleromalacia perforans is reported in <1% of patients and can lead to corneal melting and loss of vision (Wu et al., 2005). These complications can be managed with anti-inflammatory drugs or the disease-modifying antirheumatic drugs (DMARDs) anti-TNF-α or anti-CD20 (rituximab) (Atchia et al., 2006, Iaccheri et al., 2010).

1.3.8 Haematologic abnormalities

Haematologic manifestations include anaemia, which is considered the most common symptom of RA, along with thrombocytopenia, thrombocytosis, eosinophilia, and haematological malignancies (Bowman, 2002, Agrawal et al., 2006). Felty's syndrome is a rare, severe condition reported in <1% of patients (Balint and Balint, 2004). This syndrome is characterised by chronic polyarthritis, neutropenia, and splenomegaly and usually develops in the late stages of RA. In these patients, susceptibility to bacterial infection is high because of the development of neutropenia, which can be managed by DMARDs, methotrexate, and rituximab (Newman and Akhtari, 2011).

1.4 Treatment of rheumatoid arthritis

The pharmacological mainstays of treatment of RA and its complications include DMARDs, non-steroidal anti-inflammatory drugs (NSAIDs), and glucocorticoids. Moreover, when used in combination with pharmacological treatments, physical and occupational therapy may help patients cope with RA complications. In the mid-1990s, research revealed that biological treatments such as antibodies targeting TNF, IL-6, and IL-1 exhibited greater efficacy than previously used pharmacological compounds. However, the positive impact of these biological inhibitors occurred in only about 50% of the RA patients studied (Bartok and Firestein, 2010).

1.4.1 Disease-modifying antirheumatic drugs (DMARDs)

DMARDs are described as the mainstay of treatment for RA. All RA patients should receive one or more DMARDs once RA is diagnosed. It has been found that using of DMARDs within the first 3 months of RA has more beneficial effects in controlling disease activity and improves the long-term outcome (Demoruelle and Deane, 2012). Clinical response to DMARDs requires approximately 3 to 6 months for the full effect of treatment. DMARDs can be divided into non-biologic and biologic drugs.

1.4.1.1 Non-biologic DMARDs

1.4.1.1.1 Methotrexate

Methotrexate is considered to be the first-line therapy (drug of choice) for RA patients. Methotrexate is a folic acid metabolism inhibitor that appears to exert its action by binding to dihydrofolate reductase (Lopez-Olivo et al., 2014). Supplementation with folic acid can decrease common side effects of methotrexate such as stomatitis, nausea, and diarrhoea. The main concern with using methotrexate is the potential hepatotoxicity,

which is increased by alcohol consumption and pre-existing liver disease, diabetes, and obesity (Brasington). Liver damage is very unlikely in patients who do not have liver disease and consume minimal amounts of alcohol. Regular liver function tests and complete blood counts should be performed after 1 month of therapy until the optimal dose is established.

1.4.1.1.2 Sulfasalazine

In the 1940s sulfasalazine was used as a treatment for rheumatic polyarthritis and established as a DMARD in the past two decades (Rains et al., 1995). Side effects of sulfasalazine include changes in blood counts, nausea or vomiting, dizziness, rash, and myelosuppression (Plosker and Croom, 2005). Bacterial azoreductases in the large intestine are thought to act on sulfasalazine and split it into sulphapyridine and mesalazine; however, the exact mode of sulfasalazine action remains uncertain (Rains et al., 1995). This drug should not be prescribed for patients with true sulpha allergy or glucose- 6-phosphate dehydrogenase deficiency.

1.4.1.1.3 Leflunomide

Leflunomide is a pyrimidine synthesis inhibitor that can be used as an add-on agent to methotrexate. This agent can improve all clinical outcomes of RA; however, toxicity and long-term efficacy need to be evaluated (Osiri et al., 2003).

1.4.1.1.4 Hydroxychloroquine

Hydroxychloroquine has shown the ability to slow the progression of RA compared with placebo in double-blind studies (Pavelka et al., 1989). The risk of retinal damage is increased when the agent is used long-term at a high dose (Brasington), so it is important

for RA patients receiving hydroxychloroquine to be monitored by an ophthalmologist every 6–12 months. Hydroxychloroquine can be used alone or as an add-on to methotrexate.

1.4.1.2 **Biologic DMARDs**

1.4.1.2.1 TNF inhibitors (anti-TNF)

All biologic DMARDs are considered as second-line therapy for RA treatment. Among biologic DMARDs, the drugs of choice are TNF inhibitors (anti-TNF agents), which include etanercept and infliximab, then adalimumab and, most recently, certolizumab and golimumab. These agents improve RA treatment and can be used as monotherapy or in combination with non-biologic DMARDs (Kahlenberg and Fox, 2011). The clinical response to biologic DMARDs is more rapid than response to non-biologic drugs and requires approximately 3–4 weeks (Kahlenberg and Fox, 2011). TNF inhibitors block an overexpressed signalling protein in RA; however, they also inhibit an important signalling protein required for the normal immune response, thereby increasing the risk of opportunistic infections. For that reason it is essential for RA patients to receive pneumococcal and influenza vaccines prior to treatment with TNF inhibitors (Saag et al., 2008). One study reported hepatitis B re-activation 1 month after the third dose of an anti-TNF drug in patients with chronic hepatitis B infection (Carroll and Bond, 2008). An elevated risk of lymphoma in RA remains a concern; however, Askling et al. (Askling et al., 2009) concluded that anti-TNF inhibitors do not increase the already elevated risk of lymphoma in RA. However, other rare diseases have been reported with anti-TNF therapy including new-onset multiple sclerosis, optic neuritis, and transverse myelitis (Sicotte and Voskuhl, 2001, Simsek et al., 2007, Mohan et al., 2001).

1.4.1.2.2 Rituximab

Rituximab is a genetically modified chimeric IgG1 monoclonal antibody that targets CD20+ B cells and rapidly depletes circulating B lymphocytes (Reff et al., 1994). When used in conjunction with methotrexate and glucocorticoids, rituximab has shown significant clinical benefits for RA patients by inhibiting the progression of structural joint damage (Reff et al., 1994, Keystone et al., 2009). Rituximab is an alternative treatment for RA patients who show an inadequate response to anti-TNF therapies (Keystone et al., 2009).

1.4.1.2.3 Abatacept (Orencia)

Abatacept is a selective costimulation modulator that inhibits T-cell activation. The mechanism of action involves binding CD80 or CD86 on the antigen-presenting cell to inhibit the interaction with CD28 on the T cell, thus preventing T cell activation and the B cell immunological response (Herrero-Beaumont et al., 2012).

1.5 Rheumatoid arthritis pathogenesis within the inflamed joint

RA is characterised by inflammation and destruction of the synovial cartilage and bone, which is mediated by uncontrolled and tumour-like growth of synovial fibroblasts, as shown in Figure 1.2. This process is referred to as pannus tissue expansion (Muller-Ladner and Gay, 2002). This expansion of cells results in a depletion of the oxygen supplied to the joint, rendering the synovial microenvironments hypoxic (Stevens et al., 1991).

1.5.1 Cartilage damage in RA and OA

Cartilage damage is a key feature of osteoarthritis (OA) and RA. In OA, the cartilage damage is caused by mechanical, cellular, and biochemical processes (Hinton et al., 2002). The exact cause of OA is unknown; however, risk factors that may include age, sex, joint injuries, obesity, and bone deformities (Heidari, 2011). The loss of CXC chemokines containing the ELR motif (ELR-CXC chemokines) during cartilage breakdown in OA appears to be involved in the loss of phenotypic stability of articular chondrocytes (Sherwood et al., 2015). Chondrocyte hypertrophy-like changes have been described as contributing to OA progression (van der Kraan and van den Berg, 2012). The formation of osteophytes (new bone at joint margins) and subchondral plate thickening are two features associated with OA but not seen in RA (Pap and Korb-Pap, 2015). Inflammation of the synovium, which is associated with OA, is characterised by cellular infiltrate composed largely of lymphocytes and monocytes (Haraoui et al., 1991). However, the formation of tumour-like pannus is considered to be the key difference between RA and OA synovitis (Pap and Korb-Pap, 2015).

1.5.2 Joint damage and disability in RA

Early diagnosis and treatment of RA (within 12 weeks of symptom onset) improves long-term outcomes and reduces disability, joint damage, and complications. Three main signs of inflammatory arthritis that may progress to RA include early morning stiffness (>30 minutes), swelling (clinical synovitis) of multiple joints, and tenderness of metacarpophalangeal (MCP) or metatarsophalangeal (MTP) joints (upon lateral squeezing). Early specialist referral is necessary for patients who are suffering from these symptoms (Wiesinger et al., 2013).

Any joint can be affected in RA. The MCP, proximal interphalangeal (PIP), and MTP joints of the hands and feet are most commonly affected in RA, followed by large joints such as elbows, shoulders and knees (Jeffery). Juxta-articular erosion in early RA is considered to be the main sign of progressive damage (Scott et al., 2000). X-ray is the most commonly used method to clinically evaluate structural damage in RA joints (Ory, 2003). A strong relationship exists between later disability and anatomical joint damage, which increases over time in RA patients (Ory, 2003, Scott et al., 2000). Joint damage in RA can be assessed by semi-quantitative scoring methods, such as those developed by Sharp and Larsen (Sharp et al., 1971, Larsen et al., 1979). In Sharp's scoring system, 29 areas in each hand and wrist are evaluated for erosion (scores range from 0 to 5 for each joint, and the total score ranges from 0 to 290), whereas 27 joints are evaluated for joint space narrowing (scores range from 0 to 4, and the total score ranges from 0 to 219). On the other hand, Larsen's scoring system evaluates joint abnormalities of the hand, wrist, and foot as follows: stage 0 = normal, stage 1 = slight abnormalities, stage 2 = definite early abnormalities, stage 3 = medium destructive abnormalities, stage 4 = severe definite abnormalities, and stage 5 = mutilating abnormalities. Disability in RA is commonly assessed by using the Health Assessment Questionnaire (HAQ) (Scott et al., 2000). The HAQ scores functional ability from 0 to 3 as follows: 1–2 = moderate to severe disability, and 2–3 = severe to very severe disability (Bruce and Fries, 2003). In early RA there is no correlation between joint damage on X-rays and disability; however, once radiological scores exceed 33% of maximum joint damage, the relationship becomes more linear (Ory, 2003). In previous studies, 103–142 RA patients were evaluated for joint damage by using Larsen's score in the first 2 years of RA and were followed up for

approximately 20 years. The mean Larsen's score increased with the duration of the disease as follows: in the first 2 years of RA the score was 25, from 5–8 years of RA the score increased to 30–70, and after 20 years the score exceeded 75 (Egsmose et al., 1995, Mottonen et al., 1996, Paimela et al., 1997). A correlation between HAQ score and disease duration was also observed in various studies. Analysis of 725 RA patients showed a significant relationship between HAQ score and RA duration (Scott et al., 2000). Another study of 400 RA cases reported a HAQ score of ≤1.0 for RA duration of 7 years, and ≥2.0 for RA duration of 20 years (Wolfe et al., 1988). Furthermore, it has been found that the correlation between Larsen's score and HAQ disability score was significant by 5 years of RA duration (Scott et al., 2000). The HAQ disability score can be influenced by other factors including demographic factors (age, sex), genetic factors including HLA-DR4, low socioeconomic and educational status, RF positivity, markers of active synovitis including erythrocyte sedimentation rate and C-reactive protein, and treatments such as DMARDs. Mortality can occur within first few years of the RA diagnosis, and the mortality rate may increase with disease duration. Other extra-articular manifestations of RA, such as cardiovascular disease, infections, and malignancy, are the main causes of death in RA patients (Dougados et al., 2014). RF positivity and the presence of nodules are associated with the tendency to develop severe cardiovascular disease, infections, osteoporotic fractures, lung disease, and functional disability (Naz et al., 2008, Dougados et al., 2014).

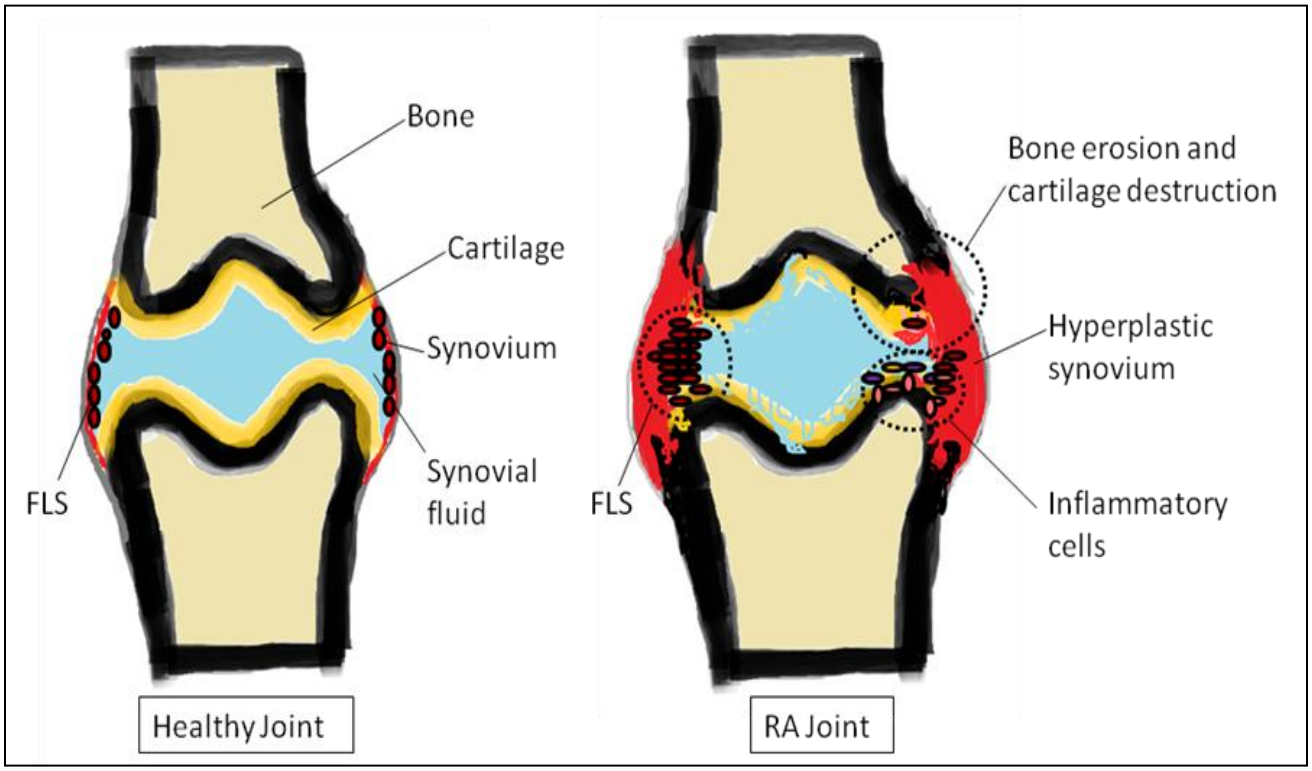

Figure 1.2 Inflamed joint in RA as compared to healthy joint.

This figure illustrates the involvement of hyperplastic synovium, FLS, and other inflammatory cells, including macrophages, dendritic cells, B cells, T cells, and plasma cells, in bone and cartilage destruction within a RA joint. FLS, fibroblast-like synoviocytes; RA, rheumatoid arthritis.

1.5.3 Bone and cartilage destruction at the cellular level

Inflammatory cytokines, such as IL-1, IL-6, IL-8, and TNF, and various chemokines play a vital role in RA by attracting other inflammatory cells to the inflamed joint. These cytokines also enhance the up-regulation of adhesion molecules. Moreover, cytokines such as vascular endothelial growth factor (VEGF) and fibroblast growth factor (FGF) enhance the growth of new blood vessels, or angiogenesis. Thus, an influx of blood and inflammatory cells cause further inflammation of the synovial membrane. Hyperplasia of the intimal lining results from a marked rise in FLS and macrophage-like synoviocytes.

Increased concentrations of inflammatory cytokines result in the up-regulation of multiple enzymes that degrade components of the extracellular matrix in RA (Firestein, 2003). Extracellular enzymes with reported activities in RA include serine proteases, aggrecanases, and MMPs (Firestein, 2003). Bone collagen is primarily cleaved by MMPs (Cawston and Wilson, 2006). However, matrix-remodelling enzymes can regulate one another and appear to collectively affect bone and cartilage destruction. For example, MMPs can become further activated by serine proteases (Cawston and Wilson, 2006). Thus, increased serine protease activity in a disease state, such as RA, leads to feedback up-regulation of MMPs, resulting in further breakdown of matrix components. Aggrecanases are members of the A disintegrin and metalloprotease with thrombospondin motifs (ADAMTS) family. Cartilage components, such as proteoglycan aggrecan and cartilage oligomeric matrix protein (COMP), are degraded by multiple members of the ADAMTS and MMP families (Liu et al., 2006). MMPs and ADAMTS cleave aggrecan at distinct sites. Thus, different aggrecan fragments will be released in response to MMP activity versus those released by ADAMTS activity. Elevated levels of ADAMTS and MMPs are found in synovial and cartilage samples obtained from RA

patients (Vankemmelbeke et al., 2001, Liu et al., 2006). In addition, specific aggrecan fragments corresponding to MMP or ADAMTS activity are found in cartilage samples or synovial fluid from RA patients (Vankemmelbeke et al., 2001, Nagase and Kashiwagi, 2003). Membrane-type MMPs are elevated in the synovial lining, synovial fibroblasts, macrophages, and multinucleated osteoclast-like cells of RA patients (Pap et al., 2000). Thus, multiple cell types and the potential interplay between these cell types may affect the expression and/or secretion of enzymes that promote bone and cartilage destruction in RA patients. Interestingly, serum concentrations of COMP are increased in patients with early RA who have evidence of bone destruction by magnetic resonance imaging, in contrast to patients without detectable bone erosion (Fujikawa et al., 2009). Furthermore, elevated COMP levels in patients with early RA and bone erosion are also associated with increased serum MMP-3 (Fujikawa et al., 2009). Conversely, various studies have debated which major aggrecanase or ADAMTS are involved in cartilage destruction. Among the ADAMTS family members, three have been investigated, including ADAMTS4, ADAMTS5, and ADAMTS17. Researchers have reported that ADAMTS4 and 5 are expressed in joint tissue and may play pivotal roles in cartilage destruction. However, the exact roles and contributions of these two enzymes in cartilage destruction remain elusive. In murine models of arthritis, ADAMTS4 deletion did not provide any protective effect on cartilage erosion in ADAMTS4 knockout mice, whereas the protection of cartilage was significant in ADAMTS5 knockout mice (Glasson et al., 2004, Glasson et al., 2005). However, Song et al. (Song et al., 2007) showed that both ADAMTS4 and 5 are effective in aggrecan degradation in human articular cartilage explants. Then again, ADAMTS17 has been associated with a significant increase in

synovial cells after the induction of TNF and hypoxia (Charbonneau et al., 2007). That study reported that the effect of TNF on ADAMTS17 induction was mediate through nuclear factor-kappa B (NF-κB), and the hypoxia effect was mediated via both hypoxia-inducible factor (HIF)-1 and NF-κB pathways.

Similar to MMPs, the cysteine proteases cathepsins B and L have shown a broad proteolytic activity on proteoglycans and type II, IX, and XI collagen under acidic conditions (Maciewicz et al., 1990). In the Maciewicz et al. study, cathepsins B and L degraded rat chondrosarcoma collagens at 20°C to 37°C and pH values of 3.5 to 7.0. Moreover, another study reported that TNF enhances the expression of cathepsin B in FLS (Lemaire et al., 1997). In addition, FLS invasiveness activity and cartilage destruction were reduced after cathepsin L cleavage by ribozymes in a severe combined immunodeficient mouse model (Pierer et al., 2003). Among cathepsins, cathepsin K plays a pivotal role in osteoclast-mediated degradation of bone matrix through its ability to degrade type I collagen (Garnero et al., 1998). Cathepsin K expression was reported higher in RA than in OA synovium (Hou et al., 2002). Previous studies demonstrated that IL-1B enhances the production of polysulphated glycosaminoglycans in FLS, which in turn boosts the expression and activity of cathepsin K (Akimoto et al., 2000, Li et al., 2000). Cathepsin K knockout mice showed no signs of bone degradation as compared to wild-type mice (Stroup et al., 2001). In addition, the same study identified a selective cathepsin K inhibitor, SB-357114, that impaired human osteoclast activity in bovine cortical bone slices. Taken together, this evidence suggests the involvement of cathepsins, specifically cathepsin K, in bone degradation of the RA inflamed joint. These

findings support the pathological relevance of proteases in the erosion of articular cartilage and bone in RA.

During the process of physical remodelling, the amount of bone that forms is usually equivalent to the amount that degenerated during bone resorption. Remodelling enables the skeleton to adapt to biomechanical changes. Bone formation and resorption are disturbed by inflammation. This imbalance is usually responsible for "articular bone losses" (Goldring, 2003). Numerous factors can act directly on osteoclasts to boost their resorbing activity, including TNF and receptor activator of nuclear factor kappa-B ligand (RANKL). RANKL has sparked interest because of its potent ability to regulate osteoclastogenesis. RANKL has been identified by many different laboratories, which have designated it as an osteoclast-distinguishing factor and a TNF ligand superfamily member, TNF-related activation-induced cytokine (Hofbauer et al., 2000). RANKL exerts its actions by binding to its associated receptor, receptor activator of nuclear factor kappa-B (RANK). RANKL activity is regulated by a naturally occurring inhibitor called osteoprotegerin (OPG). OPG is a soluble protein that works as a decoy receptor by binding to RANKL, preventing interaction between RANKL and RANK, thereby disrupting osteoclastogenesis (Simonet et al., 1997).

Recently, various studies have provided additional evidence that osteoclasts are the main cell type mediating bone loss in inflammatory arthritis. These studies examined animal models in which osteoclast differentiation or activity was inhibited by the genetic knockout of factors that are essential for osteoclast creation or by RANKL inhibition (Pettit et al., 2001). The results showed minimal evidence of focal bone erosion. IL-1 and TNF have dual effects on osteoclastogenesis. These factors up-regulate RANKL in the

bone-lining and marrow stromal cells. Moreover, TNF and RANKL act synergistically to enhance osteoclast differentiation, whereas IL-1 primarily activates osteoclasts and delays osteoclast apoptosis (Romas et al., 2002). IL-1 and TNF contribute to bone loss in RA by inducing programmed cell death of osteoblasts and damaging bone development (Tsuboi et al., 1999). Unlike bone, cartilage has limited turnover. Hence, it cannot be continuously repaired. Synovial products that promote cartilage loss include TNF-α and IL-1. IL-1 causes chondrocytes to produce more MMPs and nitric oxide, which products that promote cartilage loss include TNF-α and IL-1. IL-1 causes chondrocytes to produce more MMPs and nitric oxide, which inhibits collagen and proteoglycan synthesis, enhances MMPs activity and induces chondrocytes apoptosis (Abramson et al., 2001). Moreover, IL-1 increases synthesis of peptidoglycans and collagens, which help degrade cartilage matrix (Goldring, 2003). Other researchers have reported that TNF has the same mechanism of action as IL-1. Therefore, TNF also contributes to cartilage destruction. In addition, cytokines also contribute to cartilage degeneration by decreasing proteoglycans and collagens that are essential to cartilage formation (Goldring, 2003). Cytokines and other mediators released from the synovium can also indirectly cause cartilage breakdown.

The specific mechanisms by which TNF promotes cartilage and bone destruction include increased production of matrix-digesting proteases. TNF induces expression of MMPs (Burrage et al., 2006, Moelants et al., 2013) and ADAMTS (Moelants et al., 2013) in RA. Interestingly, these proteases cleave pro-TNF from the membrane and release active TNF, which promotes downstream signalling and further production of MMPs and ADAMTS (Moelants et al., 2013). MMPs and ADAMTS collectively degrade all

components of the extracellular matrix. Thus, production of MMPs and ADAMTS downstream of TNF promotes erosion of cartilage and bone. TNF antibody blockade with infliximab or treatment with etanercept, a recombinant TNF receptor-Fc fusion protein, suppresses the expression of MMPs in RA (Huang et al., 2013, Catrina et al., 2002). The major downstream signalling effectors activated by TNF are NF-κB, p38 mitogen-activated protein kinase (MAPK), c-Jun N-terminal kinase (JNK), and extracellular-regulated kinase (ERK) (Baud and Karin, 2001). Transgenic mice that over-express human TNF develop synovial inflammation and arthritis (Gortz et al., 2005). Interestingly, these mice demonstrate increased phosphorylation of p38 MAPK and ERK but not JNK in synovial inflammatory tissues (Gortz et al., 2005). TNF antibody blockade with infliximab suppresses phosphorylation of p38 MAPK and ERK in synovial tissues, confirming that these are major signalling pathways downstream of TNF in RA (Gortz et al., 2005). ERK phosphorylates c-Jun, a member of the activating protein-1 (AP-1) family, which pairs with c-Fos to drive the expression of MMPs (Vincenti and Brinckerhoff, 2002). Further, p38 indirectly activates the expression of AP-1 genes, leading to MMP up-regulation (Vincenti and Brinckerhoff, 2002). In addition to contributions by MAPK signalling, TNF-mediated bone and cartilage degradation also appear to be partially dependent upon IL-1 expression. Human TNF transgenic mice that are IL-1-null have significantly reduced bone erosion and osteoclast formation and undetectable cartilage damage in association with lower expression levels of ADAMTS-5 and MMP-3 (Zwerina et al., 2007). Thus, TNF contributes to loss of bone and cartilage in RA by inducing the expression of matrix-degrading proteases. These effects may be

further potentiated by increased expression of other cytokines, such as IL-1. This is illustrated in Figure 1.3.

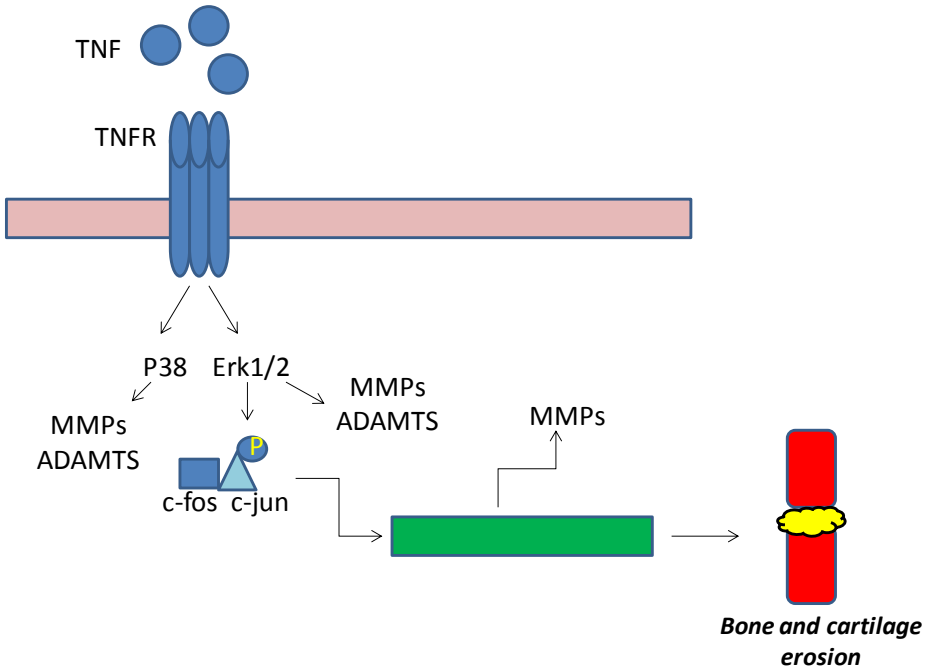

Figure 1.3 Mechanism of TNF-mediated bone and cartilage erosion.

TNF signalling in RA promotes increased production of matrix-digesting proteases. TNF binds to the TNF receptor and induces major signalling pathways, including p38 MAPK and Erk1/2. These signalling pathways induce the expression of MMPs and ADAMTS in part through the phosphorylation of transcription factors such as c-Jun. MMPs and ADAMTS digest major extracellular matrix proteins, resulting in erosion of cartilage and bone. TNF, tumour necrosis factor; TNFR, TNF receptor; p38, p38 mitogen-activated protein kinase; Erk, extracellular-regulated kinase; MMP, matrix metalloproteinase; ADAMTS, a disintegrin and metalloprotease with thrombospondin motifs.

1.5.4 Hypoxia

Active synovium metabolically consumes more oxygen. Chronically inflamed joints with large effusions have increased pressure and, consequently, a reduced supply of blood (Ahn et al., 2008). The rheumatoid synovial microenvironment is normally hypoxic (Stevens et al., 1991). In a hypoxic environment, the vascular system starts to adapt its structure to facilitate blood flow to the tissues and cells of the inflamed joints. Macrophages and proliferating synovial cells produce cytokines and angiogenic factors, such as VEGF and FGF, which activate angiogenesis. A master regulator of the adaptation response to the change in oxygen supply is HIF. Activation of HIF signalling leads to extensive changes in gene expression, which allows cells and tissues to adapt to reduced oxygen levels. The changes that happen in response to HIF activation include enhanced glucose uptake, increased expression of glycolytic enzymes, and increased expression of angiogenic factors. However, the formation of new blood vessels is insufficient to cope with cellular proliferation. Thus, inadequate oxygen delivery creates a hypoxic environment (Stevens et al., 1991).

1.5.5 Acid and acid build-up

Cells require an adequate supply of oxygenated blood to prevent possible disturbances in the cellular membrane and to generate energy. Synoviocytes start to adapt their metabolic pathways in hypoxic conditions by shifting the metabolic pathway from the aerobic pyruvate to the anaerobic glycolytic pathway. Thus, lactic acid accumulates inside the inflamed joint (Lund-Olesen, 1970, Treuhaft et al., 1971).

In 1970, oxygen tension (pO_2) was measured in synovial fluid samples from 58 RA patients. The mean pO_2 was 27 mmHg, which was significantly lower than the mean pO_2 of 43 mmHg reported for patients with OA. Similar to the Treuhaft and McCarty study, another study reported that the pO_2 was less than 15–20 mmHg in 27% of synovial samples from 55 RA patients (Stevens et al., 1991). Moreover, various studies identified physiological alterations in synovial fluid from RA patients, including elevated pCO_2, as high as 150 mmHg, high lactic acid (10 mmol/L), and low pH (as low as 6.6) (McCarty, 1974, Falchuk et al., 1970). In addition, an acid-base analyser measured the H^+ concentration in synovial fluids from 130 patients with arthritis. Synovial fluid from 60 RA patients showed a mean H^+ concentration of 64.4 nmol/L, with pH ranging from 7.41 to 6.85. In contrast, the mean H^+ concentration in OA synovial fluid was approximately 44 nmol/L, and the pH ranged from 7.41 to 7.06 (Farr et al., 1985). The impact of extracellular acidification on bone and cartilage cells has been studied. Arnett and Dempster showed that acid stimulation of rat osteoclasts led to bone erosion (Arnett and Dempster, 1986). Moreover, recent studies suggest that acid-sensing proteins play critical roles in osteoclast (Jahr et al., 2005) and chondrocyte (Jahr et al., 2005, Yuan et al., 2010c) activity.

1.6 **Acid-sensing proteins**

Recently, three different types of acid-sensing proteins have been found in various tissues and synoviocytes. First, acid-sensing ion channels (ASICs) are highly expressed in central neurons and peripheral sensory neurons (Waldmann et al., 1997). ASICs are members of the epithelial sodium channel/degenerin family. Members of this family have two characteristic transmembrane areas: (i) a large cysteine-rich extracellular loop and (ii) short extracellular N- and C-termini (Krishtal, 2003, Waldmann, 2001). Six subunits have been cloned. ASIC1a, 2a, and 2b are found in central neurons (Alvarez de la Rosa et al., 2002). ASIC1a, 1b, 2a, and 3 are expressed in sensory neurons. Kolker et al. (2010) conducted an in-depth study of ASIC3 expression in FLS. ASIC3 plays a vital role in the regulation of hyaluronan release, as observed in FLS of ASIC3-/- mice.

Second, G-protein-coupled receptors (GPCRs or GPRs) play vital roles in intracellular calcium mobilization and generation of inositol phosphates in hypoxic conditions. A study by Christensen et al. (2005) identified GPCR activity in human synoviocytes. However, the molecular identity of the protein is unknown.

Third, transient receptor potential cation channel subfamily V member 1 (TRPV1), also known as the vanilloid receptor 1, is expressed in synoviocytes of patients with OA and RA (Engler et al., 2007). These studies suggest that functional acid-sensing proteins are expressed in synoviocytes. However, the roles of specific acid-sensing proteins in modulating functional responses of synovial cells to acidic conditions remain unknown.

1.6.1 Acid-sensing ion channels (ASICs)

Studies showed that external protons are responsible for the activation of sodium ion (Na^+) channels, which are ASICs. These channels were duplicated according to their resemblance to a larger subfamily of channels called degenerin/epithelial Na^+ channels (ENaCs).

1.6.1.1 **Structure**

ASICs open in response to reduced extracellular pH due to acidification (Krishtal, 2003, Waldmann, 2001). The degenerin ion channel superfamily includes ASICs that are ENaCs (Waldmann and Lazdunski, 1998, Kellenberger and Schild, 2002). These channels are specific for sodium ions and are inhibited by diuretic drugs, such as amiloride. They are membrane-spanning proteins that contain two transmembrane regions, each of which has a large extracellular loop, an intracellular amino group, and a terminal carboxyl group (Figure 1.4). Multiple ASIC subunits must assemble to form a functional ion channel (Waldmann, 2001).

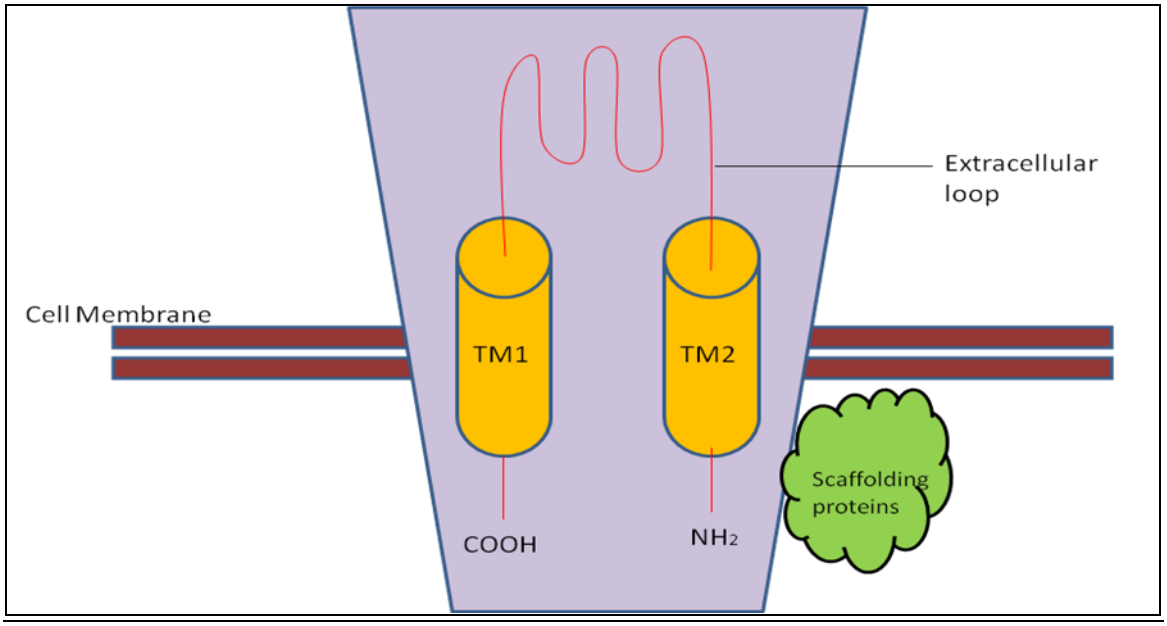

Figure 1.4 Structure of an ASIC.

The ASIC monomeric structure is composed of two transmembrane regions connected by an extracellular loop. An ASIC has an intracellular amino and terminal carboxyl group. Na^+ enters the channel, and small concentrations of Ca^{2+} usually accompany the influx of sodium. Diuretics, such as amiloride, inhibit ASIC activity. PDZ-containing scaffolding proteins, such as PSD-95 and PIST, bind to ASICs. Scaffolding proteins form unique docking sites for additional signalling molecules, propagating downstream signalling diversity. For example, PIST interacts with Rho GTPase family members, whereas other signalling pathways may be activated by PSD-95 or another scaffolding protein. TM, transmembrane region; COOH, carboxyl group; NH_2, amine group; ASIC, acid-sensing ion channel; Na^+, sodium ion; Ca^{2+}, calcium ion; PDZ, post-synaptic density, Drosophila discs large, and zonula occludens-1; PSD-95, post-synaptic density protein 95; PIST, PDZ domain protein interacting specifically with TC10; GTPase, hydrolase that acts on guanosine triphosphate.

ASICs exhibit all of the features and traits of ENaCs despite showing only approximately 20%–25% similarity with the superfamily. Functional ASICs are either heterotetramers or homotetramers that have diverse functional properties. The functional ENaC is mainly composed of four subunits. Both ENaCs and ASICs are sensitive to low concentrations of amiloride (Krishtal, 2003).

The six recognized proteins of the ASIC family are as follows. ASIC1a and ASIC1b are variants encoded by *ASIC1*. ASIC2b and ASIC2a are derived from *ASIC2*. The other two members are ASIC3 and ASIC4. Both ASIC4 and ASIC2b are inactive if expressed alone. ASIC4 cannot function as a proton-gated channel, whereas ASIC2b can alter the structures of ASIC3 and ASIC2 if they are co-expressed (Lingueglia et al., 2006). Both extracellular and intracellular aspects can effectively adjust the functions of an ASIC. For example, the neuropeptides FF (Phe-Leu-Phe-Gln-Pro-Arg-Phe amide) and FMRFamide (Phe-Met-Arg-Phe amide) transform the ASIC current by limiting or enhancing channel desensitisation following pH activation (Askwith et al., 2000). Moreover, protein kinase C (PKC) specifically targets ASIC1 and ASIC2 through its PDZ (post-synaptic density, Drosophila discs large, and zonula occludens-1) domain, whereas protein kinase A (PKA) effectively modulates ASIC1 (Bronstein-Sitton, 2004). Additionally, ASIC3 interacts with channel-interacting PDZ protein primarily to adjust cell-surface expression of the channels.

1.6.1.2 **Mechanisms**

ASICs have various pathological and physiological roles due to their specific localisation and functional traits. Expression of ASICs in the central nervous system and peripheral

tissues plays a crucial role in various diseases, such as multiple sclerosis, anxiety, memory lapses, musculoskeletal pain, and learning disorders (Kolker et al., 2010).

Studies in ASIC1-/- mice have implicated this particular channel in memory and learning (Bronstein-Sitton, 2004). Destruction of long-term potentiation (LTP) was observed in hippocampal neurons from these mice. Damaged LTP may cause memory and learning problems. In these knockout mice, ASIC flow shortages in the hippocampal neurons significantly reduced the movement of N-methyl-D-aspartate receptors. In addition, ASIC2a, which can create heterodimers with ASIC1, failed to form functional channels in ASIC1-/- mice (Bronstein-Sitton, 2004). In contrast, ASIC3-/- and ASIC2-/- mice had fewer defects. Nonetheless, both ASIC3-/- and ASIC2-/- mice had deficiencies in mechanosensation and light touch.

Two major studies established the immunoreactivity of ASIC3 in sensory neurons. The first one showed that ASIC3 and ASIC2 are co-expressed in the dorsal root ganglion (DRG) and that these proteins are more commonly found in large neurons (Alvarez de la Rosa et al., 2002). However, co-expression of ASIC3 with a calcitonin gene-related peptide (CGRP) is found in large and small trigeminal ganglion neurons (Ichikawa and Sugimoto, 2002).

In the central and peripheral nervous systems, ASIC1 and ASIC3, respectively, play key roles together with extracellular modulators and interacting proteins. ASIC3 activity is up-regulated by activators of the PKC pathway, which are released during peripheral inflammation. Inflammation leads to an elevation of ASIC3 mRNA transcription levels in the DRG and spinal cord. Protons released at either the pre- or post-synaptic membranes could activate ASIC3 (Molliver et al., 2005).

Interestingly, ASIC3 has been identified as the most sensitive ion channel. It is more widely distributed in human beings than in mice, which indicates its extensive role in human beings (Kolker et al., 2010). During episodes of cardiac ischemic pain, ASIC3 senses changes in pH and mediates the sensation of pain. This is caused by large fluxes in current at the DRG of sensory neurons that supply nervous impulses to the heart (Benson et al., 1999, Sutherland et al., 2001), resulting in angina. In addition, ASIC3 detects and responds to small changes in the extracellular pH of muscles due to metabolic stress (pH 7.4 to 7.0).

The axon reflex caused by the peripheral release of CGRP occurs due to the activation of C fibres with subsequent vasodilation and extravasation (Willis, 1999, Sann and Pierau, 1998). ASIC3, TRPV1, and CGRP are co-expressed on the afferent vessels of the arterial muscle. This suggests all three function as sensors and effectors of localised blood influx in response to elevated lactic acid levels and rising temperatures in muscle. This co-expression assists cellular detection of a broad range of acid levels.

Activation of ASICs by acidosis increases the influx of Na^{+} into cells (Zha, 2013). Small concentrations of calcium ions (Ca^{2+}) accompany Na^{2+} through ASICs, which results in the activation of voltage-gated calcium channels and increased intracellular Ca^{2+} concentrations (Figure 1.5). Thus, although the roles of ASICs in Ca^{2+} influx are indirect, these ion channels contribute to the overall increase in Ca^{2+} that occurs in response to acidosis. ASIC knockout mouse models accumulate reduced amounts of Ca^{2+} in synoviocytes under acidic conditions (Kolker et al., 2010). Further, ASIC inhibition reduces cellular Ca^{2+} levels and articular cartilage breakdown in rats (Yuan et al., 2010b).

These results are consistent with the notion that ASICs are important regulators of Ca^{2+} accumulation and cartilage destruction in RA.

Signalling molecules that interact with ASICs include components of the cytoskeleton, such as α-actinin (Zha, 2013). Scaffolding proteins bind ASICs through PDZ motifs and include protein interacting with C-kinase 1 (PICK1), PDZ domain protein interacting specifically with TC10 (PIST), A-kinase anchoring protein 150 (AKAP150), and post-synaptic density protein 95 (PSD-95) (Zha, 2013). Interactions between ASICs and PICK1 depend upon PKA and PKC signalling and regulate trafficking of ASICs to the membrane (Zha, 2013). PIST interacts with ASICs and members of the Rho GTPase family (Neudauer et al., 2001). However, the specific functional consequences of ASIC interactions with PIST remain unknown. Disruption of AKAP150-ASIC binding reduces ASIC signalling, indicating that AKAPs may be involved in the activation or maintenance of ASIC function (Chu et al., 2011). Further, PSD-95 reduces cell-surface levels and signalling of ASICs (Zha, 2013). Thus, multiple binding partners and downstream signalling effectors modulate ASIC function and affect intracellular ion concentrations and cartilage destruction in response to altered cellular pH.

ASIC function may be further enhanced by GPCR signalling, which induces intracellular Ca^{2+} accumulation and activation of PKA (Christensen et al., 2005) as discussed below. PKA increases surface levels and signalling from ASICs. Thus, GPCRs lead to increased activation of ASIC function. Signalling from ovarian cancer GPCR 1 (OGR1 or GPR68), a membrane receptor for protons and lipids, is associated with osteoclast differentiation (Yang et al., 2006), which leads to bone resorption. Thus, GPCR signalling in the synovial environment may contribute to bone destruction in RA. TRPV1 also becomes

activated during acidic conditions. ASICs are usually activated in the presence of mild acidosis, whereas TRPV1 activity occurs during severe acidosis (Bohlen and Julius, 2012). TRPV1 is activated by GPCR signalling due to changes in phosphorylation or lipid status (Bohlen and Julius, 2012). Thus, cross-signalling from GPCRs appears to activate ASICs and TRPV1, two critical ion channel families, in response to acidic pH in the synovial environment in RA.

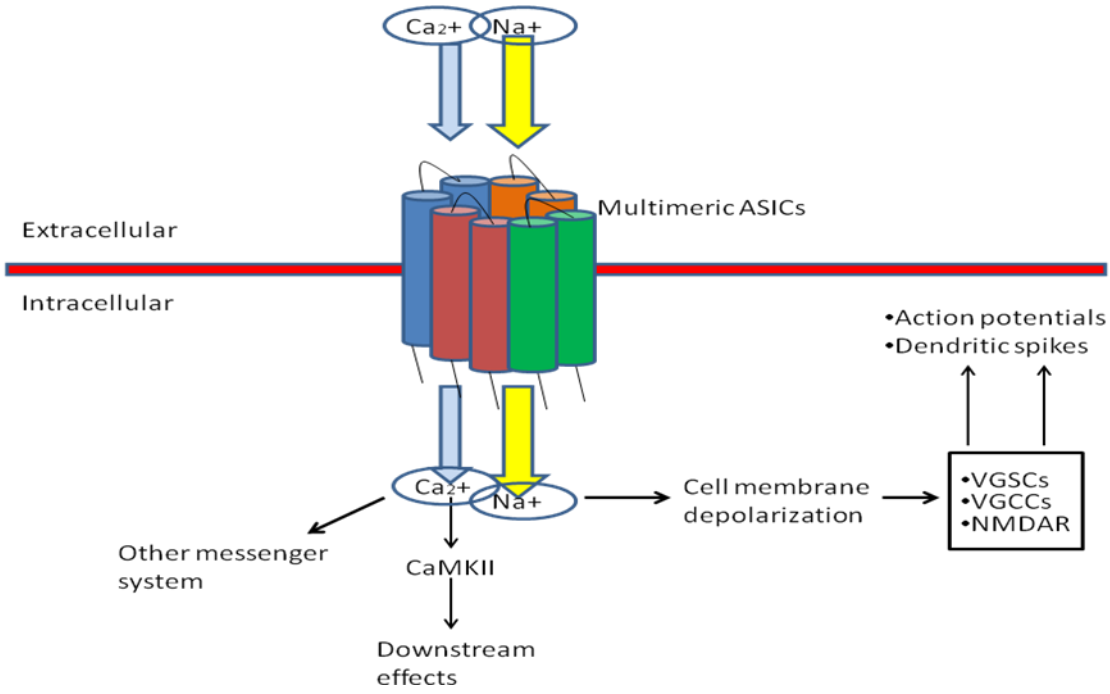

Figure 1.5 ASICs multimeric structure and function.

Upon ASICs activation, there is Na^+ and, to a lesser degree, Ca^{2+} influx into the cell, which depolarizes the cell membrane. The inward current activates other voltage-gated channels, such as VGCCs, VGSCs, and NMDARs; this will enhance the generation of dendritic spikes and action potentials. Moreover, Ca^{2+} influx activates CaMKII, which in turn influences other messenger pathways (Wemmie et al., 2013). Ca^{2+}, calcium ion; Na^+, sodium ion; CaMKII, Ca^{2+}/calmodulin-dependent protein kinase II; VGSC, voltage-gated sodium channel; VGCC, voltage-gated calcium channel; NMDAR, N-methyl-D-aspartate receptor.

1.6.2 ASIC3 in inflammatory disorders and rheumatoid arthritis

ASIC3 expression is increased in various inflammatory conditions. For example, a three-fold increase in ASIC3 expression was found in inflamed intestinal tissue from a patient with Crohn's disease (Yiangou et al., 2001). In addition, ASIC3 appears to be involved in the metabolic and inflammatory conditions associated with obesity and type 2 diabetes (Huang et al., 2008). ASIC3 knockout mice show reduced adiposity, increased insulin sensitivity, and improved performance in glucose tolerance tests compared with their wild-type counterparts (Huang et al., 2008). Furthermore, ASIC expression increases in sensory neurons in response to inflammation-associated pH reduction (Voilley et al., 2001). However, NSAIDs suppress increased ASIC expression and reduce currents from ASICs (Voilley et al., 2001). These data indicate that the expression and function of ASICs are inhibited by anti-inflammatory drugs. Thus, inflammation is a major trigger for ASIC activity. These findings are consistent with our hypothesis that acid-sensing proteins play critical roles in the development and maintenance of the inflammatory environment found in RA.

Acid build-up leads to pain and harms the joints. A correlation exists between the degree of pain and joint damage and the acidity of the synovial fluid present in arthritic joints (Revici et al., 1949, Geborek et al., 1989). A study by Kolker et al. (Kolker et al., 2010) showed that ASIC3 may be expressed in synoviocytes, type B FLS, and the epiphyseal plates of ASIC3+/+ mice. Immunostaining for ASIC3 was not detected in tissues from control ASIC3-/- mice. However, the role that ASIC3 plays in synoviocytes remains unclear (Waldburger et al., 2008).

Activated ASIC3 is more permeable to Ca^{2+} and facilitates an increase in intracellular Ca^{2+} mobilization. Increased intracellular Ca^{2+} activates several signalling pathways,

leading to increased production of hyaluronan by type B synoviocytes (Kolker et al., 2012). High levels of Ca^{2+} in the cell are also associated with Ca^{2+}/calmodulin-dependent protein kinase II activation, which may further aggravate inflammation. Increased intracellular Ca^{2+} in FLS activates intracellular signalling pathways that enhance the inflammatory response. In turn, increased inflammation and destruction of cartilage aggravates disease. Studies show that GPCR and TRPV1 are also activated in FLS, resulting in increased intracellular Ca^{2+}. Based on this, researchers have suggested that ASIC3 is not the only pH sensor in FLS (Hu et al., 2008, Christensen et al., 2005b).

The roles of ASIC3 in sensing acidity, as well as in the modulation of hyaluronan expression and release, were evaluated at a pH of 5.5. However, in RA the prevailing pH is usually between 6.0 and 6.9 (Kolker et al., 2012). In addition, researchers have shown that responses to changes in acidity by ASICs are dependent on the level of acidity (Benson et al., 2002). Consequently, future studies should evaluate these parameters at a range of different acidic conditions.

1.6.2.1 **Transient receptor potential cation channel subfamily V member 1 (TRPV1)**

Cloning of TRPV1 provided evidence that transient receptor potential (TRP) channels participate in the pain pathway. Research shows that TRPV1 is the most studied receptor in the TRP superfamily (Caterina and Julius, 2001). It is expressed in the trigeminal ganglia, DRG, and nodose ganglion neurons and works together with nociceptive fibres at an activation temperature of 43°C. Sensing of an acid or vanilloid compound is a clear indication of the significance of TRPV1 in mediating responses to

harmful stimuli (Caterina et al., 1997, Tominaga et al., 1998). TRPV1 is encoded by *TRPV1* in humans. This group of ion channels detects and regulates body temperature and is involved in sensing heat and pain. Structurally, TRPV1 is 838 amino acids long, with a molecular weight of 95 kDa. It has six transmembrane domains, a C-terminal cytosolic region that is 132 amino acids long, and an N-terminal region that is 432 amino acids long (Figure 1.6).

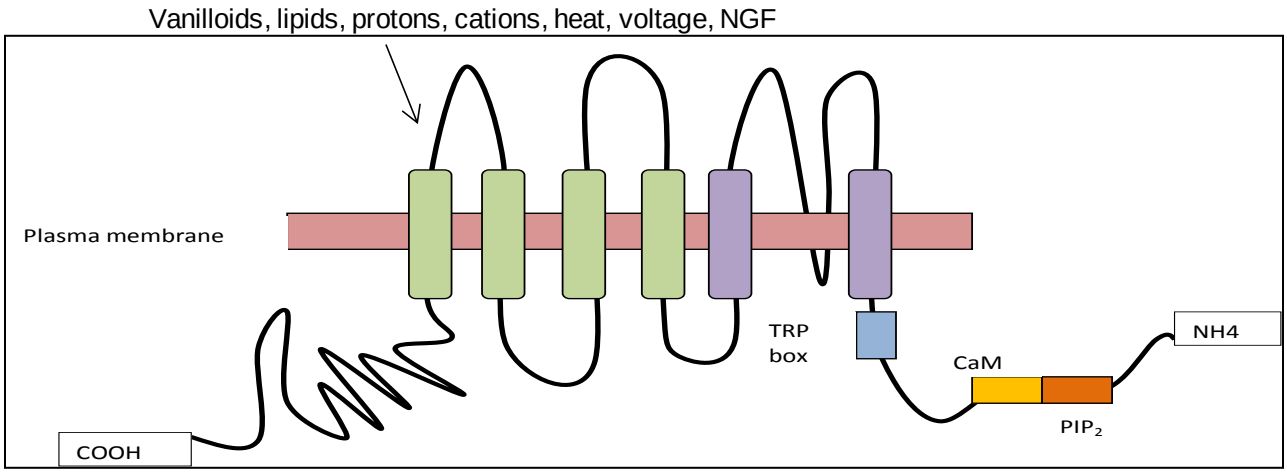

Figure 1.6 TRPV1 structure.

The structure of TRPV1 consists of six transmembrane domains. There are amino-terminal sequences that mediate CaM and PIP_2 signalling. TRPV1 activators are shown above the structure. NGF, nerve growth factor; COOH, carboxyl group; TRP, transient receptor potential; NH_4, amine group; CaM, calcium-modulated protein; PIP_2, phosphatidylinositol 4,5-bisphosphonate; TRPV1, transient receptor potential cation channel subfamily V member 1. TRPV1 is widely distributed across many tissues and is activated in a polymodal manner by both chemical and physical stimuli. Different TRPV1 activators are shown in Table 1 below.

Table1 Physical and chemical activators of TRPV1

Activator	**Examples**
Vanilloids	Capsaicin, olvanil, resiniferatoxin
Lipids	Anandamide, N-oleoyldopamine, endocannabinoid, N-arachidonoyl dopamine, 18–20 carbon N-acylethanolamines, 12-hydroperoxyeicosatetraenoic acid
Protons	H^+
Cations	K^+, Rb^+, Cs^+, Na^+, and Li^+ ions
Heat	
Voltage	

Source: (Devesa et al., 2011)

1.6.2.1.1 Functionality

TRPV1 is non-selective and can be stimulated by a wide range of endogenous and exogenous stimuli, such as acidic conditions; N-arachidonoyl dopamine; vanilloids like capsaicin; and heat, which leads to a painful and burning sensation. Located in the nociceptive neurons of the peripheral nervous system, TRPV1 receptors modulate pain sensation and play a role in the integration of diverse painful stimuli. TRPV1-/- mice were shown to lack effective responses to harmful heat stimuli or to the pungent vanilloids. Other studies note that gene knockdown or knockout is crucial for examining

the role that TRP channels play in detecting certain painful stimuli in nociceptive neurons. For example, TRPV3-/- mice do not exhibit sensitivities to noxious and innocuous heat (Moqrich et al., 2005). TRPV4-/- mice present with other characteristics, such as reduced sensitivity at the tail when pressure is exerted on it (Suzuki et al., 2003). The best description for TRPV1 function is as a mediator of hyperalgesia and allodynia. In fact, TRPV1-/- mice did not respond effectively to severe chemical or thermal stimuli and did not develop inflammatory hyperalgesia (Caterina et al., 2000, Davis et al., 2000).

1.6.2.1.2 Sensitisation and desensitisation

Prostaglandins and bradykinin are released as inflammatory mediators and lead to increased nociceptor sensitivity to noxious stimuli in the presence of tissue damage, injury, and inflammation. This manifests as an increased sensitivity to painful stimuli or to the increased sensation of pain in response to non-painful stimuli. The phospholipase C (PLC) pathway is activated by these pro-inflammatory agents, leading to phosphorylation of TRPV1 by PKC and sensitization. Cleavage of phosphatidylinositol 4,5-bisphosphate (PIP_2) by PLC results in re-activation of TRPV1 and contributes to TRPV1 sensitivity to stimuli. However, desensitisation may occur with prolonged exposure to stimuli due to increased intracellular Ca^{2+} influx from the extracellular space, which leads to decreased TRPV1 activity.

TRPV1 synthesis occurs in the DRG sensory neurons, and TRPV1 is transported along the central and peripheral axons to the spinal dorsal horn and to the skin and visceral organs, respectively (Guo et al., 1999, Tominaga et al., 1998). TRPV1 is critical to a

number of sensory issues in the skin, such as heat sensation, nociception, inflammatory hyperalgesia, allodynia, and neuropathic nociception (Hudson et al., 2001).

Capsaicin, which is a treatment for arthritic pain, works by temporarily desensitising its only known receptor, TRPV1 (Holzer, 1991),(Szallasi, 2002) Capsaicin also reduces blood flow in capsaicin-sensitive afferents (Tang et al., 2004, Helyes et al., 2004) (Bolcskei et al., 2005), (Barton et al., 2006, Keeble et al., 2005, Szabo et al., 2005).

Despite TRPV1's role in arthritis, the exact mechanisms by which TRPV1 exerts its effects are not fully understood. Sensing acid stimulates the expression of immediate early genes in sensory neurons. The ERK pathway is part of the serine/threonine MAPK family. ERK signalling links nociception to altered gene expression by transducing extracellular stimuli through its signalling pathway to achieve an intracellular transcriptional and post-translational response. After activation by mediators of cellular stress, inflammation, growth factors, and mitogens, MAPK translocates into the nucleus and binds to transcription factors. Transcription of specific genes is regulated to achieve many types of cellular activities, such as proliferation and production of cytokines and other inflammatory response factors (Seger and Krebs, 1995, Lewis et al., 2000). MAPKs exist in numerous isoforms and are activated by kinases, resulting in the formation of a complex biochemical cascade that is critical for the overall regulation of the inflammatory process (Karin, 2004, Thiel et al., 2007).

1.6.2.1.3 Role of TRPV1 in inflammatory disorders and rheumatoid arthritis

TRPV1 signalling is associated with numerous inflammatory conditions, including RA. Similar to RA, chronic pancreatitis is characterised by neurogenic inflammation (Schwartz et al., 2013). Increased expression of TRPV1 and its upstream regulator, nerve growth factor (NGF) is found in chronically inflamed rat pancreatic tissues (Zhu et al., 2011). However, a blockade of NGF reduces TRPV1 expression and function in rat pancreatic sensory neurons (Zhu et al., 2011). Further, TRPV1 antagonists reduce inflammation and pain in a mouse model of chronic pancreatitis (Schwartz et al., 2013). Up-regulation of TRPV1 expression and activity is also found in acute pancreatitis in mice (Schwartz et al., 2011). Thus, expression and activation of TRPV1 in pancreatic sensory neurons are believed to be a major mechanism mediating pancreatic inflammation (Liddle, 2007). Consistent with these studies, TRPV1 also appears to be an important mediator of pancreatic inflammation in diabetes (Suri and Szallasi, 2008). In fact, loss of TRPV1 signalling in rats results in reduced age-related weight gain and improved glucose tolerance (Suri and Szallasi, 2008). These results implicate TRPV1 as a critical mediator and potential therapeutic target in obesity and diabetes, which are major inflammatory disorders. However, the role of TRPV1 in diabetes appears to include not only type 2 diabetes but also autoimmune type 1 diabetes (Suri and Szallasi, 2008), which is also characterised by pancreatic inflammation. TRPV1 activation is also associated with inflammatory bowel disease (Akbar et al., 2010). Thus, TRPV1 antagonism is a potentially beneficial approach for multiple pathological conditions characterised by chronic inflammation. These studies suggest a general link between TRPV1 activity and

inflammation, which is consistent with the concept that TRPV1 is an important mediator of inflammation in RA.

Engler et al. (Engler et al., 2007) demonstrated that TRPV1 is expressed in FLS of OA and RA patients. Synoviocytes can be exposed to TRPV1 stimuli, especially thermal stress and acidic conditions, if there is chronic or acute inflammation (Kochukov et al., 2006). Moreover, over-expression of TRPV1 has been identified in joint synovial fluids and contributes to the OA pathogenesis. TRPV1 and CGRP were expressed in a rat model of OA that was enhanced by complete Freund's adjuvant (CFA) or iodoacetate (Kochukov et al., 2006, Nilius et al., 2007). CFA decreased mechanonociceptive thresholds and allodynia, and increased arthritic changes at the tibiotarsal joints of wild-type mice. CFA-induced swelling at the knee joint is significantly reduced in TRPV1-/- mice compared to wild-type mice (Kochukov et al., 2006). TRPV1 protein expression is abundant in synoviocytes. However, its role in pathological conditions, such as arthritic inflammation, remains under debate (Kochukov et al., 2006).

The role of TRPV1 in inflammation is thought to be largely neuronal, although some evidence indicates that it may contribute to immune responses. These receptors are sensitized by neurons to generate the perception of pain. Sensitization occurs through an enhanced expression of TRPV1 and modification of the channel. Sensitized TRPV1 may also increase the release of substance P and CGRP from sensory neurons. These pro-inflammatory mediators cause vasodilation and movement of pro-inflammatory mediators and immune cells to the injury site, contributing to swelling and plasma extravasation. In RA, the levels of neuropeptides in the synovial fluid are high. Even though the role of TRPV1 in RA has not been clearly elucidated, TRPV1 is widely

considered to play a critical role in the accumulation of neuropeptides and in the integration of different noxious stimuli (Fernandes et al., 2011). Protons affect TRPV1 function by reducing the threshold for channel activation by agonists and heat and by promoting channel opening at a low pH (Tominaga and Tominaga, 2005).

TNF-α enhances the expression of TRPV1, activates TRPV1 contributing to inflammation-related pain, enhances capsaicin-induced Ca^{2+} influx, and contributes to TRPV1 sensitization. Bradykinin, histamine, adenosine triphosphate, and prostaglandin E2 have also been shown to mediate the excitation and sensitization of TRPV1 (Devesa et al., 2011).

1.6.3 G-protein-coupled receptors (GPCRs)

GPCRs have seven transmembrane domains (Figure 1.7). Members of this transmembrane receptor family recognize biomolecules in the extracellular space and initiate the activation of signal transduction pathways and appropriate cellular responses.

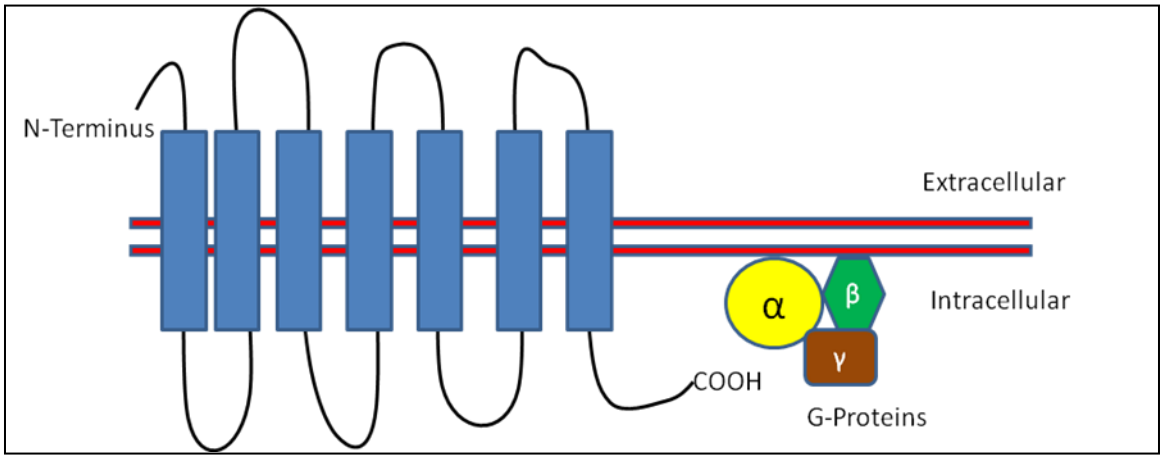

Figure 1.7 Structure of GPCR

A GPCR consists of an intracellular C-terminal domain, seven transmembrane domains, and an extracellular N-terminal domain. The G-α/β/γ subunits attach near the carboxyl terminus. GPCR, G-protein-coupled receptor.

These receptors are activated when they bind their ligands, which are normally peptides of varying sizes. GPCRs have two main transduction pathways: the cyclic adenosine monophosphate (cAMP) and phosphatidylinositol signalling pathways (Figure 8) (Gilman et al., 1987). G-proteins are composed of three different subunits: G-alpha, G-beta, and G-gamma. Once the ligand binds to the GPCR, guanine diphosphate is replaced by guanine triphosphate, inducing activation of the G-alpha protein subunit and

dissociation from the beta and gamma subunits. G-alpha has four different isoforms: G-alpha o, G-alpha s, G-alpha i, and G-alpha 12/13.

The activity of phosphatidylinositol-specific phospholipases is controlled by the G-alpha o family. For example, PLC-beta hydrolyses PIP_2 and generates the second messengers, diacylglycerol and inositol 1,4,5-trisphosphate. These messengers increase intracellular Ca^{2+} concentrations and activate proteins kinases, such as PKC (Ludwig et al., 2003). G-alpha o can work directly or through PKC and regulates different phospholipase-D isoforms. G-alpha o induces the transcription factor NF-κB via proline-rich tyrosine kinase-2. Conversely, G-alpha s induces the adenylyl cyclase pathway, leading to cAMP accumulation in cells. cAMP binds to PKA and induces GPCR phosphorylation (Gilchrist et al., 2002).

GPCRs have some acid-sensitive units, such as GPR4, GPR65, GPR68, and GPR132. These subunits are activated as ASICs if extracellular pH declines to between 6.4 and 6.8. These G-protein receptors were initially de-orphanised as receptors of lipid messengers. Recently, GPR4, GPR68 (OGR1), GPR65 (T-cell death-associated gene 8 [TDAG8]), and GPR132 (G2A) have been reported to be proton-sensing receptors that activate either the phosphoinositol or cAMP pathways. Expression of these proteins is observed in DRG and small neurons that are responsible for nociception. More than half of these proteins contribute to inflammation and neuropathic diseases. However, their functions in chronic inflammation, such as RA, remain unclear. Recently, researchers have found that OGR1 and G2A respond to low pH by increasing inositol phosphatases (IPs). In contrast, GPR4 and TDAG8 accumulate cAMP in response to extracellular acidification (Christensen et al., 2005a).

1.6.3.1 **Role of GPCR in inflammatory disorders and rheumatoid arthritis**

Many inflammatory mediators activate GPCR signalling. In addition, chronic inflammatory conditions such as asthma demonstrate increased GPCR activity (Druey, 2003). Allergens stimulate GPCR signalling in endothelial and respiratory smooth muscle cells (Druey, 2003). Activated GPCR signalling is a major therapeutic target for allergy medications (Druey, 2003), demonstrating the major role that GPCRs play in allergic conditions. Furthermore, down-regulation of G-protein-coupled receptor kinase 2, which results in increased GPCR signalling, is observed in multiple sclerosis, which is characterised by neuronal inflammation (Vroon et al., 2005). In addition to being associated with numerous inflammatory conditions, GPCR signalling is active during bone remodelling. Expression of OGR1 (GPR68) has been observed during osteoclast differentiation in a study of toothless osteoporotic rats. Colony stimulating factor-1 injection and RANKL treatment were administered to restore the osteoclast population. In that study, over-expression of OGR1 (GPR68) was noticed after 2 days of injection. Moreover, mRNA expression increased after treatment with RANKL to induce osteoclast differentiation. Inhibition of OGR1 by anti-OGR antibody or by small inhibitory RNA inhibited RANKL-induced differentiation of mouse bone marrow mononuclear cells and raw cells in vitro (Gilchrist et al., 2002). That study indicated that OGR1 might play a critical role in the development of RA because of its role in early osteoclastogenesis and osteoclast differentiation. GPR4 has been reported as a receptor for sphingosylphosphorylcholine (SPC) and lysophosphatidylcholine (LPC). However, this observation has not been confirmed yet. Zhu et al. (Zhu et al., 2001) showed that SPC and LPC enhanced intracellular Ca^{2+} in GPR4-transfected cells. However, in another

study by Ludwig et al., SPC and LPC were not considered activators or ligands for GPR68 and GPR4 (Ludwig et al., 2003). Another experiment found that LPC had no effect on cytosolic Ca^{2+}, whereas SPC activated intracellular Ca^{2+} release in synoviocytes (Christensen et al., 2005a). Because the function of GPR4 is not yet confirmed, whether GPR4 directly or indirectly mediates the effects of LPC and SPC remains unclear. Recently, various studies have shown that GPR4 senses extracellular acidification (Chen et al., 2011). Activation of GPR4 by acidic pH transduces downstream signals via cAMP and PLC. A new effector of cAMP has recently been identified and is referred to as an exchange protein directly activated by cAMP (Epac). Epac is involved in various cellular processes, including cell adhesion (Lorenowicz et al., 2007, Roscioni et al., 2008). Moreover, Epac signalling regulates PKA-independent processes, such as B2-adrenergic receptor-mediated ovarian carcinoma cell adhesion, chemotaxis, and monocyte adhesion. Activation of GPR4 at an acidic pH (6.4) enhanced human umbilical vein endothelial cell (HUVEC) adhesiveness and binding to U937 monocytes. These effects were decreased upon knockdown of GPR4 in HUVECs (Chen et al., 2011).

GPCR expression has been found in synoviocytes. Two separate studies examined synoviocytes from two groups of patients. One group of patients had RA, and the other had psoriatic arthritis. The results showed a significant increase in intracellular Ca^{2+} at pH 6.7 in both groups. Moreover, IP production was examined to confirm the role of GPCR. A significant increase in IP was found in cultured synoviocytes (SW982) at pH 6.7 (Christensen et al., 2005a). However, the identity of the GPCR detected in the previous study remains unknown. Further studies are needed to identify and characterise

the functions of these proteins in synoviocytes, including how they contribute to the pathology and progression of RA.

1.7 **Hypothesis**

In this research project we test the hypothesis that human synoviocytes (FLS) express acid sensing proteins that regulate the functional responses to acidification and that blocking expression of acid sensing mechanism in synoviocytes reduces destructive responses in human synoviocytes.

1.8 **Aims and Objectives**

1- To determine the expression and localisation of acid sensing proteins in synovium from patients with RA.

2- To determine the affect of acidic environment on acid sensing proteins and matrix metalloproteinase (MMP) expression in RA-FLS at both mRNA and protein level.

3- To determine the effects of acid sensing proteins inhibition on functional responses to acid in synoviocytes.

2 Chapter 2: Materials and Methods

2.1 List of materials

2× qPCR mastermix (plus SYBR green plus ROX)	Primerdesign, Southampton, UK
3-(4,5-Dimethylthiazol-2-yl)-2,5-Diphenyltetrazolium Bromide (MTT)	Sigma Aldrich, MO, USA
3,3'-Diaminobenzidine (DAB) peroxidase substrate	Vector Laboratories, CA, USA
Amersham western blotting detection reagent enhanced chemiluminescence (Thiel et al.) Plus	GE Healthcare, Chalfont St. Giles, UK
Aperio CS2 slidescanner	Leica, Wetzlar, Germany
Dharmafect 4 transfection reagent	Dharmacon, Thermo Fisher Scientific Inc, MA, USA
Dimethyl sulfoxide (DMSO) D8418	Sigma Aldrich, MO, USA
Donkey anti-rabbit Alexa Fluor® 568	Life Technologies, Thermo Fisher Scientific Inc, MA, USA
Dulbecco's Modified Eagle's medium (DMEM)/F-12 GlutaMAX™ Supplement	Life Technologies, Thermo Fisher Scientific Inc, MA, USA
Fetal Bovine Serum	Biosera, East Sussex, UK, East Sussex, UK
Goat anti-mouse horseradish peroxidase conjugated antibody	Abcam, Cambridge, UK
Goat anti-rabbit horseradish peroxidase conjugated antibody	Abcam, Cambridge, UK
Haematoxylin	Sigma Aldrich, MO, USA
HALT™ proteinase inhibitor cocktail EDTA-free 100x	Thermo Fisher Scientific Inc, MA, USA
iBlot® gel transfer stack, nitrocellulose	Invitrogen, Paisley, UK
L-Glutamine 200mM	Lonza-Biowhittaker, Cologne, Germany
Lipofectamine 2000 transfection reagent	Invitrogen, Paisley, UK
Mouse anti-human fibroblast antigen clone IB10	Abcam, Cambridge, UK
Mouse anti-human β-Actin purified antibody	Sigma Aldrich, MO, USA
NTC ON TARGET plus SMART pool siRNA	Dharmacon, Thermo Fisher Scientific Inc, MA, USA
Oligofectamine transfection reagent	Invitrogen, Paisley, UK
Penicillin-Streptomycin (100x)	Lonza-Biowhittaker, Cologne, Germany
Precast 12% 12-well polyacrylamide mini PROTEAN TGX gels	BIORAD, CA, USA

Precision Nanoscript Reverse Transcription Kit	Primerdesign, Southampton, UK
Prestained protein ladder broad range (10-230 kDa)	New England Biolabs, MA, USA
Rabbit anti-mouse Alexa Fluor® 488	Life Technologies, Thermo Fisher Scientific Inc, MA, USA
Recombinant human TNF-alpha	PeproTech, NJ, USA
RNeasy mini kit	Qiagen, Dusseldorf, Germany
Skimmed milk powder	Sigma Aldrich, MO, USA
Trypan blue 0.4% solution	Lonza-Biowhittaker, Cologne, Germany
Trypsin-Ethylenediaminetetraacetic acid (EDTA) (1X) liquid [0.05% Trypsin 0.53 mM EDTA•4Na]	Fisher Scientific, Thermo Fisher Scientific Inc, MA, USA
Vectastain universal elite avidin-biotin complex (ABC) kit	Vector Laboratories, CA, USA
Vectorshield mounting medium containing 4',6-diamidino-2-phenylindole (DAPI)	Vector Laboratories, CA, USA

2.2 **Clinical samples**

Biopsies of tissue synovium were collected from patients with RA and OA; some patients were undergoing surgery in theatre for knee replacements, the other patients were undergoing arthroscopy visual examinations. These samples were obtained by Professor A. Gerry Wilson, Dr. Mohammed Akil, and Professor J. Mark Wilkinson (Ethics were obtained – SSREC/03/106 and REC10/H0606/20).

For vascularity of synovitis, the visual analogue scale (VAS) was used. All samples for RA biopsies were issued pathological severity scores, the tests carried out are based on 100 mm, the scores were counted by a skilled arthroscopist, samples are marked on a physical 100-mm length scale and a ruler is used to take measurements starting left to right. Once the scores were obtained, the tissues were divided into two groups: A. Mild disease (score of <50 mm) and B. Severe disease (score >50 mm).

2.3 **Isolation of RA and OA FLS**

The biopsy tissue was processed and added to 1× trypsin-EDTA for approximately 1 hour at 37°C. The tissue was then cut up again and treated with 10 ml collagenase per sample at 1 mg/ml (sterilised through a 0.22-µm PES express Millex-GV filter) for 24 hours at 37°C, and the cell suspension was passed through a 70-µm nylon cell strainer. This was placed in a new T25 flask, the cells were incubated at 37°C, 5% CO_2 and 20% O_2. These cells were washed after approximately 24–48 hours with PBS. The complete culture medium was replaced every 2–3 days.

2.4 **Processing of synovial tissue for paraffin embedding**

Synovial tissue was placed in a labelled cassette of an appropriate size and dehydrated to displace the water through a series of graded alcohol baths (2 hours in each bath). The first 3 baths were 70% ethanol, the next 2 were 95% ethanol, and the last 2 were absolute ethanol and xylene. Then the cassette was incubated in two paraffin wax baths with a vacuum applied for 2 hours in each bath and then moved a warm place. The tissue was placed into a mould, surrounded with molten paraffin, and moved to a cold plate to allow the wax to set. The mould was then removed, and the block was inserted into a microtome to cut 5-µm sections. Synovial tissue sections were floated on the surface of a 37ºC water bath, transferred onto the surface of clean glass slides, and then placed on a warm block to melt the wax and bond the tissue to the glass.

2.5 **Immunohistochemistry of paraffin-embedded sections (IHC-P)**

Histochemical methods were used to study the expression of acid sensing proteins in arthroscopic biopsies from RA patients. Antibody optimization was performed prior to investigation of acid sensing proteins. The acid sensing proteins ASIC3, GPCR4, OGR1, and TRPV1 were evaluated with rabbit polyclonal primary antibodies purchased from Abcam. The detection of acid sensing proteins was optimized in sections of lung tissue, which expresses all four types of proteins and served as a positive control (Xu and Casey, 1996, Su et al., 2006, Chen et al., 2011, Deering-Rice et al., 2012). Rabbit isotype-specific IgG and lung tissues with no primary antibodies were used as negative controls.

Paraffin-embedded sections of human synovial tissue were deparaffinised (de-waxed) by placing the slides on a carrier and performing the following incubations for 3 min each: xylene, xylene with 100% ethanol (1:1), 100% ethanol, 70% ethanol, and 50% ethanol. Finally, the slides were washed under running tap water. Then, antigen retrieval was performed by incubating the slides in tri-sodium citrate (2.94 g in 1000 ml distilled water, pH 6.0), followed by microwaving at 98°C. After the solution reached the boiling point, 20 min was counted. This antigen retrieval procedure was performed to break the methylene bonds that cross-link proteins and mask antigen binding sites. Slides were removed from the microwave and washed under running tap water for 10 min. The slides were then washed twice in Tris-buffered saline (TBS) with 0.025% Triton X100, blocked in 10% goat serum with 1% BSA for 2 hours at room temperature, and washed twice prior to addition of the primary antibodies. Primary antibodies were diluted in TBS with 1% BSA as follows: ASIC3 (AB49333; 1:50), GPCR4 (AB75330; 1:100), GPCR68 (AB61420; 1:50), and TRPV1 (AB63083; 1:100). Synovial tissue sections were

incubated with primary antibodies for 24 hours at 4°C. On day 2, the slides were rinsed in TBS with 0.025% Triton X100 and incubated in 3% hydrogen peroxide (H_2O_2) in TBS for 15 min to quench endogenous peroxidases and reduce background staining. The secondary antibody (universal biotinylated anti-mouse/rabbit IgG secondary antibody) provided by Vector Laboratories was diluted at 1µl:50µl of TBS with 1% BSA, and slides were incubated at room temperature (25°C) for 1 hr. Sections were rinsed in TBS-Tween (TBST), and then avidin-biotin complex (ABC) solution was applied for 1 hr. ABC is a method of antigen detection that exploits the binding affinity between avidin and biotin using a secondary antibody conjugated to biotin to amplify the signal from the primary antibody (Figure 2.2). Horseradish peroxidase is conjugated to a large avidin-biotin complex, which is then added to the sample to enzymatically label each complex and further amplify the signal. Synovial tissue sections were washed twice with TBST. DAB stain (Vector Kit, DAB substrate kit for peroxidase), which was used to visualize the protein expression, was prepared by adding two drops of hydrogen peroxide solution, two drops of buffer stock solution, and four drops of DAB stock solution (each drop = 50 µl) to 5 ml distilled water and mixing well. DAB solution was added to the slides for 2–10 min, avoiding light exposure as much as possible. The colour development was checked under a microscope. Then, the sections were washed with TBST, counter-stained with haematoxylin for 30 sec, and washed in Scott's water to reduce the background staining. Sections were rehydrated in 50% ethanol, 70% ethanol, 100% ethanol, xylene with 100% ethanol, and xylene for 50 sec each. Sections were mounted and viewed. Aprio software was used to scan and analyse IHC slides (Figure 2.1).

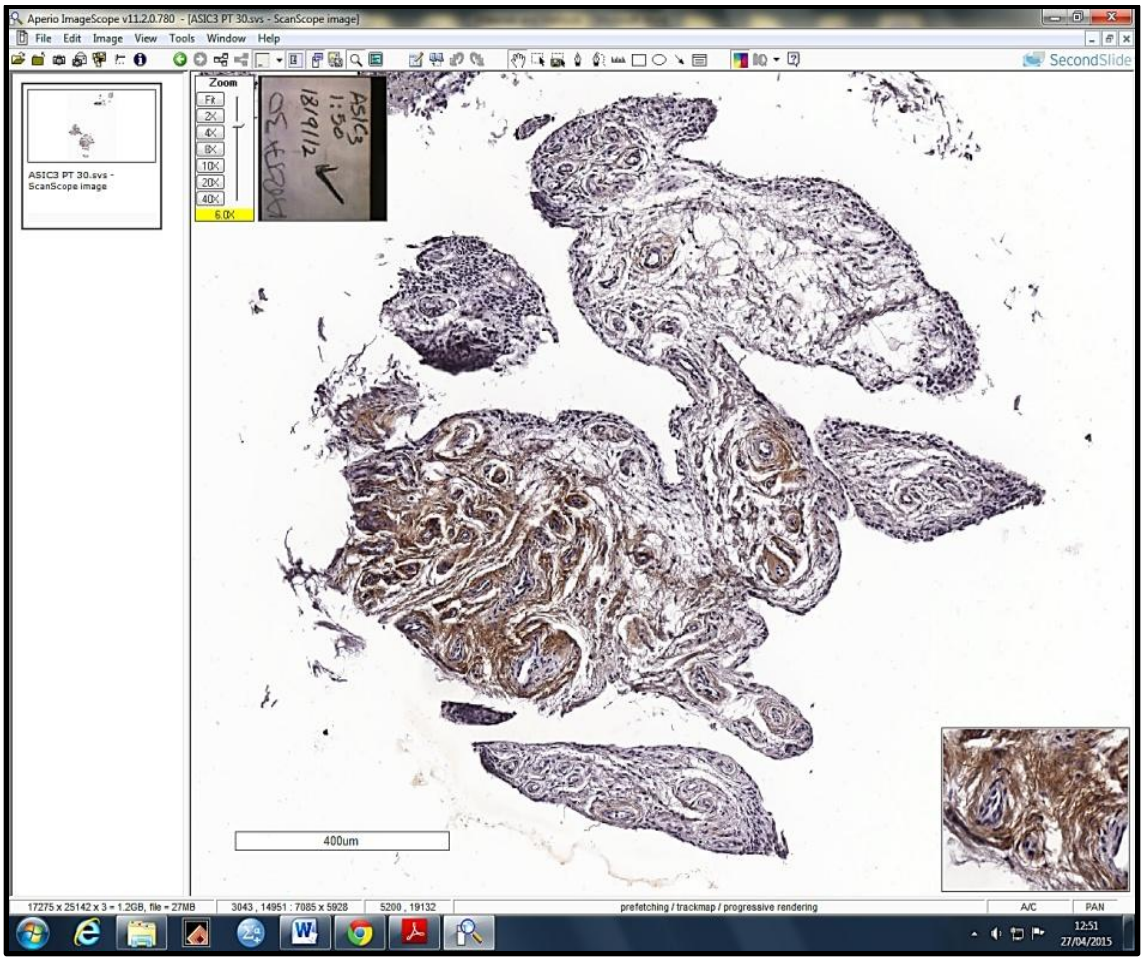

Figure 2.1 A screenshot for a scanned slide of synovial tissue using Aprio software.

All slides were scanned by Aprio software. Donor details (upper left corner), magnification of a specific area (lower right corner) and an overview of whole slide can be investigated.

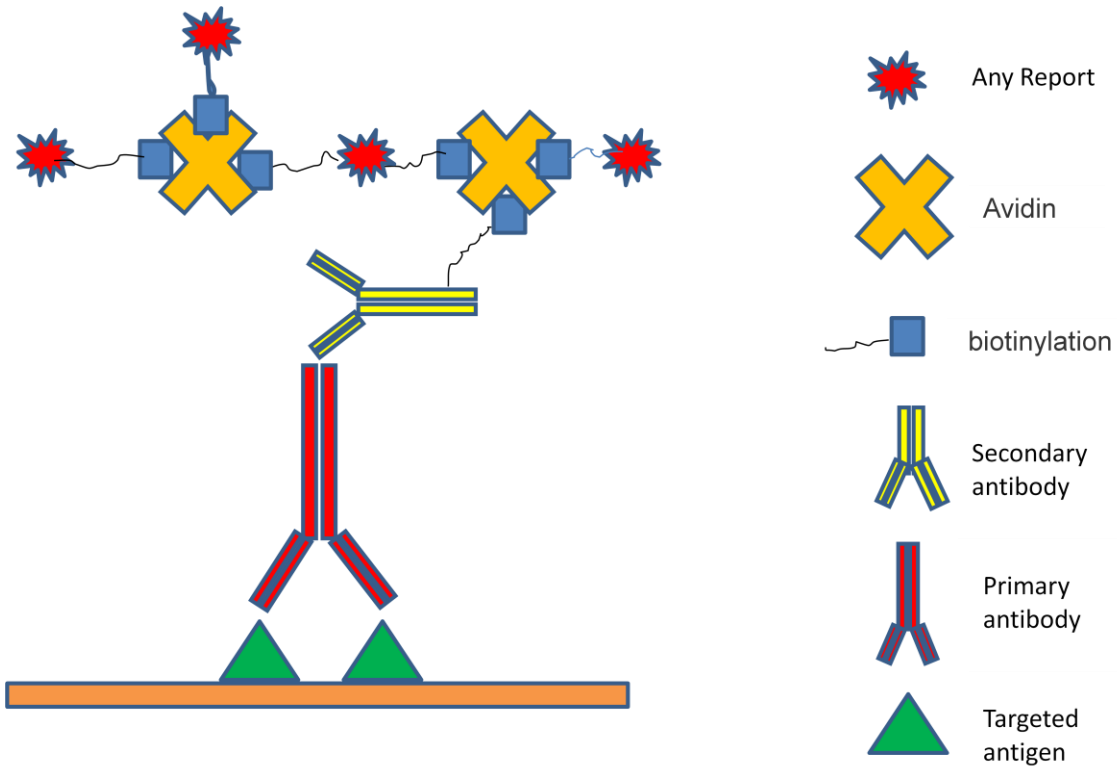

Figure 2.2 AB complex (ABC).

Avidin and biotinylated enzyme are mixed together in a specified ratio to prevent avidin saturation and incubated for about 15 min at room temperature to form the complex.

2.6 **Frozen tissue sectioning**

Synovial tissue was snap-frozen in liquid nitrogen and then stored in at -80°C. Before sectioning, the cryostat chamber and chuck temperature were set to -20°C. The frozen tissue was placed in the chamber and allowed to warm up, and the tissue or block was then frozen to a chuck using Cryoembed. Once the tissue was securely frozen in place, it was fixed into the holder and trimmed to achieve a full-face section. Sections were then taken at 7 μm and fixed to a slide using electrostatic charge. Cut sections were stored at -80°C until needed.

2.7 **Immunofluorescence (IF)**

Frozen synovial tissue sections were used to identify and co-localise the expression of acid-sensing proteins in RA FLS. RA synovial tissue was defrosted for one hour at room temperature, rinsed with PBS with 0.025% Tween 20 (PBST), and then fixed in ice-cold 4% paraformaldehyde for 10–15 min. After fixation, tissue was rinsed with PBST twice and blocked with 5% normal goat serum in PBS for 1 hr at room temperature followed by two more rinses with PBST. Rabbit anti-ASIC3 (AB49333; 1:50), GPR4 (AB75330; 1:100), GPR68 /OGR1 (AB61420; 1:50), TRPV1 (AB63083; 1:100), and mouse monoclonal to fibroblast surface protein (Anti-Fibroblast Surface Protein antibody 1B10, Abcam ab11333) were used for immunostaining. Synovial tissue was incubated with primary antibodies overnight at 4°C. Donkey anti-mouse Alexa Fluor® 488 conjugate and goat anti-rabbit IgG (H+L) Alexa Fluor® 594 conjugate were used as secondary antibodies. Samples were rinsed with PBST, and then secondary antibodies were applied (1:1000) in PBST with 1% BSA for 2 hr at room temperature in dark. Slides were washed

three times for 5 min, followed by adding one drop of mounting medium with DAPI (VECTASHIELD HardSet), which hardens after the coverslip is placed. Sections with no primary antibodies and sections treated with iso-IgG (Rabbit polyclonal IgG, ab27472) served as negative controls. All slides were examined using an inverted widefield fluorescence microscope (Leica DMI4000B) and LAS AF Lite software (Figure 2.3). Sections were investigated at 10× for whole section visualization and at 40× for specific area details.

During image collection, three different channels were used to detect acid-sensing protein expression in RA synovial tissue. Each channel is specific for a wavelength (Channel 0 to detect Alexa Fluor® 488 (green), Channel 1 for Alexa Fluor® 594 (red), and Channel 2 for DAPI stain (blue) and the exposure time was set at 6100 ms, 5072 ms, and 364 ms, with gain 6.2, 6.1, and 5.5 respectively. All sections were investigated at 10× for a whole section vision, and 40× for a specific area details. All three channels were used to detect acid-sensing proteins (red), FLS (green), and nucleus (glue) separately, and then all three channels were merged in one image as shown below.

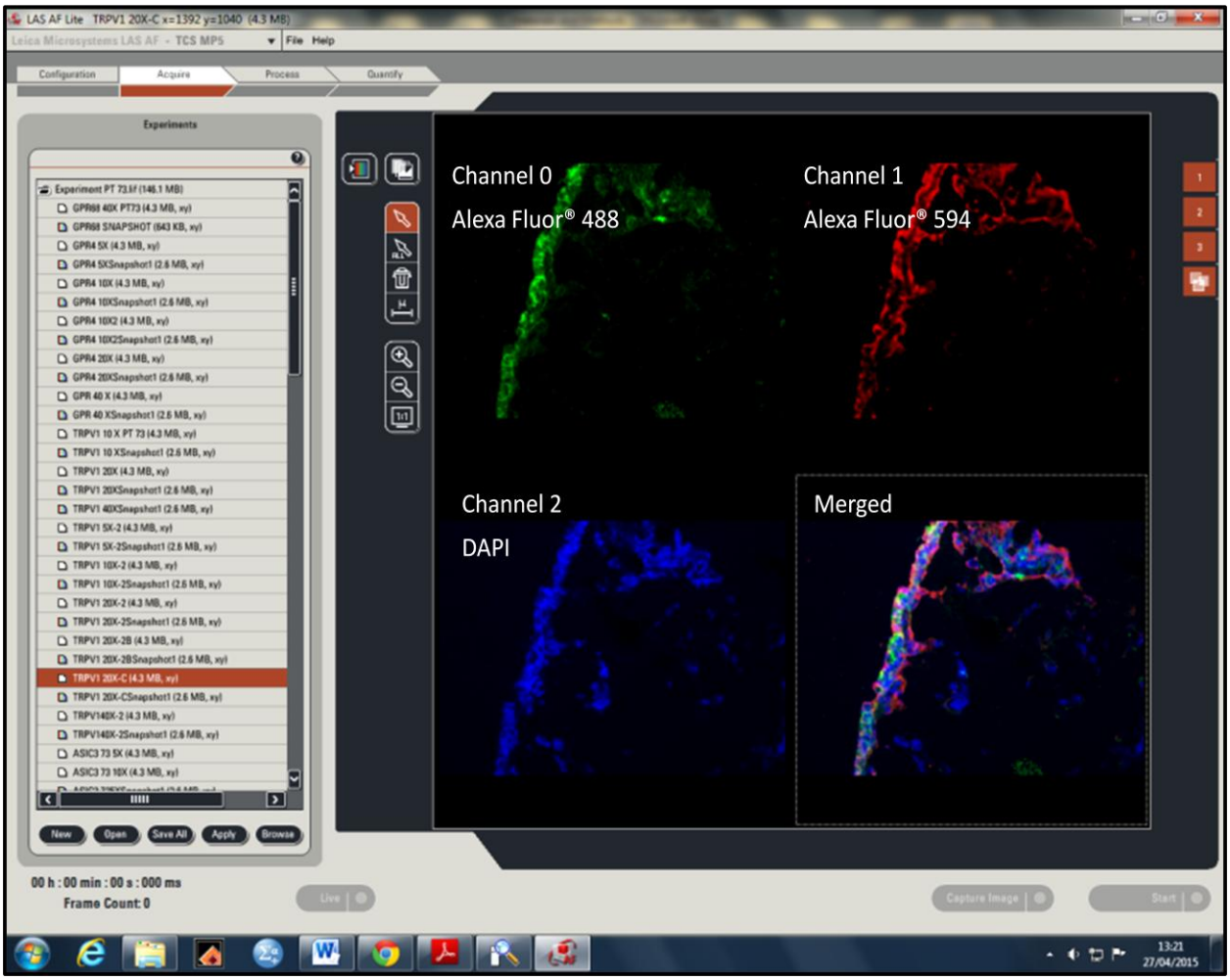

Figure 2.3 IF images

This figure illustrates the inverted widefield fluorescence microscope software LAS AF Lite and the three different channels for RA-FLS (green), acid sensing proteins interest (red), nucleus (blue), and the merged of all three channels for an RA synovial tissue section.

2.8 **RA Fibroblast-like synoviocyte (RAFLS) culture**

Dulbecco's modified Eagle's medium (DMEM)/F-12 Gluta-Max medium (Gibco, UK) was prepared by adding 5–10% foetal bovine serum (FBS), 100 U/ml penicillin, and 100 µg/ml streptomycin (P/S), mixing well, and storing at 4°C. Upon receipt of the RA FLS cell lines, complete DMEM culture medium was warmed up at room temperature for 1 hour and then cells were counted with a haemocytometer (Figure 2.4). RAFLS were initially cultured at a density of 5×10^4 cells in five T-25 flasks and were incubated at 37°C in 5% CO_2. The complete culture medium was changed every 3 days, and the cells were harvested after 14 days (80%–90% confluent) by adding trypsin/EDTA (2 ml for a T-75 flask and 500 µl for a T-25 flask). (DMEM)/F-12 GlutaMAX medium contains calcium and magnesium ions, and foetal bovine serum contains proteins that are trypsin inhibitors. Both Mg^{2+} and Ca^{2+} inhibit trypsin. Therefore, we used PBS without Ca^{2+}/Mg^{2+} to wash the cells prior to trypsinisation to reduce the concentration of divalent cations and proteins that inhibit trypsin. EDTA is a calcium chelator, which will "mop" up the remaining divalent cations. If trypsin is allowed to stay in contact with the cells for too long, cell viability will be reduced. So, flasks were incubated with trypsin/EDTA at 37°C in 5% CO_2 for maximum 5 min, and then cells were checked to see if they were detached. Once detached, 4 ml of complete DMEM medium was added to inhibit the trypsinisation. The suspension was transferred to a universal tube, and flasks were checked for any remaining attached cells before discarding the flask. The tube was centrifuged at 500×g, the supernatant was discarded, and the pellet was collected and washed twice with PBS and then resuspended in 1 ml complete DMEM prior to counting and subculturing the cells.

Contamination tests were performed for every new DMEM bottle by incubating DMEM plus 5% FBS and 1× P/S at 37°C in 5% CO2 for 24 hr and examining the medium with light microscopy at 40X for microbe growth. Moreover, incubator cleaning and mycoplasma testing were performed monthly.

2.9 **RA FLS counting**

A 10-µl aliquot of the cell suspension (described in section 2.8) was transferred into a new microtube, and 10 µl trypan blue was added to the suspension and mixed well with a pipette. The haemocytometer was prepared, the cover slip was cleaned and fixed on its correct position, and 10 µl of the trypan blue/cell mixture was dispensed under the cover slip until it covered the counting area completely. The chamber counter was inspected under the microscope at 40×. For cell counting, the following equation was used (average of cells × dilution factor × 10^4). The dilution factor in this case was 2 (1:1 diluted with trypan blue), and 10^4 is the conversion factor to ml (Figure 2.4).

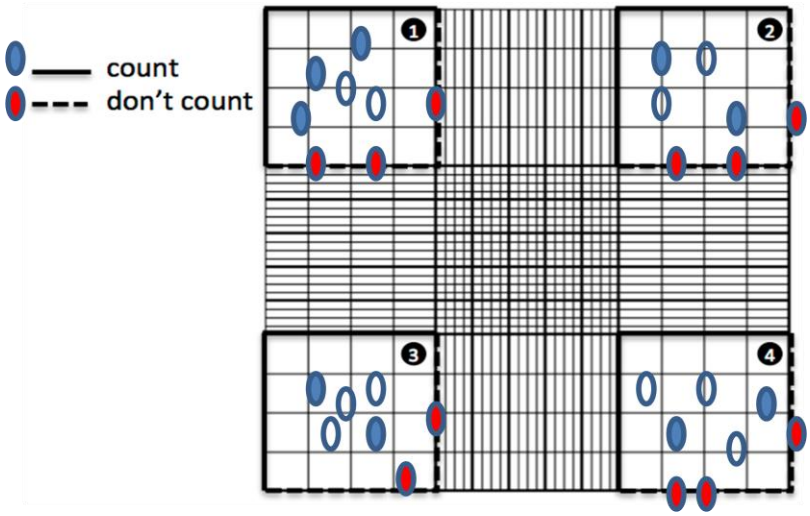

Figure 2.4 Cell counting by using Haemocytometer.

Cells in red were excluded from counting, cells in blue represent dead cells, and translucent cells represent live cells.

2.10 **RA-FLS subculture**

After re-suspending the pellet as described in the previous section (2.8), an equal volume (1 ml) of medium as the cell suspension was dispensed into four new T-25 flasks and 6-well plates, and cells were incubated at 37°C in 5% CO_2. Cells reached 90% confluence in 10–14 days, and the medium was changed every 3–4 days.

2.11 **Culture medium pH optimization**

DMEM medium was adjusted by using 1 M HCL (pH 7.4, 7.0, 6.5, 6.0), transferred into T-25 flasks, and then incubated at 37°C in 5% CO_2 for 24 hr. on day 2, acidified medium were collected in sealed tube and pH was measured by using pH meter from METTLER TOLEDO. The pH measurements for all acidified medium ranged between 7.10 and 7.50, which reflects that the buffering system ($NaHCO_3$) was effectively changing the acidity of the medium to neutral pH or pH≈7.4. So, DMEM culture medium with no $NaHCO_3$ was used. However, inside the incubator CO_2 dissolves in water and forms carbonic acid (H_2CO_3), which dissociates and form a proton H^+ and bicarbonate HCO_3^-, and that will acidify the medium to an extremely low pH in the absence of a buffering system.

$$\boldsymbol{CO_2 + H_2O \leftrightarrow H_2CO_3 \leftrightarrow H+ + HCO_3}$$

The presence of sodium bicarbonate as a buffering system in the culture medium will maintain medium condition at neutral pH under maintained CO_2 tension.

$$NaHCO_3 + H2O \leftrightarrow Na+ + HCO_3- + H_2O \leftrightarrow Na+ + H_2CO_3 + OH- \leftrightarrow Na+ + H_2O + OH- + [CO_2(aq) \leftrightarrow CO_2(g)]$$

The amount of dissolved CO_2 in the culture medium is dependent on the amount of environmental CO_2 and the temperature of the incubator. Inside the incubator CO_2 tension is maintained, but when CO_2 escapes, the reaction is driven to the right and sodium carbonate is produced, which will increase pH and turn the medium more alkaline.

HEPES has a superior buffering capacity and does not require a controlled gaseous atmosphere (Shipman, 1969). However, HEPES is relatively expensive and toxic at higher concentrations for some cell types. HEPES also greatly increases the sensitivity of media to phototoxic effects induced by exposure to fluorescent light (Zigler et al., 1985). In addition, our RAF-FLS cells were optimized to grow under a controlled gaseous atmosphere with 5% CO_2. Moreover, most incubators were in use by other researchers, and it was difficult to find an available incubator without a controlled gaseous atmosphere. The concentration of HEPES when used in a CO_2 environment must be more than double the amount of bicarbonate for adequate buffering, and that may be toxic to RA-FLS. Incubation of HEPES buffer without bicarbonate in a CO_2 atmosphere will turn the medium extremely acidic. Thus, the complexity of using HEPES as pH monitor prevented its use.

So the pH of MEM culture medium should be adjusted by changing CO_2 tension or the buffering system (HCO_3) concentration, not only by addition of HCl or lactic acid (C_3H6O_3) as illustrated in the equations below.

$$NaHCO_3 + HCL \longrightarrow NaCL + H_2O + CO_2$$

$$NaHCO_3 + C_3H_6O_3 \longrightarrow CO_2 + H_2O + NaC_3H_5O$$

NaHCO3 concentration in DMEM culture medium is 3.7 g/L, which will maintain a pH of 7.4 in a 5% CO_2 environment. The concentration of $NaHCO_3$ was manipulated to achieve desired acidic condition.

The 10× MEM with no buffering system (sodium bicarbonate) was diluted to 1× (pH=2.10–2.31) with sterile filtered distilled water, then 5% FBS, 1% penicillin streptomycin, and 1% L-Glutamine were added. The pH of the medium was measured and adjusted to be maintained at desired acidic condition by using 7.5% $NaHCO_3$ (75 g $NaHCO_3$ per litre of distilled water) (Table 1). Then all acidified medium were adjusted to pH 7.4 using 1 M NaOH and stored at 4°C. Different volumes of 1 M lactic acid were used to acidify culture medium at pH 7.4, 7.0, 6.5, and 6.0. Acidified medium was transferred into flasks with and without RA-FLS and incubated at 37°C in 5% CO_2 for 24 hr to evaluate the acidic condition and pH stability

1X MEM Volume	Components	(Control) pH 7.4	pH 7.0	pH 6.5	pH 6.0
20ML	7.5% NaHCO3	850 µl	575 µl	310 µl	160 µl
	1M NaOH	-	30 µl	65 µl	92 µl
	1M LA	-	32 µl	90 µl	100 µl
	7.5% NaHCO3	1000 µl	550 µl	270 µl	155 µl
	NaOH	-	35 µl	65 µl	100 µl
	LA	-	45 µl	75 µl	115 µl
25ML	7.5% NaHCO3	1150 µl	750 µl	450 µl	300 µl
	NaOH	-	40 µl	75 µl	90 µl
	LA	-	55 µl	110 µl	140 µl
	7.5% NaHCO3	850 µl	630 µl	400 µl	225 µl
	NaOH	-	35 µl	70 µl	97 µl
	LA	-	40 µl	90 µl	100 µl
30ML	7.5% NaHCO3	970 µl	580 µl	285 µl	200 µl
	NaOH	-	35 µl	70 µl	95 µl
	LA	-	42 µl	60 µl	42 µl
	7.5% NaHCO3	1050 µl	735 µl	420 µl	270 µl
	NaOH	-	60 µl	100 µl	130 µl
	LA	-	40 µl	120 µl	140 µl
	7.5% NaHCO3	820 µl	590 µl	390 µl	270 µl
	NaOH	-	30 µl	60 µl	100 µl
	LA	-	60 µl	90 µl	120 µl
	7.5% NaHCO3	765 µl	550 µl	440 µl	255 µl
	NaOH	-	35 µl	85 µl	115 µl
	LA	-	13µl	40µl	100 µl
80ML	7.5% NaHCO3	3410 µl	2220 µl	1160 µl	600 µl
	NaOH	-	180 µl	260 µl	320 µl
	LA	-	180 µl	310 µl	370 µl

Table 2 *shows different volumes of culture 1x MEM (20, 25, 30 and 80ml) and the amount of NaHCO3, NaOH and lactic acid needed to adjust the pH to (7.4, 7.0, 6.5, and 6.0). The amount of all components depends on the initial pH of the sterile distilled water used to prepare 1X culture medium.*

Medium pH	pH Before incubation	pH After incubation
7.0	7.07	6.98
6.51	6.55	6.50
6.0	6.0	5.94
7.0	7.17	7.04
6.50	6.50	6.47
6.07	6.10	6.0
7.0	7.11	7.08

Table 3 1X MEM pH reading before and after 24 hr incubation in T-25 flasks with no cells at 37^{o}C in 5% CO_2

Medium pH	pH Before incubation with RAFLS	pH After incubation with RAFLS
7.10	7.15	6.87
6.50	6.51	6.45
6.0	6.0	5.90
7.0	7.17	6.99
6.52	6.50	6.42
5.99	6.0	6.1
7.0	7.05	7.01

Table 4 1X MEM pH reading before and after 24 hr incubation in T-25 flasks with RA FLS cells at 37^{o}C in 5% CO_2

2.12 **RA FLS treatment with TNF**

Equal numbers (30,000 cells) of RAFLS cells were seeded in six T-25 flasks and incubated at 37°C in 5% CO_2. Once they reached confluence (80%–90%), the complete DMEM was removed, and cells were washed with phosphate-buffered saline (PBS). Cells were serum starved by adding DMEM without FBS and incubating the flasks for 24 hr at 37°C in 5% CO_2. On day 2, starvation medium was removed and replaced with 1× DMEM containing 5% FBS and 10 ng/ml TNF. Cells were treated for different times: 0, 30 minutes, 2 hours, 4 hours, and 24 hours with TNF. Each time point with TNF treatment had its own control (four controls for four treated FLS cultures). FLS cells were then harvested with trypsin/EDTA, and total RNA was extracted using the Qiagen spin column method (RNeasy Mini Kit). Then qPCR was performed using β-actin as a reference gene.

2.13 **RAFLS treatment with acidified medium**

RA-FLS ($1.5–2.0\times10^5$/ml) were seeded into T-25 flasks using complete DMEM medium and incubated at 37°C in 5% CO_2. When the cells reached 80%–90% confluency, the complete culture medium was replaced with serum starvation medium (1% PS, 1% LG, 1% FBS), and the cells were incubated for 24 hr. On day 2, the serum starvation medium was discarded, and the cells were washed twice with PBS. The cells were then treated with acidified culture medium at pH 7.4, 7.0, 6.5, and 6.0 (prepared as described in section 2.11) and incubated for another 24 hrs at 37°C in 5% CO_2. After incubation, the acidified culture medium was discarded, and the RA-FLS were washed twice with PBS

and harvested by using trypsin/EDTA. The cell pellets were collected in Falcon 15-mL conical centrifuge tubes to extract total RNA.

2.14 **Total RNA extraction**

Cell pellets were washed twice in PBS prior to RNA extraction by using a spin column. All reagents and columns were purchased from Qiagen (RNeasy Mini Kit, Qiagen). For RNA extraction, buffer RLT (lysis buffer) and 70% ethanol (600 µl each) were added to the cell pellet and mixed well by pipetting. Then up to 700 µl of the suspension was transferred to an RNeasy Mini spin column placed in a 2-ml collection tube, which was centrifuged for 15 seconds at ≈ 8000×g. The flow-through was discarded, and then 700 µl buffer RW1 was added to the RNeasy spin column, which was centrifuged again for 15 seconds at ≈ 8000×g. The flow-through discarded again, followed by addition of 500 µl buffer RPE to the spin column, which was centrifuged. The flow-through was discarded (this step was repeated once again), and then the collection tube was replaced by new one, and 50 µl RNase free water was added to the spin column, which was centrifuged for 2 min at 8000×g. Precision DNase (Primerdesign Ltd.) was used to eliminate gDNA contamination of the RNA prior to reverse transcription/real-time PCR. The 10× Precision DNase reaction buffer (5 µl) was added directly to 50 µl RNA, and then 1 µl Precision DNase enzyme was added. The reaction mixture was incubated for 10 minutes at 30°C for DNase treatment, followed by 5 minutes at 55°C for DNase inactivation. All extracted total RNA was quantified by using the NanoDrop spectrophotometer before the first-strand synthesis step. After quantification, all total mRNA samples were diluted at a single concentration (10 ng/µl) by following the equation below.

*[(Desired Concentration (10 ng)) / (total mRNA concentration)] * (Desired volume) =* ***X***

*X - Desired volume=****Y***

Whereas***:***

X is the amount of sample that needed to be diluted

Y is the diluent volume to be added to ***x***

2.15 **First-strand synthesis**

First-strand synthesis (cDNA) was done using the Primer Design Ltd. Precision Nanoscript Reverse Transcriptase kit. In a microtube, 1 µl each of oligo-dt, which is single-stranded sequence of deoxythymine (dT), was used for priming reactions catalysed by reverse transcriptase. The transcript was primed in the poly (A) tail of mRNA molecules, and random nonamer primers were added to 10 ng RNA template. RNAse-/DNase-free water was added to a final volume of 10 µl. The reaction was heated to 65°C for 5 min in a hot block (T100™ Thermal Cycler, Bio-Rad), and samples were then transferred directly to ice. Then, 10 µl of a mixture of nanoScript 10× Buffer, RNAse-DNase-free water, 1.0µl of 10 mM of nucleotide triphosphates mix (dNTP), and Nano-Script enzyme (reverse transcriptase enzyme) were added to the samples, which were

briefly vortexed, spun down quickly, and incubated at 25°C (room temperature) for 5 min, 55°C for 20 min, and 75°C for 15 min to inactivate the reaction then stored at -20°C.

Component	Volume for 1 reaction
RNA template	5.0µl (50ng)
Oligo-dT primer	1.0µl
Random nonamer primer	1.0µl
RNase/DNase free water	3.0µl
Final volume	10µl

Heat to 65°C for 5 minutes then immediately cool the tubes in an ice water bath.

Component	Volume for 1 reaction
nanoScript2 4X Buffer	5.0µl
dNTP mix 10mM	1.0µl
RNase/DNase free water	3.0µl
nanoScript2 enzyme	1.0µl
Final volume	10µl

55°C for 20 minutes

Heat inactivate the reaction by incubation at 75°C for 10-15 minutes

Figure 2.5 Flow chart of cDNA synthesis.

Shows tables of reagents concentration and incubation period and temperature

2.16 **Quantitative polymerase chain reaction (qPCR)**

RA-FLS mRNA was evaluated for expression of the acid sensing proteins, ASIC3, GPR4, OGR1, and TRPV1. Total mRNA from each sample was reverse transcribed into cDNA using the precision nanoscript reverse transcriptase kit (Primer Design Ltd., UK) as described above. Relative gene expression levels were determined with semi-quantitative real-time PCR using 10 µl MasterMix with SYBR Green and Rox using primers purchased from Primer Design Ltd. According to Primerdesign Ltd., all primers were designed without regards to intron-exon boundaries, as this is restrictive, and the most efficient location for the primers may not be on an exon-exon junction. However, to prevent gDNA contamination, the mRNA samples were treated with precision DNase, as described in section 2.14. A 348-well plate was used in which the final volume in each well was 20 µl and contained 10 µl MasterMix, 1 µl specific primers purchased from Primerdesign ltd , 4 µl RNase-/DNase-free water, and 5 µl cDNA. All reactions were run in duplicate.

Component	Volume
MasterMix	10 µl
RNase/DNase free H_2O	4 µl
Specific Primers	1 µl
cDNA	5 µl
Final volume	20 µl

All real-time PCR assays were run on the ABI Prism 7900HT Sequence Detection System (Applied Biosystems SDS). PCR amplifications were performed in duplicate wells using universal temperature cycles: 10 min at 95°C, followed by 40 two-temperature cycles (15 sec at 95°C and 1 min at 60°C).

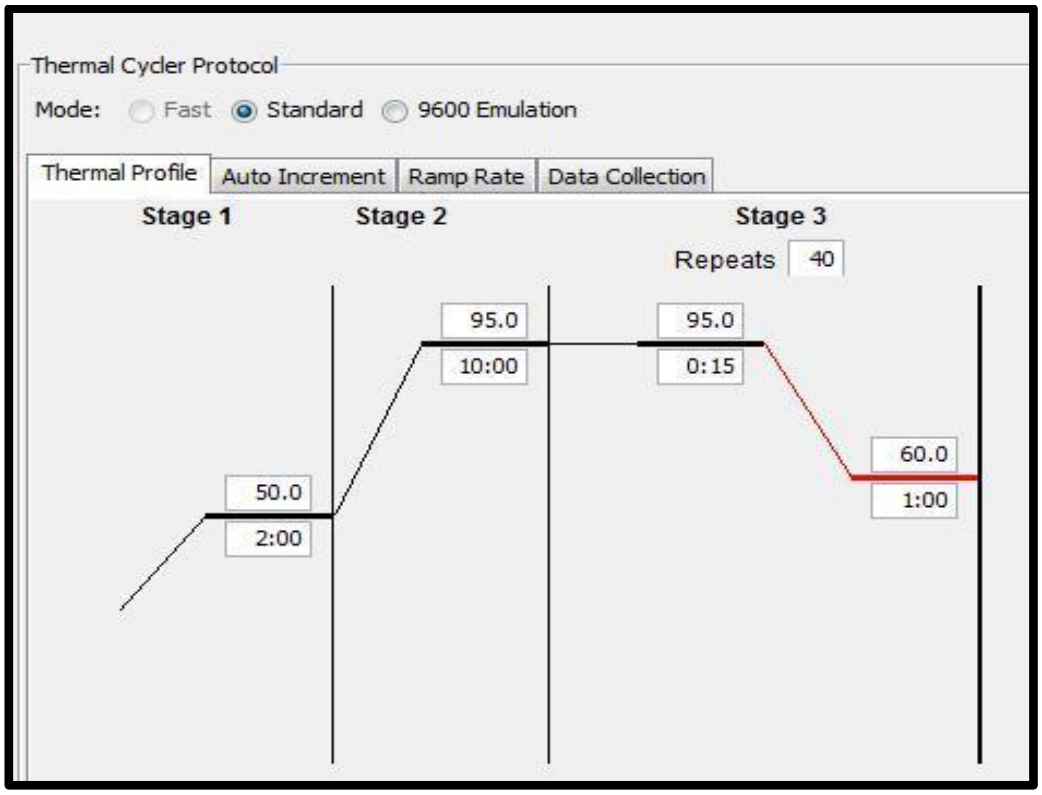

Figure 2.6 Real-time PCR standard cycles parameters.

Thermal cycles start with incubation at 50°C for 2 minutes prior to raise the temperature to initial denaturation (stage 2) at 95°C for 10 minutes followed by 40 cycles of denaturation, annealing and extension at 95°C and 60°C for 15 seconds and 1 minute, respectively (stage 3).

2.17 **qPCR raw data collection and analysis**

After each qPCR run, Applied Biosystems SDS2.4 software was used to collect raw data and analyse it using the comparative C_T method ($\Delta\Delta C_T$ method), where C_T is the point in which SYBR Green florescence exceeds the detection threshold, and the curve starts to take off (Figure 2.7). Each gene target and endogenous controls were run in duplicate and C_T values were accepted only if they were within 0.5 C_T of each other. The mRNA levels of all samples were normalized to levels of glyceraldehyde 3-phosphate dehydrogenase (GAPDH), B2M, and β-actin, as screening of all samples determined no variability in GAPDH, B2M, and β-actin expression. ΔC_T was calculated by subtraction the average endogenous control C_T value from the average of target C_T value

$$\Delta C_T = C_T \text{ target} - C_T \text{ endogenous}$$

Then $\Delta\Delta C_T$ was calculated by subtraction ΔC_T of the untreated (control) from the ΔC_T of treated

$$\Delta\Delta C_T = \Delta C_T \text{ test sample} - \Delta C_T \text{ control/untreated sample}$$

Then fold difference to the control was calculated as $2^{\wedge -(\Delta\Delta C_T)}$.

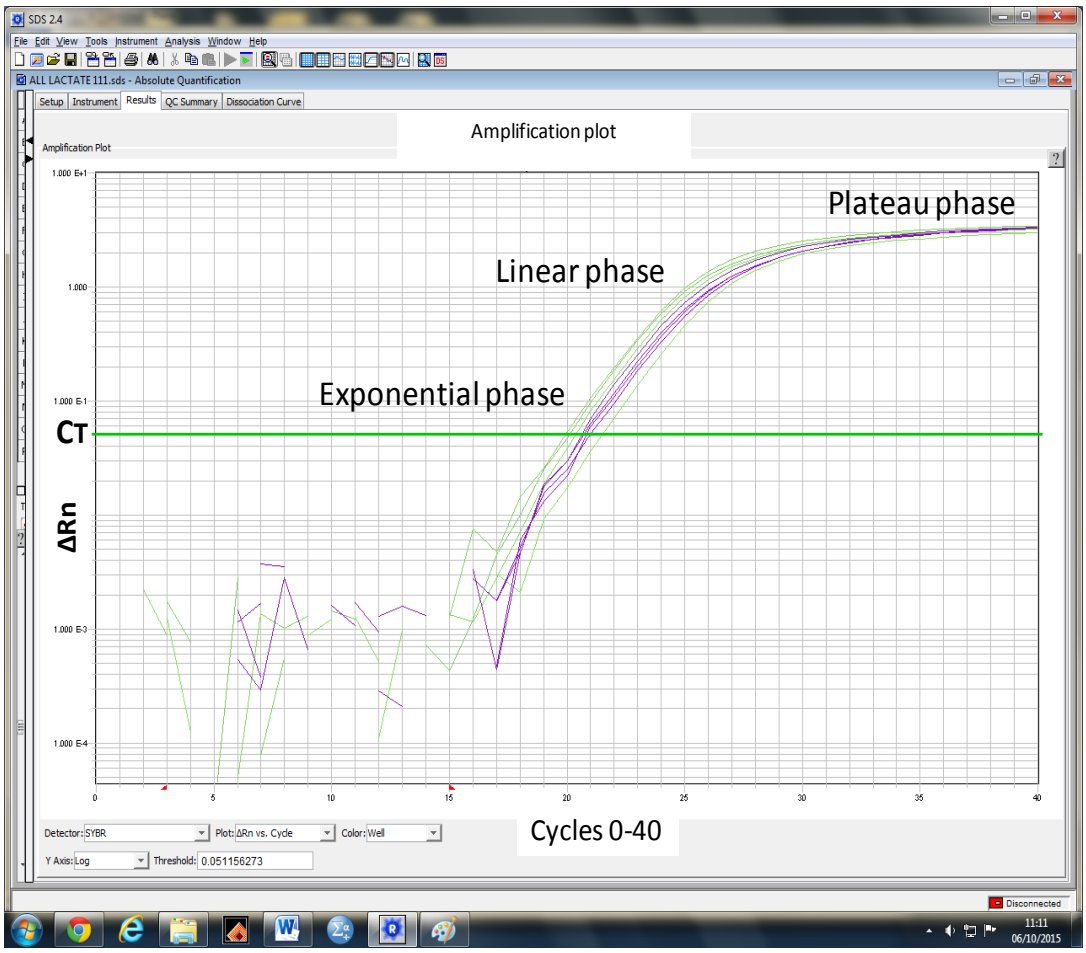

Figure 2.7 qPCR amplification phases.

CT refers to threshold cycles when fluorescent rises above the baseline, the **Exponential phase** starts when the target yields reached the detection threshold. During the amplification the amount of template increases while the concentration of DNA polymerase reduces, which in turn reduces the reaction rate, and this is called **Linear phase**. Once there are insufficient enzymes to continue amplification, the **Plateau phase** starts.

2.18 **Western Blotting (WB)**

RA-FLS (2×10^5) were washed with PBS and harvested by trypsin/EDTA. The cell suspension was centrifuged at 500×g for 7 minutes. The cell pellet was collected and washed with PBS twice then lysed by 200–400 µl Radio-Immunoprecipitation Assay (RIPA) buffer to extract total protein, and 1 µl protease inhibitor (Halt™ Protease Inhibitor Cocktail, Thermo Fisher Scientific) was added per 100 µl lysis buffer. RA-FLS lysate was incubated for 30 minutes on ice with a vortex and pipetting every 10 minutes, and then the mixture was clarified by spinning for 10 minutes at approximately 500×g at 4°C. Supernatants were collected and protein concentration was measured by NanoDrop quantification. Protein concentrations were normalised to the sample with the lowest concentration, by dilution in DNase/RNase-Free water. To denature, loading buffer with the anionic denaturing detergent sodium dodecyl sulfate (SDS) was used, and mixed with the cell lysate at ratio 1:1 then boiled at 95°C –100°C for 5–10 minutes before loading onto a 12% polyacrylamide gel (12% Mini-PROTEAN® TGX™ precast gels, Bio-Rad). Protein was loaded onto the gel (24 µg/well), and electrophoresis was performed at 120 volts for 60 minutes. Nitrocellulose membrane blotting was done by using iBlot® Gel Transfer Device for 7 minutes and then washing with TBST three times 10 minutes each. Skim milk (5%) was prepared and used as blocker. The nitrocellulose membrane was blocked by skim milk for 1 hr at room temperature. Primary mouse monoclonal antibody for β-actin (1:1000) and rabbit polyclonal antibodies for MMP-1 & MMP-9 (1:1000) diluted with the blocking solution were applied to the nitrocellulose membrane overnight at 4°C, followed by washing with TBST twice for 20 minutes, and then incubation with secondary goat anti-rabbit HRP conjugated antibodies (Abcam, ab7090; 1:1000) for 2

hours at room temperature. Then membrane was washed twice, and ECL (Amersham ECL Prime Western Blotting Detection Reagent. GE Healthcare) was added for 5 minutes in a dark place. The ECL removed by using tissue and membrane was sealed by plastic cling. Results were collected and imaged by ChemiDoc XRS+ imaging system and Bio-Rad Image-Lab software. This imaging system consists of a dark hood with a charge-coupled device (CCD) camera, which offers sensitive chemiluminescence detection. The ChemiDoc XRS+ imaging system has a signal accumulation mode (SAM) that takes a series of exposures in a set period of time to choose an image with optimal signals. Once the membrane is placed inside the hood of the device, the following steps were performed using Bio-Rad Image-Lab software:

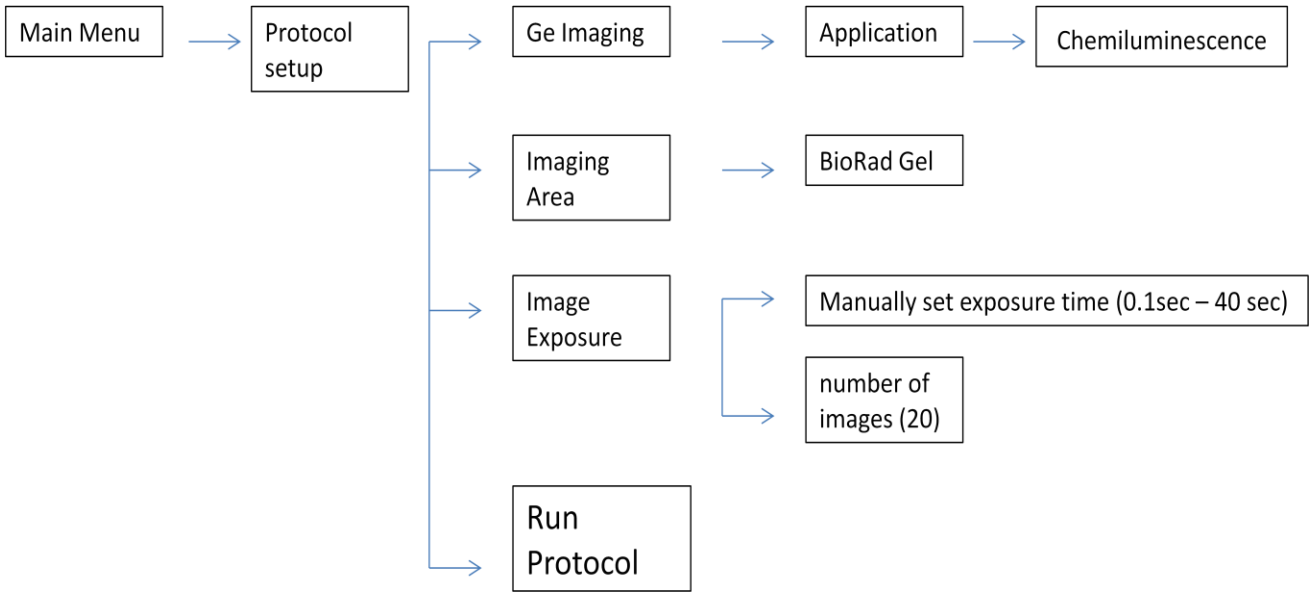

Figure 2.8 Flowchart of programming WB membrane run using Bio-Rad Image-Lab software.

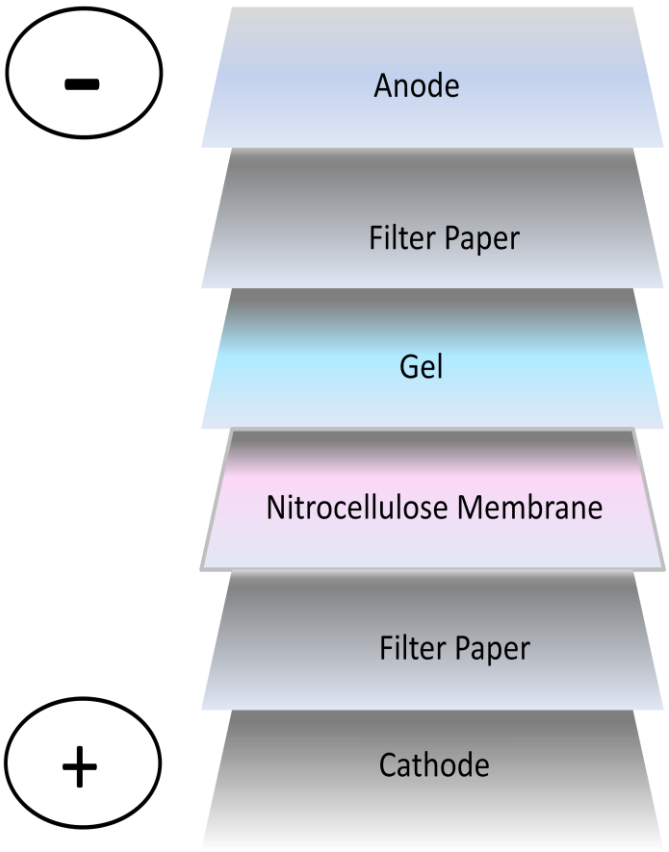

Figure 2.9 Arrangement of Western Blot transfer stack

2.19 **Migration assay 24 Trans-well plate**

RA FLS were harvested using trypsin/EDTA. Cells were re-suspended and cells were added to each of four tubes, pelleted, washed twice with PBS, and re-suspended in serum-starved acidified 1× MEM medium at pH 7.4, 7.0, 6.5, or 6.0. In 24-well plates, 700 µl of acidic MEM with 10% FBS, pH 7.4, 7.0, 6.5, or 6.0, was added to the wells, and then cell culture inserts with pore size of 8.0 µm (Falcon, 353097) were applied. Two hundred microliters of acidified serum-starved MEM containing 2.5×10^4 RA FLS cells were added into inserts. Cells in MEM at pH 7.4 were used as a control.

The plates were incubated for 24 hr in a humidified tissue culture incubator at 37°C in 5% CO_2, then inserts were removed from the chamber and washed twice with PBS. Cells were fixed by submerging the insert in 4% paraformaldehyde for 10 min, washed twice by PBS, and permeabilised with 100% methanol for 20 min at room temperature, followed by two more PBS washes. Cell inserts were stained with haematoxylin or Giemsa stain for 30 min, and then washed several times with distilled water to remove excess stain. Removal of non-invading cells was done by inserting a cotton tipped swab and gently scrubbing the upper surface of the membrane quickly to avoid drying the cells adhered to the bottom surface of the membrane. Another scrubbing was done with a second cotton swab moistened with medium or PBS. Migrated cells were counted under 60× magnification. Five to 10 high power fields (HPFs) were counted to determine the average cell number migrated per HPF.

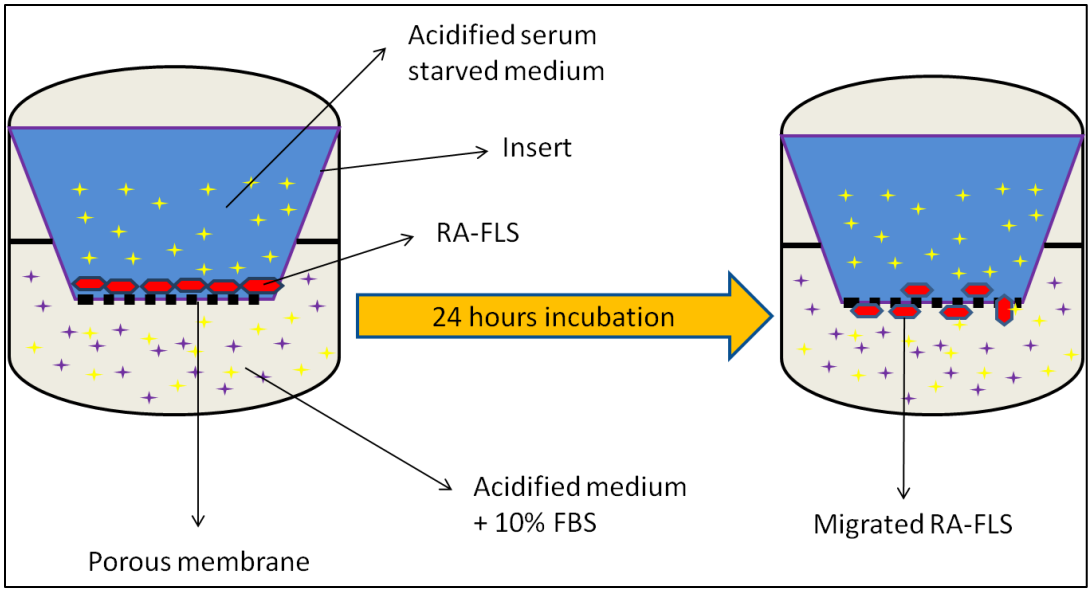

Figure 2.10 RA-FLS migration in Transwell membrane.

RAF-FLS cells were seeded in cell culture inserts with acidified serum starved medium in the upper compartment and complete acidified medium in the lower compartments followed by 24 hrs incubation at 37°C and 5% CO_2

2.20 **Migration in Oris 96 wells**

Oris 96-well plates (Platypus Technologies, LLC) were used to monitor the migration activity of RA-FLS (Figure 2.11). These plates are populated with stoppers that serve as barriers to create a cell-free detection zone in the centre of each well (Figure 2.11). RA-FLS migration was tracked by using CellTracker™ Green CMFDA (5-chloromethylfluorescein diacetate), a green fluorescent dye that freely passes through cell membranes into the cells, where it is transformed into cell membrane-impermeant reaction products. The CellTracker solution was prepared by dissolving 50 µg in 10.75 µl DMSO. Then 25 µl of the CellTracker solution was added to 10 ml 1X conditioned MEM with no FBS, and the mixture was warmed at 37°C for 5 minutes before the experiment started. Approximately 20,000 RA-FLS were seeded per well and incubated in DMEM (1% PS, 1% LG, 1% FBS) at 37˚C/5% CO_2 for 24 hours. Stoppers were gently removed, and the medium was discarded. The cells were washed twice with PBS, and then 100 µl cell tracker mixture (prepared as mentioned above) was added per well and incubated at 37°C/5% CO_2 for 30 minutes. The medium with CellTracker solution was then removed and replaced with acidified medium (1% PS, 1% LG, 1% FBS) with or without APETX2 and AMG 517, as shown in Figure 2.10. The day 1 image was taken, and then the plates were re-incubated. On day 2, images were taken, then the medium of day 1 was removed and replaced with new filtered acidified medium (1% PS, 1% LG, 1% FBS) with/without inhibitor, and then the plate was incubated again at 37°C/5% CO_2 for another 24 hours. On day 3, the image was taken, and the medium was replaced with fresh medium, and the plates were re-incubated again for day 4. The same procedure was followed for day 4

images. Multimode plate reader (Ensight,PerkinElmer) and Kaleido 1.3 software were used to capture the images as illustrated in Figure 2.11 .

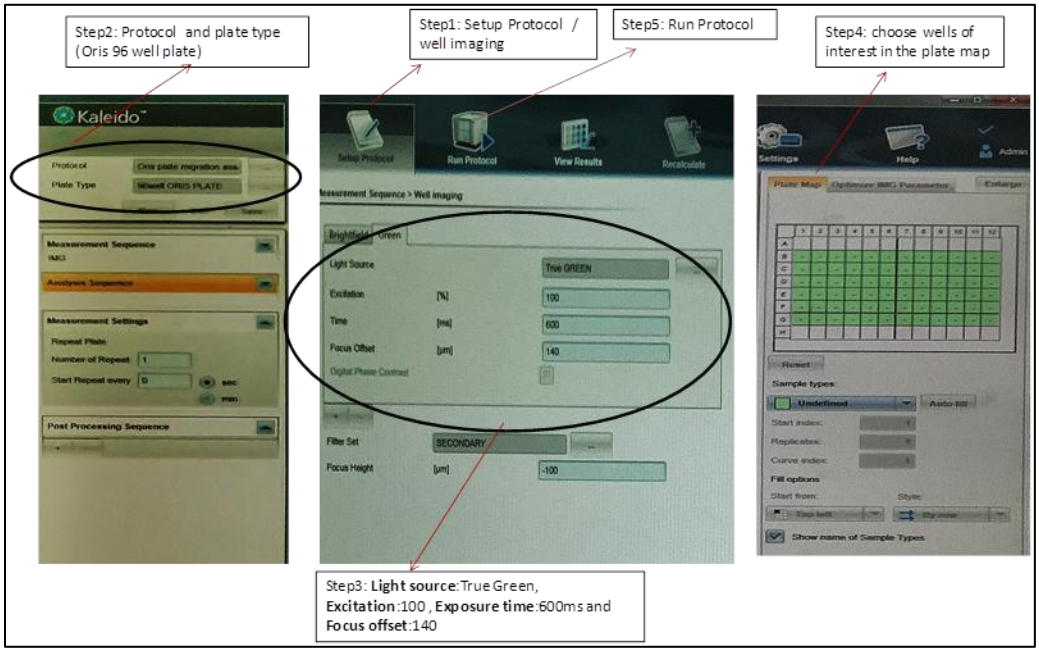

Figure 2.11 Kaleido 1.3 software

Shows the steps and settings of well imaging to analyse RA-FLS migration using Oris 96 well plate and multimode plate reader (Ensight,PerkinElmer).

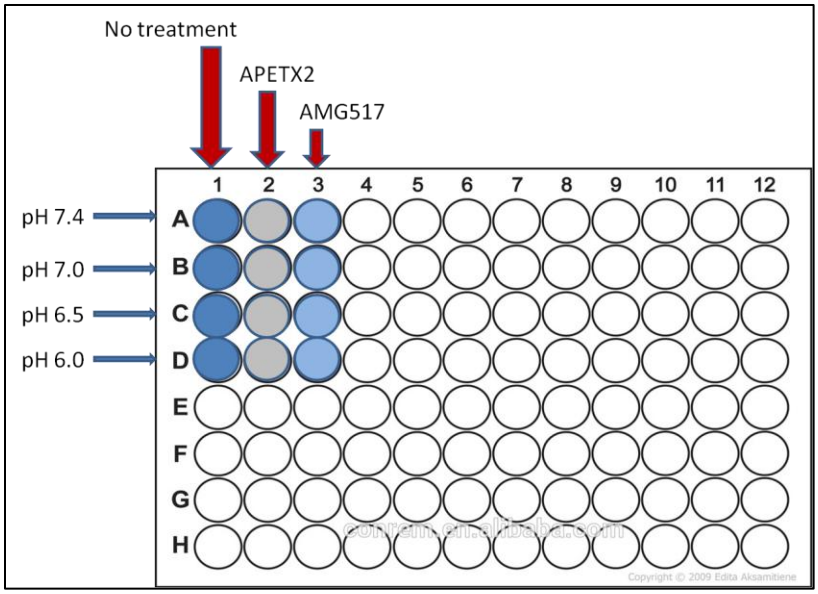

Figure 2.12 96 well plate design for RA-FLS migration experiment in Oris 96 well plate

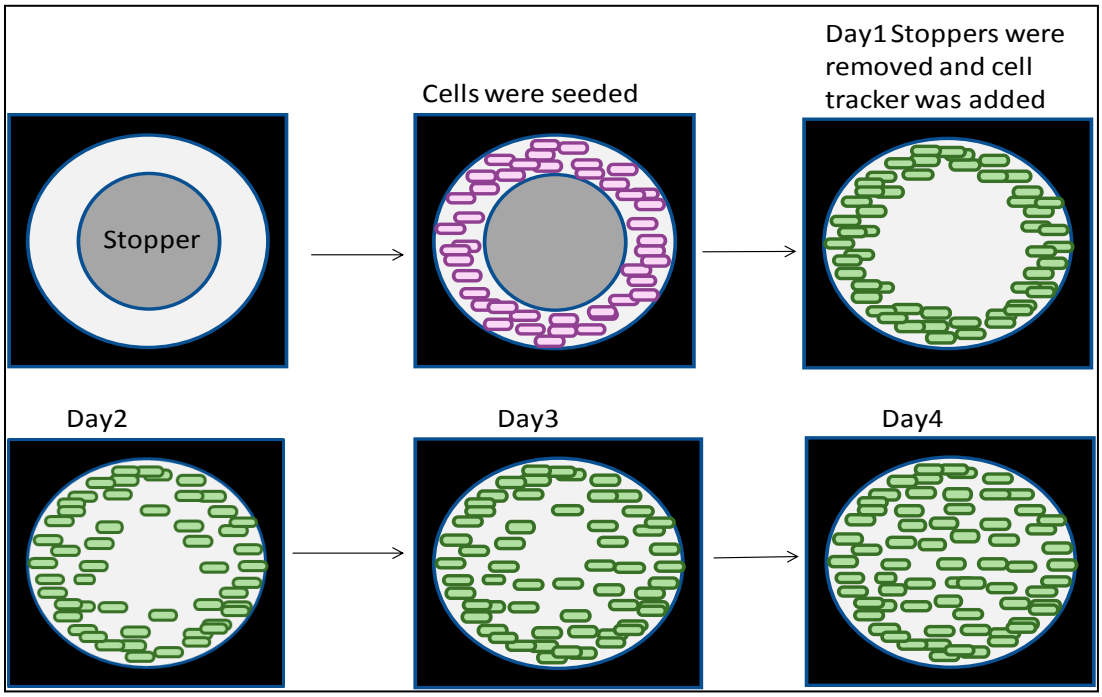

Figure 2.13 RA-FLS migration activity in Oris 96 well plate

2.21 **ASIC3 inhibition with APETX2**

APETX2 from SMARTOX BIOTECHNOLOGY (Product code**:** 07APE002-00500) was used to block ASIC3 activity. APETX2 was provided as white lyophilized solid. A stock concentration of 350 nM was prepared by dissolving 0.5 mg APETX2 in 313 ml sterilised distal water, as recommended by the supplier. The suspension was mixed well by vortexing and pipetting and then stored at -20°C. IC50 value of 175 nM was indicated for homomeric human ASIC3 channels inhibition (Diochot et al., 2004).

To prepare a 175 nM APETX2 solution, 0.5 ml MEM (10×) was transferred to a 25-ml Falcon tube, and then 2.5 ml of 350 nM APETX2 (dissolved in sterilised distilled water) was added. The total volume was increased to 5 mL, and the pH was adjusted (pH 7.4, 7.0, 6.5, and 6.0).

For RA-FLS treatment with 175 nM APETX2, cells were grown to 80%–90% confluency, and the complete culture medium was replaced with serum starvation medium (1% PS, 1% LG, 1% FBS). The cells were incubated for 24 hr prior to treatment with APTEX2. On day 2, the culture medium was replaced with acidified medium (pH 7.4, 7.0, 6.5, or 6.0). At the same time, T-25 flasks with RA-FLS from the same donors were treated with acidified medium only (no inhibitor), as illustrated in Figure 2.12, and incubated at 37°C with 5% CO_2 for 24 hrs. On day 3 the cells were harvested by trypsin/EDTA and centrifuged at 500×g for 7 min. The cell pellet was washed twice with PBS, and then total RNA was extracted and converted to cDNA. Real-time PCR was performed to determine the expression of acid sensing proteins and MMPs in RAFLS after treatment with APETX2. Cell viability was analysed before and after treatment.

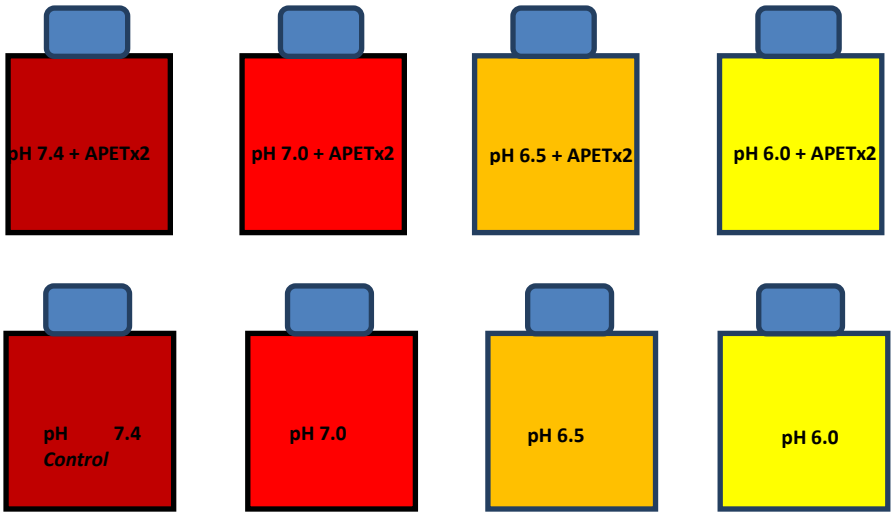

Figure 2.14 treated and untreated RA-FLS in T-25 flasks

2.22 **TRPV1 inhibition with AMG517**

A 5.0 mg potential selective TRPV1 inhibitor (AMG517) purchased from MedChem Express. A 1 mM stock solution of AMG517 was prepared by dissolving 5.0 mg AMG517 in 11.6171 ml DMSO (as recommended by the supplier) and stored at -80°C. A 250 nM solution was prepared (as a second stock solution) by adding 12.5 µl of the 1 mM AMG517 solution to 50 ml 1× MEM culture medium. It has been detected that AMG 517 inhibited acid-induced Ca^{2+} uptake into human cells expressing TRPV1 with IC_{50} values of ≈ 0.75 nM (Gavva et al., 2007),

For the 0.75 nM AMG517 solution, 15 µl of the 250 nm stock solution was added to 5 ml acidified medium (pH (7.4, 7.0, 6.5, and 6.0). The RA-FLS were treated with AMG517 using the same procedure described above for APETX2 treatment.

2.23 **RA-FLS Viability assay**

RA-FLS cells were harvested after the treatment with APETx2, AMG517, and acidified medium as described in section 2.8. The cell suspension (20 µl) was mixed with 20 µl 0.4% trypan blue dye in a microtube, and 10 µl of this mixture was uploaded into counting slid insert that has chambers in both sides (each with 10 µl). Counting slide was inserted into TC20 automated cell counter; samples of each condition were run in duplicate.

3 Chapter 3: Expression and localisation of acid-sensing proteins in synovium from patients with RA

3.1 Introduction

Recent studies have identified the expression of different acid-sensing molecules in the nervous system e.g., identification of ASIC expression in the central nervous system (Waldmann et al., 1997), expression of TRPV1 in pain sensing neurons (Caterina et al., 1997). The expression of these proteins is not restricted to neurons; other studies have shown their expression in immune cells. Tong and colleagues (Tong et al., 2011) showed that all ASICs were expressed in dendritic cells. Similarly, ASIC1 and ASIC3 were detected in bone marrow-derived macrophages (BMMs) (Kong et al., 2013). Various studies of the vanilloid receptors have described the expression of TRPV1 in macrophages and dendritic cells (Linscheid et al., 2004, Toth et al., 2009, Zhao et al., 2013). In addition to these channels, G-protein coupled receptors (GPCRs), including GPR4, GPR65 (TDAG8), GPR68 (OGR1), and GPR132 (G2A), have been investigated for their involvement in cancer cell proliferation, apoptosis, metastasis, angiogenesis, immune cell function, and inflammation (Ludwig et al., 2003, Singh et al., 2007, Yang et al., 2007, Mogi et al., 2009, Castellone et al., 2011, Chen et al., 2011, He et al., 2011, Ren and Zhang, 2011, Dong et al., 2013).

RA pathogenesis is complex, and various types of immune cells are involved in the development of the disease. Such immune cells include macrophages, mast cells, plasma cells, dendritic cells, B-cells, and T-cells (Smolen and Steiner, 2003). FLS play a vital

role in the pathogenesis of RA by producing cytokines and developing an aggressive phenotype that enhances extracellular matrix invasion and joint damage (Bartok and Firestein, 2010). Because rheumatoid joints are characterised by the acidic microenvironment, the detection of acid-sensing protein expression in RA synovium and RA-FLS is essential to investigating the role of these molecules, including their response to acid and their contribution to the development of RA.

Different methods and techniques have been used to study the expression of acid-sensing proteins in fibroblast-like synoviocytes. For example, TRPV1 was identified by qPCR in synovium of RA and OA patients (Engler et al., 2007), while ASIC3 expression was demonstrated by immunohistochemistry and immunolocalisation in murine FLS (Kolker et al., 2010). GPCR sensitivity to H^+ in synoviocytes was confirmed by measuring *inositol phosphate (*IP) production using ion exchange chromatography (Christensen et al., 2005a); however, the molecular identity of this channel is unknown. Despite this progress, it is still not clear how these acid-sensing proteins are differentially expressed in RA- and OA-FLS. In this study, several different methods were used to examine the expression of the acid-sensing molecules ASIC3, GPCR4, OGR1, and TRPV1 in the FLS of RA patients at protein and mRNA levels.

3.2 **Hypothesis**

In this study, we formulated the following hypotheses:

A- Acid-sensing proteins ASIC3, GPCR4, OGR1, and TRPV1 are differentially expressed at the protein level in RA synovium.

B- Acid-sensing proteins ASIC3, GPCR4, OGR1, and TRPV1 are differentially expressed at the mRNA level in RA-FLS and OA-FLS.

3.3 **Methods**

3.3.1 Histochemical methods

Immunohistochemistry (IHC-P) is one of the most powerful techniques to study the expression and localisation of proteins in complex tissue, such as synovium. In IHC-P, the antigen-antibody interaction can be visualized by means of colour signal through light microscopy, so different colours can be used to detect the expression and localisation of different antigens. In this study, IHC-P was used to identify and evaluate the expression of acid-sensing proteins in arthroscopic biopsies from RA patients while immunofluorescence microscopy (IF) was used to localise the expression of these acid-sensing molecules in RA-FLS.

To confirm the specificity of the primary antibodies in IHC-P, positive and negative controls were used for every experiment. The positive control was lung tissue, which is known to express all antigens of interest. The negative controls were lung tissue with no primary antibodies and lung tissue stained with non-specific rabbit iso-IgG.

Paraffin-embedded RA synovium specimens (thickness = 5 μm) were run as described in section (2.5).

3.3.2 H-SCORE and statistical analysis

Immunohistochemical scoring (H-SCORE) is a valuable semi-quantitative method used to study protein expression in a complex tissue. The results of IHC-P can be evaluated for staining intensity and percentage of stained cells. Staining intensity is categorised as follows: 0 for “no staining,” 1+ for “weak staining,” 2+ for “intermediate staining,” and 3+ for “strong or dark staining.” The percentage of stained cells can be calculated as the number of cells at different staining intensities divided by total number of cells, multiplied by 100. The H-SCORE can then be calculated by multiplying staining intensity by the percentage of cells showing that staining intensity using the following equation: 1×(% of 1+ cells) + 2×(% of 2+ cells) + 3×(% of 3+ cells). The IHC H-score scale ranges from 0 to 300 based on the percentage of cells at different staining intensities. The H-SCORE was originally developed during a study of breast and endometrial carcinoma in 1986 by McCarty et al. (1986). This method combines stain distribution and stain. There are two different methods for IHC scoring. The first method is a manual procedure to count positive cells and evaluate the intensity of the stain using light microscopy. The second method is automated and is based on digital scan of IHC slides and software analysis to calculate the number of stained cells and intensities. To evaluate the expression of each acid-sensing protein of interest, manual method was used and confirmed by the automated method.

3.3.2.1 **Manual H-SCORE**

The expression of each acid-sensing protein was evaluated in synovial tissue of four different patients. Positive and negative synovium cells were counted using light microscopy (at 60×) and computer monitor for scanned slides. Five viewing fields in each slide were examined and the average was calculated. The intensity of DAB-stained cells was evaluated and divided into four categories: negative, weak positive, positive, and strong positive, with scores of 0, 1+, 2+ and 3+, respectively (Figure 3.1).

The H-SCORE was calculated as follows:

$$H\text{-}SCORE = [(Nwp/Ntotal)\times(1)]x100 + [(Np/Ntotal)\times(2)]x100 + [(Nsp/Ntotal)\times(Bingham)]x100$$

Where Nwp = Number of weakly positive; Np = Number of moderately positive; Nsp = Number of strongly positive; Ntotal = Total number negative + positive cells.

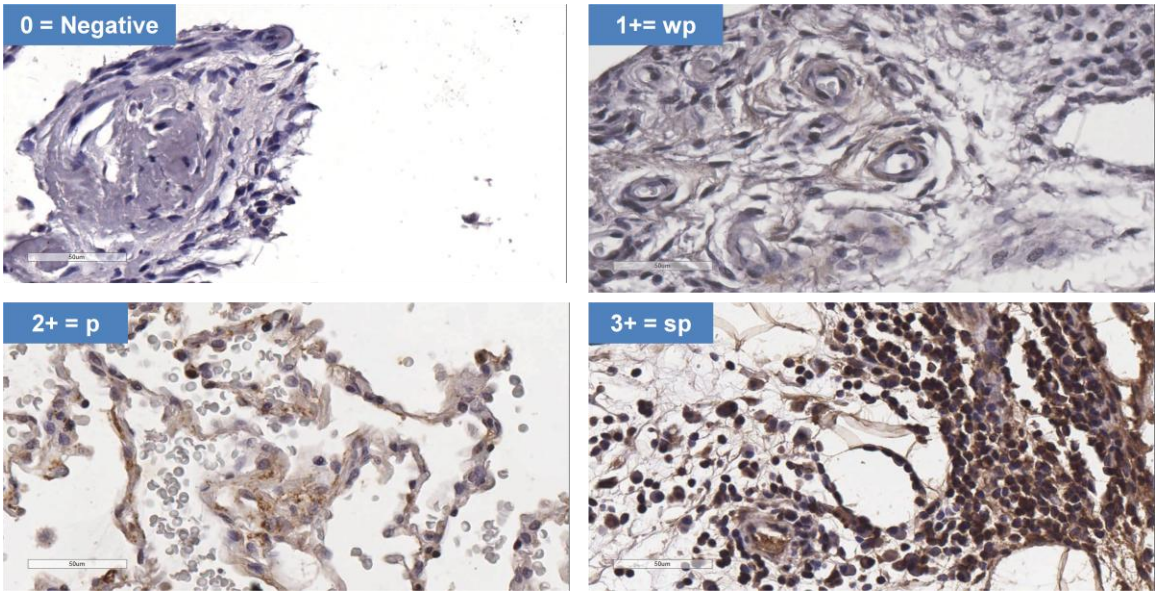

Figure 3.1 Manual evaluation of staining intensity.

The intensity of cells was evaluated as follows: 0 score or negative, (wp) = weak positive, with a score of 1+; (p) = positive, with a score of 2+; and (sp) = strong positive, with a score of 3+.

3.3.2.2 **Automated H-SCORE**

The manual method depends on visual evaluation of intensity, which may affected by perception bias due to the counter stain (Varghese et al., 2014). In contrast, the automated method is based on software analysis, which may give more accurate calculations and avoid visual perception bias. This method applies positive pixel counts and intensity algorithms to the digital image. Automated method was used to confirm the outputs of the manual method.

The IHC-P slides of lung and synovial sections were scanned using the Aperio CS2 slide scanner. The scanned slides (saved as digital images) were evaluated on the computer monitor using Aperio ImageScope to evaluate staining intensity and count the number of stained cells. The section of interest was opened as illustrated in Figure 3.2.

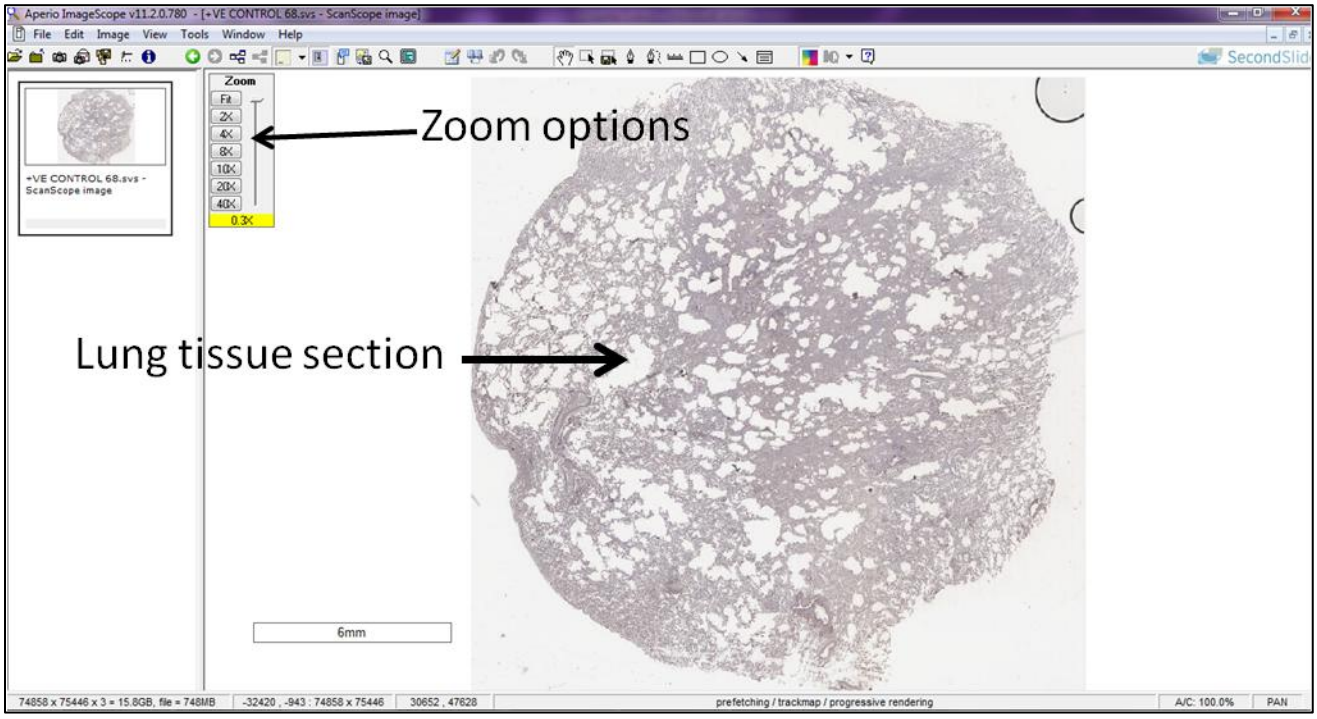

Figure 3.2 Digital scanned picture of lung tissue inspected by using Aperio ImageScope software.

Five random areas of the section were chosen at 8× magnification (300 µm), as shown below.

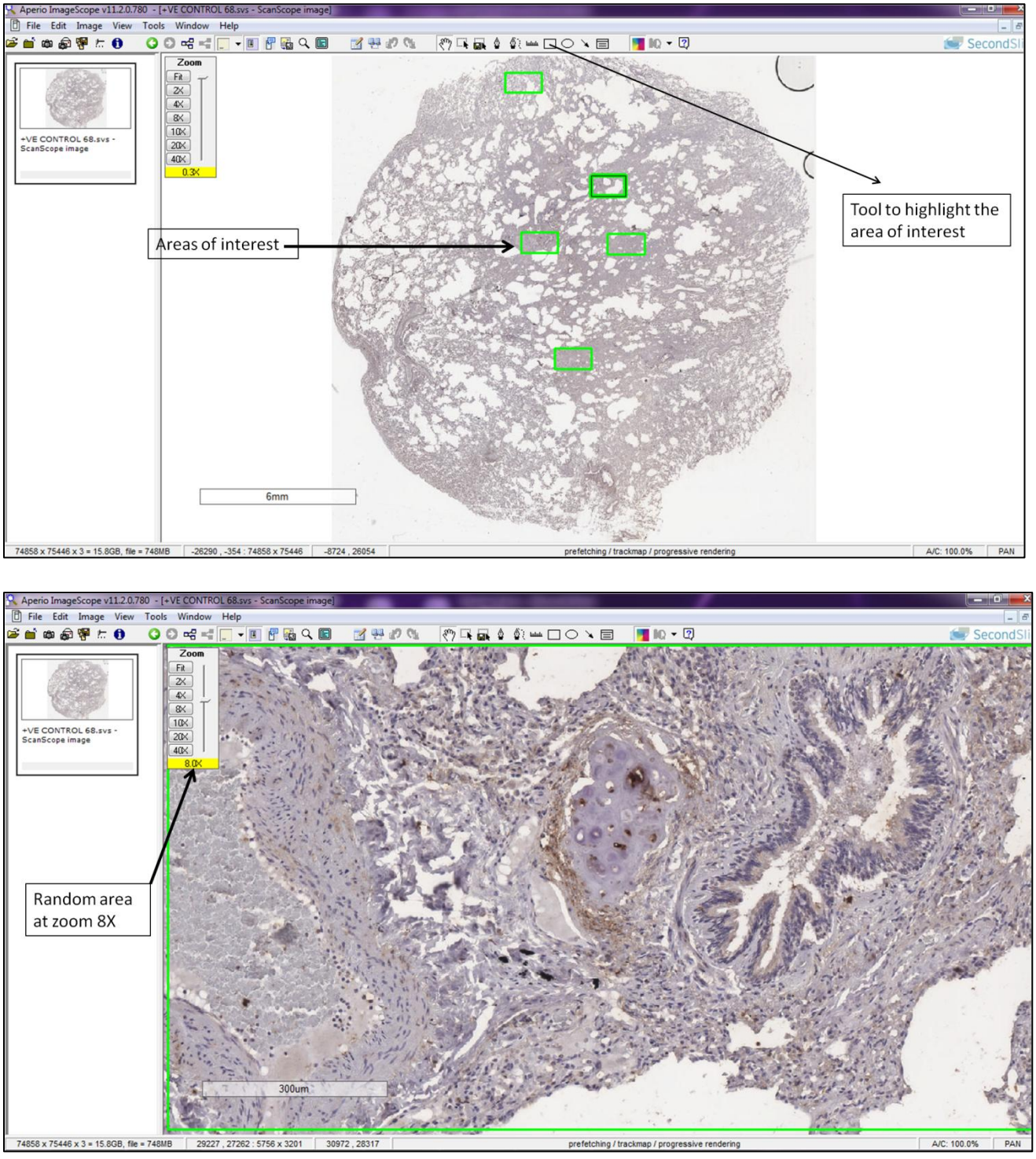

Figure 3.3 Slide analysis using ImageScope Software.
The first image shows the selected five areas to be analysed, and the second image shows an area at 8× magnification.

From the tool bar (under View), Analysis was chosen, and from the window on the right side, the region of analysis was chosen (Current Screen), and the analysis was run. Once the run was completed, Annotations was chosen to show the results of the analysed area, as illustrated in Figure 3.4. The H-SCORE we calculated using the following equation: 1×(% of 1+ cells) + 2×(% of 2 + cells) + 3×(% of 3+ cells).

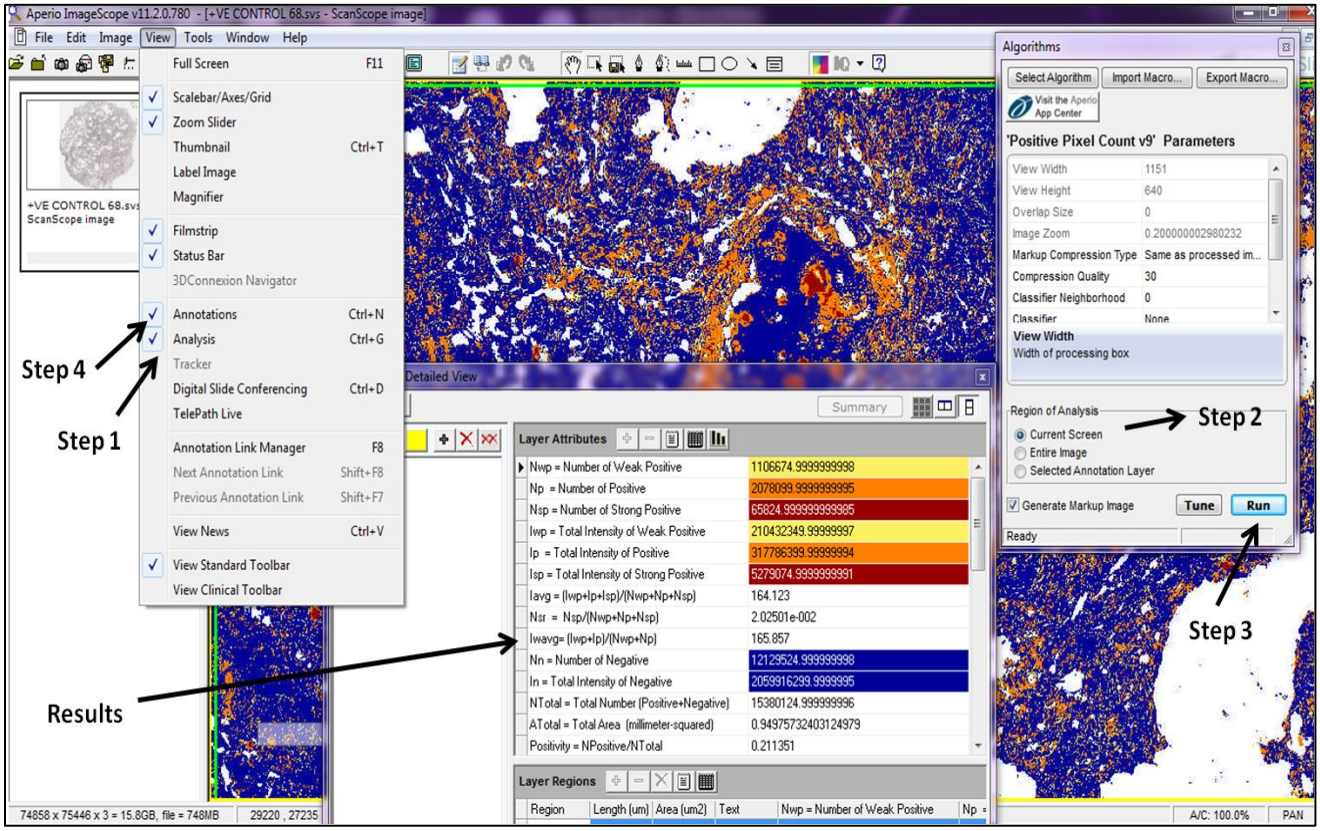

Figure 3.4 Illustrates the steps of analysis to retrieve the number of stained cells and intensities.

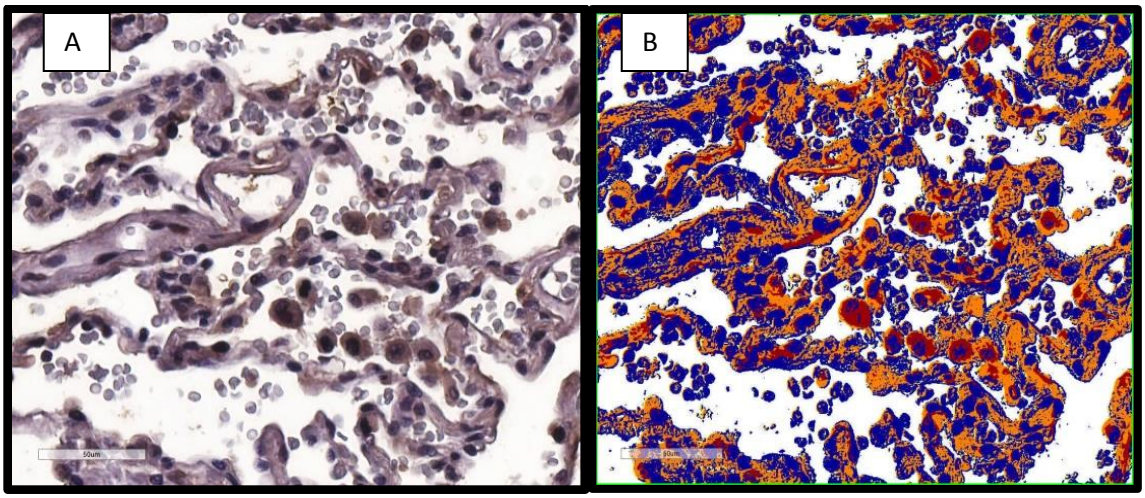

Figure 3.5 Image analysis at 40× using the Aperio system.

The different pixel colours correlate with the intensity of DAB and haematoxylin stain. Panels **A** & **B** illustrate one area of interest in lung tissue before (**A**) and after (**B)** the software analysis.

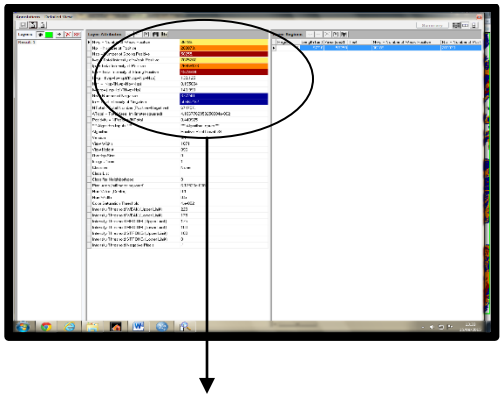

Nwp: number of weak positive	36189
Np: number of positive	203073
Nsp: number of strong positive	56055
Iwp: intensity of weak positive	7075260
IP: intensity of positive	26659123
Isp: intensity of strong positive	4979904
Nn: number of negative	377240
In: intensity of negative	50665482

Figure 3.6 Sample of the annotation result calculations.

A screen shot of the automated calculations. Yellow = number and intensity of weak positive cells (wp); red = number and intensity of positive cells (p); brown = number and intensity of strong positive (sp); blue = negative cells.

3.3.3 Dual immunofluorescence (IF)

The IHC-P results showed the expression of acid sensing proteins in the synovium without specifying cell type. Therefore, dual IF was performed to localise the expression of acid sensing proteins in RA-FLS. FLS and the protein of interest were targeted in the synovial tissue using two primary antibodies of differing species and two secondary antibodies labelled with different fluorescent dyes. Frozen tissue section were stained with polyclonal primary antibodies to ASIC3, GPR4, OGR1, TRPV1 (rabbit), or FLS (mouse) surface protein for 24 h at 4°C followed by incubation with Alexa Fluor-conjugated secondary antibodies and nuclear DAPI stain as described in material and methods section.

3.3.4 RA-FLS treatment with TNF

The 80%–90% confluent RA-FLS cells were incubated with a serum starved medium (1% FBS) for 24 hr. Starvation medium was replaced by a complete culture medium with 10 ng/ml TNF and re-incubated at different time points as described in section 2.12. RA-FLS cells were harvested as described in material and methods section prior to run real time PCR. RA-FLS without TNF treatment was used as control.

3.3.5 Polymerase chain reaction (PCR)

RA-FLS cells from different RA patients were used to measure the expression of mRNA of acid-sensing protein. RA-FLS cell cultures were treated with 10 ng/ml TNF at varying acidic pH conditions (7.0, 6.5, and 6.0). Treated RA-FLS cell cultures were compared to untreated RA-FLS pH 7.4 in this study. Quantitative real-time PCR (qPCR) was used to

determine the mRNA expression levels of acid-sensing proteins in RA-FLS under standard growth culture conditions with respect to the housekeeping genes GAPDH, B2M, and β-actin. The expression stability of these housekeeping genes was evaluated in RA-FLS by qPCR before examining the genes of interest. A master mix containing SYBR Green was used to measure cDNA amplification. The following primers were used to amplify cDNA of acid-sensing proteins:

Gene	Forward	Reverse
ASIC3	CTCCCTGCCTTAACCTT	AAGAAGCGAGAGAGAGTCAGT
GPR4	TCCACAGACCGAGCCTTTTA	CCAGAAAGCAACAGAGATAAGTAAC
GPR68/OGR1	GTGCGGCATCCTCCTGTAC	AACTGGTGGAAGCGGAACG
TRPV1	CTGGACCAACATGCTCTACTAC	AAACCCGAACAAGAAGACGAT

The reaction mixture of SYBR Green, cDNA, primers, and RNase-free water were prepared in duplicate for each sample in 384-well plates. The plate was briefly centrifuged and loaded onto to ABI 7900HT device to quantify gene of interest. SDS 2.4 software was used to set up 40 cycles of qPCR run and data collection.

3.3.5.1 **SYBR Green assessment**

SYBR Green is a non-specific fluorescent dye that will bind to any double-stranded DNA in the mixture of the reaction. It will detect primer dimers, genomic DNA, and PCR products that result from misannealed primers, which will interfere with the accuracy of the final result (King, 2010). To evaluate and assess the specificity of the primers and SYBR Green after each run of qPCR, two different methods are used. The first method is to analyse the PCR products by agarose gel electrophoresis. The presence of multiple

bands indicates contamination, while a single band that matches the predicted protein of interest size reflects a specific PCR reaction. The second, more precise method of contamination detection is a melt-curve analysis described by (Kochan et al., 2008). In this method, a high temperature 95°C is applied for one minute to denature the DNA strands and release the SYBR Green, decreasing the fluorescent signal. Then the temperature is dropped to 55°C and increased by 0.5 every 30 seconds from 55–95°C. During this process, SYBR Green will bind to any annealed DNA, and the resulting fluorescent signals are detected. A single peak reflects one product, while multiple peaks usually indicate multiple products.

3.4 **Results**

3.4.1 Acid-sensing proteins are expressed in human RA synovial tissues

The negative control (lung tissue treated with non-specific rabbit polyclonal iso-IgG) showed no staining indicative of the proteins of interest, while the positive control (lung tissue treated with specific, rabbit, polyclonal antibodies) displayed staining specific to all acid-sensing proteins (Figure 3.7). Immunohistochemistry (IHC-P) using ASIC3-, GPR4-, OGR1-, and TRPV1-specific primary antibodies showed expression of these proteins in different patterns in RA synovial tissue. All four acid-sensing proteins are distributed across the tissue and around the blood vessels, concentrated in the tissue lining as shown in Figures 3.8–3.11.

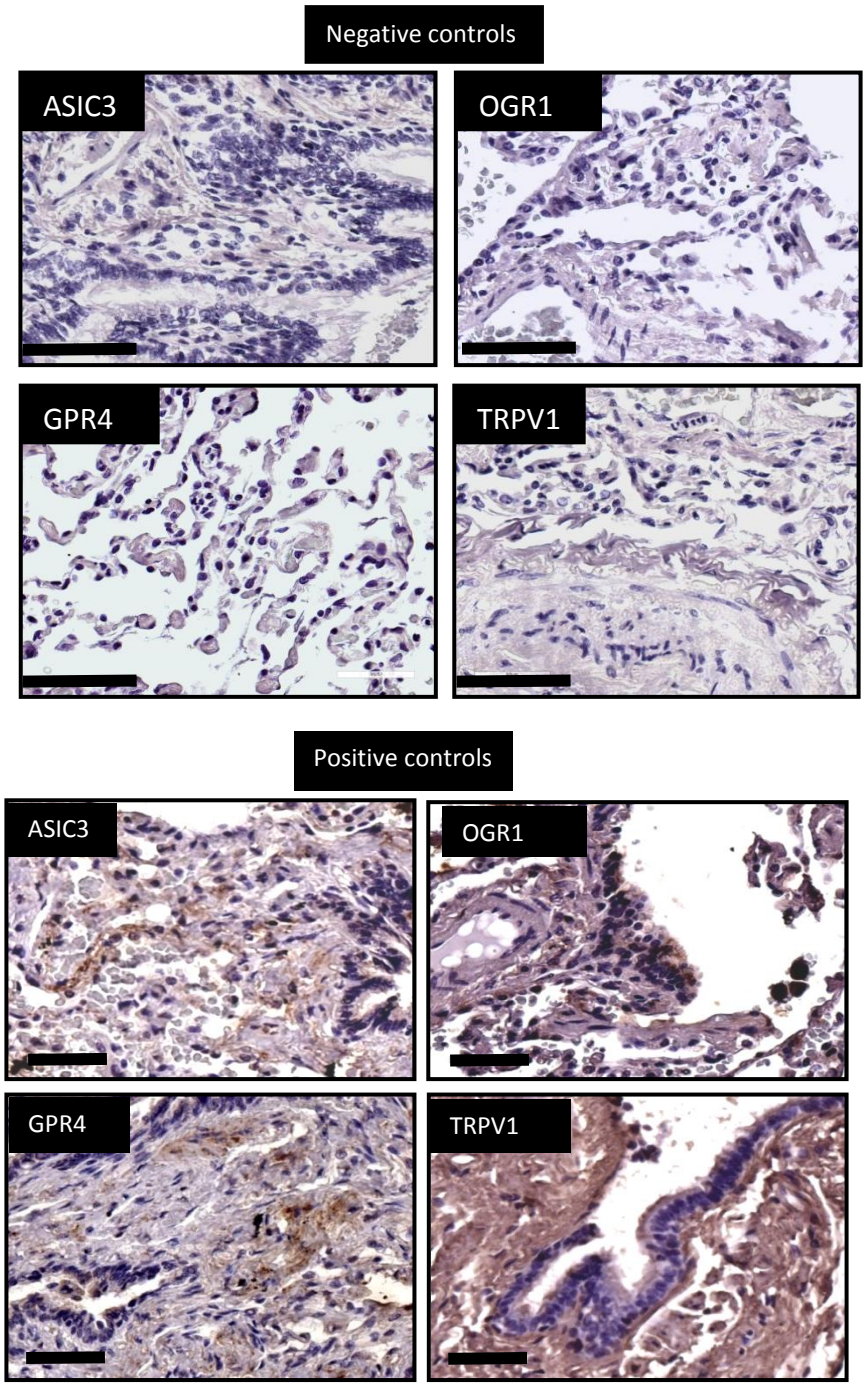

Figure 3.7 IHC-P positive and negative controls.

Lung tissue sections were used as positive controls for all four acid-sensing molecules. Lung tissues treated with Iso-IgG only were used as negative controls. DAB stain was used to indicate the expression of acid-sensing proteins (brown colour), while haematoxylin is for the nuclear staining (purple colour).

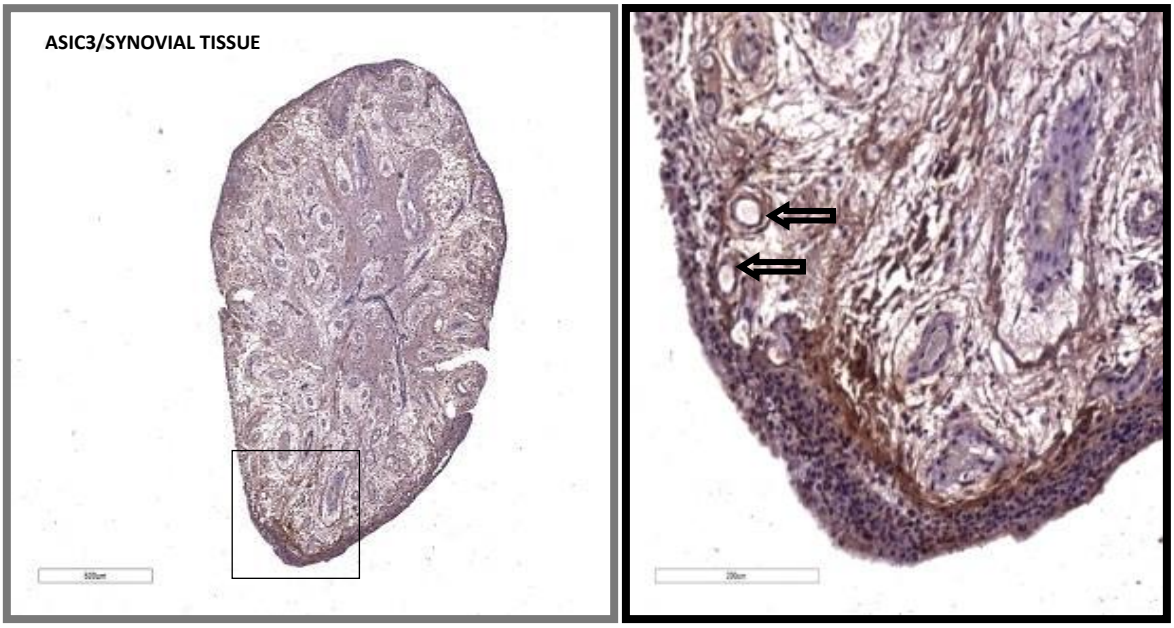

Figure 3.8 Acid-sensing ion channel 3 expression in synovial tissue.

ASIC3 was expressed around the blood vessels (arrows), close to the tissue lining. Within the tissue, ASIC3 expression was high in the fibrous regions, with clear areas around the vessels. ASIC3 was distributed over the entire tissue section, image (**A**). ASIC3 was expressed in tissue lining (4–6 cells thick) and concentrated in the inner and outer tissue lining, with moderate expression in the middle layer, image (**B**). These images are representative of four biological replicates (600 μm and 200 μm).

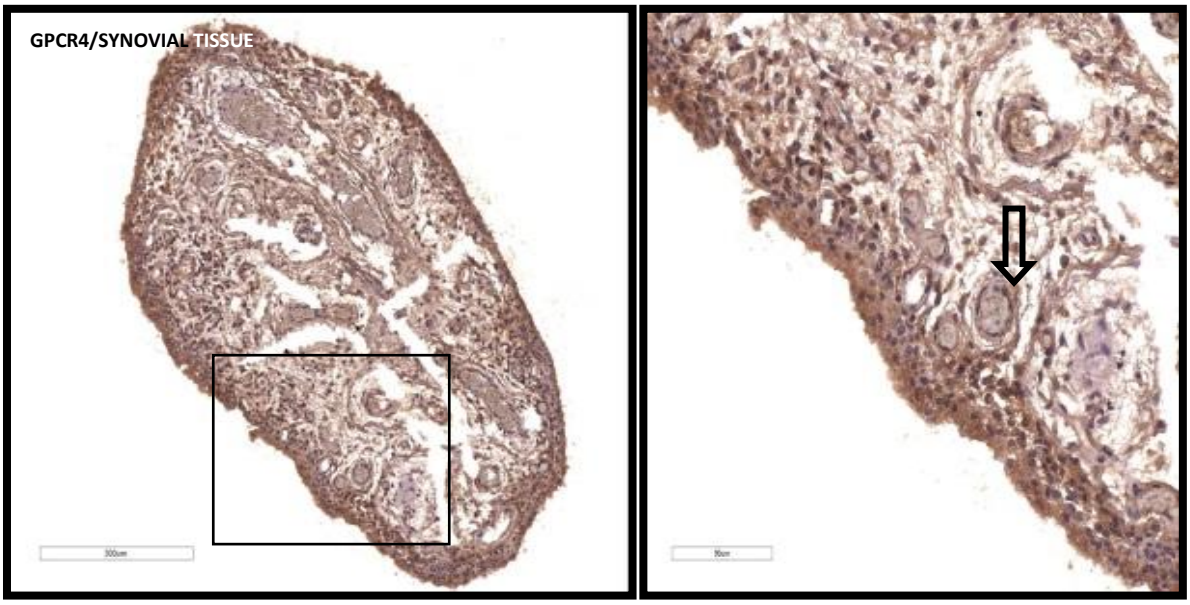

Figure 3.9 G-protein coupled receptor 4 expression in synovial tissue.

IHC-P showed high expression of GPCR4 in the outer issue lining layer, image (**A).** GPR4 was expressed throughout the synovium (**A**). Moreover, GPR4 expression concentrated around the blood vessels and distributed within the fibrous tissue between the vessels, image (**B).** These images are representative of four biological replicates (600 μm and 100 μm).

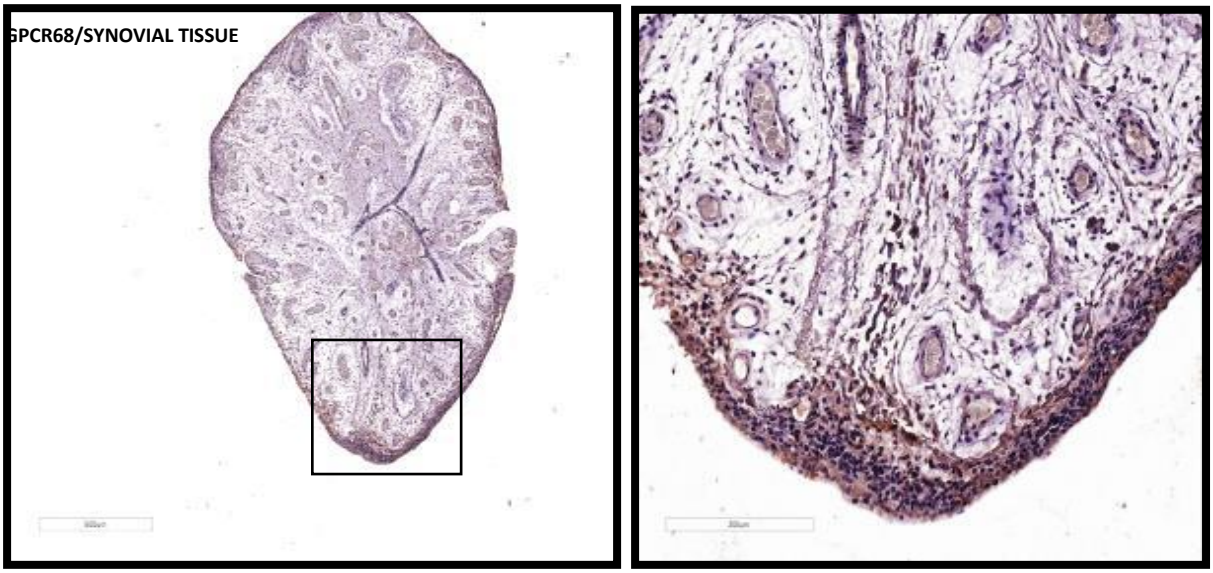

Figure 3.10 G-protein coupled receptor 68 (OGR1) expressions in synovial tissue.
GPR68 was expressed predominantly in the inner and outer layers of the synovium, with moderate to high expression in the middle layer (B). Within fibrous tissues, GPR68 was expressed in the entire arthroscopic section (A) and around the blood vessels at different concentrations (B). Weak expression was visible around some blood vessels and high expression in the outer layer of tissue lining (B). These images are representative of four biological replicates (600 μm and 200 μm).

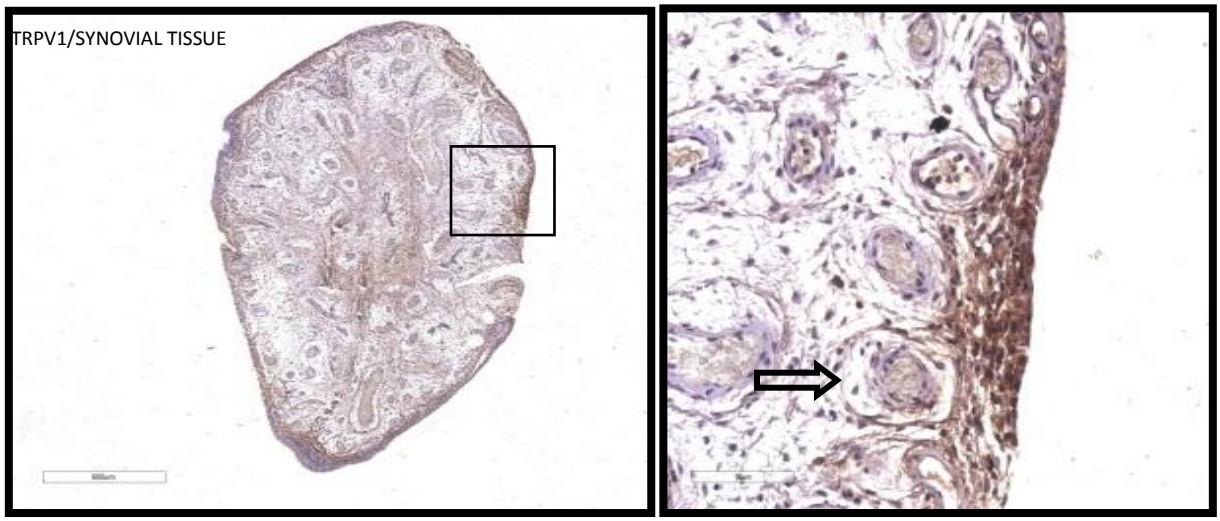

Figure 3.11 The vanilloid receptor 1 expressions in synovial tissue.

TRPV1 is expressed around the blood vessels with a clear area (1–2 cells thick) between the vessels, and highly expressed in the outer and inner tissue lining layers, image. TRPV1 expression was distributed within the fibrous tissue and around some blood vessels (arrows), concentrated in the lining **(A)**. TRPV1 expression was concentrated in the outer and inner edges of tissue lining, with low to moderate expression in the middle layer (**B)**. These images are representative of four biological replicates (600 μm and 100 μm).

3.5 **H-score of acid sensing proteins in lung tissue and RA synovial tissue**

GPR4 showed the highest expression in RA synovial tissue with a score of (211) and recorded 41% higher than its expression in lung tissue (H-score =149.5), followed by TRPV1 which is expressed 30% higher in lung tissue than in RA synovium with a score of (129). ASIC3 scored (91) in RA synovium, while the lung tissue showed 34% higher expression of ASIC3 than in synovium with score of (139). OGR1 showed lowest expression in RA synovial tissue with a score of (75) and (153) in the lung tissue, which reflects that OGR1 is expressed 50% higher in lung tissue than in RA synovial tissue. The results of acid sensing protein expression in lung and RA synovium tissue are not statistically significant. Data was calculated and analysed by GraphPad Prism 6 using two-tailed unpaired t-test.

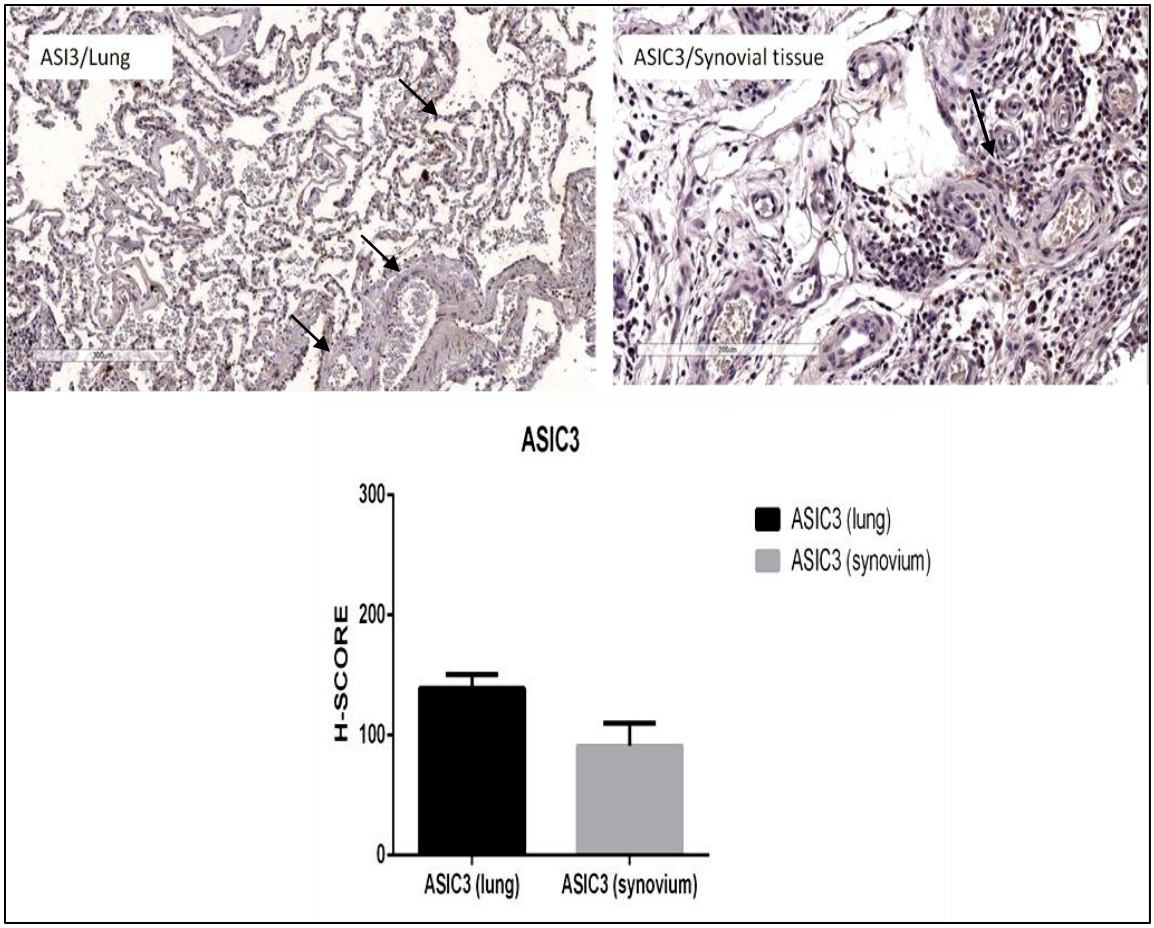

Figure 3.12 H-score of Acid sensing protein (ASIC3) in lung and tissue and RA synovial tissue.

ASIC3 is expressed 34% higher in lung tissue than in RA synovium. ASIC3 was distributed within the lung tissue including bronchioles and alveoli (arrows). The H-SCORE method assigned a value of 0–300 to each protein, based on the percentage of cells stained at different intensities using automated method by Aperio system slide scanner and analysis of five random fields (n=4).

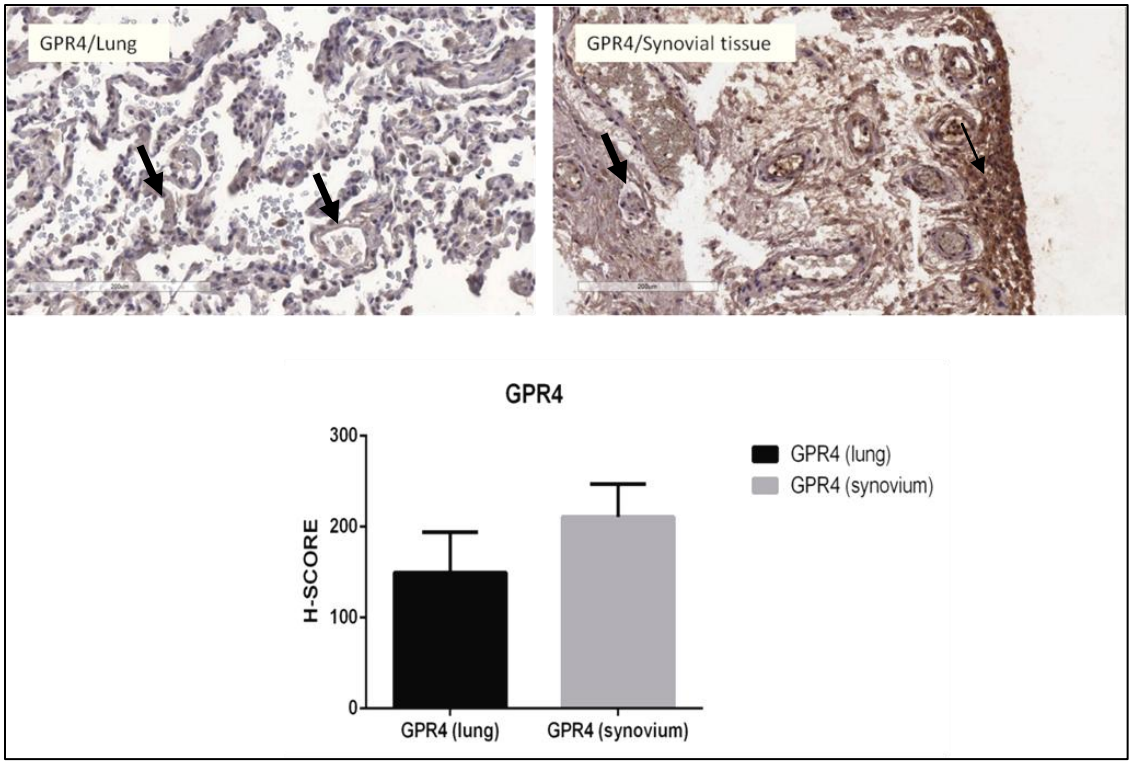

Figure 3.13 H-score of GPR4 in lung and tissue and RA synovial tissue.

GPR4 showed about 41% higher expression in lung compared to the expression in RA synovial. GPR4 was expressed within the lung epithelial tissue and around alveoli, while it concentrated in the lining of the synovial tissue with mild to expression around the blood vessels (n=4).

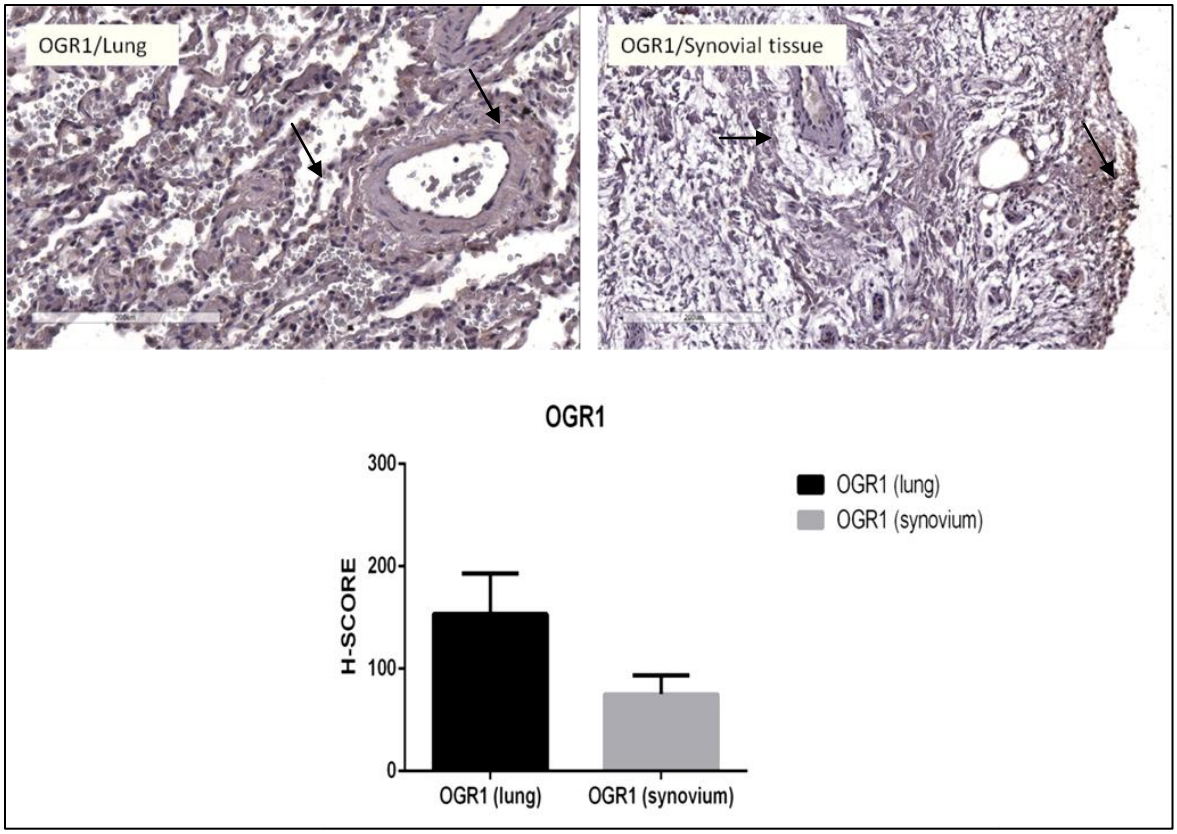

Figure 3.14 H-score of OGR1 in lung and tissue and RA synovial tissue.

OGR1 is expressed more in lung tissue than in RA synovium. OGR1 distributed within the lung tissue and around bronchioles and alveoli. While in RA synovium it is indicated in the tissue lining layers with low expression around the blood vessels (n=4).

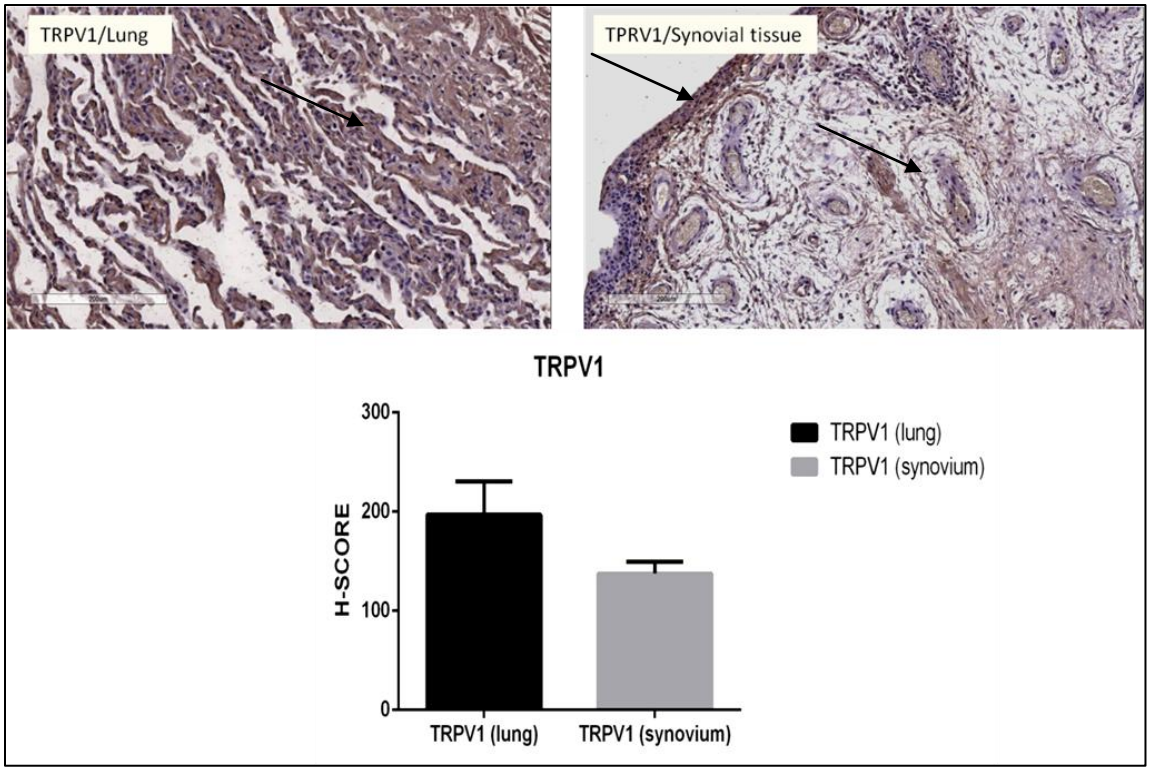

Figure 3.15 H-score of OGR1 in lung and tissue and RA synovial tissue

TRPV1 shows higher H-score in lung tissue compared to RA synovial tissue. TRPV1 expression is highly expressed within the epithelial tissue, around bronchioles and alveoli. TRPV1 in RA synovium is mildly distributed within the tissue and around the blood vessels while highly expressed in the tissue lining layers (n=4).

3.5.1 Acid-sensing proteins are expressed in RA-FLS, which reside in the synovial tissue lining

IHC-P data showed the expression of acid-sensing proteins in the synovium; however, the identity of the cells that expressed these proteins remains unknown. IF was used to determine the tissue localisation of acid-sensing proteins in synovium. These data showed that FLS reside in synovial tissue lining (Figure 3.16) A&B, with low localisation within the tissue shown in green (Alexa Fluor 488) (B). In addition, acid-sensing proteins, red (Alexa Fluor 594) co-localised with the FLS in the RA synovium. ASIC3 was expressed mainly on the cell membrane and the cytoplasm (represented by yellow colour) (Figure 3.17). GPR4 (Figure 3.18), OGR1 (Figure 3.19), and TRPV1 (Figure 3.20) were highly expressed in the nucleus (pink colour), with moderate to high expression on the cell surface and in the cytoplasm. Other types of unknown immune cells that expressed acid-sensing proteins were detected in RA synovium as illustrated by the arrow in figures (3.18-3.20).

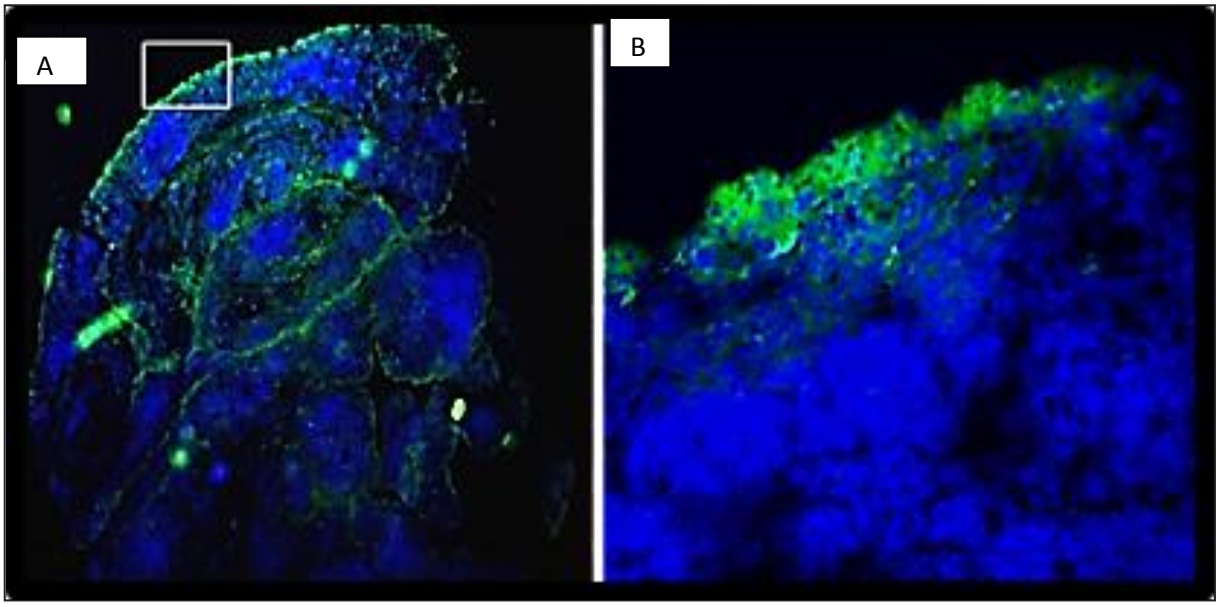

Figure 3.16 Detection of FLS in the RA synovium.

Synovial tissue was treated with nuclear DAPI stain and Alexa Fluor 488 to target the FLS surface protein, 1B10. FLS were distributed over the entire synovial tissue section **(A)**. The FLS surface protein was highly expressed in the tissue lining, where FLS reside **(B)**. These images are representative of four biological replicates.

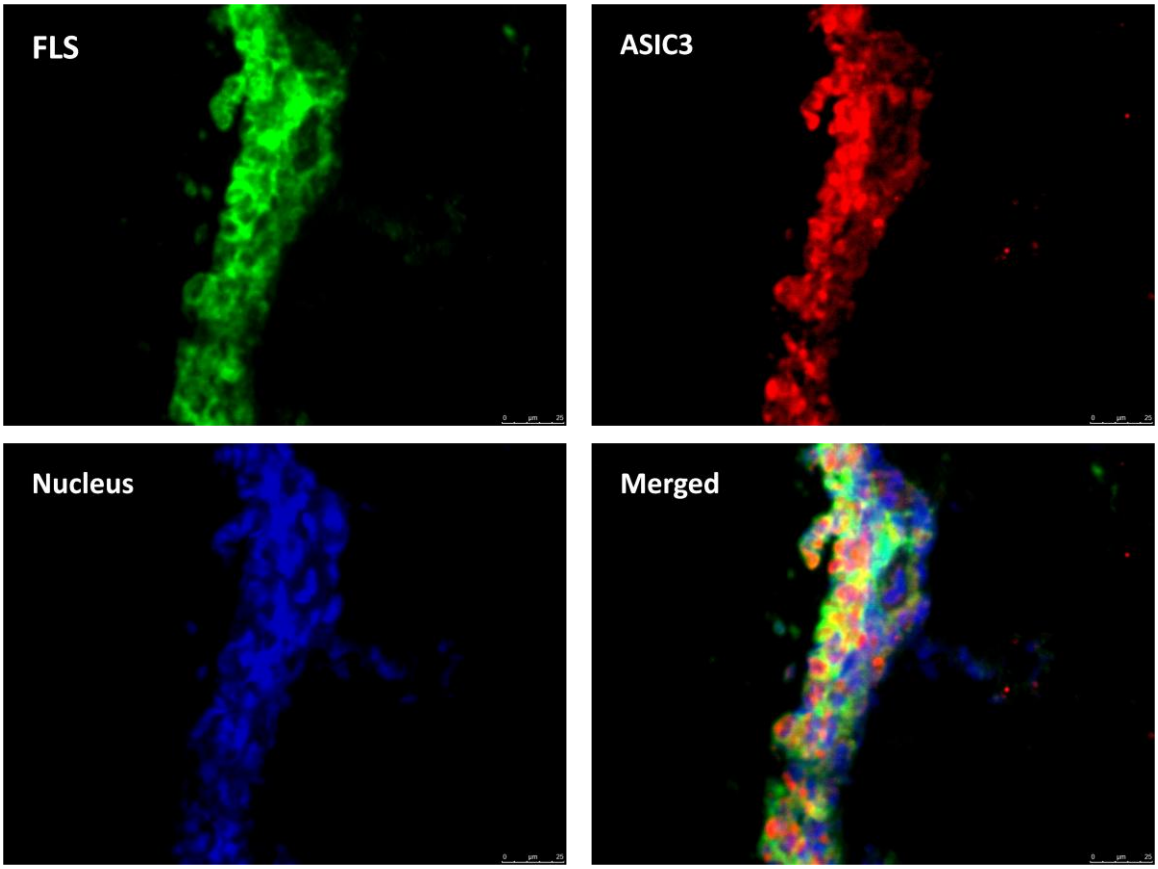

Figure 3.17 Co-localisation of the FLS surface marker 1B10 and ASIC3.

ASIC3 is highly expressed in the FLS of the RA synovial tissue. ASIC3 and FLS surface proteins are concentrated in the synovial tissue lining (yellow colour in merged image). These images are representative of four biological replicates.

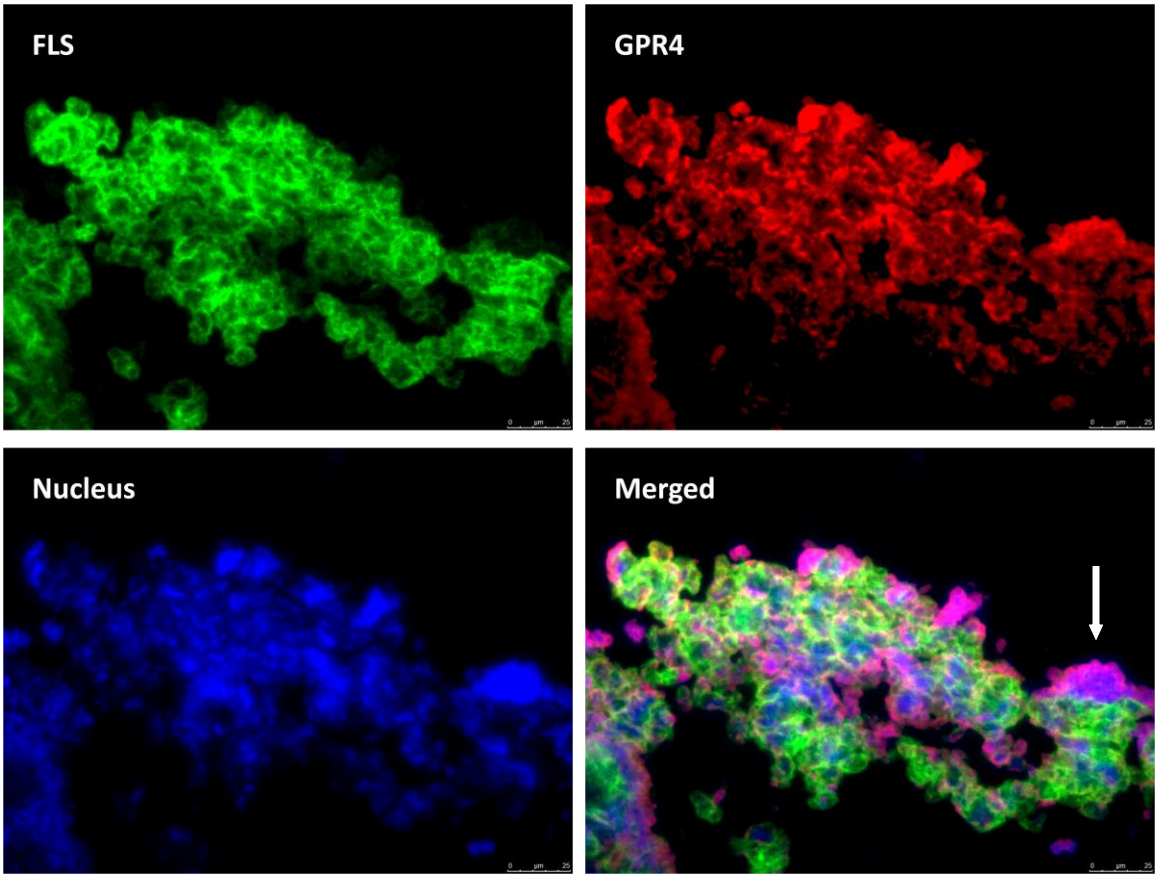

Figure 3.18 Co-localisation of the FLS surface marker 1B10 and GPR4 in RA synovial tissue.

GPR4 was expressed in the tissue lining where FLS were found, the expression is nuclear (pink colour) and surficial (yellow). Additionally, other types of cells were expressing GPR4 in the synovium . These images are representative of four biological replicates.

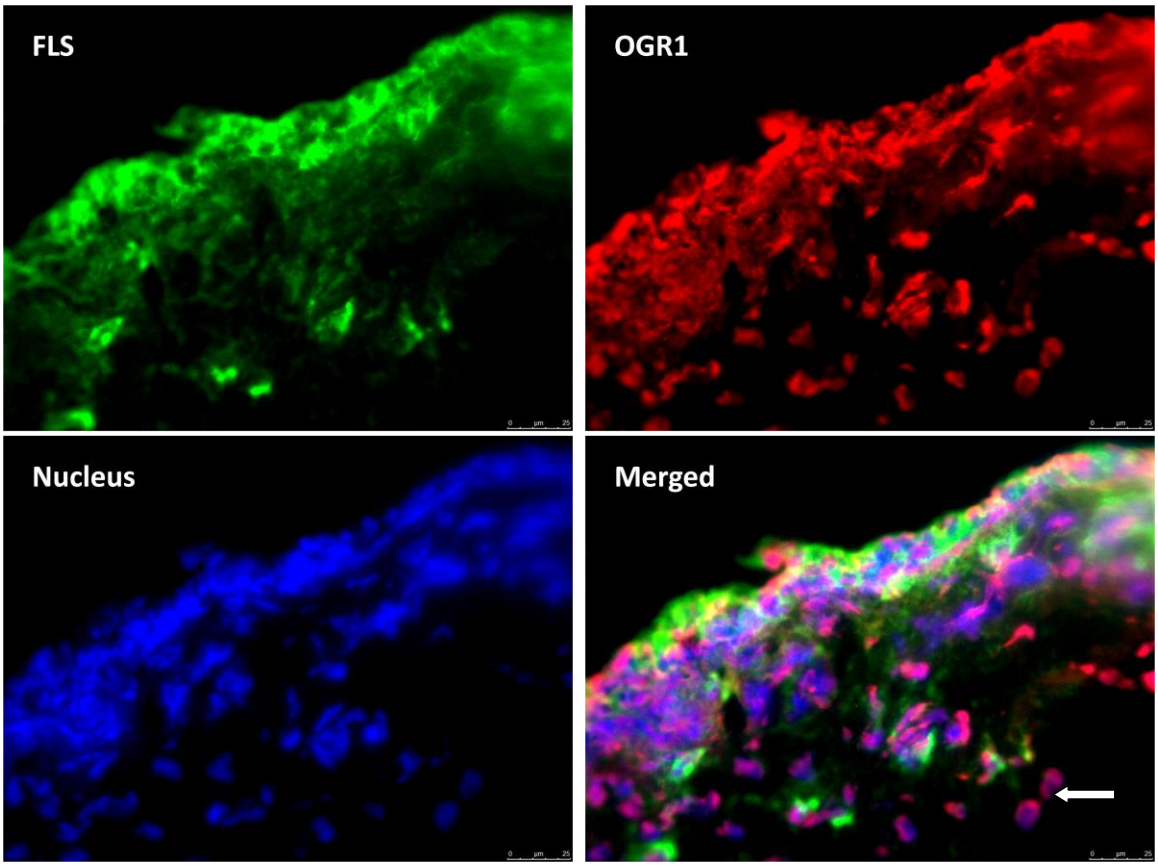

Figure 3.19 Co-localisation of the FLS surface marker 1B10 and OGR1 in RA synovium.

OGR1 (red) is predominantly expressed in the synovial tissue lining with mild expression within the synovium. OGR1 expression was detected in RA-FLS and other types of cells in the synovium as illustrated by the arrow. Co-localisation is depicted by yellow colour. These images are representative of four biological replicates.

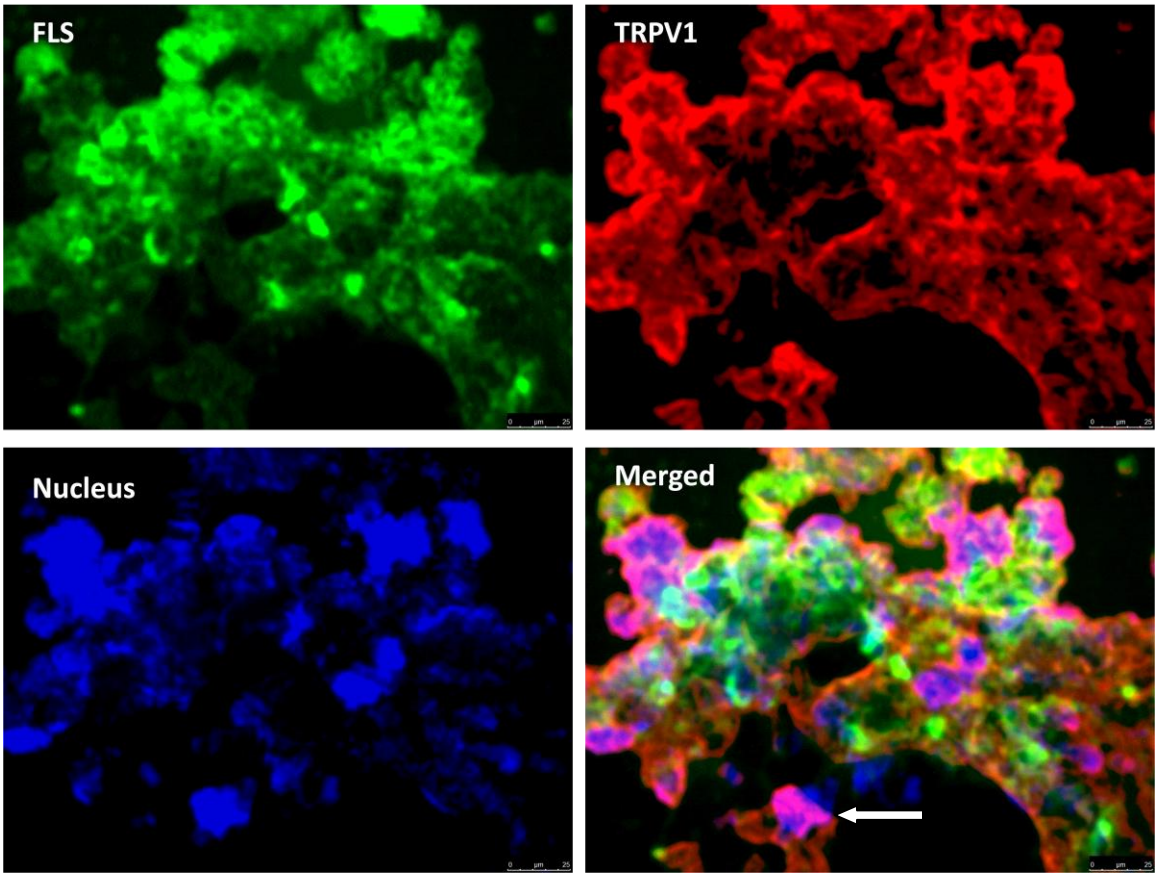

Figure 3.20 Localisation of FLS marker surface protein (1B10) and TRPV1 in synovial tissue.

TRPV1 was expressed in the tissue lining, with mild to low expression within the nuclear (pink) and surface (yellow, in the merged image) regions of RA-FLS. TRPV1 was detected in other immune cells than RA FLS in the synovium. These images are representative of four biological replicates.

3.5.2 Validation of primers for acid-sensing proteins and housekeeping genes expression by using RT-PCR reaction

According to MIQUE guidelines, qPCR efficiency is highly dependent on the validity of the primers used in the reaction (Bustin et al., 2009). To test primer efficiencies for this study, standard curves were constructed from 10-fold serial dilutions of known copy numbers of the genes of interest (Figure 3.21). The qPCR reaction efficiency was calculated with the equation: ($Efficiency = -1 + 10^{(-1/slope)}$). ASIC3 primer efficiency was 94.06%, with a calculated slope of -3.473. GPR4 primer efficiency was 94.25%, with a calculate slope of -3.468. The OGR1 and TRPV1 primer sets has efficiencies of 103.94% and 95.07%, respectively. Their respective slopes were -3.231 and -3.446. The efficiencies of the two housekeeping gene primer sets (for GAPDH and B2M) were 103.67% and 104.98%, respectively. Their respective slopes were -3.237 and -3.208. Acceptable amplification efficiencies range from 90% to 110% (D'Haene et al., 2010).

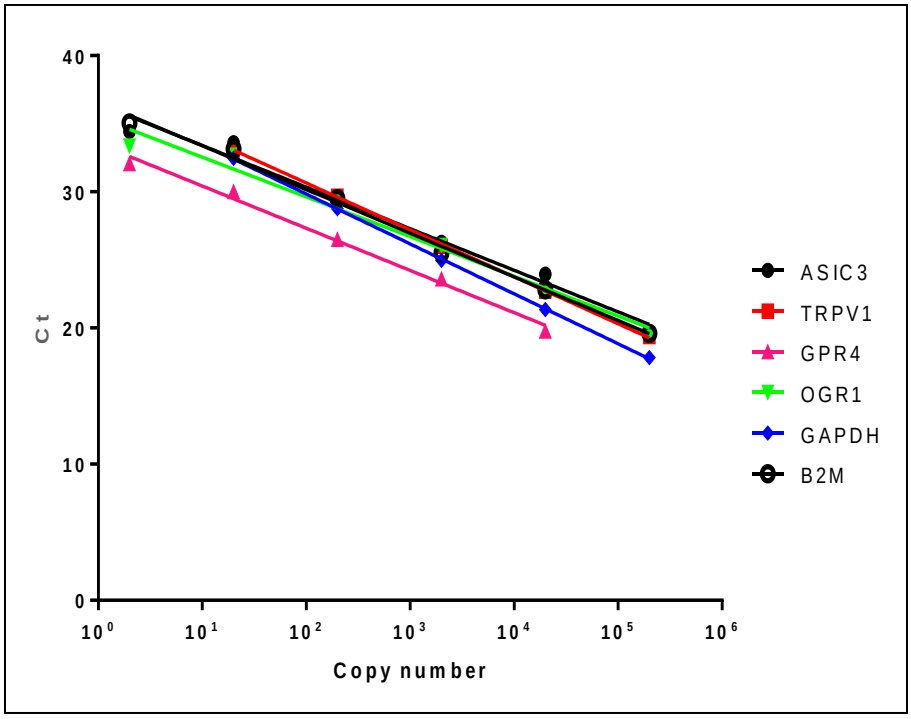

Figure 3.21 Standard curves for primer efficiency

Curves were constructed from a known copy number of genes of interest and two housekeeping genes, GAPDH and B2M. Ten-fold serial dilutions of target genes templates were assayed using real-time PCR and SYBR Green.

3.5.3 SYBR Green assessment after qPCR runs

Melt-curve analysis following qPCR shows a single peak for each amplicon (denoting the target gene). This result reflects the specificity of the primers and excludes interference from genomic DNA or primer dimers.

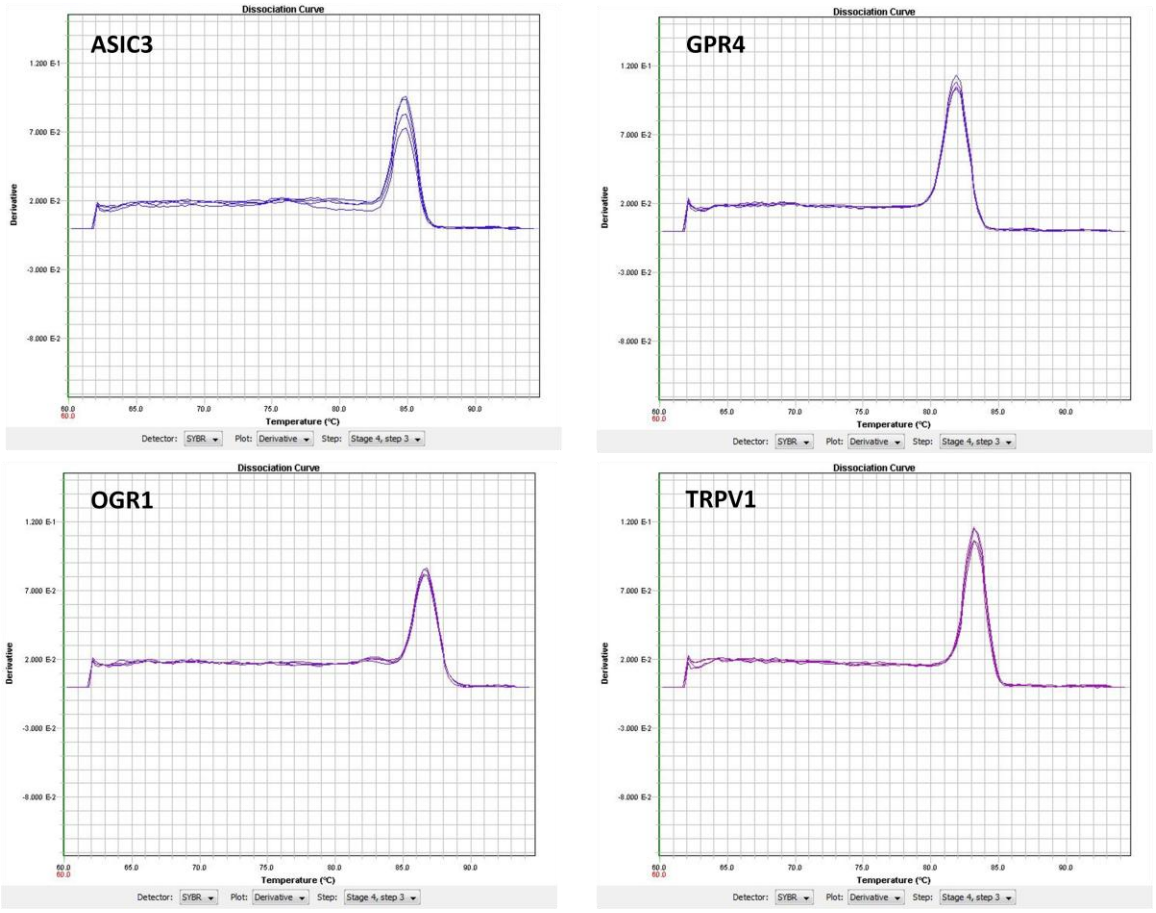

Figure 3.22 Disassociation curve results following qPCR reaction.

Each qPCR reaction was evaluated by melt curve analysis to determine SYBR Green specificity and identify any contamination with genomic DNA or primer dimers.

3.5.4 Expression of ASIC3, GPR4, OGR1 and TRPV1 in OA- and RA-FLS

All acid-sensing proteins of interest were expressed at the mRNA level in both OA- and RA-FLS. The gene with the highest expression was OGR1, with ΔC_T (-10,-12) in OA and (-5,-7) in RA FLS (Figures 3.23 and 3.24). TRPV1 was reported to have the lowest expression at mRNA in both OA and RA FLS, with ΔC_T (-15,-19) and (-11,-14), respectively (Figures 3.23 and 3.24). The ΔC_T values were calculated relatively to GAPDH. Data were collected and analysed by *SDS* 2.2 and GraphPad Prism 6 software.

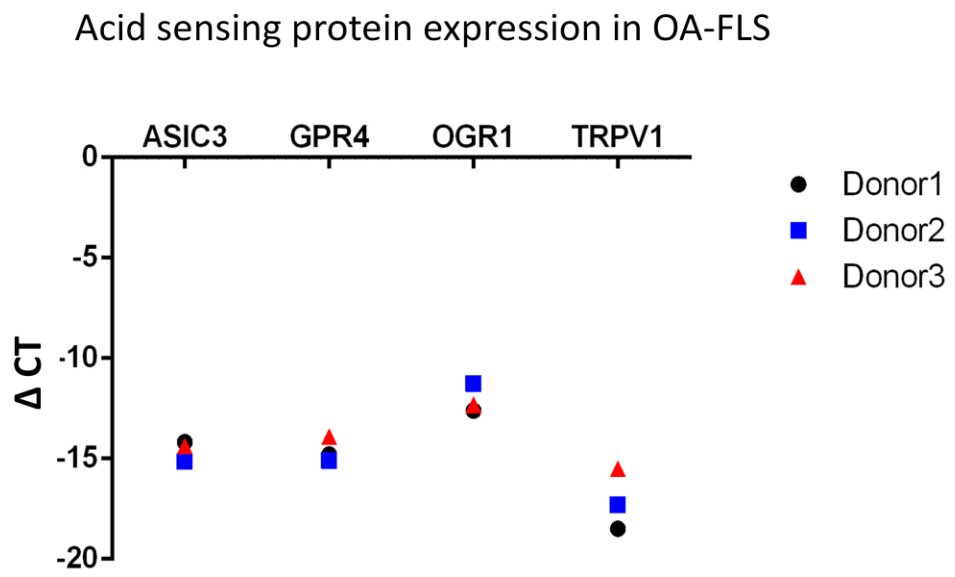

Figure 3.23 Expression of acid-sensing proteins in OA-FLS.

Total RNA was extracted from OA-FLS under normal cell culture conditions. RNA was reverse-transcribed, and cDNA for acid-sensing proteins ASIC3, GPR4, OGR1, and TRPV1 were measured using qPCR. All four acid-sensing proteins were detected at the mRNA level. Expression data are reported relative to the housekeeping gene, GAPDH (n=3).

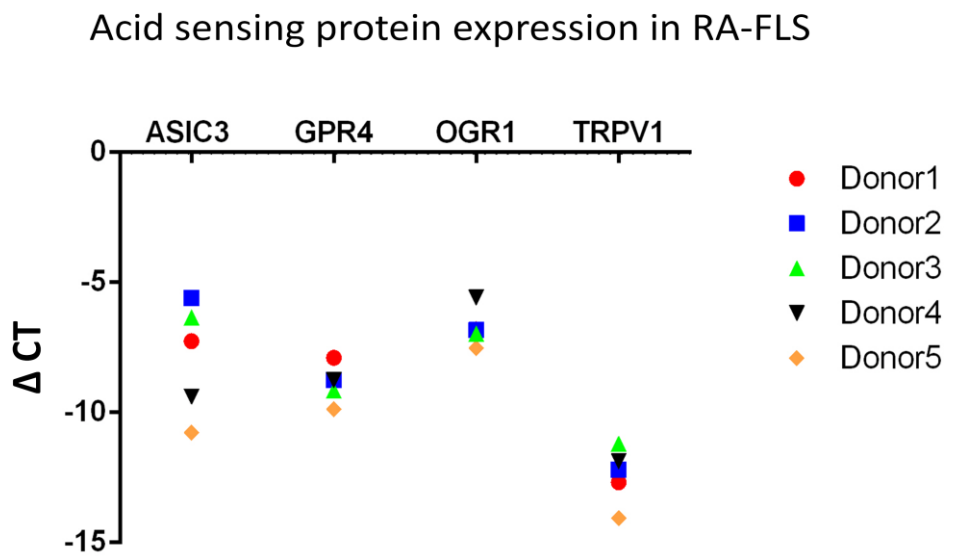

Figure 3.24 Expression of acid-sensing proteins in RA-FLS.

Total RNA was extracted from synovial FLS under maintenance cell culture conditions (described in the materials and methods section). RNA was reverse-transcribed, and cDNA for acid-sensing proteins ASIC3, GPR4, OGR1, and TRPV1 were measured using qPCR. All four acid-sensing proteins were detected at the mRNA level. Expression data are reported relative to the housekeeping gene, GAPDH (n=5).

3.5.5 Variation of acid-sensing protein expression mRNA in RA and OA

Results of qPCR showed that the expression of acid-sensing mRNA molecules was significantly higher in RA-FLS (n=3) than in OA-FLS (n=3) with $P \leq 0.0001$ (Figure 3.25). The mRNA was extracted from OA- and RA-FLS and converted to cDNA at a final concentration of 10 ng. This cDNA library was used for qPCR analysis. Averages of ΔC_T were calculated and analysed by GraphPad Prism 6 using two-way analysis of variance (two-way ANOVA) and the Sidak's multiple comparisons test.

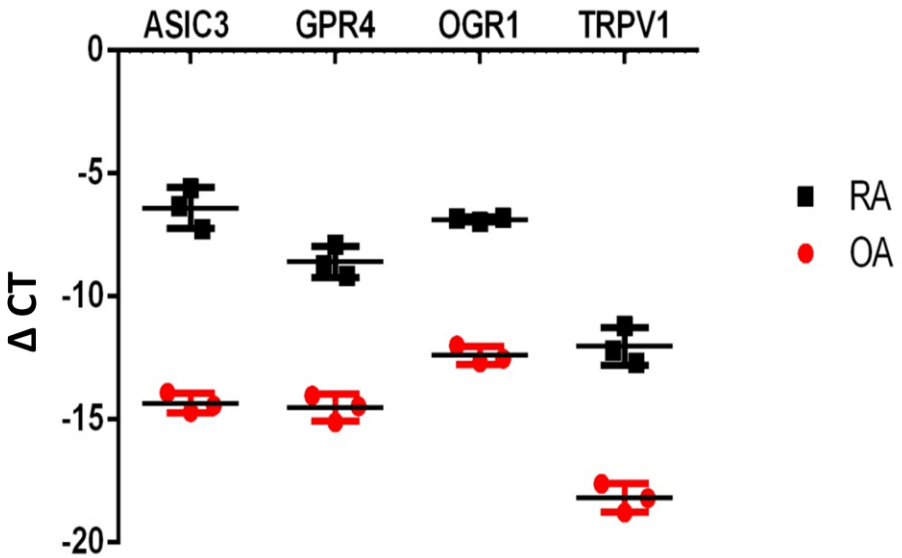

Figure 3.25 Expression of acid-sensing proteins at mRNA level in OA and RA-FLS. The data above demonstrates the variation in the expression of ASIC3, GPR4, OGR1 and TRPV1 at mRNA level in OA and RA-FLS. Data was analysed using two-way ANOVA, $P \leq 0.0001$ for all acid-sensing proteins. Data are presented as mean ± SEM. OA, n=3; RA, n=3.

3.5.6 TNF has no effect on acid-sensing proteins expression in RA-FLS

The qPCR data shows no significant alteration for ASIC3 and OGR1. GPR4 showed a slight but not significant increase after the incubation RA-FLS with 10ng/ml TNF for 24 hours. TRPV1 was insignificantly increased after 30 min of TNF and gradually reduced with the time up to 24 hrs. Data was calculated and analysed by GraphPad Prism 6 using two-tailed paired t-test.

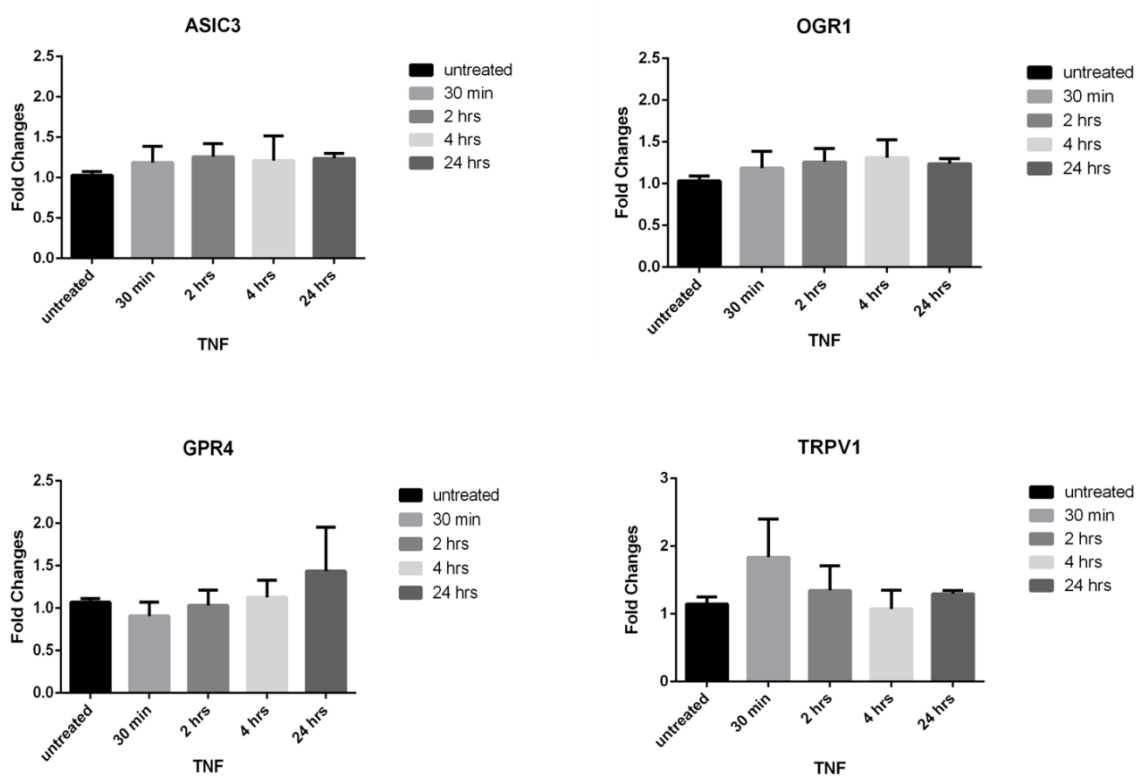

Figure 3.26 Acid-sensing protein expression in RA-FLS after treatment with TNF at different time points

The qPCR data analysis shows insignificant upregulation of acid sensing proteins (GPR4 and TRPV1) expression at mRNA level in RA-FLS treated with 10 ng/ml TNF as compared to untreated RA-FLS. Data are presented as mean ± SEM (n=4).

3.6 **Discussion**

From biopsies we have examined, our data suggest that at least four independent mechanisms for sensing acid exist in the RA synovium at the protein level. ASIC3, GPR4, OGR1, and TRPV1 were detected at the mRNA and protein levels in synovial biopsies and in RA-FLS. All four of the proteins were present in the synovial lining layer, which is where the FLS reside. However, the expression levels are varied between the proteins. GPR4 and TRPV1 were present in the majority of cells, whereas OGR1 and ASIC3 were detected in approximately one-third of cells. Moreover, ASIC3 expression in lung tissue was also detected in a previous study, which concluded that cystic fibrosis transmembrane conductance regulator (CFTR) and ASIC3 down-regulate each other and contribute to sodium reabsorption in cystic fibrosis epithelia (Su et al., 2006). Another study reported that TRPV1 activation by endogenous agonists may contribute to the induction of lung cell death (Thomas et al., 2007). Furthermore, the expression and involvement of OGR1 and GPR4 in lung were detected, and these proteins were described as inflammatory proton-sensing receptors (Tsurumaki et al., 2015). In our study we also detected the expression of these acid sensing proteins in lung tissue. The expression of these proteins (other than GPR4) was higher in the lung than in RA synovium. Specifically, H-SCORE analysis showed that ASIC3 expression was 34% higher in the lung than in the RA synovium, OGR1 expression was 50% higher in the lung, and TRPV1 expression was 30% higher in the lung. In contrast, GPR4 was the only ion channel among the proteins of interest with higher expression in RA synovial tissues (41% higher than in lung tissue).

Synovial tissue is complex and composed of different types of immune cells such as FLS, macrophages, and dendritic cells. The IF analysis shows that FLS cells are highly concentrated in RA-synovial tissue lining (Figure 3.16), where all four acid-sensing proteins are presented. Localisation of acid-sensing proteins in synoviocytes is varied. ASIC3 is expressed mainly on the surface and in the cytoplasm of RA-FLS, with low nuclear expression. GPR4 expression was high on the cell surface and in the cytoplasm with medium expression in the nucleus. In contrast, OGR1 and TRPV1 are expressed moderately on the cell surface and in the nucleus. Interestingly, our data showed that ASIC3, GPR4, OGR1 and TRPV1 were also expressed by other types of cells of the synovium. However, the identity of these cell types remains unknown. Previous studies have reported the expression of these acid-sensing proteins in other immune cells, such as dendritic cells (Tong et al., 2011). While TRPV1 is expressed in both macrophages and dendritic cells (Linscheid et al., 2004, Toth et al., 2009). Although this study focussed on fibroblasts like synoviocytes, the identity of these other cells expressing acid-sensing proteins in the synovium is an important future research direction. Our qPCR results show the expression of these proteins at the mRNA level in OA- and RA-FLS. All acid-sensing proteins were detected at the mRNA level; however, the abundance of these transcripts varied. For both OA- and RA-FLS, OGR1 mRNA expression was highest. GPR4 and ASIC3 mRNAs are expressed in similar abundance, followed by TRPV1, with the lowest level of expression in both OA- and RA-FLS. It has been reported that TNF induces glucose uptake and lactate production in different types of cells such as Sertoli cells, muscle cells, and adipocytes (Nehar et al., 1997, Boussouar et al., 1999, Porter et al., 2002, Remels et al., 2015). Although acidification is enhanced by TNF, our data

showed that TNF slightly altered the expression of GPR4 and TRPV1 at the mRNA level in RA-FLS; however, this effect was not significant. The expression of ASIC3 and OGR1 was not changed after TNF treatment.

By comparing IHC-P data with the expression at mRNA by qPCR, we can conclude that the expression of acid-sensing proteins is inconsistent between the protein mRNA levels. It is possible that this inconsistency is due to different types of cells that express acid-sensing proteins in the synovium, such as macrophages and dendritic cells. At the mRNA level, the expression of these proteins was investigated in only RA-FLS. Moreover, dual immunofluorescence staining of acid-sensing proteins and FLS in RA synovium showed that other, unknown cell types expressed acid-sensing proteins. Finally, synovial tissue and RA-FLS samples were collected from different patients, which may explain the observed inconsistencies.

The raw qPCR data show variation in the expression of acid-sensing proteins at mRNA level between OA- and RA-FLS. Our data indicate that the expression of ASIC3, OGR1, GPR4, and TRPV1 is higher in RA-FLS than in OA-FLS. Interestingly, the expression variation between OGR1, GPR4, and TRPV1 in OA-FLS is similar to the expression variation among these proteins in RA-FLS.

In conclusion, this histological study demonstrates that ASIC3, GPR4, OGR1, and TRPV1 are differentially expressed in the RA synovium. These acid-sensing molecules are expressed by FLS and other types of cells in the synovium. qPCR data demonstrate that the expression of acid-sensing proteins ASIC3, GPR4, OGR1, and TRPV1 is greater in RA-FLS than in OA-FLS. Thus, consistent with our hypothesis, our results show that acid-sensing proteins are expressed in RA synovial biopsies, and the genes are expressed

at the mRNA level in RA-FLS patients. Moreover, mRNA levels of these proteins are higher in RA-FLS than in OA-FLS.

4 Chapter 4: Effect of acidification on the expression of acid-sensing proteins and MMPs in RA-FLS

4.1 Introduction

The pH of tissue and blood is maintained at 7.4 under normal physiological conditions. However, various studies have shown that acidosis correlates with injuries and various diseases. For example, cerebral ischemia can drop extracellular pH to 6.3 and below (Siesjo et al., 1996), while in severe cardiac ischemia, the extracellular pH drops to 6.7 (Cobbe and Poole-Wilson, 1980, Cobbe et al., 1982). Moreover, pH 7.2 was reported in other kinds of systemic acidosis, although these examples did not have accompanying pain sensation (Sutherland et al., 2001). Finally, tumour microenvironment was described as an acidic space with pH range 5.5 to 7.0 (Vaupel et al., 1989, Gatenby and Gillies, 2004, Yan et al., 2014).

In all of above studies, lactic acid was described as the primary metabolite produced in response to low oxygen, which reduces the physiological pH of the extracellular microenvironment and enhances acidosis. The molecular identity of different acid sensors has been described in correlation with acidosis. In rat cardiac sensory neurons, ASIC3 has high sensitivity to acid pH 7.0 with a very steep activation curve when pH dropped to 6.7 (Sutherland et al., 2001). With regards GPCRs, sphingosylphosphorylcholine (SPC), lysophosphatidylcholine (LPC), and psychosine were described as agonists for GPR4 and OGR1 (Zhu et al., 2001); however, this finding has been challenged by Seuwen and colleagues, who showed that GPR4 and OGR1 are unaffected by SPC or LPC concentration (Seuwen et al., 2006). For the vanilloid receptor, research suggests that H^+

is a major participant that induces TRPV1 activity. One study has described that extracellular pH 6.7 can activate the TRPV1 channel at body temperature (37.4°C) (Jordt et al., 2000), while further acidification to pH <6.0 is needed to activate the channel at room temperature (Tominaga et al., 1998).

As mentioned in the introduction, poor blood perfusion and hypoxia lead to H^+ export and lactic acid production, which creates an acidic microenvironment in RA inflammatory joints. Recently, the effect of low pH on acid-sensing proteins activity was described. ASIC3 is permeable to Ca^{++} and activated under pH 5.5. Furthermore, the intracellular Ca^{++} concentration in FLS from $ASIC3^{+/+}$ mice was greater than in FLS from $ASIC3^{-/-}$ mice at pH 5.5 (Kolker et al., 2010). On the other hand, a second study has shown that the intracellular Ca^{++} was significantly higher in human FLS treated with IL-1B at pH 6.0 compared to FLS incubated at pH 6.0 alone (Gong et al., 2014). TRPV1 activation by capsaicin showed a significant increase in cytosolic Ca^{++} concentration in human synoviocytes at pH 7.0–7.2 (Kochukov et al., 2006). GPCRs responded to H^+ by increasing intracellular calcium mobilization at various pH conditions and induction of IP production in cultured SW982 synoviocytes, with maximum production at pH 6.8 (Christensen et al., 2005a, Kochukov et al., 2006).

The previous studies of acid-sensing molecules have been focussed primarily on identifying these molecules in RA-FLS and investigating the activities of these proteins under low pH. However, it is possible that acid-sensing protein expression may vary under different acidic conditions, in addition to the activity.

Bartok and Firestein have described FLS as potential cellular players in the pathogenesis of RA by contributing to the local production of inflammatory modulators, cytokines, and proteolytic enzymes that induce bone resorption (Bartok and Firestein, 2010). In addition, cathepsins K&L expression can be induced by cytokines, such as TNF and IL-1 (Bartok and Firestein, 2010). Another study in a severe combined immunodeficiency mouse model (SCID) has identified that reduction in mRNA expression for either cathepsin K or L in FLS reduces cartilage destruction and invasion (Pierer et al., 2003). Matrix metalloproteases were described as effective players in bone degradation. A study in 2002 investigated the expression of MMPs 1–14, 17, 19 in RA and OA patients and concluded that expression of MMP-1, MMP-3, MMP-9, and MMP-10 in FLS enhances the invasiveness of the cells (Tolboom et al., 2002). Additionally, MMP-1 and MMP-9 are expressed in both RA and OA; however, the expression of these two enzymes was significantly higher in RA-FLS than in OA-FLS (Tolboom et al., 2002). This same study concluded that MMP-3 and MMP-10 expression does not correlate significantly with RA. MMP-1, MMP-3, and MMP-13 expression has been reported in the lining layer cells, where FLS and macrophages reside (Firestein et al., 1991, Lindy et al., 1997). In addition to MMPs, a group of metallopeptidases related to ADAMs, ADAMTS-4 and ADAMTS-4, were identified at mRNA level in bovine synovium and human OA synovium (Kaushal and Shah, 2000, Vankemmelbeke et al., 2001). ADAMTS-5 proteinases may contribute in cartilage destruction in the synovium; however, the process of this breakdown is unknown (Vankemmelbeke et al., 2001). As described in main introduction, RANK and RANKL upregulation is induced by proinflammatory cytokines, such as interleukins and

TNF. These cytokines enhance osteoclast differentiation and increase rate of bone degradation rate in RA as described in the main introduction. The involvement of RANK/RANKL in bone destruction was reduced when IL-1, TNF, and IL-17 were inhibited (Page and Miossec, 2005). Despite these important finding, it is not known whether extracellular acidosis influences the expression of acid-sensing proteins or other bone or cartilage destruction modulators in RA-FLS.

4.2 **Hypothesis**

Based on the data above, we hypothesized that the acidified milieu of the RA joint alters the expression of acid-sensing proteins MMP-1, -3, -9, and -14, cathepsin K, ADAMTS-5, and RANKL at the mRNA level in RA-FLS.

4.3 **Methods**

4.3.1 RA-FLS viability after the treatment MEM acidified by lactic acid at pH 7.4, 7.0, 6.5, and 6.0

1.5×10^5 RA-FLS were seeded in T-25 flasks using DMEM GlutaMAX with 10% FBS, 1% penicillin and streptomycin, and then they were incubated in 5% CO_2 at 37°C. At 80–90% confluency, the cells were washing with PBS and placed in serum-free medium, then incubated under normal culture conditions for 24 h. Serum-starved medium was replaced with MEM acidified with lactic acid buffered to at pH 7.4, 6.5, or pH 6.0 with 10% FBS, 1% penicillin, 1% streptomycin, and 1% glutamine, and then cells were incubated in 5% CO_2 at 37°C for 24 h. After incubation, RA-FLS were harvested and

counted with a haemocytometer using trypan blue as described in material and methods section.

4.3.2 Validation of primers for MMP -1, -3, and -9, CathK, RANKL, and ADAMTS-5 genes expression by using RT-PCR reaction

Primers of bone modulator genes described in the table below were purchased from Primerdesign Ltd. The primers were designed without regards to intron-exon boundaries, as this is restrictive, and the most efficient location for the primers may not be on an exon-exon junction. However, to prevent gDNA contamination, the mRNA samples were treated with precision DNase, as described in the Material and Methods section.

Gene	Forward	Reverse
MMP-1	GCACTGGAGAAAGAAGACAAAGG	CTAAGTCCACATCTTGTCTTG
MMP-3	ATGAACAATGGACAAAGGATAC	AGTGTTGGCTGAGTGAAAGAG
MMP-9	CTTCCAGTACCGAGAGAAAGC	CAGGATGTCATAGGTCACGTAG
MMP-14	TCGCAGTCAGTCAAGTTCCT	CCCATCCAAGGCTAACATTCG
Cath K	ACTGCCTCCTTCCCTCCTC	GGGTGCTAGATTTATTCCATCGG
RANKL	AAAGATGTATATAGGTGTGTGAGACT	CTCCCACTGGCTGTAAATACG
ADAMTS-5	GCAGCACCAACACAACCAG	CCAGGGTGTCACATGAATGATG

Table forward and reverse primers of bone modulator genes (MMP-1, MMP-3, MMP-9, MMP-14, CathK, RANKL, ADAMTS-5) that were used for the qPCR assay.

4.3.3 Detection of acid-sensing proteins MMP1, MMP-3, MMP-9, MMP-14 and bone degradation modulators cathepsin K, RANKL and ADAMTS-5 expression at mRNA in RA-FLS by real-time PCR

RA-FLS exposed to different acidic conditions were harvested, and mRNA was extracted, and cDNA was synthesized as described in section 2.12. Samples were prepared in 384-well plate using MasterMix with SYBR Green with primers for each gene of interest. Each sample was run in duplicate using ABI Prism 7900HT Sequence Detection System (Applied Biosystems SDS). Data were collected and analysed using SDS 2.2 and GraphPad Prism software. Dissociation curve analysis was used after each qPCR run to check for any genomic DNA or primer dimers in the samples.

4.3.4 Migration of RA-FLS under low pH conditions using Oris 96-well plates with stoppers

RA-FLS (2×10^4) were seeded in Oris 96-well plates, and the migration assay was performed as described in section 2.20. Migrated cells were counted and Graph Pad Prism was used to analyse the data collected.

4.4 **Results**

4.4.1 Evaluation of primers efficiency by using RT-PCR reaction

All evaluated primers showed efficiency within the acceptable rage (90%–110%: MMP-1 (slope = -3.543 with 91.53% efficiency), MMP-3 (slope = -3.182 with 106.9% efficiency), MMP-9 (slope = -3.027 with 113.97% efficiency), RANKL (slope = -3.531 with 91.96% efficiency), CathK (slope = -3.412 with 96.37 %), and ADAMTS-5 (slope = -3.159 with 107.29% efficiency).

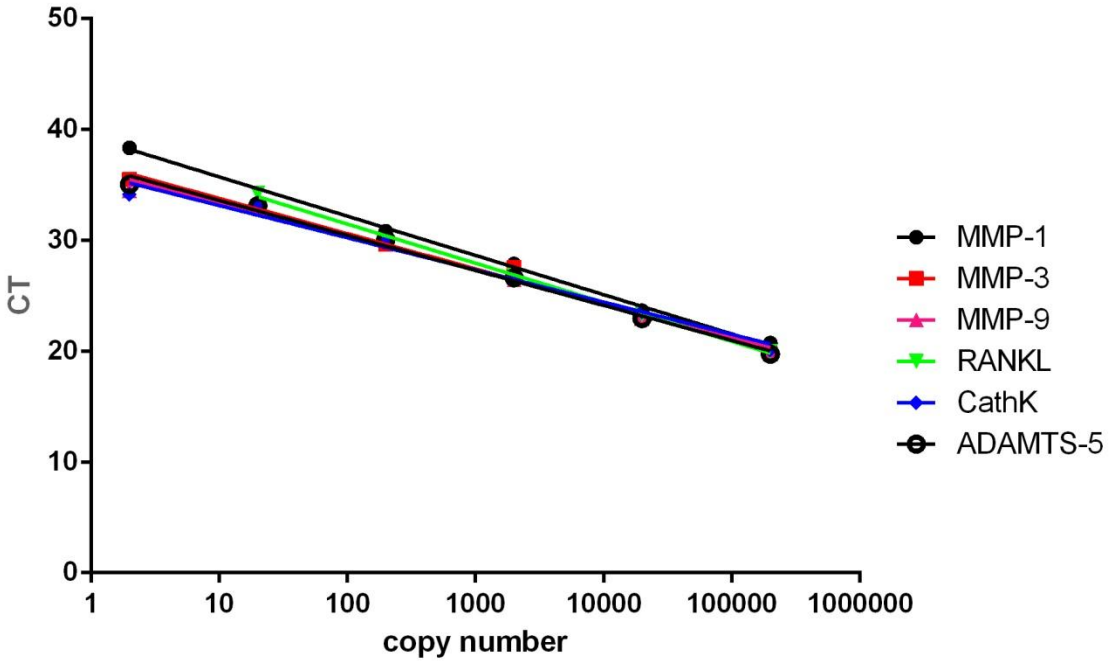

Figure 4.1 Standard curves for primer efficiency.

Curves were constructed from a known copy number of *MMP-1*, *MMP-3*, *MMP-9*, *RANKL*, *CathK*, and *ADAMTS-5* genes. Ten-fold serial dilutions of target gene templates were assayed using real-time PCR and SYBR Green.

4.4.2 Expression of acid-sensing proteins, MMPs, Cathepsin K, RANKL and ADAMTS-5 in RA-FLS after the treatment with different acidic conditions for 24 hours

The mRNA expression of acid-sensing proteins in RA-FLS was not significantly increased at pH <7.4 compared to physiological pH 7.4 (Figure 4.2). However, MMP-1 expression increased by 3.6- ($P \leq 0.01$), 1.8- ($P \leq 0.05$), and 2.2-fold ($P \leq 0.01$) at pH 7.0, 6.5, and 6.0, respectively (Figure 4.3). MMP-3 expression increased by 2.3-fold at pH 7.0 and 1.7-fold at pH 6.5 with P value ≤ 0.05, but no significant increase was found at pH 6.0 (Figure 4.3). MMP-9 was increased by 4.9-fold at pH 7.0 ($P \leq 0.01$), 3.2-fold at pH 6.5 ($P \leq 0.01$), and 1.7-fold at pH 6.0 with P value ≤ 0.05. MMP-14 and the other bone and cartilage modulators, Cathepsin K, RANKL, ADAMTS-5 was not significantly altered in RA-FLS treated with acidified medium for 24 hours (Figure 4.4). Western blot analysis showed an increase in MMP-9 expression in culture medium at pH 7.0 and pH 6.5, while in cell lysates, the increase was observed at pH 7.0 compared with the control (Figure 4.3). GraphPad Prism and SDS 2.4 software was used to collect and analyse data using a non-parametric paired two-tailed t-test.

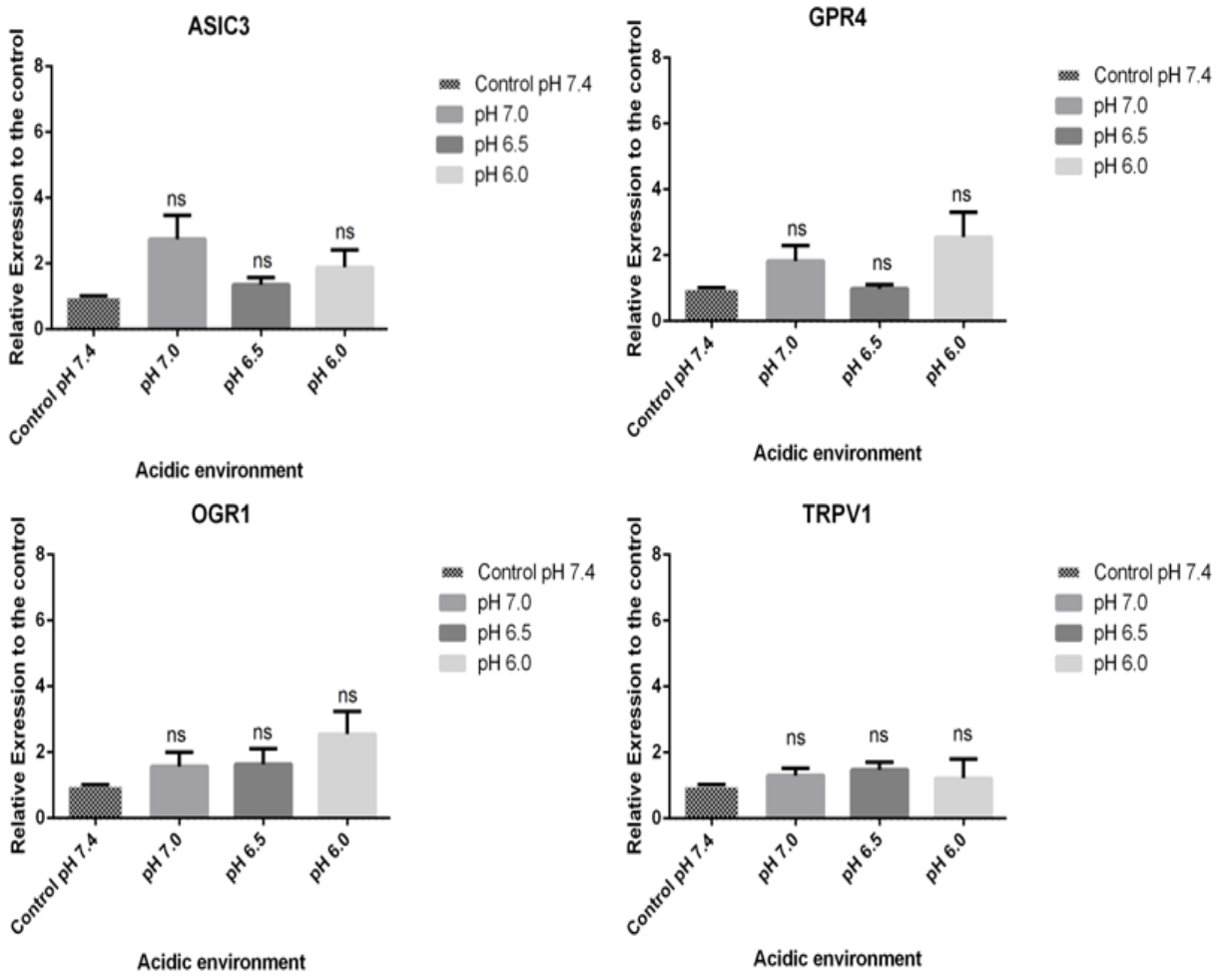

Figure 4.2 Expression of acid-sensing proteins.

Real-time PCR data showed the expression of four different acid-sensing molecules ASIC3, GPR4, OGR1, and TRPV1 in RA-FLS treated with acidified medium at pH 7.0, 6.5, and 6.0 for 24 hours. The expression levels were measured relative to the housekeeping gene GAPDH and compared to control RA-FLS treated at pH 7.4. The qPCR data analysis showed no significant increase in acid-sensing protein expression in RA-FLS after the treatment with acidified medium. The two-tailed paired t-test was used and data are presented as mean ± SEM. n = 15, ns = $P > 0.05$.

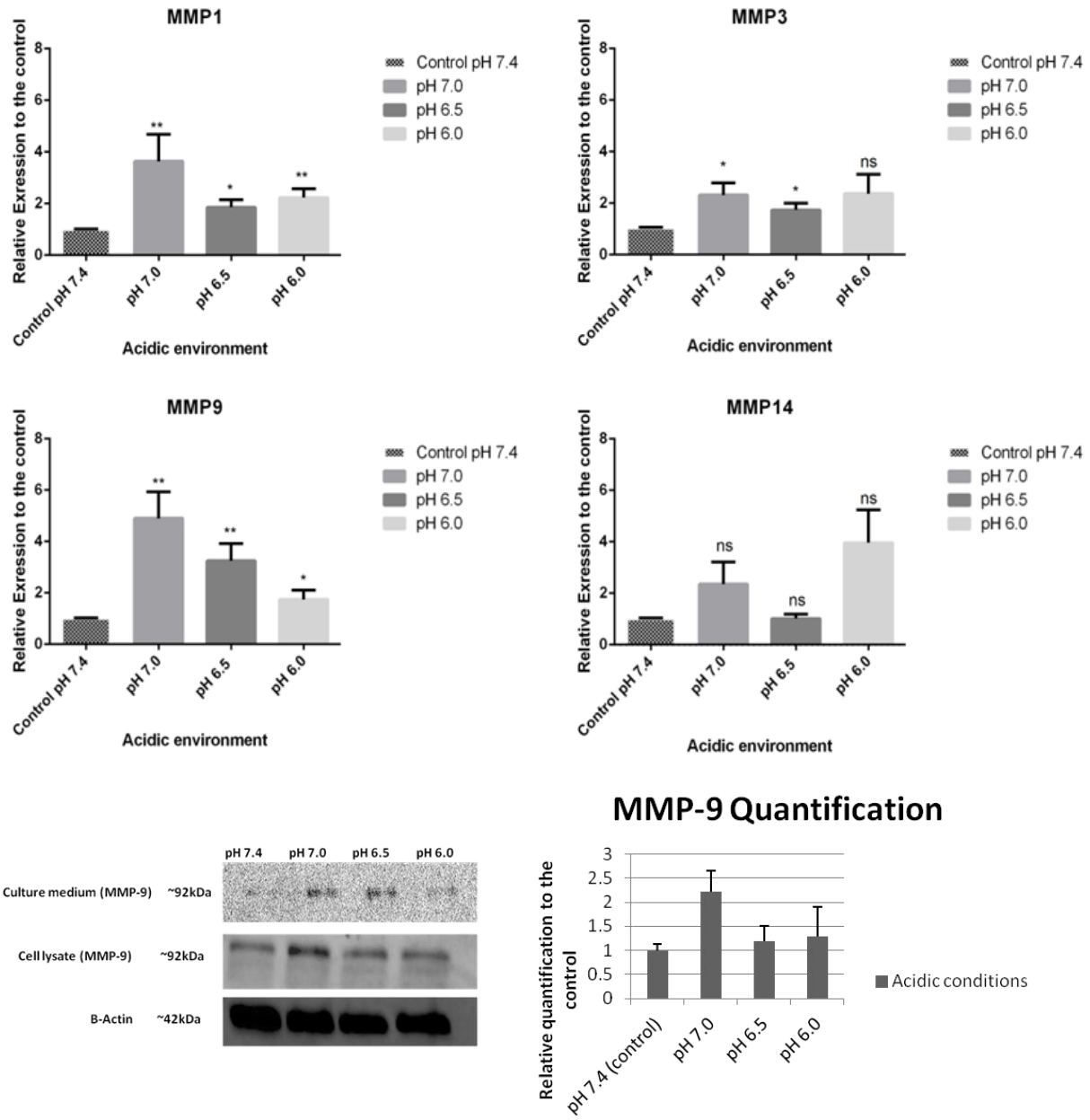

Figure 4.3 Expression of matrix metalloproteases in RA-FLS after the induction of acidic condition.

Data of qPCR showed a significant increase in MMP-1 and MMP-9 expression at low pH, while MMP-3 expression was not significantly altered at pH 6.0. MMP-14 showed a non-significant increase after treatment with acidified medium. WB showed an increase in MMP-9 in the culture medium at pH 7.0 and 6.5 respectively and at pH 7.0 in the cell lysate. Data were analysed using two-tailed t-test and presented as mean ± SEM. n = 10, ns = $P > 0.05$, * = $P \leq 0.05$, and ** = $P \leq 0.01$.

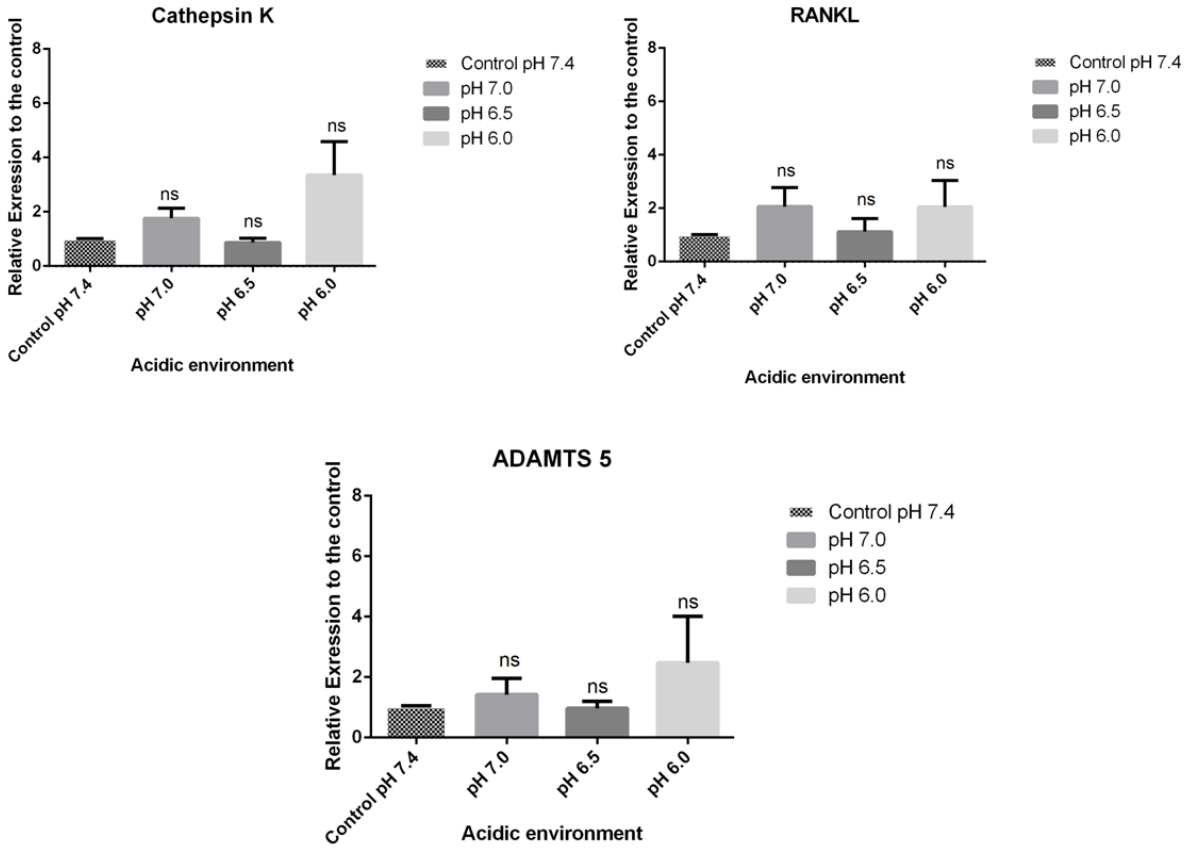

Figure 4.4 Expression of bone and cartilage modulators at the mRNA level in RA-FLS under low pH.

The expression of cathepsin K, RANKL, and ADAMTS-5 in RA-FLS was evaluated after incubation in acidified culture medium (pH 7.4, 7.0, 6.5, and 6.0) for 24 hours. The mRNA was extracted, reverse-transcribed to cDNA, and analysed by qPCR relative to GAPDH expression. None of the tested bone modulators was altered at the mRNA level at low pH. Results were analysed using SDS 2.4 and GraphPad Prism. Two-tailed paired t-test was used, and data are presented mean ± SEM (n = 10, ns = P > 0.05).

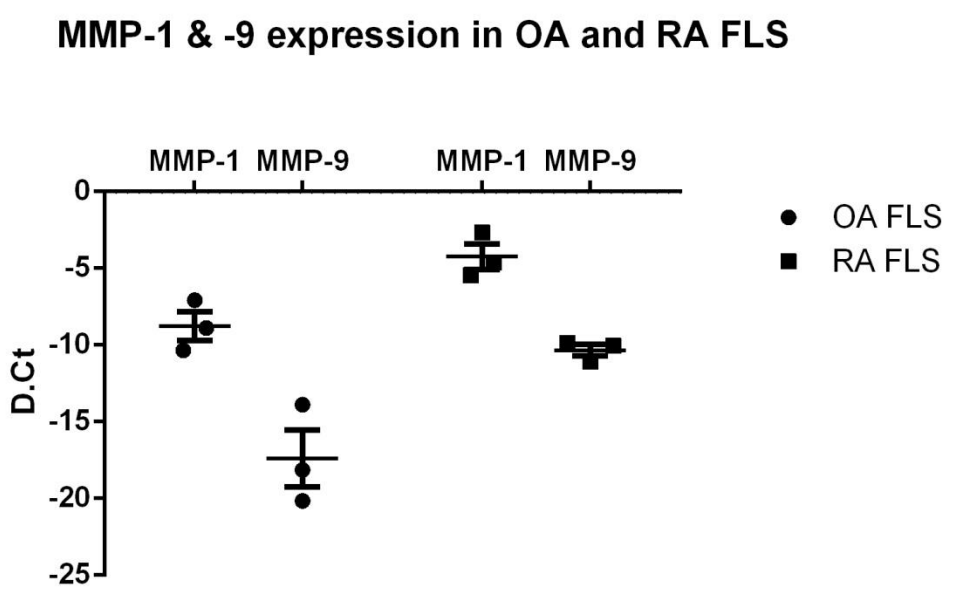

Figure 4.5 ΔCT variation in the expression of MMP-1 and MMP-9 in OA- and RA-FLS.

Real-time PCR showed a significant increase in the expression of MMP-1 and MMP-9 in RA-FLS compared to the expression of these proteases in OA-FLS with $P \leq 0.05$ and $P \leq 0.01$ respectively. Expression data were analysed relative to the housekeeping gene, B2M. Data were collected and analysed with GraphPad Prism by two-way ANOVA. Data are presented as mean ± SEM. n=3.

4.4.3 Migration of RA-FLS under different acidic conditions

In Oris 96-well plates, RA-FLS migration after 24 h incubation showed a gradual reduction at pH 7.0, pH 6.5, and pH 6.0 compared to cells incubated at pH 7.4 (Figure 4.6 and 4.7). Average number of cells migrated at neutral pH was 153, while it was 143 at pH 7.0. Migration was significantly reduced at pH 6.5 and 6.0 with 105 and 55 migrated cells and P value > 0.05 & 0.001, respectively as shown in (Figure 4.7). RA-FLS from three different donors were tested. Data was collected and analysed by GraphPad Prism using one-way ANOVA.

	RA-FLS Day 1	RA-FLS Day 4
Control **pH 7.4**	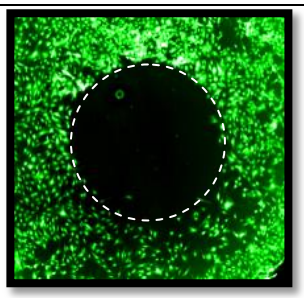	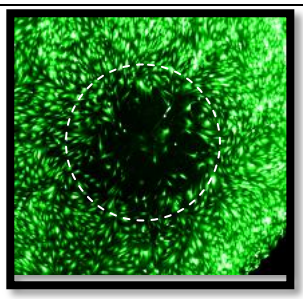
pH 7.0	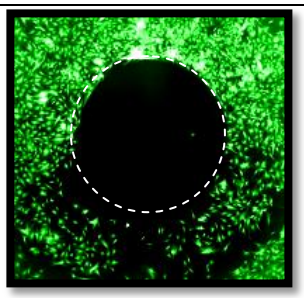	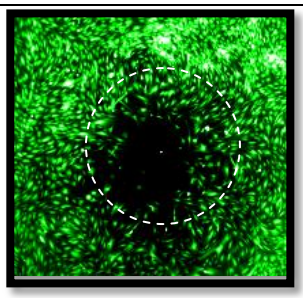
pH 6.5	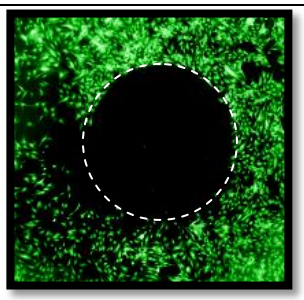	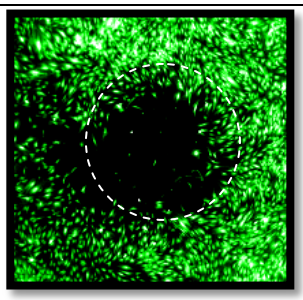
pH 6.0	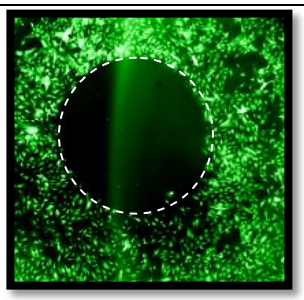	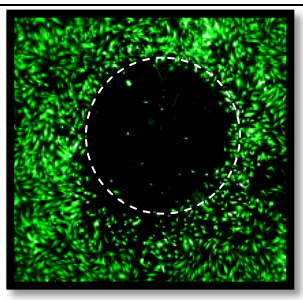

Figure 4.6 RA-FLS migration under acidic conditions.

RA-FLS were seeded (2.5×10^4 to 3.0×10^4) and allowed to adhere. Stoppers were removed and different acidic conditions were induced for 24 h. CellTracker™ Green CMFDA (5-chloromethylfluorescein diacetate) was used to monitor RA-FLS migration after four days (n = 3).

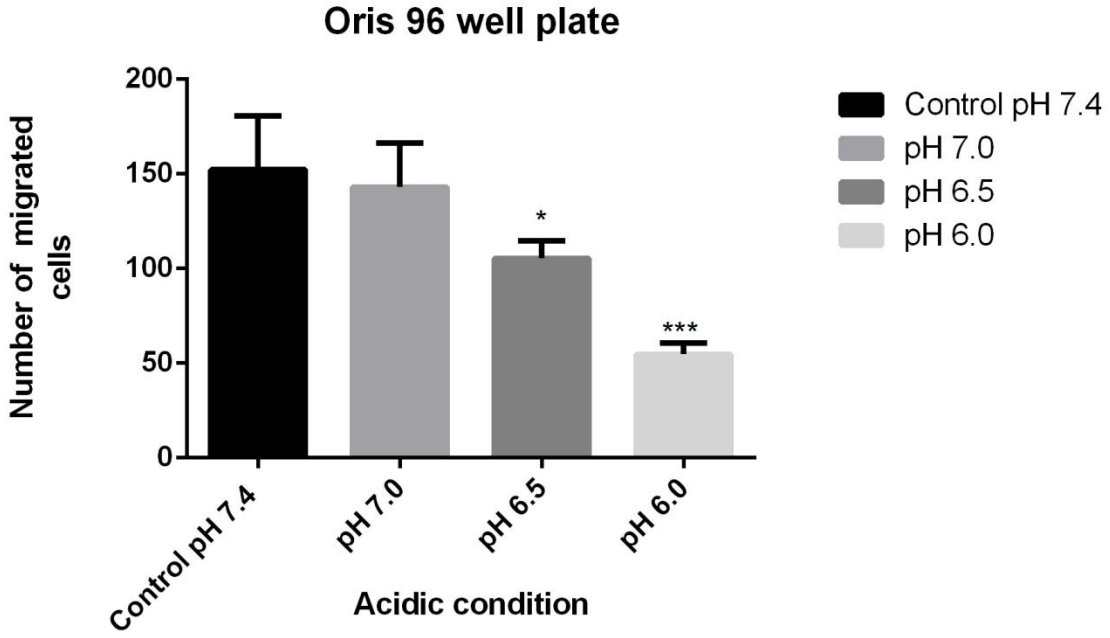

Figure 4.7 Average number of migrated RA-FLS in Oris 96-well plate.

The average number of migrated cells was calculated after incubation in acidified medium for 24 h, and then the data were analysed by GraphPad Prism using one-way ANOVA. Results are presented as mean ± SEM, where * = $P \leq 0.05$ and *** = $P \leq 0.001$ (n =3).

4.5 **Discussion**

The qPCR data revealed an insignificant increase in the expression of acid-sensing proteins in RA-FLS exposed to conditioned medium at pH 7.0, 6.5, and 6.0. OGR1 expression increased gradually, up to 2-fold, (Figure 4.1) compared to the expression in control RA-FLS maintained at pH 7.4. MMP-1 and MMP-9 exhibited a significant increase in cells from RA patients compared to OA patients, and that observation coincides with our findings (Figure 4.2). After treatment in acidified medium, cultured RA-FLS increased expression of MMP-1 at pH 7.0, 6.5, and 6.0. The maximum expression for MMP-9 was at pH 7.0; however, this increase gradually diminished by two-fold as the pH continued to decrease (Figure 4.2). A previous stud has shown no significant increase in MMP-3 expression in RA patients (Tolboom et al., 2002); however, our qPCR data suggest that MMP-3 expression increased in RA-FLS at pH 7.0 and pH 6.5, but not at pH 6.0. A recent study on the role of ASIC3 showed that MMP-3 and MMP-13 expression did not increase significantly in FLS incubated at pH 6.0 compared to those incubated at pH 7.4, even after IL-1B induction (Gong et al., 2014). Our results of MMP-3 expression were consistent with that finding. Previously, ASIC3 was shown to suppress MMP-3 and MMP-13 mRNA expression in FLS at pH 6.0 (Sluka et al., 2013), and our result with MMP-3 has shown no significant increase. However, we report a slight, albeit significant, increase in MMP-3 expression at pH 7.0 and 6.5 compared to the expression at physiological pH. ASIC3 is the most sensitive among ASICs at pH ≈ 6.7 (Sutherland et al., 2001), and that sensitivity may contribute to the reduced expression we observed at pH 6.5. MMP-14 expression was unaltered in RA-FLS under acidic conditions. As mentioned in the introduction, Cathepsin K, RANKL,

and ADAMTS 5 are expressed in the synovium and play a pivotal role in the involvement of bone and cartilage destruction. Our data show that there was no significant increase in the expression of any of these molecules in RA-FLS.

A recent investigation of human FLS migration showed a significant increase of MMP-1, MMP-2, and MMP-13 expression in FLS after the induction of a canonical Wnt antagonist, Dickkopf-1 (DKK-1). This study concluded that DKK-1 enhances FLS migration, as well as MMP-1 and -13 expression, via JNK phosphorylation and JNK-2 signalling process. However, MMP-9 and MMP-3 expression was decreased under the same conditions. A second study reported that the inhibition of PI3K/AKT activity via sphingosine kinase 1 (SPHK1) knockdown in RA-FLS reduces MMP-9 and MMP-2 expression and inhibits the migration and invasion of human RA-FLS (Yuan et al., 2014b). Our results show a significant reduction of RA-FLS migration at pH 6.5 and pH 6.0, but no significant changes in migration at pH 7.0 compared to pH 7.4 (Figure 4.5 & 4.6). Altogether, these data suggest that the acidic environment hinders RA-FLS migration and enhances the production of MMP1, MMP-3, and MMP-9 in RA-FLS independently of the hypoxia.

Previous studies investigated the invasiveness of RA-FLS via MMP activity and suggested that MMPs play a role in the invasive growth of FLS and may contribute to bone and cartilage degradation in RA (Tolboom et al., 2002, Zhu et al., 2006). However, in our study we investigated the roles of specific members of the MMP family (MMP-1, -3, -9, and -14). Because MMPs have poor substrate sequence specificity, it is difficult to use a peptide substrate alone to differentiate the activity of a specific MMP from other MMPs. Therefore, we used a plate pre-coated with antibodies targeting a particular

MMP. AnaSpec provides assay kits designed to detect the activity of a specific MMP. A monoclonal human MMP antibody is used to pull down both pro and active MMP forms from the sample, and proteolytic activity is detected by using a 5-FAM/QXL™ 520 FRET peptide. However, for this assay medium without phenol red and sodium bicarbonate is needed. Because RA-FLS are optimized to grow in DMEM and MEM medium, which contain phenol red, we could not perform MMP activity assays. Moreover, the quantities of primary RA-FLS were limited, so we used the available cells to perform other experiments such as qPCR, western blot, and migration assays under various acidic conditions.

At pH 5.5, a rapid increase of intracellular calcium was observed in cultured FLS from $ASIC3^{+/+}$ mice compared to those from $ASIC3^{-/-}$ mice. The expression of MMP-3 and MMP-13 in ASIC3 knockdown FLS was significantly higher at pH 6.0 (Kolker et al., 2010, Sluka et al., 2013). TRPV1 also alters expression of MMP-1 in human keratinocytes, and an influx of Ca^{2+} and involvement of PKC signal transduction may contribute in this process (Lee et al., 2008). The combination of low pH (7.1–7.2) and capsaicin showed a potential increase in cytosolic calcium in synoviocytes via activity of TRPV1 (Kochukov et al., 2006). Another contribution of GPCRs in response to extracellular acidification and increase intracellular Ca^{2+} mobilization in synoviocytes was reported by (Christensen et al., 2005a). This study suggested a modest and high intracellular Ca^{2+} mobilization at pH 6.8 and pH 6.4 respectively with high generation of IP. Moreover, It has been found that activation of GPCRs by homocysteine induced PTKs, Ca^{2+}-dependent PKC, and oxidative stress signal transduction process which induce ERK1/2 signalling pathway and regulate MMP-9 activity in microvascular

endothelial cells (Moshal et al., 2006). Taken together, these data suggest that intracellular calcium influx via acid-sensing protein activity modulates various intercellular signalling pathways and enhances the production of MMPs in RA-FLS in an acidic microenvironment. In our study, we reported increases in MMP-1, MMP-3, and MMP-9 and reduction of RA-FLS migration under acidic conditions. Moreover, we reported no significant increase of acid-sensing protein expression that would suggest the enhancement of MMP expression is mediated by the activity of acid-sensing molecules under acidic conditions.

The findings reported in this section show acidification alters the migration of RA-FLS. However, it is unclear which types of acid-sensing proteins are most involved in this process. In order to answer this question, we used selective ASIC3 and TRPV1 pharmacological inhibitors to test the expression of MMPs and investigate the RA-FLS migration rate.

5 Chapter 5: Use of pharmacological inhibitors APETX2 and AMG517 to investigate the roles of ASIC3 and TRPV1 in MMP modulation under acidic conditions

5.1 Introduction

The involvement of acid-sensing proteins in bone resorption and cartilage destruction of the RA joint remains unknown. There is accumulating evidence that ASIC3 is involved in the pathogenesis of RA. In a murine model of arthritis, ASIC3 was described as a protective molecule that enhances FLS death in RA joints and prevents excessive inflammation (Sluka et al., 2013). Additionally, ASIC3 was described as the most sensitive of the ASICs to acidic pH (6.7) in sensory neurons, and it has been reported that responsiveness to pain simulation was reduced in ASIC3$^{-/-}$ mice compared to wild type (Sutherland et al., 2001, Sluka et al., 2013). The sensitivity of this channel to pH is attributed to residues Phe20 and Thr25 in the intracellular pre-TM1 domain and Gly430 in the extracellular pre-TM2 domain (Yuan et al., 2010a).

On the other hand, under acute inflammatory conditions, hyperalgesia to noxious heat produced by carrageenan induction was significantly inhibited in TRPV1-/- mice relative to the wild type (Davis et al., 2000). In contrast, the role of TRPV1 under chronic inflammatory conditions was studied in a murine model of arthritis using CFA. Paw enlargement and oedema were reported in wild type mice, while TRPV1-/- mice did not exhibit these responses. Moreover, synovial pannus expansion, as well as bone and cartilage destruction, were reported in wild type mice, but these responses were minimal in TRPV1-/- mice (Szabo et al., 2005). To elucidate the possible mechanism for this observation, the capability of proton concentration to modulate TRPV1 was investigated.

Specific TRPV1 extracellular amino acids residues at the E600 site were described as the site of proton interaction, which modulates the channel's activity (Jordt et al., 2000). Heat-evoked currents at pH ranging from 6 to 8 were greater in TRPV1-expressing cells than in cells with a mutated E600 site in TRPV-1 (Jordt et al., 2000). Recent studies have shown that GPCRs contribute to the acid sensing at the site of ischemia and inflammation (Lardner, 2001, Tomura et al., 2005).

Extracellular acidification may activate OGR1 and enhances the production of COX-2 and prostaglandin PGE_2 through the OGR1/$G_{q/11}$/PLC/PKC signalling pathway in human osteoblasts (Tomura et al., 2008). In addition, activation OGR1/$G_{q/11}$ in human airway smooth muscle cells (ASMCs) enhances intracellular Ca^{2+} mobilization and production of IL-6 via phosphorylation of ERK and p38MAPK (Ichimonji et al., 2010). On the other hand, GPR4 responds to acidosis through the G_S/cAMP pathway and induces the production of adhesion molecules VCAM-1 and ICAM-1 in human umbilical vein endothelial cells (HUVECs) (Chen et al., 2011). Another study reported an expression of chemokines, cytokines, and other various inflammatory genes, including stress response genes and the NF-κB pathway genes, when GPR4 was activated by acid (Dong et al., 2013).

5.1.1 ASICs Inhibitors

ASICs inhibitors can be categorized into specific, nonspecific, and non-discriminative molecules. A potassium-sparing diuretic or amiloride was the first ASICs blocker described (Waldmann et al., 1996). It has been reported that this molecule was able to increase the rate of sodium excretion in deoxycorticosterone acetate-induced hypertensive rats, while maintaining potassium levels. Moreover, amiloride was

described as safe compound for long-term treatment of hypertension, as it reduced the risk of hypokalemia (Qadri et al., 2010). However, amiloride and its derivatives such as benzamil and ethylisopropyl *amiloride* **(**EIPA) were indicated as non-discriminative molecules and poor reversible blockers of ASICs (Deval et al., 2010). Moreover, non-steroid anti-inflammatory drugs (NSAIDs) can also inhibit the activity of ASICs with relatively low affinity (IC_{50} ranging from 92 to 249 μM) as described by (Voilley et al., 2001). This study showed that both flurbiprofen and ibuprofen blocked the activity of ASIC1a, while ASIC3 is de-activated by salicylic acid, aspirin and diclofenac. Four organic compounds known as anti-protozoal diarylamidines (DAPI, diminazene, HSB and pentamidine) were described as a potent ASIC inhibitors in primary cultures of hippocampal neurons with apparent affinities ranging from 300 nM to 38 μM (Chen et al., 2010). In addition to organic compounds, Bi- and trivalent cations were also defined as ASICs inhibitor. For instance, gadolinium (Gd^{3+}) inhibited both ASIC2a ($IC_{50} \geq 1$ mM) and ASIC2a-ASIC3 heteromers at higher potency ($IC_{50} \sim 40$ μM) as (Babinski et al., 2000) described. Moreover, CU^{2+} was described as an inhibitor of ASICs in hypothalamic neurons with IC_{50}=46.8 μM (Wang et al., 2007). However, none of these molecules is absolutely specific for ASIC channels (Diochot et al., 2004).

Two peptide toxins isolated from the venoms of the spider *Psalmopoeus cambridgei* (PcTx1) and the sea anemone *Anthopleura elegantissima* (APETx2) were described as selective blockers for ASIC1a and ASIC3 channels, respectively (Diochot et al., 2004). It has been reported that PcTx1 toxin inhibited the activity of ASIC1a channel in animal models of acute and chronic pain when injected intrathecally or intracerebroventricularly (Duan et al., 2007, Mazzuca et al., 2007). It has been described that the binding site of

PcTx1 is on the extracellular loop of ASIC1a, a site close to the H^+ sensing site (which involves in pH sensing) at the interface between two subunits in the trimeric channel, and stabilizes it (Qadri et al., 2009). On the other hand, it has been reported that ASIC3-like currents were expressed by ~60% of rat cutaneous sensory neurons (Deval et al., 2008). This study showed that after the induction of moderate cutaneous acidifications (at pH 6.9–6.6) the skin C-fibres firing was totally inhibited after the treatment with ASIC3-specific toxin APETx2 in rat models (Deval et al., 2008). Moreover, heat hyperalgesia was inhibited when APETx2 is co-injected with CFA in the hind paw, whereas PcTx1 has no significant effect. This finding was also confirmed when pain behaviour experiments was performed by using an ASIC3 knockdown model, and the results showed no signs of heat hyperalgesia (Deval et al., 2008). APETX2 directly inhibits the ASIC3 channel by acting at its external side, and it does not modify the channel unitary conductance. This peptide is composed of 24 amino acids, linked together by three disulfide bridges, and reversibly inhibits ASIC3 peak current in both rat and human cell culture with an IC_{50} =63 nM and 175 nM, respectively, without any effect on ASIC1a, ASIC1b, or ASIC2a (Diochot et al., 2004). Also, it has been reported that the heteromeric ASIC2b-ASIC3 channel was inhibited by APETx2 with an IC_{50} of 117 nM and heteromeric ASIC1a-ASIC3 and ASIC1b-ASIC3 channels with lower affinities (IC_{50}=2 and 0.9 μM, respectively). APETx2 was tested on various heterologously expressed Kv channels. None of Kv channels subtypes (Kv1.4, HERG, Kv2.2, Kv3.1, Kv4.1, Kv4.2, Kv4.3) was significantly inhibited by APETx2. Only a partial inhibition of Kv3.4 current was reported when much higher concentrations (3 μM) of APETx2 applied (Diochot et al., 2004).

5.1.2 TRPV1 inhibitors

TRPV1 channel can be blocked by two different methods. One method is by targeting TRPV1 using agonists to activate and desensitize the receptor (such as Capsaicin). Capsaicin desensitized TRPV1 and has been described as an effective treatment for pain produced by RA, OA and peripheral neuropathy (Brito et al., 2014). The other method is by using antagonists that able to inhibit all TPRV1 receptor activation modes. Several TRPV1 antagonists have been developed and tested. Capsazepine was the first described antagonist that blocks the capsaicin-binding site on TRPV1 and inhibits channel activation in rat DRG (Bevan et al., 1992). However, due to its low metabolic stability and non-selectivity, it has been not considered as a candidate for clinical trials (Broad et al., 2008, Pal et al., 2009, Vriens et al., 2009, Wong and Gavva, 2009). in contrast, selective TRPV1 inhibitors A-425619 and SB-705498 were tested in rats and humans and demonstrated effective reduction of hyperalgesia and allodynia, as well as increased heat pain tolerance (Jara-Oseguera et al., 2008). Another chemical compound (AMG517) was described as a potent selective inhibitor for TRPV1. It has been reported that capsaicin, pH 5, and heat-induced Ca^{2+} uptake and inward currents were inhibited in human TRPV1-expressing CHO cells when after the treatment with AMG517 at IC50 values of 0.76 nM, 0.62 nM and 1.3 nM, respectively (Gavva et al., 2007). In addition, as measured by Ca^{2+} uptake into TRPV1-expressing cells it has been reported that AMG 517 did not activate TRPV1 at concentrations up to 40 μM. Among the recombinant TRP family members it has been found that AMG517 selective for TRPV1 as the IC50 value for AMG 517 was >20 μM against 2-APB-activated TRPV2 and TRPV3, 4-PDD-activated TRPV4, allyl isothiocyanate-activated TRPA1, and icilin-activated TRPM8 (Gavva et al.,

2007). Moreover, capsaicin-activated TRPV1 was inhibited by AMG517 in rat dorsal root ganglion neurons with an IC50 value of 0.68 nM (Gavva et al., 2007).

5.1.3 GPCRs inhibitors

Different GPCRs inhibitors, such as CU^{++} for OGR1 (Yuan et al., 2014a) and *2-Ethyl-3-{4-[(E)-3-(4-isopropyl-piperazin-1-yl)-propenyl]-benzyl}-5,7-dimethyl-3H-imidazo[4,5-b] pyridine* (EIDIP) for GPR4 have been used previously (Dong et al., 2013); however, no specificity data were provided. Therefore, the selectivity of these compounds cannot be inferred.

All above data illustrate the critical role of acid-sensing proteins in proton sensing and regulation of multiple intracellular signalling pathways. However, no study in RA-FLS has compared the contribution of each of these acid sensors in the development of RA.

As we reported previously, MMPs (1, 3, and 9) were increased and the migration rate was reduced in RA-FLS under low pH conditions. To investigate the involvement of acid-sensing proteins in MMP modulation and cellular migration, two potent selective inhibitors, APETX and AMG517, were used. Expression of MMPs and bone resorption modulators, as well as RA-FLS migration rate, were investigated after exposure to these specific inhibitors.

5.2 **Hypothesis**

ASIC3 and TRPV1 modulate the expression of MMPs and bone destruction modulators in RA-FLS under acidic conditions.

5.3 **Methods**

5.3.1 RA-FLS treatment with ASIC3 (APETX2) and TRPV1 (AMG517) selective inhibitors

1.5×10^4 RA-FLS were seeded in T-25 flasks and allowed to grow to 80-90% confluence. Culture medium was replaced with serum-free medium for 24 h in 5% CO_2 at 37°C. APETX2 (0.5 mg), provided by Smartox Biotechnology (Product code**:** 07APE002-00500), was prepared at 175 nM as described in section 2.21. Meanwhile, 5 mg AMG517 (SelleckChem) was prepared at 0.75 nM as described in section 2.22. Serum-free medium was replaced with acidified MEM and APETX2 or AMG517 (separate treatments) and incubated for 24 h at 37°C in 5% CO_2. Culture medium and cell pellet were collected for western bolt, qPCR and RA-FLS migration assays. T-25 flasks with RA-FLS treated with only acidified MEM were run in parallel with T-25 RA-FLS treated with acidified medium and selected antagonist.

5.3.2 RA-FLS viability assay after APETX2 and AMG 517 induction

To monitor RA-FLS viability, cells were stained with trypan blue. A haemocytometer was used, as described in section 2.23, to count cells before and after exposure to APETX2 or AMG517.

5.3.3 Western blot (WB)

RA-FLS lysates were analysed to measure the expression of MMP-1 and MMP-9. Rabbit polyclonal antibodies targeting MMP-1, MMP-9, and mouse monoclonal β-actin was used as loading control then WB was performed as described in section 2.18.

5.3.4 Real-time PCR

RA-FLS mRNA was extracted and converted to cDNA (section 2.15) to analyse the expression of acid-sensing proteins, MMPs, Cathepsin K, RANKL, and AMADTS5 before and after exposure to APETX2 or AMG 517. SYBR Green chemistry was used as a cDNA amplification indicator, followed by disassociation curve analysis as described previously.

5.3.5 RA-FLS migration assay using 96-well Oris plate

20,000 RA-FLS cells were seeded in a 96-well Oris plate and incubated in a serum starved medium (1% FBS) for 24 hr. Starvation medium was removed and cell tracker was applied for 30 minutes then replaced by acidified medium with and without 175 nM APETX2 and 0.75 nM AMG 517 and incubated for 24 hr. Images was collected as described in section 2.20.

5.4 **Results**

5.4.1 Viability of RA-FLS after the induction of APETX2 and AMG517

RA-FLS showed a slight reduction in viability after exposure to acidic conditions and ASIC3 and TRPV1 antagonists. We observed a 2.5%–4.0% reduction in viability when cells were treated with acidified medium only. In contrast, viability was reduced between 1.33%–7.0 % when cells were exposed to acidified medium and 175 nM APETX2, while exposure to acidified medium and 0.75 nM AMG517 reduced viability between 2.0% and 8.3%.

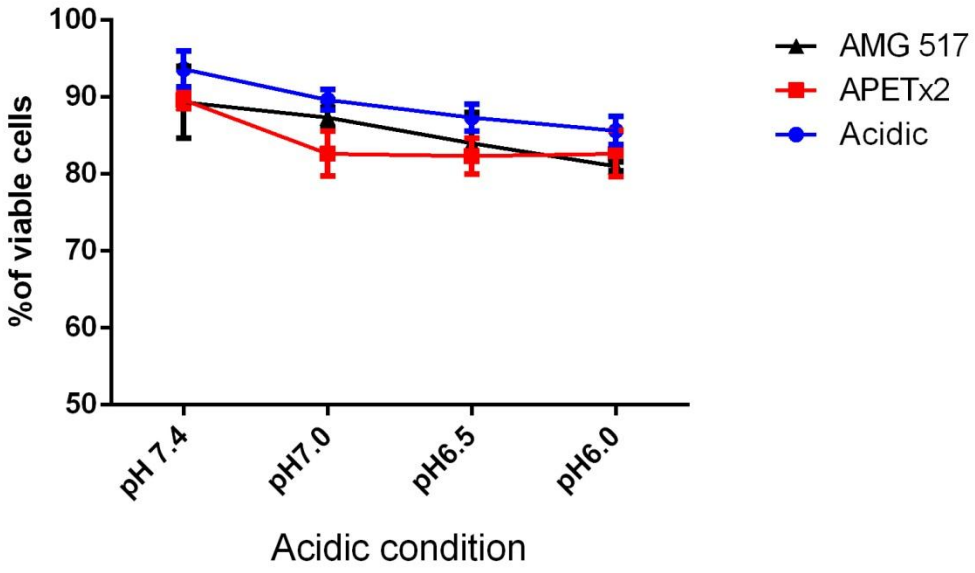

Figure 5.1 Viability of RA-FLS after 24 h incubation in different acidic conditions, with or without 175 nM ASIC3 and 0.75 nM TRPV1 inhibitors.

RA-FLS were grown in T-25 flasks to 90% confluence. The culture medium replaced with acidified medium with or without APETX2 and AMG517. No significant changes in cell viability were observed. The two-tailed paired t-test was used, and results are presented as proportional change of three separate experiments.

5.4.2 Expression of MMPs -1, -3, -9, and acid-sensing proteins after treatment with APETX2

RA-FLS treated with 175 nM APTEX2 exhibited no significant change in mRNA expression of acid-sensing proteins compared to cells treated with acidified medium only (Figure 5.2). However, real-time PCR data showed a significant reduction of 1.7-fold in MMP-1 expression ($P \leq 0.001$), and 1.2-fold of MMP-9 expression at pH 7.0 after 24 h exposure to 175 nM APETX2 ($P \leq 0.0001$) (Figure 5.3). No significant changes were reported in the expression of MMP-3 (Figure 5.3) or the tested bone destruction modulators after exposure to 175 nM ASIC3 selective antagonist (APETX2) (Figure 5.4).

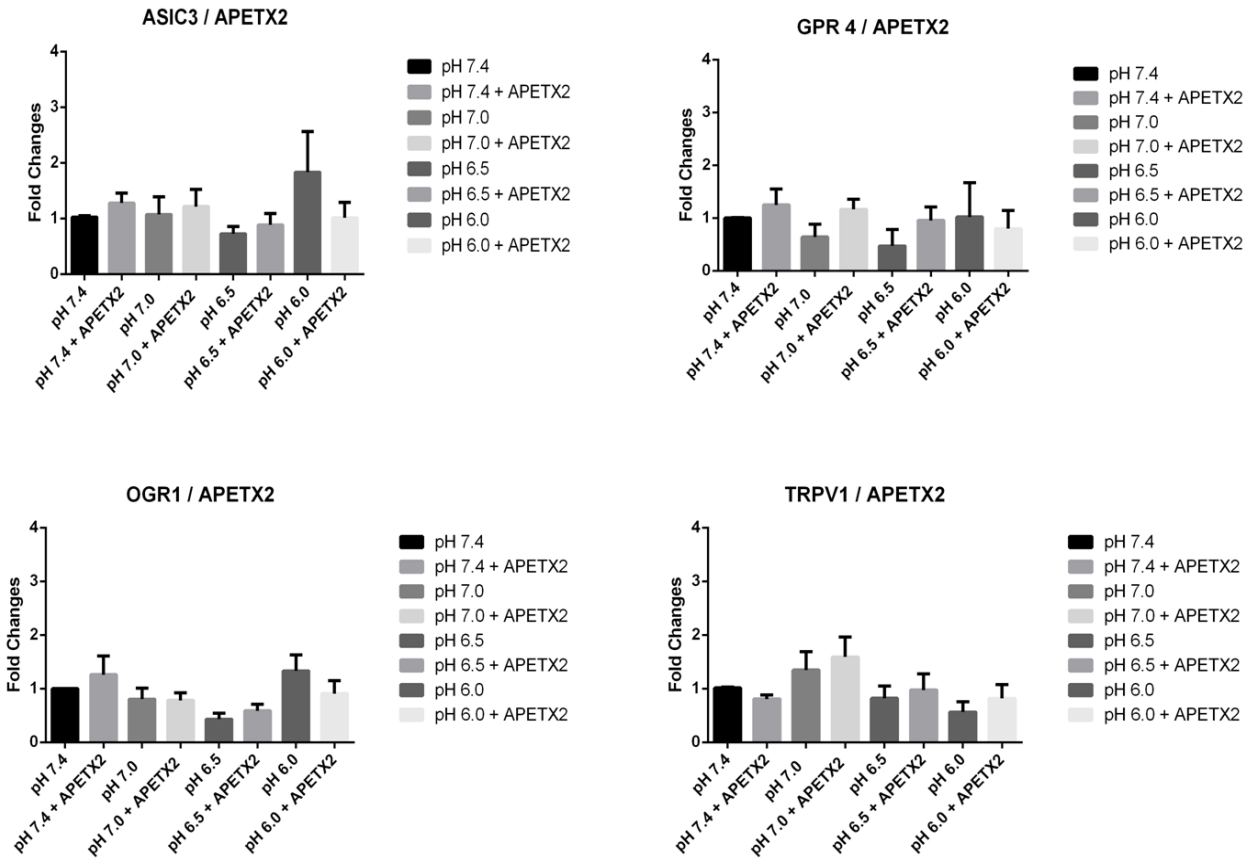

Figure 5.2 mRNA quantification of acid sensing proteins in RA-FLS after the treatment with APETX2

No significant changes in ASIC3, GPR4, OGR1 and TRPV1 expression were observed at mRNA level after exposure to APETX2. Results were calculated using two-tailed paired t-test. Data are presented as mean ± SEM, n=4.

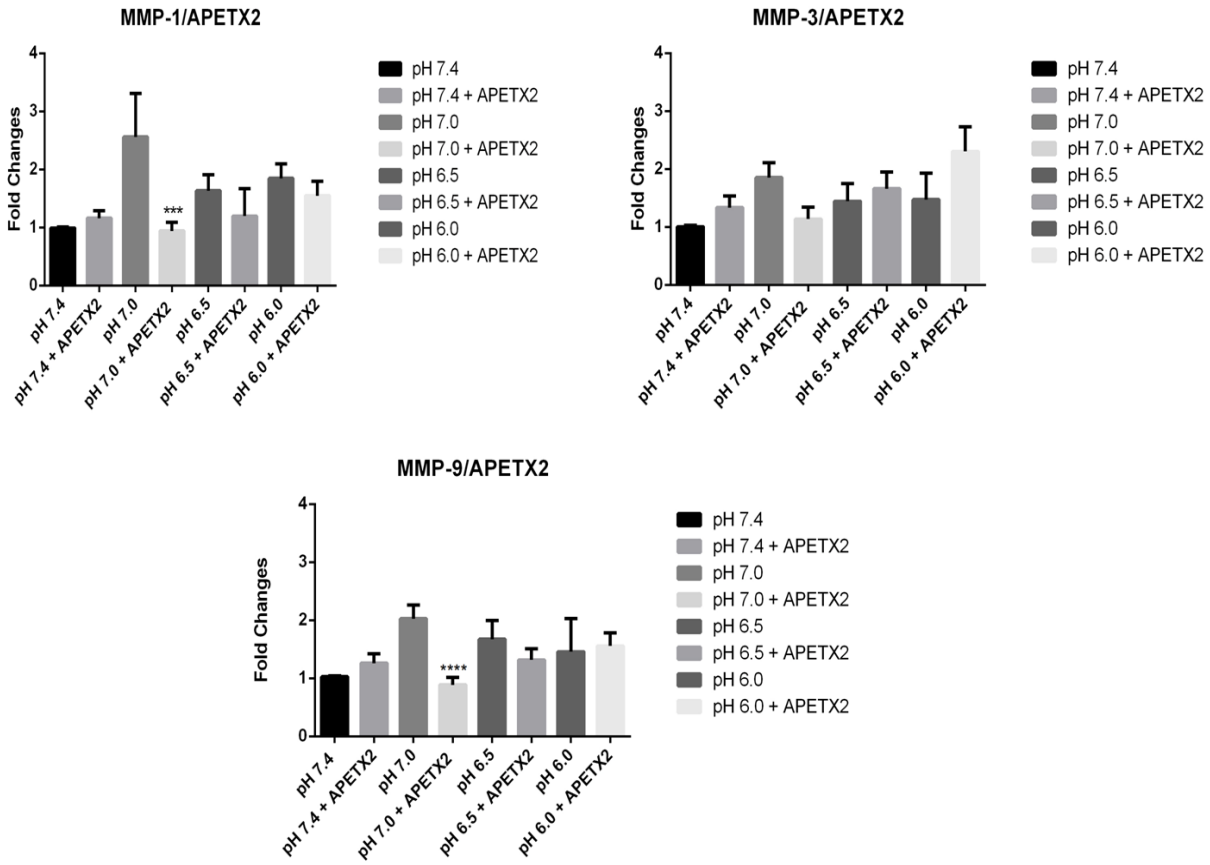

Figure 5.3 Quantification of transcript levels for MMPs -1, -3, and -9 with real-time PCR after the inhibition of ASIC3 with 175 nM APETX2.

MMP-1 and MMP-9 exhibited significant reductions in expression at pH 7.0 after exposure to APETX2. No significant changes in MMP-3 expression were observed. Results were calculated using two-tailed paired t-test. Data are presented as mean ± SEM. *** = $P \leq 0.001$ and **** = $P \leq 0.0001$ (n = 7).

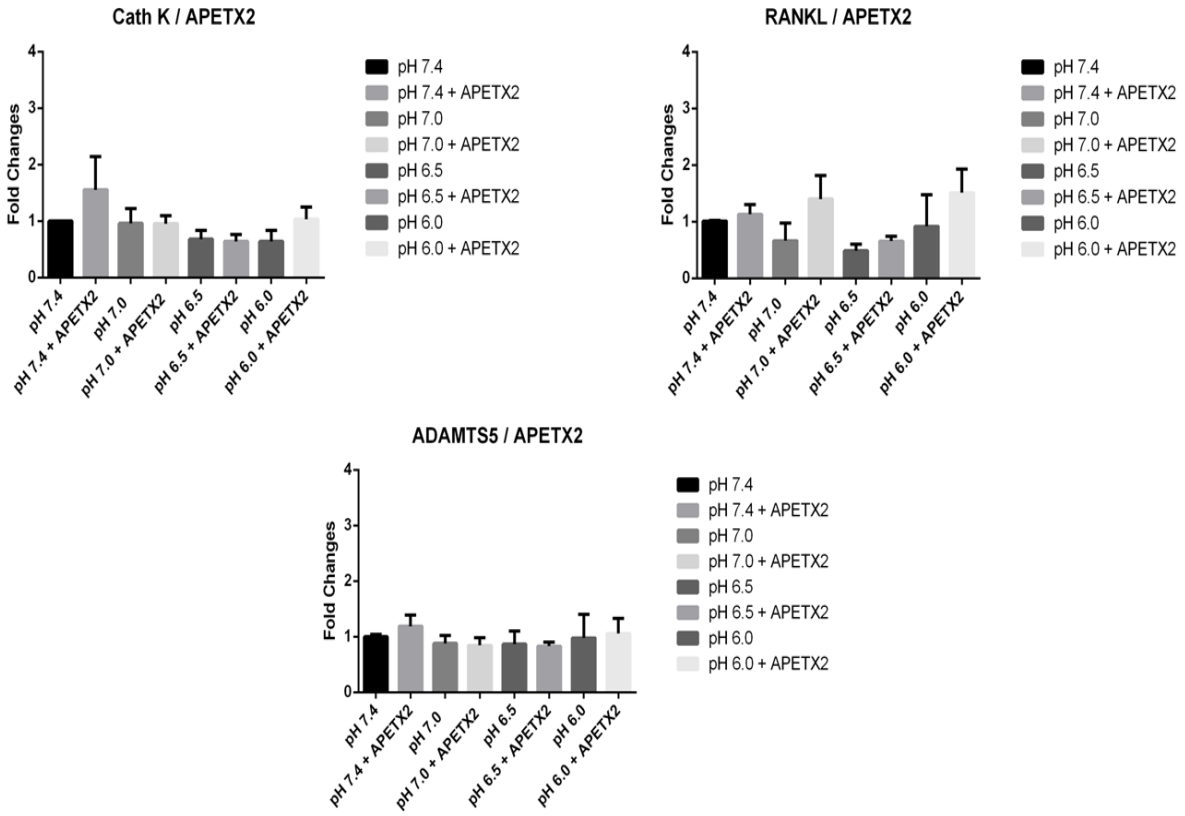

Figure 5.4 CathK, RANKL, and ADAMTS5 expression at the mRNA level in RA-FLS after APETX2 induction.

No significant alterations were indicated at mRNA level of these proteins in RA-FLS after exposure to APETX2. Results were calculated using two-tailed paired t-test. Data are presented as mean ± SEM, n=4.

5.4.3 The effect of TRPV1 inhibition on the expression of MMP-1, -3, 9, acid-sensing proteins, and bone resorption modulators

RA-FLS treated with the TRPV1 selective inhibitor, AMG 517 (0.75 nM), showed no significant alteration in ASIC3, GPR4, OGR1, or TRPV1 expression at the mRNA level (Figure 5.5). On the other hand, a significant reduction of MMP-1 expression of about one-fold at pH 7.0 ($P \leq 0.05$). MMP-9 expression was reduced at pH 7.0 by approximately 2.5-fold reduction and pH 6.5 of about 1.5-fold ($P \leq 0.05$) (Figure 5.6). No significant changes in MMP-3 and bone resorption modulators (CathK, RANKL and ADAMTS5) expression were observed in any of the tested conditions (Figure 5.7). The expression of these genes in RA-FLS treated with AMG517 was compared to the expression in RA-FLS exposed only to acidified medium. Data were collected and analysed by GraphPad Prism using the two-tailed paired t-test.

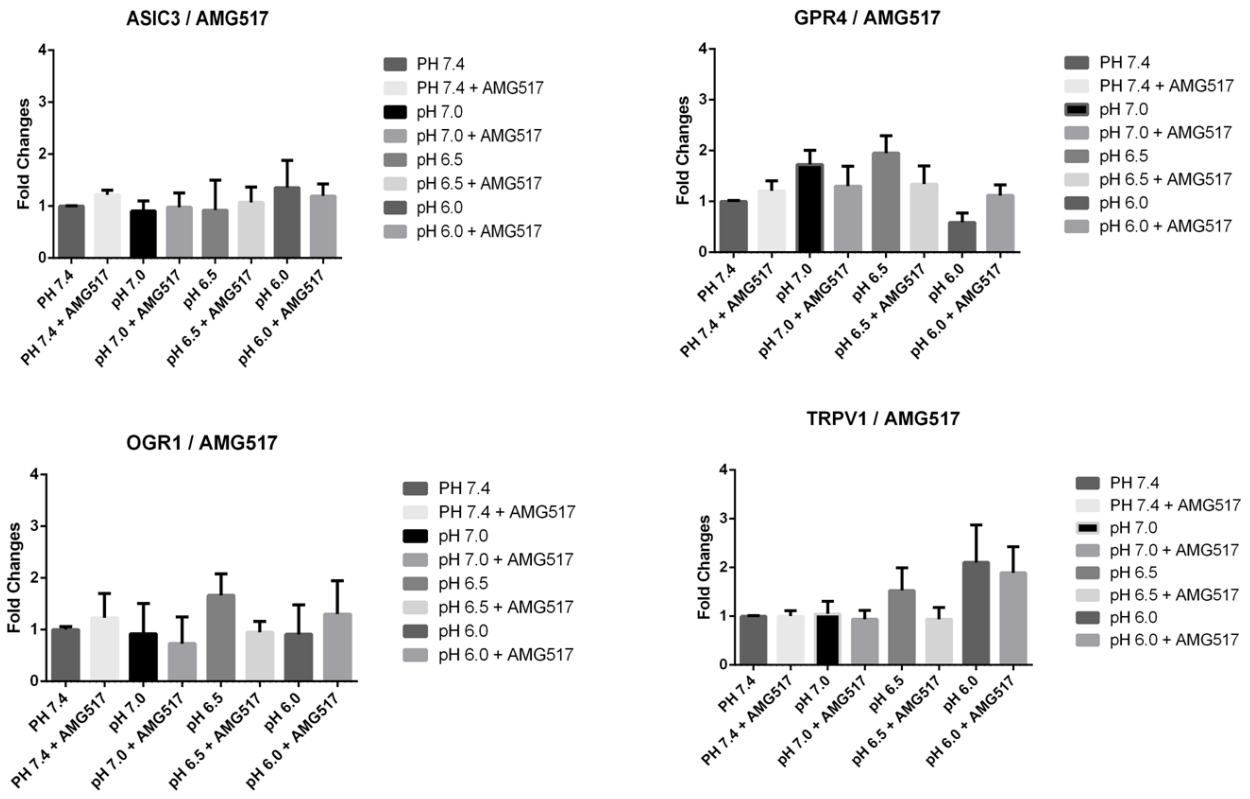

Figure 5.5 mRNA expression of acid sensing proteins in RA-FLS after the treatment with TRPV1 antagonist

No significant alterations in ASIC3, GPR4, OGR1 and TRPV1 expression were indicated at mRNA level after exposure to AMG517. Results were calculated using two-tailed paired t-test. Data are presented as mean ± SEM, n=4.

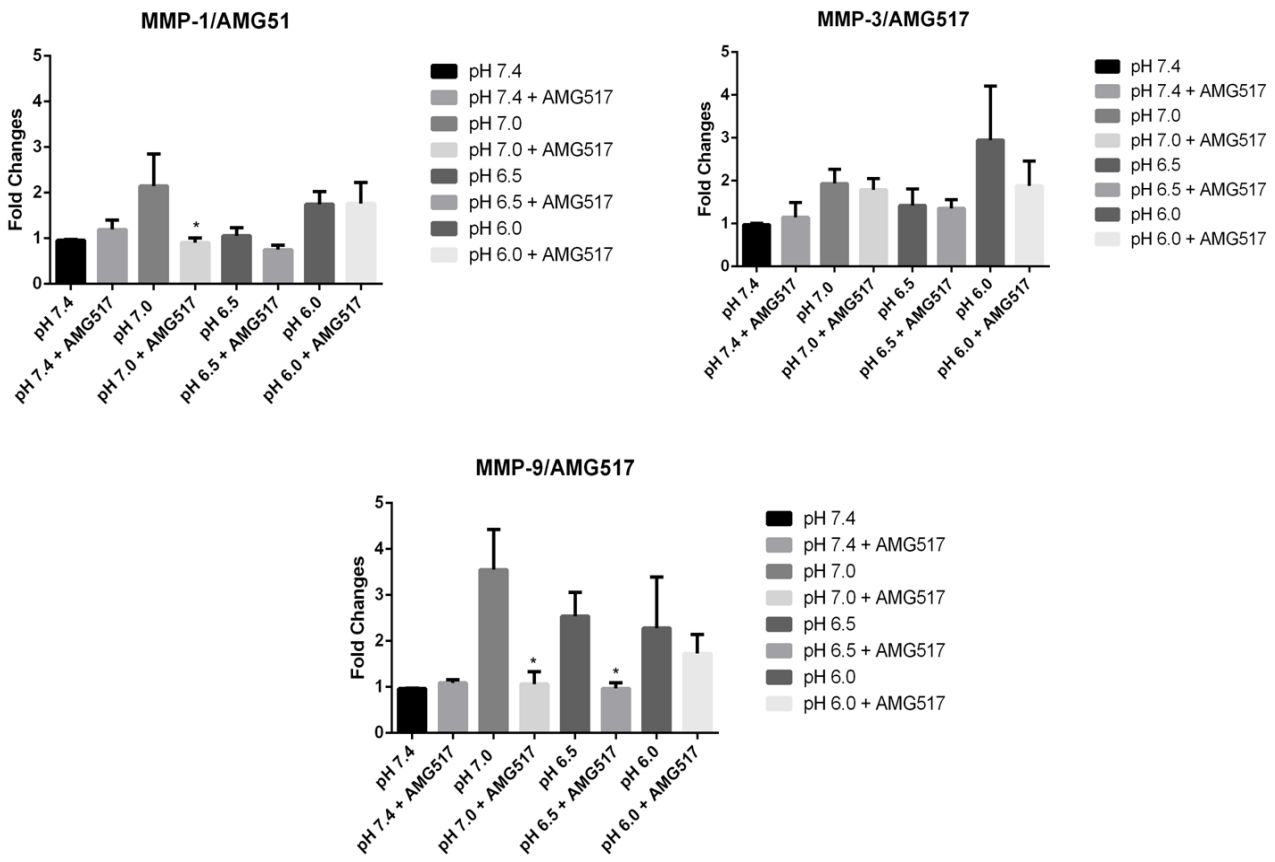

Figure 5.6 Expression of MMPs under various acidic conditions and after exposure to 175 nM AMG517.

MMP-1 showed a significant reduction in expression at pH 7.0, while MMP-9 expression was reduced at both pH 7.0 and 6.5. No significant changes in MMP-3 expression were observed after exposure to AMG517 relative to acidified medium only controls. Results are presented as mean ± SEM. * = $P \leq 0.05$, n=7.

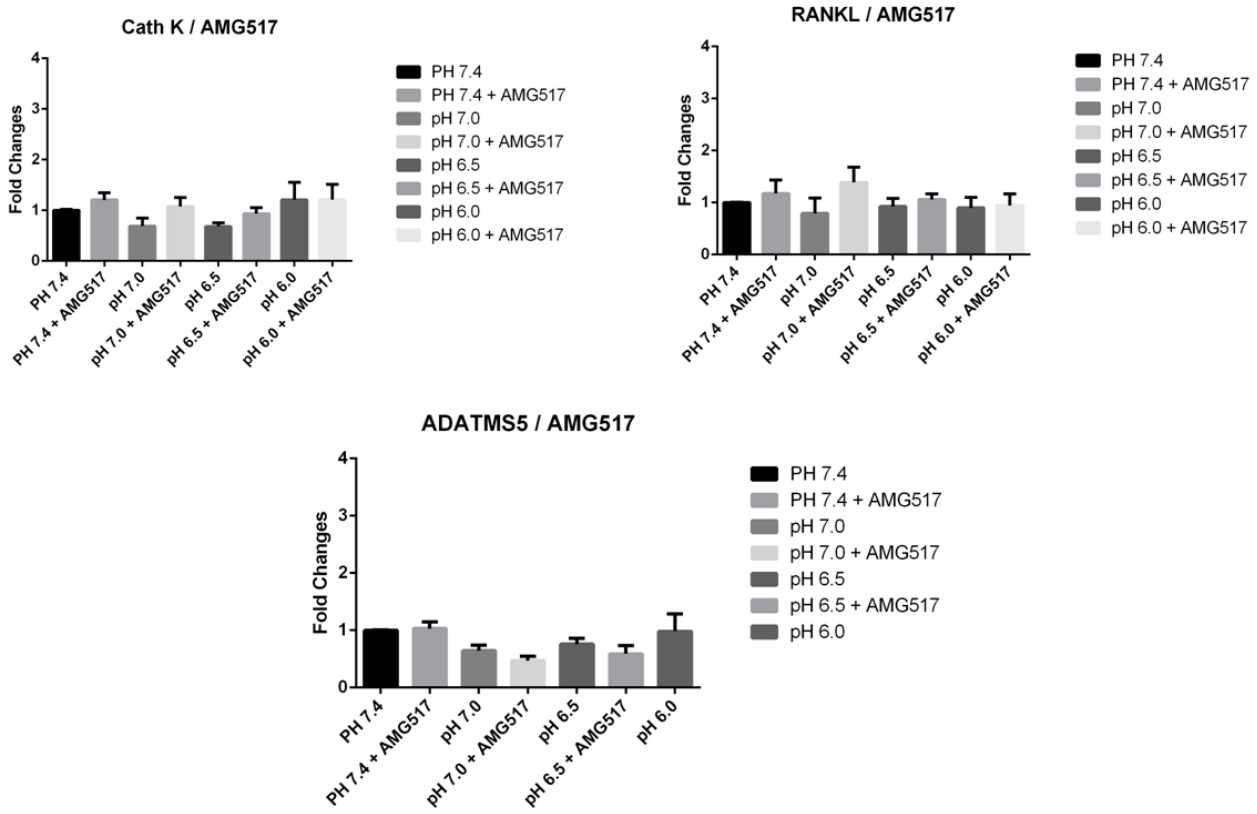

Figure 5.7 mRNA expression of bone formation modulators in RA-FLS after the treatment with TRPV1 antagonist

CathK, RANKL, and ADAMTS5 showed no significant alteration at mRNA level in RA-FLS after exposure to AMG517. Results were calculated using two-tailed paired t-test. Data are presented as mean ± SEM, n=4.

5.4.4 Pro-MMP-9 Expression was reduced in RA-FLS after the induction of AMG517

Western blot results showed a reduction in the expression of pro-MMP-9 (~92 kDa) in RA-FLS at pH 7.0, 6.5, and 6.0 after treatment with 0.75 AMG517, compared to expression in untreated RA-FLS. No protein bands were observed for MMP-1 or MMP-3, even after treatment with the ASIC3 and TRPV1 inhibitors. Protein quantification was analysed by using ImageJ software and calculated relative to the control (untreated cells at pH 7.4).

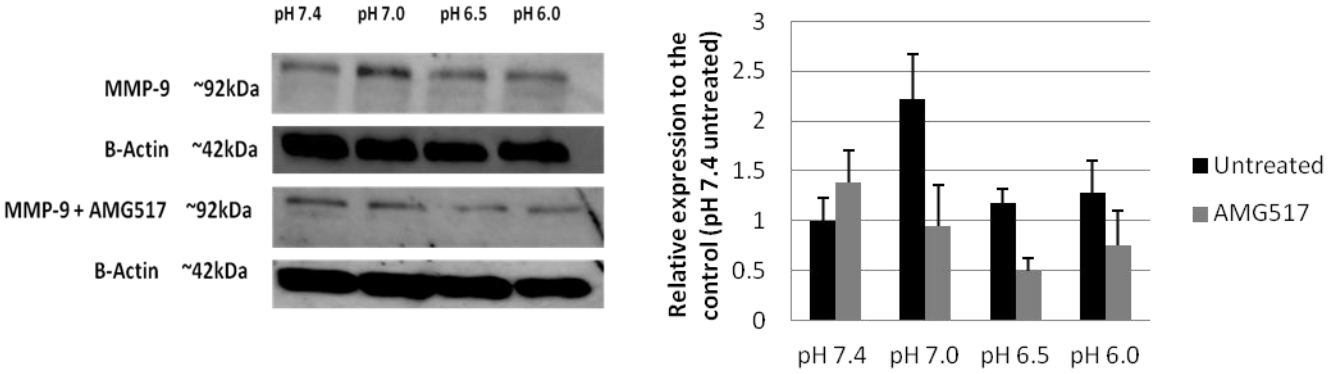

Figure 5.8 MMP-9 expression at the protein level before and after treatment with AMG517

Western blot analysis of MMP-9 showed lower expression at pH 7.0, 6.5, and 6.0 after TRPV1 inhibition compared to untreated cells cultured under acidic conditions (n=2).

5.4.5 RA-FLS migration after the induction of APETX2 and AMG517

No significant change in migration was reported after treatment with APETX2 and/or AMG517 compared to untreated cells cultured under various pH conditions (Figures 5.9-5.10). RA-FLS migration was reported as the average of three separate experiments. Treatment groups were compared using the two-tailed unpaired t-test, and data were analysed using GraphPad Prism.

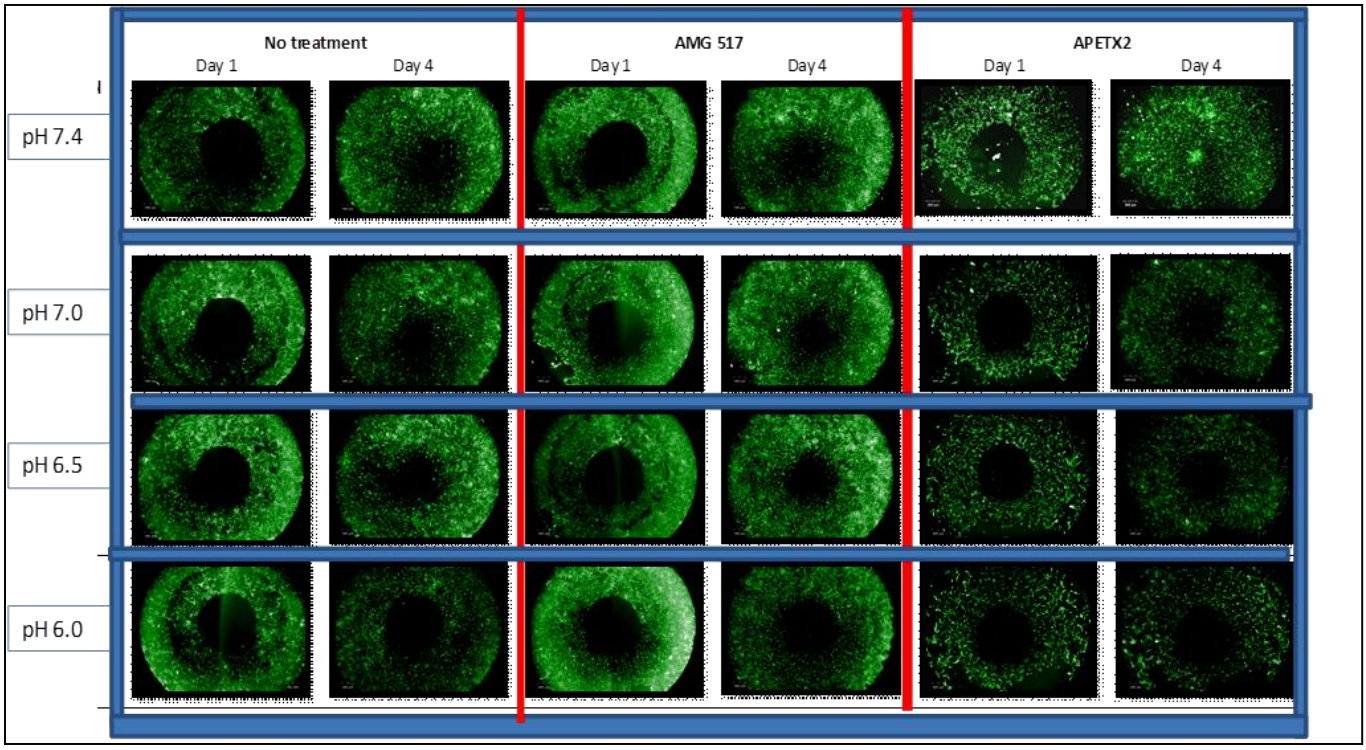

Figure 5.9 RA-FLS migration after exposure to of 0.75 nM AMG517 and 175nM APETX2

Approximately 2.5×10^4–3.0×10^4 RA-FLS were seeded and allowed to adhere for 24 h in Oris 96-well plates with stoppers. Stoppers were removed and cell migration was imaged at day 1 and day 4 after AMG517 and APETX2 were applied. This experiment was completed in triplicate.

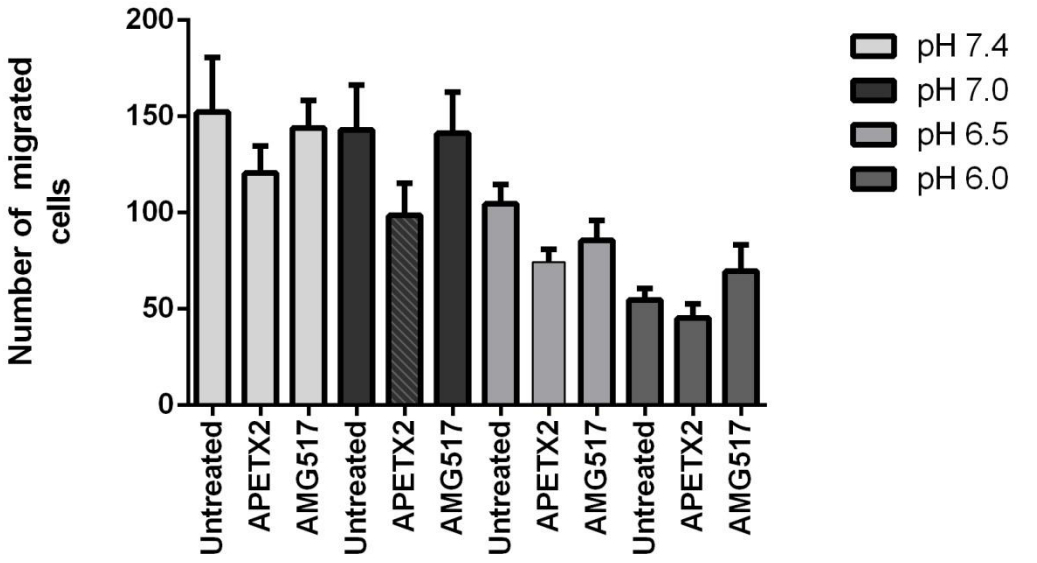

Figure 5.10 Alteration in RA-FLS migration rate under acidic conditions and after exposure to ASIC3 and TRPV1 specific inhibitors.

RA-FLS migratory activity was evaluated before and after exposure to ASIC3- and TRPV1-specific inhibitors. No significant migration was indicated when treated RA-FLS compared to untreated. Unpaired t-test was used to analyse each condition. Results are presented as mean ± SEM. This experiment was conducted in triplicate.

5.5 **Discussion**

The cell viability assay showed a slight non-significant reduction in RA-FLS viability after exposure to acidified medium and either 175 nM APETX2 or 0.75 nM AMG517 / 24 h. pH 6.0, in combination with IL-1B, has been shown to enhance death in FLS from ASIC3-/- mice compared to those from wild type mice exposed to a solution pH 6.0 only (Sluka et al., 2013). Other studies have reported no significant reduction in viability of cells such as monocytes and macrophages after exposure to lactic acid-modified medium (Mogi et al., 2009, Dietl et al., 2010). These data agree with our observations that extracellular acidification has no significant effect on cell viability, enhances the expression of MMP-1 and MMP-9 and reduces the migration rate of RA-FLS.

We hypothesized that acid-sensing proteins contribute to the modulation of MMPs and RA-FLS migration. To determine whether acid-sensing proteins affect expression of MMPs or bone destruction modulators, we inhibited the activity of ASIC3 and TRPV1 using two selective inhibitors: APETX2 and AMG517. However, to investigate the electrophysiological properties of these acid-sensing proteins and the inhibition efficiency of the inhibitors, we needed to use the patch-clamp technique (Diochot et al., 2004). This technique requires a large amount of time to identify the IC50 and extensive optimization of the inhibitor concentrations. Thus, we followed the recommended concentrations acquired from the providers and previous studies on human cells (Diochot et al., 2004, Gavva et al., 2007). With 175 nM APETX2 induction, qPCR data showed no change in expression of acid-sensing proteins and modulators of bone degradation in RA-FLS. Furthermore, at the mRNA level, we observed a significant reduction in MMP-1 and MMP-9 at pH 7.0 after treatment with APETX2. MMP-3 was reportedly increased in

a ASIC3$^{-/-}$ arthritis mouse model relative to wild type (Sluka et al., 2013). In contrast, our data suggest a gradual increase in MMP-3 expression in RA-FLS after ASIC3 is inhibited; however, this increase is not statistically significant.

Studies have suggested that MMP-1 stimulates cellular migration in myoblasts, epithelial cells, and fibroblasts (Wang et al., 2009, Herrera et al., 2013). In addition, MMP-9 overexpression enhanced migratory activity in vascular smooth muscle cells (VSMCs) both *in vitro* and *in vivo* (Galis et al., 2002, Herrera et al., 2013). However, our data show no significant change in RA-FLS migration despite the down-regulation of MMP-1 and MMP-9 with APETX2 compared to untreated RA-FLS. Conversely, TRPV1 inhibition had no effect on expression of acid-sensing proteins or bone destruction modulators in RA-FLS. However, our qPCR data reported a reduction in MMP-1 expression at pH 7.0 and MMP-9 at both pH 7.0 and pH 6.5. In addition, WB results showed a reduction in MMP-9 expression at the protein level at pH 7.0, 6.5 and 6.0 after treatment with AMG517. Despite the reduction in MMP-1 and MMP-9 expression upon AMG517 treatment, our data indicate that RA-FLS exhibited no significant changes in migratory activity when compared to RA-FLS treated with acidified medium. Our results suggest that, under extracellular acidification, ASIC3 and TRPV1 modulate the expression of MMP-1 and MMP-9 in RA-FLS, implicating a new role for these two acid-sensing proteins in RA-FLS migratory activity. Moreover, extracellular acidification impaired RA-FLS migration despite overexpression or down-regulation of MMP-1 and MMP-9.

MMP-1 and MMP-9 enhance cellular migration rate and various factors are thought to be cell migration enhancers, including TNF, IL-1B and IL-6. TNF/IL-1B were reported to enhance the production of IL-6 in dermal fibroblasts, which in turn induces MMP-9

production and enhances cellular migration (Saalbach et al., 2010). Another study reported that two migration markers, N-cadherin, and β-catenin, were upregulated by MMP-1 and myoblast migration was enhanced (Wang et al., 2009). Migration toward fibrinogen coincides with active integrin $\alpha_V\beta3$ and the production of mature MMP-9 in breast cancer cells (Rolli et al., 2003). Furthermore, expression of IL-6, MMP-3, and MMP-13 were significantly increased in ASIC3$^{-/-}$ mice relative to wild type after exposure to CAIA. Altogether, the data suggest vital roles for proinflammatory cytokines TNF, IL-1B and IL-6 in MMP expression, and thus in migration activity.

We have reported that ASIC3 and TRPV1 modulate the expression of MMP-1 at mRNA level, and MMP-9 at both mRNA and protein levels in RA-FLS after treatment with acidified medium with lactic acid. Similarly, RA-FLS migratory activity was impaired gradually with pH reduction. The role of acidification via lactic acid in TNF and IL-6 inhibition has been reported in monocytes and macrophages (Mogi et al., 2009, Dietl et al., 2010). It has been reported by Dietl et al., 2010 that low concentration of lactic acid (10 mM) inhibits TNF expression in monocytes, while inhibition of IL-6 requires a higher concentration (20 mM). This study identified that acidification of the medium to pH 7.1 has a minimal inhibition effect on TNF secretion, while a decrease in pH to 6.6 had stronger effect on TNF production. Our data showed that pH 7.0 has no significant effect on RA-FLS migration rate, but media acidified to pH 6.5 and 6.0 decreased migration significantly. Moreover, the highest expression of MMP-1 and MMP-9 was observed at pH 7.0.

Taken together, our data suggest that extracellular acidification enhances the activity of ASIC3 and TRPV1, which in turn increases the production of MMP-1 and -9 in RA-FLS.

Acidification seems to be a dominant factor that affects the production of proinflammatory cytokines TNF and IL-6 and inhibits RA-FLS migration. Moreover, ASIC3 and TRPV1 inhibition reduces MMP-1(mRNA) and MMP-9 expression and has no effect on RA-FLS migration rate.

Because there are no selective inhibitors for OGR1 and GPR4, we have attempted OGR1 knockdown in RA-FLS. However, the expression of OGR1 mRNA in RA-FLS was very low when 6-well plates were used. Thus, future studies of OGR1 will require optimization using T-75 flasks, which would generate a greater quantity of OGR1 mRNA. RA-FLS invasion assay was planned; however, due to the limitation of samples (primary RA-FLS), we used the migration assay. The invasion assay usually uses 12- or 24-well plates, which require large numbers of cells, whereas the migration assay can evaluate three different treatments and/or subjects in a single 96-well plate. We plan to carry out the invasion assay in the future when primary cells are available.

6 Chapter 6: Final Discussion

Acid-sensing protein expression and localisation were investigated previously in different cells. However, to our knowledge, no study has investigated the expression of four different acid-sensing molecules in RA-FLS. In chapter 3 of this research project, we indicated the expression and localisation of ASIC3, OGR1, GPR4 and TRPV1 in RA-FLS at both the mRNA and protein levels and in OA-FLS at the mRNA level. IHC-P reported that all four acid-sensing molecules were expressed in the synovial tissue of RA patients. Acid-sensing proteins were expressed in different patterns within fibrous tissue and around blood vessels; however, all were concentrated in the tissue lining in which FLS resides. In addition, we have detected acid-sensing protein expression in other immune cells of the synovial tissue. Furthermore, we have indicated that the expression of these molecules was higher in RA than in OA at the mRNA level. TNF is considered one of the main cytokines that promotes bone and cartilage destruction in the RA joint. TNF enhances downstream signalling pathways and promotes the production of bone and cartilage erosion modulators such as MMPs and ADAMTs (Moelants et al., 2013). Thus, we investigated whether TNF affects acid-sensing protein expression by treating RA-FLS with 10 ng of TNF. All four acid-sensing molecules were increased; however, the difference was insignificant possibly due to the small number of samples examined. A large number of samples may be needed to indicate the actual effect of TNF on acid-sensing protein expression because signs of increase were reported in a small number of RA patient samples. rheumatoid joint characterised by an acidic microenvironment with pH as low as (6.6) (Falchuk et al., 1970), we investigated the expression of acid-sensing proteins in RA-FLS under different acidic conditions (pH 7.4-6.0). The expression of

these acid sensors was indicated in human RA-FLS with a slight but not significant alteration at low pH compared with that at pH 7.4. Bone and cartilage destruction are a major complication of RA, and this process is modulated by multiple enzymes such as serine proteases, aggrecanases, and MMPs. Few studies have focussed on the effect of an acidic microenvironment on the expression of such modulators in RA-FLS, while no study has shown how the expression of these proteins may be altered by a change in pH. In the current study, we investigated the effect of extracellular acidification on the expression of bone and cartilage modulators, including MMP-1, -3, -9, and -14, Cathepsin K, RANKL and ADAMTS-5, in human RA-FLS. MMP-1, -3 and -9 were upregulated under acidic conditions at pH 7.0-6.0 compared with the control at pH 7.4. MMP-9 expression in RA-FLS was dramatically upregulated at pH 7.0 compared with that in the control. Furthermore, we reported that MMP-1 and -9 were highly expressed in RA-FLS compared with that in OA-FLS. It has been known that MMP-1 and -9 play important roles in cell migration as reported in myoblasts, epithelial cells, and vascular smooth muscle cells (VSMCs) (Galis et al., 2002, Wang et al., 2009, Herrera et al., 2013) .Thus, we tested the migratory activity of RA-FLS under different acidic environments. Our data reported a reduction in the RA-FLS migration rate under low pH. Taken together, our data suggest that the acidic microenvironment of the RA joint enhances the activity of acid-sensing proteins that, in turn, promote the production of MMP-1, -3, and -9. Furthermore, TNF/IL-1B and IL-6 were reported to be key players that enhance MMP-9 expression, which then enhances the migratory activity of dermal fibroblasts (Saalbach et al., 2010). However, under acidified conditions created by lactic acid, the production of TNF and IL-6 are down-regulated as reported previously (Mogi et al., 2009, Dietl et al.,

2010). Our data reflect that acid (lactic acid build up) is a key factor that enhances MMP-1 and -9 expression and impairs RA-FLS migration activity. It would be interesting to study the expression of MMPs in RA-FLS under the effect of a combination of both TNF and an acidified medium.

It has been reported that ASIC3 modulates the expression of MMP-3 and MMP-9 in ASIC3-/- mice (Sluka et al., 2013), and TRPV1 activation enhances the expression of MMP-1 in human keratinocytes (Lee et al., 2008). However, there is a lack of knowledge concerning the roles of these two acid-sensing proteins in RA. To understand the role of acid-sensing proteins in RA-FLS migration and MMP expression, ASIC3 and TRPV1 were targeted by specific and potent inhibitors (APETx2 and AMG517). We reported that these two acid-sensor molecule alterations modulate the expression MMP-1 and -9 in RA-FLS but has no effect on the migration rate of RA-FLS under low pH. Our data suggest that both ASIC3 and TRPV1 activity may promote the expression of MMP-1 and -9, while the migration of RA-FLS could be modulated by other acid-sensing proteins such as OGR1 and/or GPR4. Moreover, ASIC3 and TRPV1 could be considered potential therapeutic targets that may reduce bone and cartilage erosion in RA. In vivo studies would provide interesting knowledge regarding the role of these two molecules in the development of RA. Understanding the intracellular signalling pathways underlying the activation of ASIC3 and TRPV1 would provide a wide range of therapeutic targets that may help to suppress RA complication. Different studies have investigated ASIC3 and TRPV1 signalling pathways for their activation in different inflammatory disorders. Active ASIC3 enhances Ca^{2+} influx, which, in turn, increases intracellular calcium mobilisation and activates several signalling pathways. Increased Ca^{2+} in the cell is also

associated with Ca^{2+}/calmodulin-dependent protein kinase II activation, further aggravating inflammation. Additionally, TRPV1 activation is associated with different inflammatory conditions such as RA. It has been described that TRPV1 activation mediates numerous signalling pathways, including the activation of PKC and PKA.

To our knowledge, we are the first to report the expression of OGR1 and GPR4 in RA-FLS and synovial tissue. However, the role of these two proteins in the development of RA remains elusive. In vitro and in vivo studies have reported that OGR1 was strongly upregulated during the activation of osteoclastogenesis (Yang et al., 2006). Another study demonstrated that OGR1 responds to extracellular acidification and enhances osteoclast viability through an NFAT-independent, protein kinase C-dependent pathway, while the inhibition of this channel by Cu^{2+} or siRNA suppressed the survival of osteoclasts under acidified conditions (Pereverzev et al., 2008). These findings suggest that OGR1 expressed in RA-FLS may also be involved in bone degradation and cartilage destruction in the RA joint. Interestingly, different studies have described OGR1 as a cell migration suppressor; it has been found that OGR1, but not GPR4, inhibits both breast and prostate cancer cell migration and metastasis via the increased expression of Gαi1 (Singh et al., 2007) and the Gα12/13-Rho-Rac1 pathway (Li et al., 2013). By contrast, another in vivo study demonstrated the role of GPR4 in melanoma and prostate cancer cells under an acidic environment. It has been reported that GPR4 activation at pH 6.4-6.9 enhances the production of active RhoA and actin stress fibre formation, which, in turn, reduces cell migration activity (Castellone et al., 2011). Our study reported a reduction in the RA-FLS migration rate under low pH and may reflect the involvement of OGR1 and GPR4 in RA-FLS migration activity despite the increase in MMP-1, -3 and -9. In conclusion, our study

demonstrated that at least four mediating factors exist for sensing acid are expressed in the RA synovium at the mRNA and protein levels. To our knowledge, we are the first to indicate the expression of OGR1 and GPR4 in RA-FLS. Moreover, we reported that an acidified microenvironment has no effect on acid-sensing protein expression; however, the activity needs further investigation by using the patch clamp technique. Acidic conditions upregulate the expression of MMP-1, -3 and -9 in RA-FLS. Furthermore, our study indicated that ASIC3 and TRPV1 inhibition down regulate the expression of MMP-1 and -9 under low pH. Additionally, the migration activity of RA-FLS was gradually reduced with the reduction in pH despite the inhibition of ASIC3 and TRPV1 activity. Taken together, these findings suggest that an acidic microenvironment within the rheumatoid joint promotes the activities of ASIC3 and TRPV1, which, in turn, increase the production of MMP-1, -3 and -9. In addition, OGR1 and GPR4 may be activated and halt the migration activity of RA-FLS, thus aggravating RA complication through bone erosion and cartilage destruction. Targeting acid-sensing receptors may represent a novel means to inhibit bone invasion and cartilage destruction in response to microenvironmental acidosis in RA.

7 FUTURE WORK:

As we reported the expression of acid-sensing proteins by immune cells other than FLS, identifying the identities of these cells will provide valuable knowledge concerning how these cells may be involved in RA development. We will also investigate the activity of the acid-sensing proteins ASIC3, OGR1, GPR4 and TRPV1 under different acidic conditions and how they might contribute to the expression of MMPs. It is crucial to

explore the intracellular signalling pathways induced by acid-sensing protein activity after RA-FLS exposure to an acidic environment. To better understand the exact role of OGR1 and GPR4 in RA-FLS migration and invasion, we will use small interfering RNA (siRNA) targeting these two molecules. An in vivo study using a murine model of RA and an acid-sensing protein knock-out model will provide interesting knowledge concerning the role of these molecules in the development of RA.

Bibliography

ABRAMSON, S. B., AMIN, A. R., CLANCY, R. M. & ATTUR, M. 2001. The role of nitric oxide in tissue destruction. *Best Pract Res Clin Rheumatol,* 15**,** 831-45.

AGRAWAL, S., MISRA, R. & AGGARWAL, A. 2006. Anemia in rheumatoid arthritis: high prevalence of iron-deficiency anemia in Indian patients. *Rheumatol Int,* 26**,** 1091-5.

AHN, J. K., KOH, E. M., CHA, H. S., LEE, Y. S., KIM, J., BAE, E. K. & AHN, K. S. 2008. Role of hypoxia-inducible factor-1alpha in hypoxia-induced expressions of IL-8, MMP-1 and MMP-3 in rheumatoid fibroblast-like synoviocytes. *Rheumatology (Oxford),* 47**,** 834-9.

ALARCON, G. S., KOOPMAN, W. J., ACTON, R. T. & BARGER, B. O. 1982. Seronegative rheumatoid arthritis. A distinct immunogenetic disease? *Arthritis Rheum,* 25**,** 502-7.

AKBAR, A., YIANGOU, Y., FACER, P., BRYDON, W. G., WALTERS, J. R., ANAND, P. & GHOSH, S. 2010. Expression of the TRPV1 receptor differs in quiescent inflammatory bowel disease with or without abdominal pain. *Gut,* 59**,** 767-74.

AKIMOTO, H., YAMAZAKI, R., HASHIMOTO, S., SATO, T. & ITO, A. 2000. 4'-Hydroxy aceclofenac suppresses the interleukin-1-induced production of promatrix metalloproteinases and release of sulfated-glycosaminoglycans from rabbit articular chondrocytes. *Eur J Pharmacol,* 401**,** 429-36.

ALVAREZ DE LA ROSA, D., ZHANG, P., SHAO, D., WHITE, F. & CANESSA, C. M. 2002. Functional implications of the localization and activity of acid-sensitive channels in rat peripheral nervous system. *Proc Natl Acad Sci U S A,* 99**,** 2326-31.

ARNETT, T. R. & DEMPSTER, D. W. 1986. Effect of pH on bone resorption by rat osteoclasts in vitro. *Endocrinology,* 119**,** 119-24.

ASKLING, J., BAECKLUND, E., GRANATH, F., GEBOREK, P., FORED, M., BACKLIN, C., BERTILSSON, L., COSTER, L., JACOBSSON, L. T., LINDBLAD, S., LYSHOLM, J., RANTAPAA-DAHLQVIST, S., SAXNE, T., VAN VOLLENHOVEN, R., KLARESKOG, L. & FELTELIUS, N. 2009. Anti-tumour necrosis factor therapy in rheumatoid arthritis and risk of malignant lymphomas: relative risks and time trends in the Swedish Biologics Register. *Ann Rheum Dis,* 68**,** 648-53.

ASKWITH, C. C., CHENG, C., IKUMA, M., BENSON, C., PRICE, M. P. & WELSH, M. J. 2000. Neuropeptide FF and FMRFamide potentiate acid-evoked currents from sensory neurons and proton-gated DEG/ENaC channels. *Neuron,* 26**,** 133-41.

ATCHIA, II, KIDD, C. E. & BELL, R. W. 2006. Rheumatoid arthritis-associated necrotizing scleritis and peripheral ulcerative keratitis treated successfully with infliximab. *J Clin Rheumatol,* 12**,** 291-3.

BABINSKI, K., CATARSI, S., BIAGINI, G. & SEGUELA, P. 2000. Mammalian ASIC2a and ASIC3 subunits co-assemble into heteromeric proton-gated channels sensitive to Gd3+. *J Biol Chem,* 275**,** 28519-25.

BALINT, G. P. & BALINT, P. V. 2004. Felty's syndrome. *Best Pract Res Clin Rheumatol,* 18**,** 631-45.

BALSA, A., BARRERA, P., WESTHOVENS, R., ALVES, H., MAENAUT, K., PASCUAL-SALCEDO, D., CORNELIS, F., BARDIN, T., RIENTE, L., RADSTAKE, T. R., DE ALMEIDA, G., LEPAGE, V., STRAVOPOULOS, C., SPAEPEN, M., LOPES-VAZ, A., CHARRON, D., MARTINEZ, M., PRUDHOMME, J. F., MIGLIORINI, P. & FRITZ, P. 2001. Clinical and immunogenetic characteristics of European multicase rheumatoid arthritis families. *Ann Rheum Dis,* 60**,** 573-6.

BARTOK, B. & FIRESTEIN, G. S. 2010. Fibroblast-like synoviocytes: key effector cells in rheumatoid arthritis. *Immunol Rev,* 233**,** 233-55.
BARTON, N. J., MCQUEEN, D. S., THOMSON, D., GAULDIE, S. D., WILSON, A. W., SALTER, D. M. & CHESSELL, I. P. 2006. Attenuation of experimental arthritis in TRPV1R knockout mice. *Exp Mol Pathol,* 81**,** 166-70.
BAUD, V. & KARIN, M. 2001. Signal transduction by tumor necrosis factor and its relatives. *Trends Cell Biol,* 11**,** 372-7.
BENSON, C. J., ECKERT, S. P. & MCCLESKEY, E. W. 1999. Acid-evoked currents in cardiac sensory neurons: A possible mediator of myocardial ischemic sensation. *Circ Res,* 84**,** 921-8.
BENSON, C. J., XIE, J., WEMMIE, J. A., PRICE, M. P., HENSS, J. M., WELSH, M. J. & SNYDER, P. M. 2002. Heteromultimers of DEG/ENaC subunits form H+-gated channels in mouse sensory neurons. *Proc Natl Acad Sci U S A,* 99**,** 2338–2343.
BEVAN, S., HOTHI, S., HUGHES, G., JAMES, I. F., RANG, H. P., SHAH, K., WALPOLE, C. S. & YEATS, J. C. 1992. Capsazepine: a competitive antagonist of the sensory neurone excitant capsaicin. *Br J Pharmacol,* 107**,** 544-52.
BHARADWAJ, A. & HAROON, N. 2005. Interstitial lung disease and neuropathy as predominant extra-articular manifestations in patients with rheumatoid arthritis: a prospective study. *Med Sci Monit,* 11**,** 26.
BINGHAM, C. O., 3RD 2002. The pathogenesis of rheumatoid arthritis: pivotal cytokines involved in bone degradation and inflammation. *J Rheumatol Suppl,* 65**,** 3-9.
BOHLEN, C. J. & JULIUS, D. 2012. Receptor-targeting mechanisms of pain-causing toxins: How ow? *Toxicon,* 60**,** 254-64.
BOLCSKEI, K., HELYES, Z., SZABO, A., SANDOR, K., ELEKES, K., NEMETH, J., ALMASI, R., PINTER, E., PETHO, G. & SZOLCSANYI, J. 2005. Investigation of the role of TRPV1 receptors in acute and chronic nociceptive processes using gene-deficient mice. *Pain,* 117**,** 368-76.
BOUSSOUAR, F., GRATAROLI, R., JI, J. & BENAHMED, M. 1999. Tumor necrosis factor-alpha stimulates lactate dehydrogenase A expression in porcine cultured sertoli cells: mechanisms of action. *Endocrinology,* 140**,** 3054-62.
BOWMAN, S. J. 2002. Hematological manifestations of rheumatoid arthritis. *Scand J Rheumatol,* 31**,** 251-9.
BRASINGTON, R. Disease-Modifying Antirheumatic Drugs. *Journal of Hand Surgery,* 34**,** 347-348.
BRITO, R., SHETH, S., MUKHERJEA, D., RYBAK, L. P. & RAMKUMAR, V. 2014. TRPV1: A Potential Drug Target for Treating Various Diseases. *Cells,* 3**,** 517-45.
BROAD, L. M., KEDING, S. J. & BLANCO, M. J. 2008. Recent progress in the development of selective TRPV1 antagonists for pain. *Curr Top Med Chem,* 8**,** 1431-41.
BRUCE, B. & FRIES, J. F. 2003. The Stanford Health Assessment Questionnaire: Dimensions and Practical Applications. *Health and Quality of Life Outcomes,* 1**,** 20-20.
BURRAGE, P. S., MIX, K. S. & BRINCKERHOFF, C. E. 2006. Matrix metalloproteinases: role in arthritis. *Front Biosci,* 11**,** 529-43.
BUSTIN, S. A., BENES, V., GARSON, J. A., HELLEMANS, J., HUGGETT, J., KUBISTA, M., MUELLER, R., NOLAN, T., PFAFFL, M. W., SHIPLEY, G. L., VANDESOMPELE, J. & WITTWER, C. T. 2009. The MIQE guidelines: minimum information for publication of quantitative real-time PCR experiments. *Clin Chem,* 55**,** 611-22.
CARROLL, M. B. & BOND, M. I. 2008. Use of tumor necrosis factor-alpha inhibitors in patients with chronic hepatitis B infection. *Semin Arthritis Rheum,* 38**,** 208-17.
CASTELLONE, R. D., LEFFLER, N. R., DONG, L. & YANG, L. V. 2011. Inhibition of tumor cell migration and metastasis by the proton-sensing GPR4 receptor. *Cancer Lett,* 312**,** 197-208.

CATERINA, M. J. & JULIUS, D. 2001. The vanilloid receptor: a molecular gateway to the pain pathway. *Annu Rev Neurosci,* 24**,** 487-517.
CATERINA, M. J., SCHUMACHER, M. A., TOMINAGA, M., ROSEN, T. A., LEVINE, J. D. & JULIUS, D. 1997. The capsaicin receptor: a heat-activated ion channel in the pain pathway. *Nature,* 389**,** 816-24.
CATRINA, A. I., LAMPA, J., ERNESTAM, S., AF KLINT, E., BRATT, J., KLARESKOG, L. & ULFGREN, A. K. 2002. Anti-tumour necrosis factor (TNF)-alpha therapy (etanercept) down-regulates serum matrix metalloproteinase (MMP)-3 and MMP-1 in rheumatoid arthritis. *Rheumatology (Oxford),* 41**,** 484-9.
CAWSTON, T. E. & WILSON, A. J. 2006. Understanding the role of tissue degrading enzymes and their inhibitors in development and disease. *Best Pract Res Clin Rheumatol,* 20**,** 983-1002.
CHARBONNEAU, M., HARPER, K., GRONDIN, F., PELMUS, M., MCDONALD, P. P. & DUBOIS, C. M. 2007. Hypoxia-inducible factor mediates hypoxic and tumor necrosis factor alpha-induced increases in tumor necrosis factor-alpha converting enzyme/ADAM17 expression by synovial cells. *J Biol Chem,* 282**,** 33714-24.
CHEN, A., DONG, L., LEFFLER, N. R., ASCH, A. S., WITTE, O. N. & YANG, L. V. 2011. Activation of GPR4 by acidosis increases endothelial cell adhesion through the cAMP/Epac pathway. *PLoS One,* 6**,** e27586.
CHEN, X., QIU, L., LI, M., DURRNAGEL, S., ORSER, B. A., XIONG, Z. G. & MACDONALD, J. F. 2010. Diarylamidines: high potency inhibitors of acid-sensing ion channels. *Neuropharmacology,* 58**,** 1045-53.
CHRISTENSEN, B. N., KOCHUKOV, M., MCNEARNEY, T. A., TAGLIALATELA, G. & WESTLUND, K. N. 2005a. Proton-sensing G protein-coupled receptor mobilizes calcium in human synovial cells. *Am J Physiol Cell Physiol,* 289**,** C601-8.
CHRISTENSEN, B. N., KOCHUKOV, M., MCNEARNEY, T. A., TAGLIALATELA, G. & WESTLUND, K. N. 2005b. Proton-sensing G protein-coupled receptor mobilizes calcium in human synovial cells. . *Am J Physiol Cell Physiol.,* 289**,** C601-8.
CHU, X. P., PAPASIAN, C. J., WANG, J. Q. & XIONG, Z. G. 2011. Modulation of acid-sensing ion channels: molecular mechanisms and therapeutic potential. *Int J Physiol Pathophysiol Pharmacol,* 3**,** 288-309.
COBBE, S. M., PARKER, D. J. & POOLE-WILSON, P. A. 1982. Tissue and coronary venous pH in ischemic canine myocardium. *Clin Cardiol,* 5**,** 153-6.
COBBE, S. M. & POOLE-WILSON, P. A. 1980. Tissue acidosis in myocardial hypoxia. *J Mol Cell Cardiol,* 12**,** 761-70.
COJOCARU, M., COJOCARU, I. M., SILOSI, I., VRABIE, C. D. & TANASESCU, R. 2010. Extra-articular Manifestations in Rheumatoid Arthritis. *Mædica,* 5**,** 286-291.
COMBE, B., DIDRY, C., GUTIERREZ, M., ANAYA, J. M. & SANY, J. 1993. Accelerated nodulosis and systemic manifestations during methotrexate therapy for rheumatoid arthritis. *Eur J Med,* 2**,** 153-6.
CRONSTEIN, B. N. 2007. Interleukin-6--a key mediator of systemic and local symptoms in rheumatoid arthritis. *Bull NYU Hosp Jt Dis,* 65**,** S11-5.
CUNNANE, G., WARNOCK, M., FYE, K. H. & DAIKH, D. I. 2002. Accelerated nodulosis and vasculitis following etanercept therapy for rheumatoid arthritis. *Arthritis Rheum,* 47**,** 445-9.
D'HAENE, B., VANDESOMPELE, J. & HELLEMANS, J. 2010. Accurate and objective copy number profiling using real-time quantitative PCR. *Methods,* 50**,** 262-70.
DAVIS, J. B., GRAY, J., GUNTHORPE, M. J., HATCHER, J. P., DAVEY, P. T., OVEREND, P., HARRIES, M. H., LATCHAM, J., CLAPHAM, C., ATKINSON, K., HUGHES, S. A., RANCE, K., GRAU, E., HARPER, A. J., PUGH, P. L., ROGERS, D. C.,

BINGHAM, S., RANDALL, A. & SHEARDOWN, S. A. 2000. Vanilloid receptor-1 is essential for inflammatory thermal hyperalgesia. *Nature,* 405**,** 183-7.
DAWSON, J. K., FEWINS, H. E., DESMOND, J., LYNCH, M. P. & GRAHAM, D. R. 2001. Fibrosing alveolitis in patients with rheumatoid arthritis as assessed by high resolution computed tomography, chest radiography, and pulmonary function tests. *Thorax,* 56**,** 622-7.
DEERING-RICE, C. E., JOHANSEN, M. E., ROBERTS, J. K., THOMAS, K. C., ROMERO, E. G., LEE, J., YOST, G. S., VERANTH, J. M. & REILLY, C. A. 2012. Transient Receptor Potential Vanilloid-1 (TRPV1) Is a Mediator of Lung Toxicity for Coal Fly Ash Particulate Material. *Mol Pharmacol,* 81**,** 411-419.
DEMORUELLE, M. K. & DEANE, K. D. 2012. Treatment Strategies in Early Rheumatoid Arthritis and Prevention of Rheumatoid Arthritis. *Current rheumatology reports,* 14**,** 472-480.
DEVAL, E., GASULL, X., NOEL, J., SALINAS, M., BARON, A., DIOCHOT, S. & LINGUEGLIA, E. 2010. Acid-sensing ion channels (ASICs): pharmacology and implication in pain. *Pharmacol Ther,* 128**,** 549-58.
DEVAL, E., NOEL, J., LAY, N., ALLOUI, A., DIOCHOT, S., FRIEND, V., JODAR, M., LAZDUNSKI, M. & LINGUEGLIA, E. 2008. ASIC3, a sensor of acidic and primary inflammatory pain. *EMBO J,* 27**,** 3047-55.
DEVESA, I., PLANELLS-CASES, R., FERNÁNDEZ-BALLESTER, G., GONZÁLEZ-ROS, J. M., FERRER-MONTIEL, A. & FERNÁNDEZ-CARVAJAL, A. 2011. Role of the transient receptor potential vanilloid 1 in inflammation and sepsis. *J Inflamm Res.,* 4**,** 67-81.
DI PAOLO, J. A., HUANG, T., BALAZS, M., BARBOSA, J., BARCK, K. H., BRAVO, B. J., CARANO, R. A., DARROW, J., DAVIES, D. R., DEFORGE, L. E., DIEHL, L., FERRANDO, R., GALLION, S. L., GIANNETTI, A. M., GRIBLING, P., HUREZ, V., HYMOWITZ, S. G., JONES, R., KROPF, J. E., LEE, W. P., MACIEJEWSKI, P. M., MITCHELL, S. A., RONG, H., STAKER, B. L., WHITNEY, J. A., YEH, S., YOUNG, W. B., YU, C., ZHANG, J., REIF, K. & CURRIE, K. S. 2011. Specific Btk inhibition suppresses B cell- and myeloid cell-mediated arthritis. *Nat Chem Biol,* 7**,** 41-50.
DIETL, K., RENNER, K., DETTMER, K., TIMISCHL, B., EBERHART, K., DORN, C., HELLERBRAND, C., KASTENBERGER, M., KUNZ-SCHUGHART, L. A., OEFNER, P. J., ANDREESEN, R., GOTTFRIED, E. & KREUTZ, M. P. 2010. Lactic acid and acidification inhibit TNF secretion and glycolysis of human monocytes. *J Immunol,* 184**,** 1200-9.
DIOCHOT, S., BARON, A., RASH, L. D., DEVAL, E., ESCOUBAS, P., SCARZELLO, S., SALINAS, M. & LAZDUNSKI, M. 2004. A new sea anemone peptide, APETx2, inhibits ASIC3, a major acid-sensitive channel in sensory neurons. *EMBO J,* 23**,** 1516-25.
DONG, L., LI, Z., LEFFLER, N. R., ASCH, A. S., CHI, J. T. & YANG, L. V. 2013. Acidosis activation of the proton-sensing GPR4 receptor stimulates vascular endothelial cell inflammatory responses revealed by transcriptome analysis. *PLoS One,* 8**,** e61991.
DOUGADOS, M., SOUBRIER, M., ANTUNEZ, A., BALINT, P., BALSA, A., BUCH, M. H., CASADO, G., DETERT, J., EL-ZORKANY, B., EMERY, P., HAJJAJ-HASSOUNI, N., HARIGAI, M., LUO, S. F., KURUCZ, R., MACIEL, G., MOLA, E. M., MONTECUCCO, C. M., MCINNES, I., RADNER, H., SMOLEN, J. S., SONG, Y. W., VONKEMAN, H. E., WINTHROP, K. & KAY, J. 2014. Prevalence of comorbidities in rheumatoid arthritis and evaluation of their monitoring: results of an international, cross-sectional study (COMORA). *Ann Rheum Dis,* 73**,** 62-8.
DRUEY, K. M. 2003. Regulators of G protein signalling: potential targets for treatment of allergic inflammatory diseases such as asthma. *Expert Opin Ther Targets,* 7**,** 475-84.

DUAN, B., WU, L. J., YU, Y. Q., DING, Y., JING, L., XU, L., CHEN, J. & XU, T. L. 2007. Upregulation of acid-sensing ion channel ASIC1a in spinal dorsal horn neurons contributes to inflammatory pain hypersensitivity. *J Neurosci,* 27**,** 11139-48.

EGSMOSE, C., LUND, B., BORG, G., PETTERSSON, H., BERG, E., BRODIN, U. & TRANG, L. 1995. Patients with rheumatoid arthritis benefit from early 2nd line therapy: 5 year followup of a prospective double blind placebo controlled study. *J Rheumatol,* 22**,** 2208-13.

ENGLER, A., AESCHLIMANN, A., SIMMEN, B. R., MICHEL, B. A., GAY, R. E., GAY, S. & SPROTT, H. 2007. Expression of transient receptor potential vanilloid 1 (TRPV1) in synovial fibroblasts from patients with osteoarthritis and rheumatoid arthritis. *Biochem Biophys Res Commun,* 359**,** 884-8.

FALCHUK, K. H., GOETZL, E. J. & KULKA, J. P. 1970. Respiratory gases of synovial fluids. An approach to synovial tissue circulatory-metabolic imbalance in rheumatoid arthritis. *Am J Med,* 49**,** 223-31.

FARR, M., GARVEY, K., BOLD, A. M., KENDALL, M. J. & BACON, P. A. 1985. Significance of the hydrogen ion concentration in synovial fluid in rheumatoid arthritis. *Clin Exp Rheumatol,* 3**,** 99-104.

FERNANDES, E. S., RUSSELL, F. A. & D, D. S. 2011. A distinct role for TRPA1, in addition to TRPV1, in TNFalpha-induced inflammatory hyperalgesia and CFA-induced mono-arthritis. . *Arthritis Rheum,* 63**,** 819–829.

FIRESTEIN, G. S. 2003. Evolving concepts of rheumatoid arthritis. *Nature,* 423**,** 356-61.

FIRESTEIN, G. S., PAINE, M. M. & LITTMAN, B. H. 1991. Gene expression (collagenase, tissue inhibitor of metalloproteinases, complement, and HLA-DR) in rheumatoid arthritis and osteoarthritis synovium. Quantitative analysis and effect of intraarticular corticosteroids. *Arthritis Rheum,* 34**,** 1094-105.

FIRESTEIN, G. S. & ZVAIFLER, N. J. 1990. How important are T cells in chronic rheumatoid synovitis? *Arthritis Rheum,* 33**,** 768-73.

FUJIKAWA, K., KAWAKAMI, A., TAMAI, M., UETANI, M., TAKAO, S., ARIMA, K., IWAMOTO, N., ARAMAKI, T., KAWASHIRI, S., ICHINOSE, K., KAMACHI, M., NAKAMURA, H., ORIGUCHI, T., IDA, H., AOYAGI, K. & EGUCHI, K. 2009. High serum cartilage oligomeric matrix protein determines the subset of patients with early-stage rheumatoid arthritis with high serum C-reactive protein, matrix metalloproteinase-3, and MRI-proven bone erosion. *J Rheumatol,* 36**,** 1126-9.

GALIS, Z. S., JOHNSON, C., GODIN, D., MAGID, R., SHIPLEY, J. M., SENIOR, R. M. & IVAN, E. 2002. Targeted disruption of the matrix metalloproteinase-9 gene impairs smooth muscle cell migration and geometrical arterial remodeling. *Circ Res,* 91**,** 852-9.

GARNERO, P., BOREL, O., BYRJALSEN, I., FERRERAS, M., DRAKE, F. H., MCQUENEY, M. S., FOGED, N. T., DELMAS, P. D. & DELAISSE, J. M. 1998. The collagenolytic activity of cathepsin K is unique among mammalian proteinases. *J Biol Chem,* 273**,** 32347-52.

GATENBY, R. A. & GILLIES, R. J. 2004. Why do cancers have high aerobic glycolysis? *Nat Rev Cancer,* 4**,** 891-9.

GAVVA, N. R., BANNON, A. W., HOVLAND, D. N., JR., LEHTO, S. G., KLIONSKY, L., SURAPANENI, S., IMMKE, D. C., HENLEY, C., ARIK, L., BAK, A., DAVIS, J., ERNST, N., HEVER, G., KUANG, R., SHI, L., TAMIR, R., WANG, J., WANG, W., ZAJIC, G., ZHU, D., NORMAN, M. H., LOUIS, J. C., MAGAL, E. & TREANOR, J. J. 2007. Repeated administration of vanilloid receptor TRPV1 antagonists attenuates hyperthermia elicited by TRPV1 blockade. *J Pharmacol Exp Ther,* 323**,** 128-37.

GEBOREK, P., SAXNE, T., PETTERSSON, H. & WOLLHEIM, F. A. 1989. Synovial fluid acidosis correlates with radiological joint destruction in rheumatoid arthritis knee joints. . *J Rheumatol.,* 16**,** 468-72.

GILCHRIST, A., LI, A. & HAMM, H. E. 2002. G alpha COOH-terminal minigene vectors dissect heterotrimeric G protein signaling. *Sci STKE,* 2002**,** pl1.

GILMAN, S. C., BERNER, P. R. & CHANG, J. 1987. Phospholipase A2 activation by interleukin 1: release and metabolism of arachidonic acid by IL 1-stimulated rabbit chondrocytes. *Agents Actions,* 21**,** 345-7.

GLASSON, S. S., ASKEW, R., SHEPPARD, B., CARITO, B., BLANCHET, T., MA, H. L., FLANNERY, C. R., PELUSO, D., KANKI, K., YANG, Z., MAJUMDAR, M. K. & MORRIS, E. A. 2005. Deletion of active ADAMTS5 prevents cartilage degradation in a murine model of osteoarthritis. *Nature,* 434**,** 644-8.

GLASSON, S. S., ASKEW, R., SHEPPARD, B., CARITO, B. A., BLANCHET, T., MA, H. L., FLANNERY, C. R., KANKI, K., WANG, E., PELUSO, D., YANG, Z., MAJUMDAR, M. K. & MORRIS, E. A. 2004. Characterization of and osteoarthritis susceptibility in ADAMTS-4-knockout mice. *Arthritis Rheum,* 50**,** 2547-58.

GOLDRING, S. R. 2003. Pathogenesis of bone and cartilage destruction in rheumatoid arthritis. *Rheumatology (Oxford),* 42 Suppl 2**,** ii11-6.

GOMEZ, E. L., GUN, S. C., SOMNATH, S. D., D'SOUZA, B., LIM, A. L., CHINNA, K. & RADHAKRISHNAN, A. K. 2011. The prevalence of rheumatoid factor isotypes and anti-cyclic citrullinated peptides in Malaysian rheumatoid arthritis patients. *Int J Rheum Dis,* 14**,** 12-7.

GONG, W., KOLKER, S. J., USACHEV, Y., WALDER, R. Y., BOYLE, D. L., FIRESTEIN, G. S. & SLUKA, K. A. 2014. Acid-sensing ion channel 3 decreases phosphorylation of extracellular signal-regulated kinases and induces synoviocyte cell death by increasing intracellular calcium. *Arthritis Res Ther,* 16**,** R121.

GORTZ, B., HAYER, S., TUERCK, B., ZWERINA, J., SMOLEN, J. S. & SCHETT, G. 2005. Tumour necrosis factor activates the mitogen-activated protein kinases p38alpha and ERK in the synovial membrane in vivo. *Arthritis Res Ther,* 7**,** R1140-7.

GUO, A., VULCHANOVA, L., WANG, J., LI, X. & ELDE, R. 1999. Immunocytochemical localization of the vanilloid receptor 1 (VR1): relationship to neuropeptides, the P2X3 purinoceptor and IB4 binding sites. *Eur J Neurosci,* 11**,** 946-58.

HARAOUI, B., PELLETIER, J. P., CLOUTIER, J. M., FAURE, M. P. & MARTEL-PELLETIER, J. 1991. Synovial membrane histology and immunopathology in rheumatoid arthritis and osteoarthritis. In vivo effects of antirheumatic drugs. *Arthritis Rheum,* 34**,** 153-63.

HE, X. D., TOBO, M., MOGI, C., NAKAKURA, T., KOMACHI, M., MURATA, N., TAKANO, M., TOMURA, H., SATO, K. & OKAJIMA, F. 2011. Involvement of proton-sensing receptor TDAG8 in the anti-inflammatory actions of dexamethasone in peritoneal macrophages. *Biochem Biophys Res Commun,* 415**,** 627-31.

HEIDARI, B. 2011. Knee osteoarthritis prevalence, risk factors, pathogenesis and features: Part I. *Caspian Journal of Internal Medicine,* 2**,** 205-212.

HELYES, Z., SZABO, A., NEMETH, J., JAKAB, B., PINTER, E., BANVOLGYI, A., KERESKAI, L., KERI, G. & SZOLCSANYI, J. 2004. Antiinflammatory and analgesic effects of somatostatin released from capsaicin-sensitive sensory nerve terminals in a Freund's adjuvant-induced chronic arthritis model in the rat. *Arthritis Rheum,* 50**,** 1677-85.

HERRERA, I., CISNEROS, J., MALDONADO, M., RAMIREZ, R., ORTIZ-QUINTERO, B., ANSO, E., CHANDEL, N. S., SELMAN, M. & PARDO, A. 2013. Matrix metalloproteinase (MMP)-1 induces lung alveolar epithelial cell migration and proliferation, protects from apoptosis, and represses mitochondrial oxygen consumption. *J Biol Chem,* 288**,** 25964-75.

HERRERO-BEAUMONT, G., MARTINEZ CALATRAVA, M. J. & CASTANEDA, S. 2012. Abatacept mechanism of action: concordance with its clinical profile. *Reumatol Clin,* 8**,** 78-83.

HINTON, R., MOODY, R. L., DAVIS, A. W. & THOMAS, S. F. 2002. Osteoarthritis: diagnosis and therapeutic considerations. *Am Fam Physician,* 65**,** 841-8.

HOFBAUER, L. C., KHOSLA, S., DUNSTAN, C. R., LACEY, D. L., BOYLE, W. J. & RIGGS, B. L. 2000. The roles of osteoprotegerin and osteoprotegerin ligand in the paracrine regulation of bone resorption. *J Bone Miner Res,* 15**,** 2-12.

HOLZER, P. 1991. Capsaicin: cellular targets, mechanisms of action, and selectivity for thin sensory neurons. *Pharmacol Rev,* 43**,** 143-201.

HOU, W. S., LI, W., KEYSZER, G., WEBER, E., LEVY, R., KLEIN, M. J., GRAVALLESE, E. M., GOLDRING, S. R. & BROMME, D. 2002. Comparison of cathepsins K and S expression within the rheumatoid and osteoarthritic synovium. *Arthritis Rheum,* 46**,** 663-74.

HU, F., SUN, W. W., ZHAO, X. T., CUI, Z. J. & YANG, W. X. 2008. TRPV1 mediates cell death in rat synovial fibroblasts through calcium entry-dependent ROS production and mitochondrial depolarization. *Biochem Biophys Res Commun,* 369**,** 989-93.

HUANG, J., XIE, B., LI, Q., XIE, X., ZHU, S., WANG, M., PENG, W. & GU, J. 2013. Infliximab reduces CD147, MMP-3, and MMP-9 expression in peripheral blood monocytes in patients with active rheumatoid arthritis. *Eur J Pharmacol,* 698**,** 429-34.

HUANG, S. J., YANG, W. S., LIN, Y. W., WANG, H. C. & CHEN, C. C. 2008. Increase of insulin sensitivity and reversal of age-dependent glucose intolerance with inhibition of ASIC3. *Biochem Biophys Res Commun,* 371**,** 729-34.

HUDSON, L. J., BEVAN, S., WOTHERSPOON, G., GENTRY, C., FOX, A. & WINTER, J. 2001. VR1 protein expression increases in undamaged DRG neurons after partial nerve injury. *Eur J Neurosci,* 13**,** 2105-14.

IACCHERI, B., ANDROUDI, S., BOCCI, E. B., GERLI, R., CAGINI, C. & FIORE, T. 2010. Rituximab treatment for persistent scleritis associated with rheumatoid arthritis. *Ocul Immunol Inflamm,* 18**,** 223-5.

ICHIKAWA, H. & SUGIMOTO, T. 2002. The co-expression of ASIC3 with calcitonin gene-related peptide and parvalbumin in the rat trigeminal ganglion. *Brain Res,* 943**,** 287-91.

ICHIMONJI, I., TOMURA, H., MOGI, C., SATO, K., AOKI, H., HISADA, T., DOBASHI, K., ISHIZUKA, T., MORI, M. & OKAJIMA, F. 2010. Extracellular acidification stimulates IL-6 production and Ca(2+) mobilization through proton-sensing OGR1 receptors in human airway smooth muscle cells. *Am J Physiol Lung Cell Mol Physiol,* 299**,** L567-77.

JAHR, H., VAN DRIEL, M., VAN OSCH, G. J., WEINANS, H. & VAN LEEUWEN, J. P. 2005. Identification of acid-sensing ion channels in bone. *Biochem Biophys Res Commun,* 337**,** 349-54.

JARA-OSEGUERA, A., SIMON, S. A. & ROSENBAUM, T. 2008. TRPV1: on the road to pain relief. *Curr Mol Pharmacol,* 1**,** 255-69.

JEFFERY, R. C. Clinical features of rheumatoid arthritis. *Medicine,* 38**,** 167-171.

JORDT, S. E., TOMINAGA, M. & JULIUS, D. 2000. Acid potentiation of the capsaicin receptor determined by a key extracellular site. *Proc Natl Acad Sci U S A,* 97**,** 8134-9.

KAHLENBERG, J. M. & FOX, D. A. 2011. Advances in the Medical Treatment of Rheumatoid Arthritis. *Hand clinics,* 27**,** 11-20.

KARIN, M. 2004. Mitogen activated protein kinases as targets for development of novel anti-inflammatory drugs. *Ann Rheum Dis,* 63 Suppl 2**,** ii62-ii64.

KARLSON, E. W., MANDL, L. A., HANKINSON, S. E. & GRODSTEIN, F. 2004. Do breast-feeding and other reproductive factors influence future risk of rheumatoid arthritis? Results from the Nurses' Health Study. *Arthritis Rheum,* 50**,** 3458-67.

KAUSHAL, G. P. & SHAH, S. V. 2000. The new kids on the block: ADAMTSs, potentially multifunctional metalloproteinases of the ADAM family. *J Clin Invest,* 105**,** 1335-7.
KEEBLE, J., BLADES, M., PITZALIS, C., CASTRO DA ROCHA, F. A. & BRAIN, S. D. 2005. The role of substance P in microvascular responses in murine joint inflammation. *Br J Pharmacol,* 144**,** 1059-66.
KELLENBERGER, S. & SCHILD, L. 2002. Epithelial sodium channel/degenerin family of ion channels: a variety of functions for a shared structure. *Physiol Rev,* 82**,** 735-67.
KEYSTONE, E., EMERY, P., PETERFY, C. G., TAK, P. P., COHEN, S., GENOVESE, M. C., DOUGADOS, M., BURMESTER, G. R., GREENWALD, M., KVIEN, T. K., WILLIAMS, S., HAGERTY, D., CRAVETS, M. W. & SHAW, T. 2009. Rituximab inhibits structural joint damage in patients with rheumatoid arthritis with an inadequate response to tumour necrosis factor inhibitor therapies. *Ann Rheum Dis,* 68**,** 216-21.
KING, N. 2010. The use of comparative quantitative RT-PCR to investigate the effect of cysteine incubation on GPx1 expression in freshly isolated cardiomyocytes. *Methods Mol Biol,* 630**,** 215-32.
KITAS, G., BANKS, M. J. & BACON, P. A. 2001. Cardiac involvement in rheumatoid disease. *Clinical Medicine,* 1**,** 18-21.
KOCHAN, K. J., AMARAL, M. E., AGARWALA, R., SCHAFFER, A. A. & RIGGS, P. K. 2008. Application of dissociation curve analysis to radiation hybrid panel marker scoring: generation of a map of river buffalo (B. bubalis) chromosome 20. *BMC Genomics,* 9**,** 544.
KOCHUKOV, M. Y., MCNEARNEY, T. A., FU, Y. & WESTLUND, K. N. 2006. Thermosensitive TRP ion channels mediate cytosolic calcium response in human synoviocytes. *Am J Physiol Cell Physiol,* 291**,** C424-32.
KOLKER, S. J., WALDER, R. Y., USACHEV, Y., HILLMAN, J., BOYLE, D. L., FIRESTEIN, G. S. & SLUKA, K. A. 2010. Acid-sensing ion channel 3 expressed in type B synoviocytes and chondrocytes modulates hyaluronan expression and release. *Ann Rheum Dis,* 69**,** 903-9.
KOLKER, S. J., WALDER, R. Y., USACHEV, Y., HILLMAN, J., BOYLE, D. L., FIRESTEIN, G. S. & SLUKA, K. A. 2012. Acid-sensing ion channel 3 expressed in type B synoviocytes and chondrocytes modulates hyaluronan expression and release. *Ann Rheum Dis,* 69**,** 903-909.
KONG, X., TANG, X., DU, W., TONG, J., YAN, Y., ZHENG, F., FANG, M., GONG, F. & TAN, Z. 2013. Extracellular acidosis modulates the endocytosis and maturation of macrophages. *Cell Immunol,* 281**,** 44-50.
KORPELA, M., MUSTONEN, J., TEPPO, A. M., HELIN, H. & PASTERNACK, A. 1997. Mesangial glomerulonephritis as an extra-articular manifestation of rheumatoid arthritis. *Br J Rheumatol,* 36**,** 1189-95.
KRISHTAL, O. 2003. The ASICs: signaling molecules? Modulators? *Trends Neurosci,* 26**,** 477-83.
LARDNER, A. 2001. The effects of extracellular pH on immune function. *J Leukoc Biol,* 69**,** 522-30.
LARSEN, A., EDGREN, J., HARJU, E., LAASONEN, L. & REITAMO, T. 1979. Interobserver variation in the evaluation of radiologic changes of rheumatoid arthritis. *Scand J Rheumatol,* 8**,** 109-12.
LEE, Y. M., LI, W. H., KIM, Y. K., KIM, K. H. & CHUNG, J. H. 2008. Heat-induced MMP-1 expression is mediated by TRPV1 through PKCalpha signaling in HaCaT cells. *Exp Dermatol,* 17**,** 864-70.
LEMAIRE, R., HUET, G., ZERIMECH, F., GRARD, G., FONTAINE, C., DUQUESNOY, B. & FLIPO, R. M. 1997. Selective induction of the secretion of cathepsins B and L by cytokines in synovial fibroblast-like cells. *Br J Rheumatol,* 36**,** 735-43.

LEWIS, T. S., HUNT, J. B., AVELINE, L. D., JONSCHER, K. R., LOUIE, D. F., YEH, J. M., NAHREINI, T. S., RESING, K. A. & AHN, N. G. 2000. Identification of novel MAP kinase pathway signaling targets by functional proteomics and mass spectrometry. *Mol Cell,* 6**,** 1343-54.

LI, Z., HOU, W. S. & BROMME, D. 2000. Collagenolytic activity of cathepsin K is specifically modulated by cartilage-resident chondroitin sulfates. *Biochemistry,* 39**,** 529-36.

LIDDLE, R. A. 2007. The role of Transient Receptor Potential Vanilloid 1 (TRPV1) channels in pancreatitis. *Biochim Biophys Acta,* 1772**,** 869-78.

LINDY, O., KONTTINEN, Y. T., SORSA, T., DING, Y., SANTAVIRTA, S., CEPONIS, A. & LOPEZ-OTIN, C. 1997. Matrix metalloproteinase 13 (collagenase 3) in human rheumatoid synovium. *Arthritis Rheum,* 40**,** 1391-9.

LINGUEGLIA, E., DEVAL, E. & LAZDUNSKI, M. 2006. FMRFamide-gated sodium channel and ASIC channels: a new class of ionotropic receptors for FMRFamide and related peptides. *Peptides,* 27**,** 1138-52.

LINSCHEID, P., SEBOEK, D., SCHAER, D. J., ZULEWSKI, H., KELLER, U. & MULLER, B. 2004. Expression and secretion of procalcitonin and calcitonin gene-related peptide by adherent monocytes and by macrophage-activated adipocytes. *Crit Care Med,* 32**,** 1715-21.

LIU, C. J., KONG, W., XU, K., LUAN, Y., ILALOV, K., SEHGAL, B., YU, S., HOWELL, R. D. & DI CESARE, P. E. 2006. ADAMTS-12 associates with and degrades cartilage oligomeric matrix protein. *J Biol Chem,* 281**,** 15800-8.

LOPEZ-OLIVO, M. A., SIDDHANAMATHA, H. R., SHEA, B., TUGWELL, P., WELLS, G. A. & SUAREZ-ALMAZOR, M. E. 2014. Methotrexate for treating rheumatoid arthritis. *Cochrane Database Syst Rev,* 10.

LORENOWICZ, M. J., FERNANDEZ-BORJA, M. & HORDIJK, P. L. 2007. cAMP signaling in leukocyte transendothelial migration. *Arterioscler Thromb Vasc Biol,* 27**,** 1014-22.

LUDWIG, M. G., VANEK, M., GUERINI, D., GASSER, J. A., JONES, C. E., JUNKER, U., HOFSTETTER, H., WOLF, R. M. & SEUWEN, K. 2003. Proton-sensing G-protein-coupled receptors. *Nature,* 425**,** 93-8.

LUND-OLESEN, K. 1970. Oxygen tension in synovial fluids. *Arthritis Rheum,* 13**,** 769-76.

MACIEWICZ, R. A., WOTTON, S. F., ETHERINGTON, D. J. & DUANCE, V. C. 1990. Susceptibility of the cartilage collagens types II, IX and XI to degradation by the cysteine proteinases, cathepsins B and L. *FEBS Lett,* 269**,** 189-93.

MARADIT-KREMERS, H., CROWSON, C. S., NICOLA, P. J., BALLMAN, K. V., ROGER, V. L., JACOBSEN, S. J. & GABRIEL, S. E. 2005. Increased unrecognized coronary heart disease and sudden deaths in rheumatoid arthritis: a population-based cohort study. *Arthritis Rheum,* 52**,** 402-11.

MAZZUCA, M., HEURTEAUX, C., ALLOUI, A., DIOCHOT, S., BARON, A., VOILLEY, N., BLONDEAU, N., ESCOUBAS, P., GELOT, A., CUPO, A., ZIMMER, A., ZIMMER, A. M., ESCHALIER, A. & LAZDUNSKI, M. 2007. A tarantula peptide against pain via ASIC1a channels and opioid mechanisms. *Nat Neurosci,* 10**,** 943-5.

MCCARTY, D. J. 1974. Selected aspects of synovial membrane physiology. *Arthritis Rheum,* 17**,** 289-96.

MCCARTY, K. S., JR., SZABO, E., FLOWERS, J. L., COX, E. B., LEIGHT, G. S., MILLER, L., KONRATH, J., SOPER, J. T., BUDWIT, D. A., CREASMAN, W. T. & ET AL. 1986. Use of a monoclonal anti-estrogen receptor antibody in the immunohistochemical evaluation of human tumors. *Cancer Res,* 46**,** 4244s-4248s.

MCDONAGH, J., GREAVES, M., WRIGHT, A. R., HEYCOCK, C., OWEN, J. P. & KELLY, C. 1994. High resolution computed tomography of the lungs in patients with rheumatoid arthritis and interstitial lung disease. *Br J Rheumatol,* 33**,** 118-22.

MCMICHAEL, A. J., SASAZUKI, T., MCDEVITT, H. O. & PAYNE, R. O. 1977. Increased frequency of HLA-Cw3 and HLA-Dw4 in rheumatoid arthritis. *Arthritis Rheum,* 20**,** 1037-42.

MOELANTS, E. A., MORTIER, A., VAN DAMME, J. & PROOST, P. 2013. Regulation of TNF-alpha with a focus on rheumatoid arthritis. *Immunol Cell Biol,* 91**,** 393-401.

MOGI, C., TOBO, M., TOMURA, H., MURATA, N., HE, X. D., SATO, K., KIMURA, T., ISHIZUKA, T., SASAKI, T., SATO, T., KIHARA, Y., ISHII, S., HARADA, A. & OKAJIMA, F. 2009. Involvement of proton-sensing TDAG8 in extracellular acidification-induced inhibition of proinflammatory cytokine production in peritoneal macrophages. *J Immunol,* 182**,** 3243-51.

MOHAN, N., EDWARDS, E. T., CUPPS, T. R., OLIVERIO, P. J., SANDBERG, G., CRAYTON, H., RICHERT, J. R. & SIEGEL, J. N. 2001. Demyelination occurring during anti-tumor necrosis factor alpha therapy for inflammatory arthritides. *Arthritis Rheum,* 44**,** 2862-9.

MOLLIVER, D. C., IMMKE, D. C., FIERRO, L., PARE, M., RICE, F. L. & MCCLESKEY, E. W. 2005. ASIC3, an acid-sensing ion channel, is expressed in metaboreceptive sensory neurons. *Mol Pain,* 1**,** 35.

MOQRICH, A., HWANG, S. W., EARLEY, T. J., PETRUS, M. J., MURRAY, A. N., SPENCER, K. S., ANDAHAZY, M., STORY, G. M. & PATAPOUTIAN, A. 2005. Impaired thermosensation in mice lacking TRPV3, a heat and camphor sensor in the skin. *Science,* 307**,** 1468-72.

MOSHAL, K. S., SEN, U., TYAGI, N., HENDERSON, B., STEED, M., OVECHKIN, A. V. & TYAGI, S. C. 2006. Regulation of homocysteine-induced MMP-9 by ERK1/2 pathway. *Am J Physiol Cell Physiol,* 290**,** C883-91.

MOTTONEN, T., PAIMELA, L., AHONEN, J., HELVE, T., HANNONEN, P. & LEIRISALO-REPO, M. 1996. Outcome in patients with early rheumatoid arthritis treated according to the "sawtooth" strategy. *Arthritis Rheum,* 39**,** 996-1005.

MULLER-LADNER, U. & GAY, S. 2002. MMPs and rheumatoid synovial fibroblasts: Siamese twins in joint destruction? *Ann Rheum Dis,* 61**,** 957-9.

NAGASE, H. & KASHIWAGI, M. 2003. Aggrecanases and cartilage matrix degradation. *Arthritis Res Ther,* 5**,** 94-103.

NANNINI, C., MEDINA-VELASQUEZ, Y. F., ACHENBACH, S. J., CROWSON, C. S., RYU, J. H., VASSALLO, R., GABRIEL, S. E., MATTESON, E. L. & BONGARTZ, T. 2013. Incidence and Mortality of Obstructive Lung Disease in Rheumatoid Arthritis: A Population-Based Study. *Arthritis care & research,* 65**,** 1243-1250.

NAZ, S. M., FARRAGHER, T. M., BUNN, D. K., SYMMONS, D. P. M. & BRUCE, I. N. 2008. The influence of age at symptom onset and length of followup on mortality in patients with recent-onset inflammatory polyarthritis. *Arthritis & Rheumatism,* 58**,** 985-989.

NEHAR, D., MAUDUIT, C., BOUSSOUAR, F. & BENAHMED, M. 1997. Tumor necrosis factor-alpha-stimulated lactate production is linked to lactate dehydrogenase A expression and activity increase in porcine cultured Sertoli cells. *Endocrinology,* 138**,** 1964-71.

NEUDAUER, C. L., JOBERTY, G. & MACARA, I. G. 2001. PIST: a novel PDZ/coiled-coil domain binding partner for the rho-family GTPase TC10. *Biochem Biophys Res Commun,* 280**,** 541-7.

NEWMAN, K. A. & AKHTARI, M. 2011. Management of autoimmune neutropenia in Felty's syndrome and systemic lupus erythematosus. *Autoimmun Rev,* 10**,** 432-7.

NILIUS, B., OWSIANIK, G., VOETS, T. & PETERS, J. A. 2007. Transient receptor potential cation channels in disease. *Physiol Rev,* 87**,** 165-217.

OLIVER, J. E. & SILMAN, A. J. 2009. Why are women predisposed to autoimmune rheumatic diseases? *Arthritis Res Ther,* 11**,** 252.

ORY, P. A. 2003. Interpreting radiographic data in rheumatoid arthritis. *Ann Rheum Dis,* 62**,** 597-604.
OSIRI, M., SHEA, B., ROBINSON, V., SUAREZ-ALMAZOR, M., STRAND, V., TUGWELL, P. & WELLS, G. 2003. Leflunomide for the treatment of rheumatoid arthritis: a systematic review and metaanalysis. *J Rheumatol,* 30**,** 1182-90.
PAGE, G. & MIOSSEC, P. 2005. RANK and RANKL expression as markers of dendritic cell-T cell interactions in paired samples of rheumatoid synovium and lymph nodes. *Arthritis Rheum,* 52**,** 2307-12.
PAIMELA, L., LAASONEN, L., KANKAANPAA, E. & LEIRISALO-REPO, M. 1997. Progression of cervical spine changes in patients with early rheumatoid arthritis. *J Rheumatol,* 24**,** 1280-4.
PAL, M., ANGARU, S., KODIMUTHALI, A. & DHINGRA, N. 2009. Vanilloid receptor antagonists: emerging class of novel anti-inflammatory agents for pain management. *Curr Pharm Des,* 15**,** 1008-26.
PAP, T. & KORB-PAP, A. 2015. Cartilage damage in osteoarthritis and rheumatoid arthritis[mdash]two unequal siblings. *Nat Rev Rheumatol,* 11**,** 606-615.
PAP, T., SHIGEYAMA, Y., KUCHEN, S., FERNIHOUGH, J. K., SIMMEN, B., GAY, R. E., BILLINGHAM, M. & GAY, S. 2000. Differential expression pattern of membrane-type matrix metalloproteinases in rheumatoid arthritis. *Arthritis Rheum,* 43**,** 1226-32.
PATATANIAN, E. & THOMPSON, D. F. 2002. A Review of Methotrexate-Induced Accelerated Nodulosis. *Pharmacotherapy: The Journal of Human Pharmacology and Drug Therapy,* 22**,** 1157-1162.
PAVELKA, K., SEN, K. P., PELÍSKOVÁ, Z., VÁCHA, J. & TRNAVSKÝ, K. 1989. Hydroxychloroquine sulphate in the treatment of rheumatoid arthritis: a double blind comparison of two dose regimens. *Ann Rheum Dis,* 48**,** 542-546.
PETTIT, A. R., JI, H., VON STECHOW, D., MULLER, R., GOLDRING, S. R., CHOI, Y., BENOIST, C. & GRAVALLESE, E. M. 2001. TRANCE/RANKL knockout mice are protected from bone erosion in a serum transfer model of arthritis. *Am J Pathol,* 159**,** 1689-99.
PIERER, M., MULLER-LADNER, U., PAP, T., NEIDHART, M., GAY, R. E. & GAY, S. 2003. The SCID mouse model: novel therapeutic targets - lessons from gene transfer. *Springer Semin Immunopathol,* 25**,** 65-78.
PLOSKER, G. L. & CROOM, K. F. 2005. Sulfasalazine: a review of its use in the management of rheumatoid arthritis. *Drugs,* 65**,** 1825-49.
PORTER, M. H., CUTCHINS, A., FINE, J. B., BAI, Y. & DIGIROLAMO, M. 2002. Effects of TNF-alpha on glucose metabolism and lipolysis in adipose tissue and isolated fat-cell preparations. *J Lab Clin Med,* 139**,** 140-6.
PRETE, M., RACANELLI, V., DIGIGLIO, L., VACCA, A., DAMMACCO, F. & PEROSA, F. 2011. Extra-articular manifestations of rheumatoid arthritis: An update. *Autoimmunity Reviews,* 11**,** 123-131.
QADRI, Y. J., BERDIEV, B. K., SONG, Y., LIPPTON, H. L., FULLER, C. M. & BENOS, D. J. 2009. Psalmotoxin-1 docking to human acid-sensing ion channel-1. *J Biol Chem,* 284**,** 17625-33.
QADRI, Y. J., SONG, Y., FULLER, C. M. & BENOS, D. J. 2010. Amiloride docking to acid-sensing ion channel-1. *J Biol Chem,* 285**,** 9627-35.
RAINS, C. P., NOBLE, S. & FAULDS, D. 1995. Sulfasalazine. A review of its pharmacological properties and therapeutic efficacy in the treatment of rheumatoid arthritis. *Drugs,* 50**,** 137-56.
REFF, M. E., CARNER, K., CHAMBERS, K. S., CHINN, P. C., LEONARD, J. E., RAAB, R., NEWMAN, R. A., HANNA, N. & ANDERSON, D. R. 1994. Depletion of B cells in vivo by a chimeric mouse human monoclonal antibody to CD20. *Blood,* 83**,** 435-45.

REMELS, A. H., GOSKER, H. R., VERHEES, K. J., LANGEN, R. C. & SCHOLS, A. M. 2015. TNF-alpha-induced NF-kappaB activation stimulates skeletal muscle glycolytic metabolism through activation of HIF-1alpha. *Endocrinology,* 156**,** 1770-81.

REN, J. & ZHANG, L. 2011. Effects of ovarian cancer G protein coupled receptor 1 on the proliferation, migration, and adhesion of human ovarian cancer cells. *Chin Med J (Engl),* 124**,** 1327-32.

REVICI, E., STOOPEN, E., FRENK, E. & RAVICH, R. A. 1949. The painful focus. II. The relation of pain to local physiochemical changes. *Bull Inst Appl Biol* 1**,** 29-38.

RISTIC, G. G., LEPIC, T., GLISIC, B., STANISAVLJEVIC, D., VOJVODIC, D., PETRONIJEVIC, M. & STEFANOVIC, D. 2010. Rheumatoid arthritis is an independent risk factor for increased carotid intima-media thickness: impact of anti-inflammatory treatment. *Rheumatology (Oxford),* 49**,** 1076-81.

ROLLI, M., FRANSVEA, E., PILCH, J., SAVEN, A. & FELDING-HABERMANN, B. 2003. Activated integrin alphavbeta3 cooperates with metalloproteinase MMP-9 in regulating migration of metastatic breast cancer cells. *Proc Natl Acad Sci U S A,* 100**,** 9482-7.

ROMAS, E., GILLESPIE, M. T. & MARTIN, T. J. 2002. Involvement of receptor activator of NFkappaB ligand and tumor necrosis factor-alpha in bone destruction in rheumatoid arthritis. *Bone,* 30**,** 340-6.

ROSCIONI, S. S., ELZINGA, C. R. & SCHMIDT, M. 2008. Epac: effectors and biological functions. *Naunyn Schmiedebergs Arch Pharmacol,* 377**,** 345-57.

SAAG, K. G., TENG, G. G., PATKAR, N. M., ANUNTIYO, J., FINNEY, C., CURTIS, J. R., PAULUS, H. E., MUDANO, A., PISU, M., ELKINS-MELTON, M., OUTMAN, R., ALLISON, J. J., SUAREZ ALMAZOR, M., BRIDGES, S. L., JR., CHATHAM, W. W., HOCHBERG, M., MACLEAN, C., MIKULS, T., MORELAND, L. W., O'DELL, J., TURKIEWICZ, A. M. & FURST, D. E. 2008. American College of Rheumatology 2008 recommendations for the use of nonbiologic and biologic disease-modifying antirheumatic drugs in rheumatoid arthritis. *Arthritis Rheum,* 59**,** 762-84.

SAALBACH, A., KLEIN, C., SCHIRMER, C., BRIEST, W., ANDEREGG, U. & SIMON, J. C. 2010. Dermal fibroblasts promote the migration of dendritic cells. *J Invest Dermatol,* 130**,** 444-54.

SAHATCIU-MEKA, V., REXHEPI, S., MANXHUKA-KERLIU, S. & REXHEPI, M. 2010. Extra-articular manifestations of seronegative and seropositive rheumatoid arthritis. *Bosn J Basic Med Sci,* 10**,** 26-31.

SANN, H. & PIERAU, F. K. 1998. Efferent functions of C-fiber nociceptors. *Z Rheumatol,* 57 Suppl 2**,** 8-13.

SARZI-PUTTINI, P., ATZENI, F., GERLI, R., BARTOLONI, E., DORIA, A., BARSKOVA, T., MATUCCI-CERINIC, M., SITIA, S., TOMASONI, L. & TURIEL, M. 2010. Cardiac involvement in systemic rheumatic diseases: An update. *Autoimmunity Reviews,* 9**,** 849-852.

SAPIR-KOREN, R. & LIVSHITS, G. 2016. Rheumatoid arthritis onset in postmenopausal women: Does the ACPA seropositive subset result from genetic effects, estrogen deficiency, skewed profile of CD4(+) T-cells, and their interactions? *Mol Cell Endocrinol,* 431**,** 145-63.

SCHWARTZ, E. S., CHRISTIANSON, J. A., CHEN, X., LA, J. H., DAVIS, B. M., ALBERS, K. M. & GEBHART, G. F. 2011. Synergistic role of TRPV1 and TRPA1 in pancreatic pain and inflammation. *Gastroenterology,* 140**,** 1283-1291 e1-2.

SCHWARTZ, E. S., LA, J. H., SCHEFF, N. N., DAVIS, B. M., ALBERS, K. M. & GEBHART, G. F. 2013. TRPV1 and TRPA1 antagonists prevent the transition of acute to chronic inflammation and pain in chronic pancreatitis. *J Neurosci,* 33**,** 5603-11.

SCOTT, D. L., PUGNER, K., KAARELA, K., DOYLE, D. V., WOOLF, A., HOLMES, J. & HIEKE, K. 2000. The links between joint damage and disability in rheumatoid arthritis. *Rheumatology (Oxford),* 39**,** 122-32.

SEGER, R. & KREBS, E. G. 1995. The MAPK signaling cascade. *FASEB J,* 9**,** 726-35.

SEUWEN, K., LUDWIG, M. G. & WOLF, R. M. 2006. Receptors for protons or lipid messengers or both? *J Recept Signal Transduct Res,* 26**,** 599-610.

SHARP, J. T., LIDSKY, M. D., COLLINS, L. C. & MORELAND, J. 1971. Methods of scoring the progression of radiologic changes in rheumatoid arthritis. Correlation of radiologic, clinical and laboratory abnormalities. *Arthritis Rheum,* 14**,** 706-20.

SHERWOOD, J., BERTRAND, J., NALESSO, G., POULET, B., PITSILLIDES, A., BRANDOLINI, L., KARYSTINOU, A., DE BARI, C., LUYTEN, F. P., PITZALIS, C., PAP, T. & DELL'ACCIO, F. 2015. A homeostatic function of CXCR2 signalling in articular cartilage. *Ann Rheum Dis,* 74**,** 2207-15.

SHIPMAN, C., JR. 1969. Evaluation of 4-(2-hydroxyethyl)-1-piperazineethanesulfonic acid (HEPES) as a tissue culture buffer. *Proc Soc Exp Biol Med,* 130**,** 305-10.

SICOTTE, N. L. & VOSKUHL, R. R. 2001. Onset of multiple sclerosis associated with anti-TNF therapy. *Neurology,* 57**,** 1885-8.

SIESJO, B. K., KATSURA, K. & KRISTIAN, T. 1996. Acidosis-related damage. *Adv Neurol,* 71**,** 209-33; discussion 234-6.

SIMONET, W. S., LACEY, D. L., DUNSTAN, C. R., KELLEY, M., CHANG, M. S., LUTHY, R., NGUYEN, H. Q., WOODEN, S., BENNETT, L., BOONE, T., SHIMAMOTO, G., DEROSE, M., ELLIOTT, R., COLOMBERO, A., TAN, H. L., TRAIL, G., SULLIVAN, J., DAVY, E., BUCAY, N., RENSHAW-GEGG, L., HUGHES, T. M., HILL, D., PATTISON, W., CAMPBELL, P., SANDER, S., VAN, G., TARPLEY, J., DERBY, P., LEE, R. & BOYLE, W. J. 1997. Osteoprotegerin: a novel secreted protein involved in the regulation of bone density. *Cell,* 89**,** 309-19.

SIMSEK, I., ERDEM, H., PAY, S., SOBACI, G. & DINC, A. 2007. Optic neuritis occurring with anti-tumour necrosis factor α therapy. *Ann Rheum Dis,* 66**,** 1255-1258.

SINGH, L. S., BERK, M., OATES, R., ZHAO, Z., TAN, H., JIANG, Y., ZHOU, A., KIRMANI, K., STEINMETZ, R., LINDNER, D. & XU, Y. 2007. Ovarian cancer G protein-coupled receptor 1, a new metastasis suppressor gene in prostate cancer. *J Natl Cancer Inst,* 99**,** 1313-27.

SLUKA, K. A., RASMUSSEN, L. A., EDGAR, M. M., O'DONNELL, J. M., WALDER, R. Y., KOLKER, S. J., BOYLE, D. L. & FIRESTEIN, G. S. 2013. Acid-sensing ion channel 3 deficiency increases inflammation but decreases pain behavior in murine arthritis. *Arthritis Rheum,* 65**,** 1194-202.

SMOLEN, J. S. & STEINER, G. 2003. Therapeutic strategies for rheumatoid arthritis. *Nat Rev Drug Discov,* 2**,** 473-488.

SONG, R. H., TORTORELLA, M. D., MALFAIT, A. M., ALSTON, J. T., YANG, Z., ARNER, E. C. & GRIGGS, D. W. 2007. Aggrecan degradation in human articular cartilage explants is mediated by both ADAMTS-4 and ADAMTS-5. *Arthritis Rheum,* 56**,** 575-85.

STEVENS, C. R., WILLIAMS, R. B., FARRELL, A. J. & BLAKE, D. R. 1991. Hypoxia and inflammatory synovitis: observations and speculation. *Ann Rheum Dis,* 50**,** 124-32.

STROUP, G. B., LARK, M. W., VEBER, D. F., BHATTACHARYYA, A., BLAKE, S., DARE, L. C., ERHARD, K. F., HOFFMAN, S. J., JAMES, I. E., MARQUIS, R. W., RU, Y., VASKO-MOSER, J. A., SMITH, B. R., TOMASZEK, T. & GOWEN, M. 2001. Potent and selective inhibition of human cathepsin K leads to inhibition of bone resorption in vivo in a nonhuman primate. *J Bone Miner Res,* 16**,** 1739-46.

SU, X., LI, Q., SHRESTHA, K., CORMET-BOYAKA, E., CHEN, L., SMITH, P. R., SORSCHER, E. J., BENOS, D. J., MATALON, S. & JI, H. L. 2006. Interregulation of

proton-gated Na(+) channel 3 and cystic fibrosis transmembrane conductance regulator. *J Biol Chem,* 281**,** 36960-8.

SURI, A. & SZALLASI, A. 2008. The emerging role of TRPV1 in diabetes and obesity. *Trends Pharmacol Sci,* 29**,** 29-36.

SUTHERLAND, S. P., BENSON, C. J., ADELMAN, J. P. & MCCLESKEY, E. W. 2001. Acid-sensing ion channel 3 matches the acid-gated current in cardiac ischemia-sensing neurons. *Proc Natl Acad Sci U S A,* 98**,** 711-6.

SZABO, A., HELYES, Z., SANDOR, K., BITE, A., PINTER, E., NEMETH, J., BANVOLGYI, A., BOLCSKEI, K., ELEKES, K. & SZOLCSANYI, J. 2005. Role of transient receptor potential vanilloid 1 receptors in adjuvant-induced chronic arthritis: in vivo study using gene-deficient mice. *J Pharmacol Exp Ther,* 314**,** 111-9.

SZALLASI, A. 2002. Vanilloid (capsaicin) receptors in health and disease. *Am J Clin Pathol,* 118**,** 110-21.

TANG, M. L., HAAS, D. A. & HU, J. W. 2004. Capsaicin-induced joint inflammation is not blocked by local anesthesia. *Anesth Prog,* 51**,** 2-9.

THIEL, M. J., SCHAEFER, C. J., LESCH, M. E., MOBLEY, J. L., DUDLEY, D. T., TECLE, H., BARRETT, S. D., SCHRIER, D. J. & FLORY, C. M. 2007. Central role of the MEK/ERK MAP kinase pathway in a mouse model of rheumatoid arthritis: potential proinflammatory mechanisms. *Arthritis Rheum,* 56**,** 3347-57.

THOMAS, K. C., SABNIS, A. S., JOHANSEN, M. E., LANZA, D. L., MOOS, P. J., YOST, G. S. & REILLY, C. A. 2007. Transient receptor potential vanilloid 1 agonists cause endoplasmic reticulum stress and cell death in human lung cells. *J Pharmacol Exp Ther,* 321**,** 830-8.

TOLBOOM, T. C., PIETERMAN, E., VAN DER LAAN, W. H., TOES, R. E., HUIDEKOPER, A. L., NELISSEN, R. G., BREEDVELD, F. C. & HUIZINGA, T. W. 2002. Invasive properties of fibroblast-like synoviocytes: correlation with growth characteristics and expression of MMP-1, MMP-3, and MMP-10. *Ann Rheum Dis,* 61**,** 975-80.

TOMINAGA, M., CATERINA, M. J., MALMBERG, A. B., ROSEN, T. A., GILBERT, H., SKINNER, K., RAUMANN, B. E., BASBAUM, A. I. & JULIUS, D. 1998. The cloned capsaicin receptor integrates multiple pain-producing stimuli. *Neuron,* 21**,** 531-43.

TOMINAGA, M. & TOMINAGA, T. 2005. Structure and function of TRPV1. *Pflugers Arch,* 451**,** 143-50.

TOMURA, H., MOGI, C., SATO, K. & OKAJIMA, F. 2005. Proton-sensing and lysolipid-sensitive G-protein-coupled receptors: a novel type of multi-functional receptors. *Cell Signal,* 17**,** 1466-76.

TOMURA, H., WANG, J. Q., LIU, J. P., KOMACHI, M., DAMIRIN, A., MOGI, C., TOBO, M., NOCHI, H., TAMOTO, K., IM, D. S., SATO, K. & OKAJIMA, F. 2008. Cyclooxygenase-2 expression and prostaglandin E2 production in response to acidic pH through OGR1 in a human osteoblastic cell line. *J Bone Miner Res,* 23**,** 1129-39.

TONG, J., WU, W. N., KONG, X., WU, P. F., TIAN, L., DU, W., FANG, M., ZHENG, F., CHEN, J. G., TAN, Z. & GONG, F. 2011. Acid-sensing ion channels contribute to the effect of acidosis on the function of dendritic cells. *J Immunol,* 186**,** 3686-92.

TOTH, B. I., BENKO, S., SZOLLOSI, A. G., KOVACS, L., RAJNAVOLGYI, E. & BIRO, T. 2009. Transient receptor potential vanilloid-1 signaling inhibits differentiation and activation of human dendritic cells. *FEBS Lett,* 583**,** 1619-24.

TREUHAFT, P. S., LEWIS, M. R. & MCCARTY, D. J. 1971. A rapid method for evaluating the structure and function of the rheumatoid hand. *Arthritis Rheum,* 14**,** 75-86.

TSUBOI, M., KAWAKAMI, A., NAKASHIMA, T., MATSUOKA, N., URAYAMA, S., KAWABE, Y., FUJIYAMA, K., KIRIYAMA, T., AOYAGI, T., MAEDA, K. & EGUCHI, K. 1999. Tumor necrosis factor-alpha and interleukin-1beta increase the Fas-mediated apoptosis of human osteoblasts. *J Lab Clin Med,* 134**,** 222-31.

TSURUMAKI, H., MOGI, C., AOKI-SAITO, H., TOBO, M., KAMIDE, Y., YATOMI, M., SATO, K., DOBASHI, K., ISHIZUKA, T., HISADA, T., YAMADA, M. & OKAJIMA, F. 2015. Protective Role of Proton-Sensing TDAG8 in Lipopolysaccharide-Induced Acute Lung Injury. *International Journal of Molecular Sciences,* 16**,** 28931-28942.

TURESSON, C. & MATTESON, E. L. 2004. Management of extra-articular disease manifestations in rheumatoid arthritis. *Curr Opin Rheumatol,* 16**,** 206-11.

TURIEL, M., SITIA, S., ATZENI, F., TOMASONI, L., GIANTURCO, L., GIUFFRIDA, M., COLONNA, V. D. G. & SARZI-PUTTINI, P. 2010. The heart in rheumatoid arthritis. *Autoimmunity Reviews,* 9**,** 414-418.

VAN DER KRAAN, P. M. & VAN DEN BERG, W. B. 2012. Chondrocyte hypertrophy and osteoarthritis: role in initiation and progression of cartilage degeneration? *Osteoarthritis and Cartilage,* 20**,** 223-232.

VANKEMMELBEKE, M. N., HOLEN, I., WILSON, A. G., ILIC, M. Z., HANDLEY, C. J., KELNER, G. S., CLARK, M., LIU, C., MAKI, R. A., BURNETT, D. & BUTTLE, D. J. 2001. Expression and activity of ADAMTS-5 in synovium. *Eur J Biochem,* 268**,** 1259-68.

VARGHESE, F., BUKHARI, A. B., MALHOTRA, R. & DE, A. 2014. IHC Profiler: an open source plugin for the quantitative evaluation and automated scoring of immunohistochemistry images of human tissue samples. *PLoS One,* 9**,** e96801.

VAUPEL, P., OKUNIEFF, P. & NEURINGER, L. J. 1989. Blood flow, tissue oxygenation, pH distribution, and energy metabolism of murine mammary adenocarcinomas during growth. *Adv Exp Med Biol,* 248**,** 835-45.

VINCENTI, M. P. & BRINCKERHOFF, C. E. 2002. Transcriptional regulation of collagenase (MMP-1, MMP-13) genes in arthritis: integration of complex signaling pathways for the recruitment of gene-specific transcription factors. *Arthritis Res,* 4**,** 157-64.

VOILLEY, N., DE WEILLE, J., MAMET, J. & LAZDUNSKI, M. 2001. Nonsteroid anti-inflammatory drugs inhibit both the activity and the inflammation-induced expression of acid-sensing ion channels in nociceptors. *J Neurosci,* 21**,** 8026-33.

VRIENS, J., APPENDINO, G. & NILIUS, B. 2009. Pharmacology of vanilloid transient receptor potential cation channels. *Mol Pharmacol,* 75**,** 1262-79.

VROON, A., KAVELAARS, A., LIMMROTH, V., LOMBARDI, M. S., GOEBEL, M. U., VAN DAM, A. M., CARON, M. G., SCHEDLOWSKI, M. & HEIJNEN, C. J. 2005. G protein-coupled receptor kinase 2 in multiple sclerosis and experimental autoimmune encephalomyelitis. *J Immunol,* 174**,** 4400-6.

WALDBURGER, J. M., BOYLE, D. L., PAVLOV, V. A., TRACEY, K. J. & FIRESTEIN, G. S. 2008. Acetylcholine regulation of synoviocyte cytokine expression by the alpha7 nicotinic receptor. *Arthritis Rheum,* 58**,** 3439-49.

WALDMANN, R. 2001. Proton-gated cation channels--neuronal acid sensors in the central and peripheral nervous system. *Adv Exp Med Biol,* 502**,** 293-304.

WALDMANN, R., CHAMPIGNY, G., BASSILANA, F., HEURTEAUX, C. & LAZDUNSKI, M. 1997. A proton-gated cation channel involved in acid-sensing. *Nature,* 386**,** 173-7.

WALDMANN, R. & LAZDUNSKI, M. 1998. H(+)-gated cation channels: neuronal acid sensors in the NaC/DEG family of ion channels. *Curr Opin Neurobiol,* 8**,** 418-24.

WANG, W., PAN, H., MURRAY, K., JEFFERSON, B. S. & LI, Y. 2009. Matrix metalloproteinase-1 promotes muscle cell migration and differentiation. *Am J Pathol,* 174**,** 541-9.

WANG, W., YU, Y. & XU, T. L. 2007. Modulation of acid-sensing ion channels by Cu(2+) in cultured hypothalamic neurons of the rat. *Neuroscience,* 145**,** 631-41.

WEMMIE, J. A., TAUGHER, R. J. & KREPLE, C. J. 2013. Acid-sensing ion channels in pain and disease. *Nat Rev Neurosci,* 14**,** 461-71.

WEYAND, C. M., SCHMIDT, D., WAGNER, U. & GORONZY, J. J. 1998. The influence of sex on the phenotype of rheumatoid arthritis. *Arthritis Rheum,* 41**,** 817-22.
WIESINGER, T., SMOLEN, J. S., ALETAHA, D. & STAMM, T. 2013. Compression test (Gaenslen's squeeze test) positivity, joint tenderness, and disease activity in patients with rheumatoid arthritis. *Arthritis Care Res,* 65**,** 653-7.
WILDER, R. L. & CROFFORD, L. J. 1991. Do infectious agents cause rheumatoid arthritis? *Clin Orthop Relat Res***,** 36-41.
WILLIS, W. D., JR. 1999. Dorsal root potentials and dorsal root reflexes: a double-edged sword. *Exp Brain Res,* 124**,** 395-421.
WOLFE, F., KLEINHEKSEL, S. M., CATHEY, M. A., HAWLEY, D. J., SPITZ, P. W. & FRIES, J. F. 1988. The clinical value of the Stanford Health Assessment Questionnaire Functional Disability Index in patients with rheumatoid arthritis. *J Rheumatol,* 15**,** 1480-8.
WONG, G. Y. & GAVVA, N. R. 2009. Therapeutic potential of vanilloid receptor TRPV1 agonists and antagonists as analgesics: Recent advances and setbacks. *Brain Res Rev,* 60**,** 267-77.
WU, C. C., YU, H. C., YEN, J. H., TSAI, W. C. & LIU, H. W. 2005. Rare extra-articular manifestation of rheumatoid arthritis: scleromalacia perforans. *Kaohsiung J Med Sci,* 21**,** 233-5.
XU, Y. & CASEY, G. 1996. Identification of human OGR1, a novel G protein-coupled receptor that maps to chromosome 14. *Genomics,* 35**,** 397-402.
YAN, L., SINGH, L. S., ZHANG, L. & XU, Y. 2014. Role of OGR1 in myeloid-derived cells in prostate cancer. *Oncogene,* 33**,** 157-64.
YANG, L. V., RADU, C. G., ROY, M., LEE, S., MCLAUGHLIN, J., TEITELL, M. A., IRUELA-ARISPE, M. L. & WITTE, O. N. 2007. Vascular abnormalities in mice deficient for the G protein-coupled receptor GPR4 that functions as a pH sensor. *Mol Cell Biol,* 27**,** 1334-47.
YANG, M., MAILHOT, G., BIRNBAUM, M. J., MACKAY, C. A., MASON-SAVAS, A. & ODGREN, P. R. 2006. Expression of and role for ovarian cancer G-protein-coupled receptor 1 (OGR1) during osteoclastogenesis. *J Biol Chem,* 281**,** 23598-605.
YIANGOU, Y., FACER, P., SMITH, J. A., SANGAMESWARAN, L., EGLEN, R., BIRCH, R., KNOWLES, C., WILLIAMS, N. & ANAND, P. 2001. Increased acid-sensing ion channel ASIC-3 in inflamed human intestine. *Eur J Gastroenterol Hepatol,* 13**,** 891-6.
YUAN, F. L., CHEN, F. H., LU, W. G. & LI, X. 2010a. Acid-sensing ion channels 3: a potential therapeutic target for pain treatment in arthritis. *Mol Biol Rep,* 37**,** 3233-8.
YUAN, F. L., CHEN, F. H., LU, W. G., LI, X., LI, J. P., LI, C. W., XU, R. S., WU, F. R., HU, W. & ZHANG, T. Y. 2010b. Inhibition of acid-sensing ion channels in articular chondrocytes by amiloride attenuates articular cartilage destruction in rats with adjuvant arthritis. *Inflamm Res,* 59**,** 939-47.
YUAN, F. L., CHEN, F. H., LU, W. G., LI, X., WU, F. R., LI, J. P., LI, C. W., WANG, Y., ZHANG, T. Y. & HU, W. 2010c. Acid-sensing ion channel 1a mediates acid-induced increases in intracellular calcium in rat articular chondrocytes. *Mol Cell Biochem,* 340**,** 153-9.
YUAN, F. L., ZHAO, M. D., JIANG, L. B., WANG, H. R., CAO, L., ZHOU, X. G., LI, X. L. & DONG, J. 2014a. Molecular actions of ovarian cancer G protein-coupled receptor 1 caused by extracellular acidification in bone. *Int J Mol Sci,* 15**,** 22365-73.
YUAN, H., YANG, P., ZHOU, D., GAO, W., QIU, Z., FANG, F., DING, S. & XIAO, W. 2014b. Knockdown of sphingosine kinase 1 inhibits the migration and invasion of human rheumatoid arthritis fibroblast-like synoviocytes by down-regulating the PI3K/AKT activation and MMP-2/9 production in vitro. *Mol Biol Rep,* 41**,** 5157-65.
ZHA, X. M. 2013. Acid-sensing ion channels: trafficking and synaptic function. *Mol Brain,* 6**,** 1.

ZHAO, J. F., CHING, L. C., KOU, Y. R., LIN, S. J., WEI, J., SHYUE, S. K. & LEE, T. S. 2013. Activation of TRPV1 prevents OxLDL-induced lipid accumulation and TNF-alpha-induced inflammation in macrophages: role of liver X receptor alpha. *Mediators Inflamm,* 2013**,** 925171.

ZHU, K., BAUDHUIN, L. M., HONG, G., WILLIAMS, F. S., CRISTINA, K. L., KABAROWSKI, J. H., WITTE, O. N. & XU, Y. 2001. Sphingosylphosphorylcholine and lysophosphatidylcholine are ligands for the G protein-coupled receptor GPR4. *J Biol Chem,* 276**,** 41325-35.

ZHU, P., LU, N., SHI, Z. G., ZHOU, J., WU, Z. B., YANG, Y., DING, J. & CHEN, Z. N. 2006. CD147 overexpression on synoviocytes in rheumatoid arthritis enhances matrix metalloproteinase production and invasiveness of synoviocytes. *Arthritis Res Ther,* 8**,** R44.

ZHU, Y., COLAK, T., SHENOY, M., LIU, L., PAI, R., LI, C., MEHTA, K. & PASRICHA, P. J. 2011. Nerve growth factor modulates TRPV1 expression and function and mediates pain in chronic pancreatitis. *Gastroenterology,* 141**,** 370-7.

ZIGLER, J. S., JR., LEPE-ZUNIGA, J. L., VISTICA, B. & GERY, I. 1985. Analysis of the cytotoxic effects of light-exposed HEPES-containing culture medium. *In Vitro Cell Dev Biol,* 21**,** 282-7.

ZWERINA, J., REDLICH, K., POLZER, K., JOOSTEN, L., KRONKE, G., DISTLER, J., HESS, A., PUNDT, N., PAP, T., HOFFMANN, O., GASSER, J., SCHEINECKER, C., SMOLEN, J. S., VAN DEN BERG, W. & SCHETT, G. 2007. TNF-induced structural joint damage is mediated by IL-1. *Proc Natl Acad Sci U S A,* 104**,** 11742-7.

Appendices

List of extra equipment

7900HT AbiPrism sequence detection system	Applied Biosystems, CA, USA
Aperio CS2 slidescanner	Leica, Wetzlar, Germany
ChemiDoc™ XRS+ System	BIORAD, CA,USA
Inverted wide-field fluorescent microscope under mercury lamp DM1400B	Leica, Wetzlar, Germany
Microscope DM500 brightfield	Leica, Wetzlar, Germany
Nanodrop Spectrophotometer ND 1000	Thermo Fisher Scientific Inc, MA, USA
Original iBlot® gel transfer device	Invitrogen, Paisley, UK
Thermo cycler T100	Bio-Rad Laboratories, CA, USA

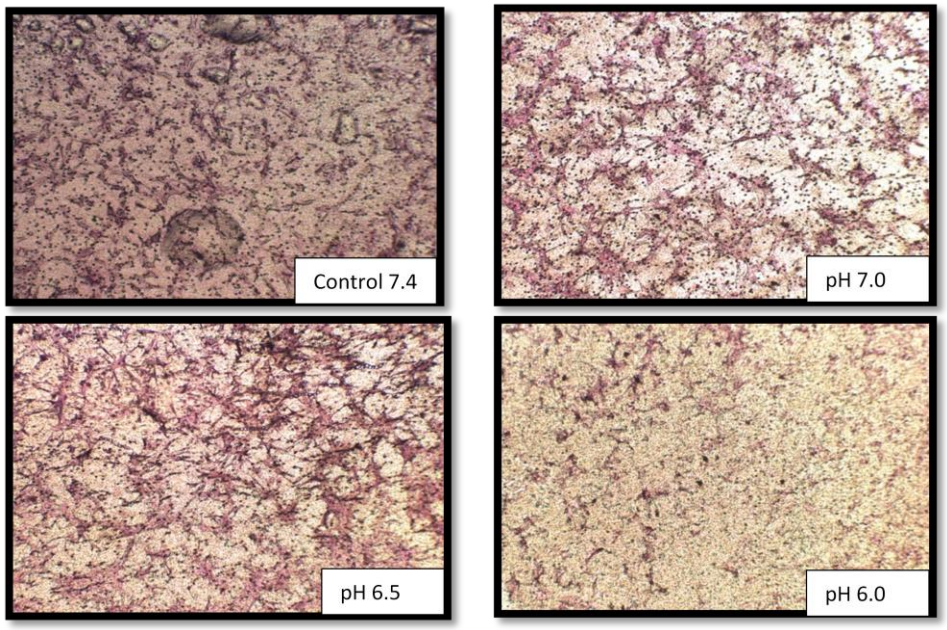

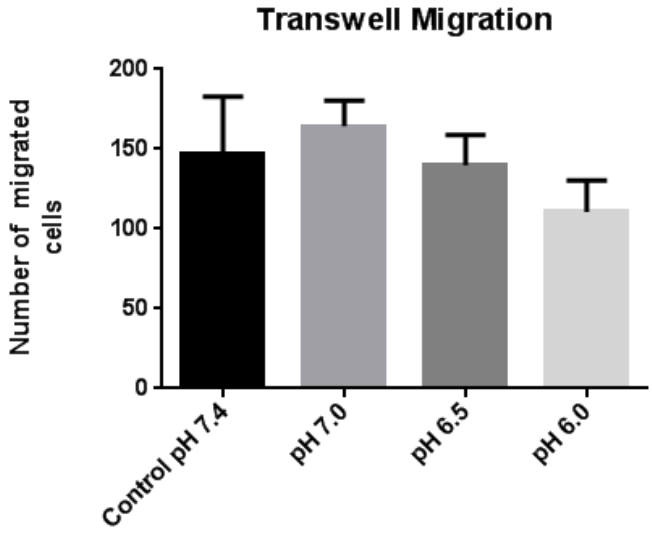

Figure, RA-FLS migration in transwell 24 well plate; Figure shows insignificant reduction in RA-FLS migration at low pH.

Manual H-score in lung and RA-synovium

ASIC3 score ≈ 164 in lung and 139 in synovial tissue. GPR4 is expressed higher in lung than in RA synovium with H-score 149 and 192, respectively. OGR1 H-score is lower in RA synoivum than in lung with H-score of 113 and 140 respectively. The average scores of TRPV1 ≈124 in RA synovium and 150 in lung tissue. No significant change was indicated. Unpaired t-test was used to analyze data. Results are presented as mean ± SEM

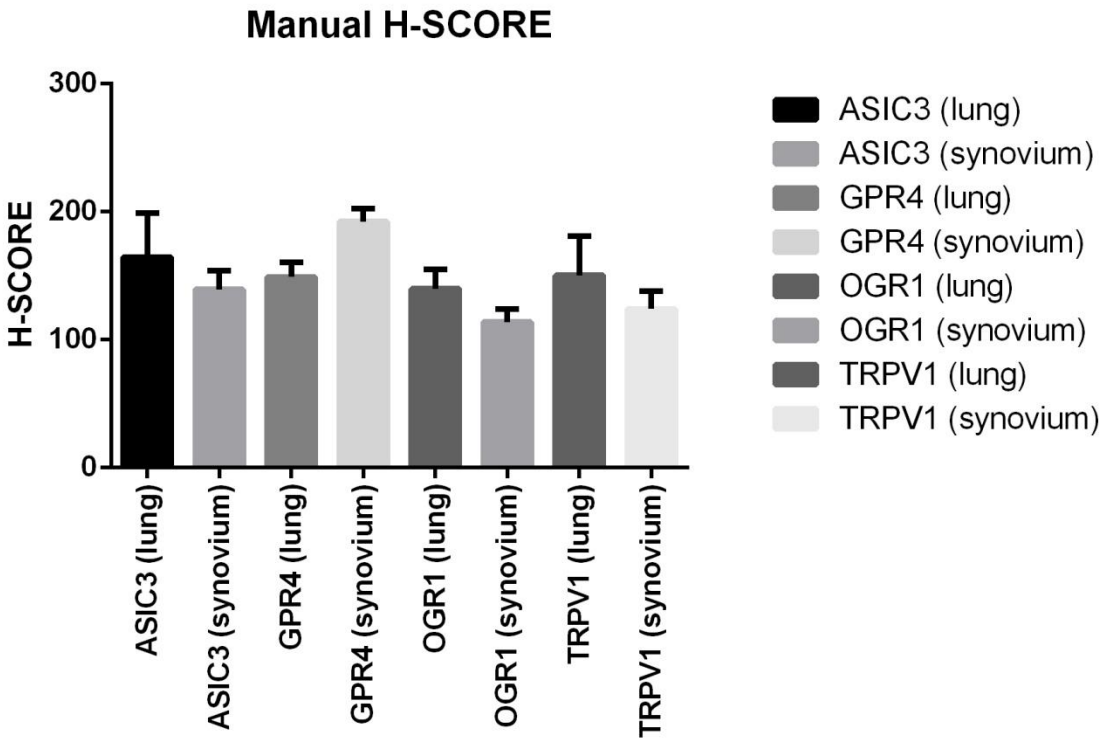

Figure; H-score of Acid sensing protein (ASIC3) in lung and tissue and RA synovial tissue.

SYBR Green assessment after qPCR runs

Melt-curve analysis following qPCR shows a single peak for each amplicon of bone and cartilage destruction modulators

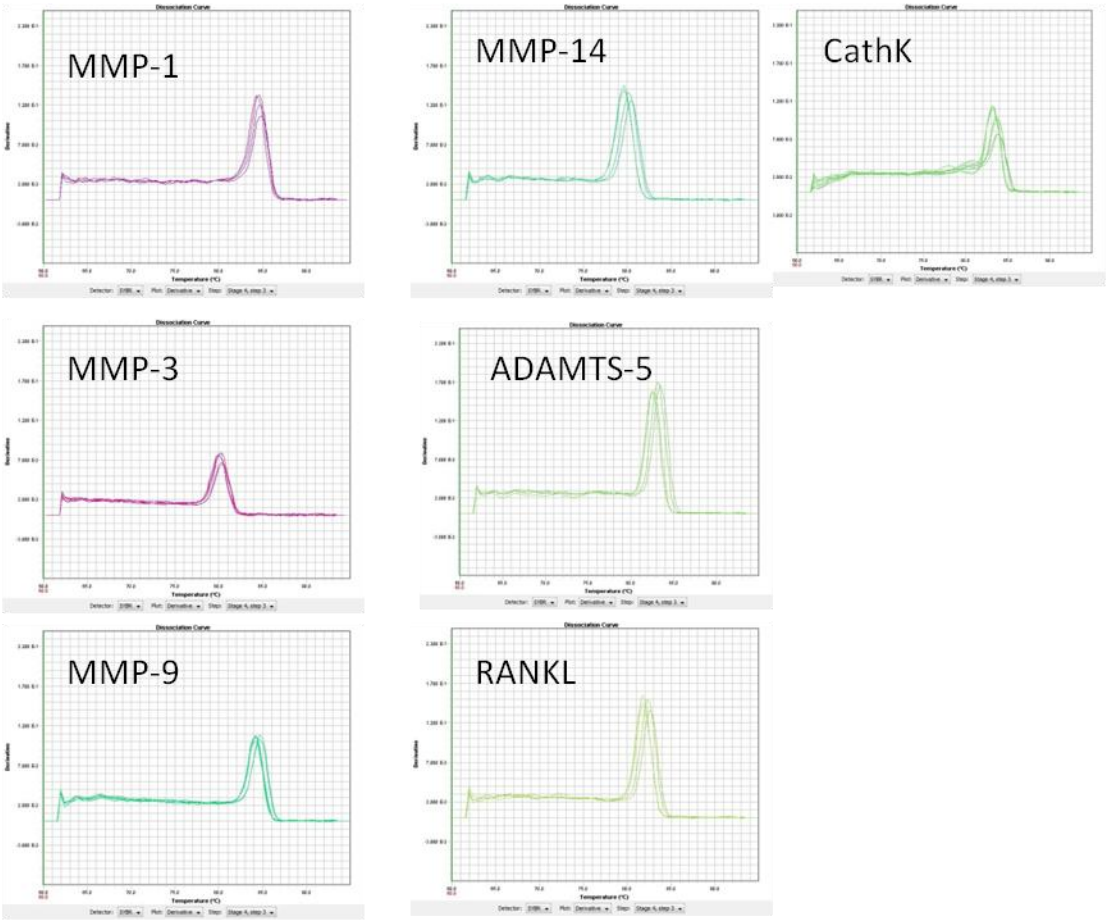

Figure Disassociation curve results following qPCR reaction.

Each qPCR reaction was evaluated by melt curve analysis to determine SYBR Green specificity and identify any contamination with genomic DNA or primer dimers.